

## INFORMATION TO USERS

This manuscript has been reproduced from the microfilm master. UMI films the text directly from the original or copy submitted. Thus, some thesis and dissertation copies are in typewriter face, while others may be from any type of computer printer.

**The quality of this reproduction is dependent upon the quality of the copy submitted.** Broken or indistinct print, colored or poor quality illustrations and photographs, print bleedthrough, substandard margins, and improper alignment can adversely affect reproduction.

In the unlikely event that the author did not send UMI a complete manuscript and there are missing pages, these will be noted. Also, if unauthorized copyright material had to be removed, a note will indicate the deletion.

Oversize materials (e.g., maps, drawings, charts) are reproduced by sectioning the original, beginning at the upper left-hand corner and continuing from left to right in equal sections with small overlaps.

Photographs included in the original manuscript have been reproduced xerographically in this copy. Higher quality 6" x 9" black and white photographic prints are available for any photographs or illustrations appearing in this copy for an additional charge. Contact UMI directly to order.

ProQuest Information and Learning  
300 North Zeeb Road, Ann Arbor, MI 48106-1346 USA  
800-521-0600

UMI<sup>®</sup>



**University of Alberta**

**A Redox-Regulated RNA Helicase Gene**

by

Sonya Louise Kujat Choy



A thesis submitted to the Faculty of Graduate Studies and Research  
in partial fulfillment of the requirements  
for the degree of Doctor of Philosophy

Department of Biological Sciences

Edmonton, Alberta

Spring 2001



National Library  
of Canada

Acquisitions and  
Bibliographic Services

395 Wellington Street  
Ottawa ON K1A 0N4  
Canada

Bibliothèque nationale  
du Canada

Acquisitions et  
services bibliographiques

395, rue Wellington  
Ottawa ON K1A 0N4  
Canada

*Your file Votre référence*

*Our file Notre référence*

The author has granted a non-exclusive licence allowing the National Library of Canada to reproduce, loan, distribute or sell copies of this thesis in microform, paper or electronic formats.

The author retains ownership of the copyright in this thesis. Neither the thesis nor substantial extracts from it may be printed or otherwise reproduced without the author's permission.

L'auteur a accordé une licence non exclusive permettant à la Bibliothèque nationale du Canada de reproduire, prêter, distribuer ou vendre des copies de cette thèse sous la forme de microfiche/film, de reproduction sur papier ou sur format électronique.

L'auteur conserve la propriété du droit d'auteur qui protège cette thèse. Ni la thèse ni des extraits substantiels de celle-ci ne doivent être imprimés ou autrement reproduits sans son autorisation.

0-612-60315-6

**Canada**



**University of Alberta**

**Library Release Form**

**Name of Author:** Sonya Louise Kujat Choy

**Title of Thesis:** A Redox-Regulated RNA Helicase Gene

**Degree:** Doctor of Philosophy

**Year this Degree Granted:** 2001

Permission is hereby granted to the University of Alberta Library to reproduce single copies of this thesis and to lend or sell such copies for private, scholarly, or scientific research purposes only.

The author reserves all other publication and other rights in association with the copyright in the thesis, and except as hereinbefore provided, neither the thesis nor any substantial portion thereof may be printed or otherwise reproduced in any material form whatever without the author's prior written permission.



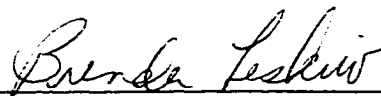
11179-62 Avenue  
Edmonton, Alberta T6H 1N3

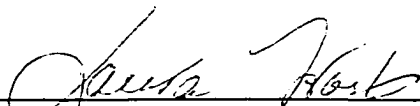
**Date:** December 7, 2000

**University of Alberta**

**Faculty of Graduate Studies and Research**

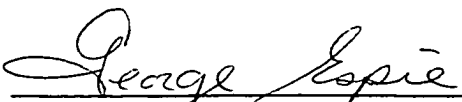
The undersigned certify that they have read, and recommend to the Faculty of Graduate Studies and Research for acceptance, a thesis entitled **A Redox-Regulated RNA Helicase Gene** submitted by **Sonya Louise Kujat Choy** in partial fulfillment of the requirements for the degree of **Doctor of Philosophy in Microbiology and Biotechnology**.

  
for Dr. George W. Owtrim, Supervisor

  
Dr. Laura Frost

  
Dr. Roseline Godbout

  
Dr. Mark Glover

  
Dr. George Espie, External Examiner

Date: November 24, 2000

So we fix our eyes not on what is seen,  
but on what is unseen.  
For what is seen is temporary,  
but what is unseen is eternal.  
(II Cor 4:18, NIV)

Dedicated to my family

## ABSTRACT

The complete genome sequence of *Synechocystis* sp. strain PCC 6803 revealed a 1401 bp open reading frame (slr0083) whose deduced amino acid sequence is characteristic of the DEAD-box family of putative RNA helicases (Kaneko *et al.*, 1995). This gene was subcloned and two mutants were engineered by insertional inactivation and/or deletion of the coding region. The dominant negative phenotype and the inability to generate homozygous mutants suggest this is an essential gene. According to the mRNA expression pattern determined by Northern analysis, conditions favoring net reduction of the plastoquinone pool correlate with the presence of the transcript, therefore this gene has been designated *crhR* for cyanobacterial RNA helicase – Redox. Determination of the *crhR* transcript half-life indicates that mRNA stability effects are also redox-responsive, attributable to changes in photosynthetic electron transport. A putative promoter region was identified by mapping the 5' termini of the *crhR* transcripts. Electrophoretic mobility shift analysis defined a 228 bp region of DNA, which includes 79 bp of coding sequence, that is bound by a soluble factor present in cell-free extracts. This suggests that *crhR* expression may be influenced by the interaction of accessory or transcription factors with *cis*-elements in the promoter region. Furthermore, the CrhR protein was successfully over-expressed as recombinant GST- and HIS-tagged proteins for the production of anti-CrhR antiserum. Western analyses indicate that the CrhR protein is stable in the cells and that the relative abundance of the CrhR protein reflects the observed transcriptional and post-transcriptional redox-regulation of its mRNA. *In vitro* biochemical analyses using affinity-purified HIS:CrhR revealed a non-specific RNA-binding capacity in addition to RNA-dependent ATP hydrolysis and ATP-dependent (5'-3') RNA-unwinding activities. This confirms that CrhR is a true RNA helicase. Potential tertiary interactions were detected between CrhR and two soluble peptides, one of which may be the ribosomal S1 protein, however the nature of the cognate RNA substrate(s) and predicted association in a ribonucleoprotein complex await

further investigation. A hypothetical model is presented in which redox changes at the thylakoid membrane regulate the signal transduction pathways that lead to *crhR* expression. Finally, the potential biological role of this RNA helicase is discussed.

## ACKNOWLEDGEMENTS

Many people have contributed to the progress and development of this thesis and its author, both professionally and personally, and it seems impossible to adequately express my gratitude in these few words.

My supervisor, Dr. George Owtrim, supplied the perfect balance of freedom and guidance in the lab, as well as sending me to various conferences and supporting me financially. Dana Chamot (who taught me the paranoia of RNA work!), Esther Yu, Wendy Magee, Ryan Blush, and Bassam El-Fahmawi have passed along valuable lab skills and, along with a steady stream of summer and project students, made the lab an enjoyable place to work. This research project also benefited from the work of Dana Chamot, Ian Le, Scott Messenger, and Rosa Spencer.

Dr. Bill Page shared his computer, scanner, and hard-drive space, plus protein apparatus and countless chemicals, reagents, and enzymes. These were graciously administered - often in a research "emergency" situation! - by Anne Tindale (Sharpe), whose friendship and encouragement both in and out of the lab has meant a great deal to me.

Within the Biological Sciences Department I have had the privilege of working with many people - profs, grad students, technicians, undergrads - who set an example of personal and professional excellence, perseverance, tenacity and good-humour, and motivated me to strive for these things too. I am grateful for the Graduate Teaching Assistantship Award which gave me valuable experience in undergraduate labs in addition to paying the rent.

My family, often bemused at my intense curiosity for cyanobacteria and microbes in general, encouraged me by showing great enthusiasm for my periodic "discoveries". Angela, especially, suffered with me through successive rites of passage such as the first departmental seminar and the candidacy exam. And then there were those stretches of time where nothing seemed to work in the lab. My parents, Irwin and Louise Kujat, instilled in me the faith and values that have sustained me through the difficulties and made it possible to truly enjoy the successes. I am deeply grateful for the emotional support - I love you.

My new husband, Peter Choy, has shared the happiness and relief of seeing this project to completion and was a constant encouragement when I felt like quitting. It is impossible to express my love and gratitude to you!

Above all, the relationship that I have through Jesus Christ with the God who created cyanobacteria and RNA helicases, has put this thesis research and writing into perspective, constantly reminding me to work for things that will last.

## TABLE OF CONTENTS

	<b>PAGE</b>
<b>CHAPTER ONE. General Introduction</b>	<b>1</b>
1.1 The Significance of RNA and RNA Metabolism	2
1.1.1 The DEAD-box Family of Putative RNA Helicase	2
1.1.2 Characteristic Biochemical Activities of RNA Helicases	3
1.1.3 Crystal Structure Predictions and a Model for RNA Unwinding	7
1.1.4 The Biological Significance of DEAD-box RNA Helicases	11
1.1.5 Generalizations Regarding RNA Helicases	15
1.2 Cyanobacteria: A Model System For The Study of RNA Helicases	16
1.2.1 General Characteristics of Cyanobacteria	16
1.2.2 Bioenergetics	19
1.2.2.1 Cyanobacterial Antenna Complexes: The Phycobilisome	22
1.2.2.2 The Photosystem Complexes (PSI and PSII)	22
1.2.2.3 The Inter-photosystem Electron Carriers and Photosynthetic Electron Transport	24
1.2.2.4 Bioenergetics: Respiration and Respiratory Electron Transport	25
1.2.3 Bioenergetics: Homeostasis	27
1.2.3.1 Long-term Changes in Light-Harvesting Capacity	27
1.2.3.2 Balance of Light-Harvesting by State Transitions	28
1.2.3.3 Photoinhibition Due to Excess Excitation of PSII	29
1.3 The Model Organism for Investigation of RNA Helicases: <i>Synechocystis</i> sp. strain PCC 6803	30
1.4 Summary and Research Objectives	30
<b>CHAPTER TWO. Materials and Methods</b>	<b>32</b>
2.1 Bacterial Strains, Growth Conditions and Media	33
2.2 DNA Procedures	38
2.2.1 Isolation of DNA from Whole Cells	41
2.2.1.1 Chromosomal DNA from Cyanobacteria	41
2.2.1.2 Plasmid DNA from <i>E. coli</i>	42
2.2.2 DNA Manipulation	42
2.2.2.1 Restriction Enzymes, Agarose Gel Electrophoresis, and Isolation of DNA Fragments	42
2.2.2.2 Ligation of DNA Fragments	43
2.2.2.3 Transformation and Electroporation of <i>E. coli</i>	43
2.2.2.4 Transformation of <i>Synechocystis</i> sp. strain PCC 6803	44
2.2.3 DNA Analysis	44
2.2.3.1 Southern Transfer and Hybridization	44
2.2.3.2 Sequencing	45
2.2.4 PCR	46



2.2.5 Site-Directed Mutagenesis	46
2.2.6 Radioactive Labeling of DNA	48
2.2.6.1 End-labeling	48
2.2.6.2 Random Primer Labeling	48
2.3 RNA Procedures	48
2.3.1 RNA Extraction	49
2.3.1.1 Cyanobacterial RNA Extraction	49
2.3.1.2 RNA Extraction from <i>E. coli</i>	49
2.3.2 Northern Analysis	50
2.3.3 Determination Of 5' Transcript Ends and Preliminary Promoter Analysis	51
2.3.3.1 Primer Extension	51
2.3.3.2 S1 Nuclease Protection Assay	52
2.3.3.3 Electrophoretic Mobility Shift Assay (EMSA)	53
2.4 Manipulation of Protein	54
2.4.1 Preparation of Cell-Free Extracts Containing Soluble Protein from <i>Synechocystis</i>	54
2.4.2 Electrophoresis of Proteins	55
2.4.2.1 SDS-Polyacrylamide Gel Electrophoresis (SDS-PAGE)	55
2.4.2.2 Non-denaturing Polyacrylamide Gel Electrophoresis	55
2.4.2.3 Staining Of Polyacrylamide Gels	56
2.4.3 Over-Expression and Purification of Recombinant CrhR Proteins	56
2.4.3.1 pGEX-2T, GST Fusion Protein System (Amersham Pharmacia Biotech)	56
2.4.3.1.1 Cloning	56
2.4.3.1.2 Over-Expression and Purification of GST:CrhR	56
2.4.3.2 pRSETA (Invitrogen)	57
2.4.3.2.1 Cloning	57
2.4.3.2.2 Over-Expression and Purification of HIS:CrhR	58
2.4.4 Generation of Rabbit Polyclonal Anti-CrhR Antiserum	59
2.4.4.1 Large-Scale Preparation and Purification of HIS:CrhR	59
2.4.4.2 Electroelution of Proteins from Polyacrylamide Gel	59
2.4.4.3 Preparation of Anti-CrhR Polyclonal Antiserum	60
2.4.5 Western Analysis	61
2.4.6 FarWestern Analysis	62
2.4.7 Biosynthetic Labeling of Cells	63
2.4.8 Immunoprecipitation	63
2.5 <i>In vitro</i> Biochemical Analyses	64
2.5.1 ATPase Assays	64
2.5.2 RNA Helicase Assays	65
2.6 Computer Analyses and Graphic Images	66

<b>CHAPTER THREE. Genetic Analysis of a Putative RNA Helicase Gene in the Cyanobacterium <i>Synechocystis</i> sp. strain PCC 6803</b>	67
3.1 Introduction	68
3.2 Results	69
3.2.1 Initial Attempts to Isolate a DEAD-box Gene from <i>Synechococcus</i> sp. strain PCC 7942	69
3.2.2 Subcloning of the <i>crhR</i> Open Reading Frame	70
3.2.3 Construction and Analysis of <i>crhR</i> <sup>-</sup> Mutants	77
3.2.3.1 Inactivation of <i>crhR</i> by Insertion of a Selectable Marker into the Coding Region	77
3.2.3.2 Transformation of <i>Synechocystis</i> to Obtain Homozygous <i>crhR</i> Mutants	80
3.2.3.3 Expression of Mutant Constructs in a Heterologous System - <i>E. coli</i>	83
3.2.3.4 Phenotypic Comparison of Wild-type and <i>crhR</i> <sup>-</sup> Mutants Of <i>Synechocystis</i>	84
3.3 Discussion	88
<b>CHAPTER FOUR. Expression of the <i>crhR</i> Transcript: Regulation by Redox</b>	91
4.1 Introduction	92
4.1.1 Redox-Responsive mRNA Expression Patterns	92
4.1.2 Light-Responsive Promoter Elements: <i>cis</i> - and <i>trans</i> -Acting Factors	94
4.1.3 Light-Responsive Differential mRNA Stability	96
4.1.4 Post-Transcriptional Modulation of Gene Expression: A Role for RNA Helicases...	96
4.2 Results	98
4.2.1 Northern Analyses	98
4.2.1.1 Preliminary Screen for Transcript(s) from the <i>crhR</i> Open Reading Frame	98
4.2.1.2 <i>crhR</i> Exhibits a Light-Responsive Pattern of Expression That is Altered in Response to Glucose Metabolism	101
4.2.1.3 Alterations in the Net Redox Status of the Plastoquinone Pool Correlate with Differential Expression of the <i>crhR</i> Transcript	102
4.2.1.4 Actinic Light-Induced Shifts in the Redox Equilibrium of the Plastoquinone Pool Yield a Corresponding Change in <i>crhR</i> Transcript Accumulation	111
4.2.1.5 <i>crhR</i> Transcript Levels Respond to the Intensity of Actinic Light	116
4.2.1.6 Re-examination of the Effects of Various Stresses on <i>crhR</i> Expression	118
4.2.2 The Post-Transcriptional Regulation of <i>crhR</i> is Mediated by Cellular Redox State	119

4.2.3 Mapping of the Putative 5' Transcription Initiation Site of the <i>crhR</i> mRNA, and Sequence Analysis in the Surrounding Region	119
4.2.3.1 Primer Extension to Determine 5' Ends of the <i>crhR</i> Transcript	119
4.2.3.2 S1 Nuclease Mapping of the 5' Ends of the <i>crhR</i> Transcript: The <i>crhR</i> Gene Has Two Redox-Regulated Transcripts	122
4.2.3.3 Identification of Potential <i>cis</i> -Elements Proximal to the Putative Transcript Initiation Site	129
4.2.4 Analysis of the Putative Promoter Region by Electrophoretic Mobility Shift Assays (EMSA)	129
4.2.4.1 Formation of a Complex Between the dsDNA Fragment 45E and a Soluble Effector	130
4.2.4.2. Formation of a Complex Between dsDNA Fragment 45B and a Soluble Effector	134
4.3 Discussion	138
4.3.1 Plastoquinol-Mediated Transcription of <i>crhR</i>	139
4.3.2 Redox Effects on <i>crhR</i> mRNA Stability	143
4.3.3 <i>cis</i> -Elements and <i>trans</i> -Acting Factors in the Expression of <i>crhR</i>	143
<b>CHAPTER FIVE. Investigation of the CrhR Protein: Over-Expression, Purification and Western Analyses</b>	147
5.1 Introduction	148
5.2 Results	149
5.2.1 Construction and Purification of Recombinant CrhR Proteins	150
5.2.1.1 The pGEX-2T System (Pharmacia)	150
5.2.1.2 The pRSETA System (Invitrogen)	156
5.2.2 Analysis of the Polyclonal Anti-CrhR Antiserum	157
5.2.3 Western Analysis of CrhR Expression Patterns	160
5.2.3.1 Evaluation of CrhR Expressed from Recombinant and Mutant Plasmid Constructs	160
5.2.3.2 Western Analysis Detects Proteins in Other Cyanobacteria and in <i>E. coli</i> that Cross-React with Anti-CrhR Antiserum	161
5.2.3.3 Relative CrhR Protein Levels Reflect the mRNA Accumulation Patterns Determined by Northern Analysis	161
5.2.3.4 Alterations in CrhR Protein Levels Reflect the Plastoquinone-Mediated Redox Regulation of the <i>crhR</i> Transcript	164
5.2.3.5 The Effect of Various Stress Treatments on CrhR Protein Levels	165
5.2.4 Interaction of Other Proteins with CrhR	166
5.2.4.1 FarWestern Analysis: Incubation of HIS:CrhR with Nitrocellulose-Immobilized Proteins	166
5.2.4.2 Addition of Anti-CrhR Antibodies Co-precipitates Two Proteins with CrhR	166

5.2.4.3	Two Proteins from <i>Synechocystis</i> Co-elute with HIS:CrhR from an Ni-NTA Agarose Column	169
5.2.4.4	Potential Candidate Proteins for Interaction with CrhR	170
5.3	Discussion	170
5.3.1	Over-Expression and Purification of Recombinant CrhR Proteins	170
5.3.2	Polyclonal Anti-CrhR Antibodies	172
5.3.3	Western Analyses to Elucidate the CrhR Expression Pattern	173
5.3.4	Potential <i>in vivo</i> Tertiary Interactions with CrhR	174
 <b>CHAPTER SIX. Biochemical Analysis of the Recombinant CrhR Protein</b>		
		176
6.1	Introduction	177
6.2	Results	179
6.2.1	ATPase Activity	180
6.2.1.1	HIS:CrhR Exhibits ATPase Activity	180
6.2.1.2	ATP Hydrolysis is RNA-dependent	183
6.2.1.3	Hydrolysis is Specific for Adenine Nucleotides	189
6.2.2	RNA Helicase Activity	190
6.2.2.1	HIS:CrhR Exhibits RNA Unwinding Activity	190
6.2.2.2	Non-specific RNA Stimulates Unwinding of the dsRNA Substrate	190
6.2.2.3	RNA Unwinding is Dependent Upon ATP	193
6.3	Discussion	193
6.3.1	CrhR Exhibits Biochemical Activities Characteristic of an RNA Helicase	193
6.3.2	CrhR and the Current Model for RNA Unwinding by DEAD-box Proteins	195
 <b>CHAPTER SEVEN. A Model for the Regulation and Physiological Role of the RNA Helicase CrhR</b>		
		196
7.1	Introduction	197
7.2	Events Leading to the Expression of <i>crhR</i>	197
7.2.1	Redox-Regulated Gene Expression: The Role of Plastoquinone	197
7.2.2	Signal Transduction Pathways Initiated in Response to Interaction of the Plastoquinone Pool with <i>cyt b<sub>6</sub>f</i> and/or PSII	200
7.2.3	Modulation of Plastoquinone-Mediated Signal Transduction Pathways by Alterations in the Thylakoid Membrane	203
7.2.4	Redox Regulation of Transcript Stability	205
7.2.5	A Potential Transcription Factor in the Putative Signal Transduction Pathway to <i>crhR</i> Expression	206
7.2.6	Interdependence of Transcriptional and Translational Control of <i>crhR</i> : The Protein Expression Pattern	208
7.3	Biological Significance of CrhR	209

7.3.1 CrhR is a True RNA Helicase That is Essential for Viability and Growth of <i>Synechocystis</i>	209
7.3.2 Biological Function of a Redox-Regulated RNA Helicase: Implications for RNA Metabolism	210
7.3.3 CrhR Expression in Response to Cold-Shock and Cold-Acclimation: Similarities to CsdA from <i>E. coli</i>	210
7.3.4 Tertiary Association of CrhR with Other Proteins	211
7.4 Significance	212
<b>CHAPTER EIGHT. References</b>	<b>213</b>
<b>APPENDIX A. Amino Acid Designations</b>	<b>233</b>

## LIST OF TABLES

<b>TABLE</b>	<b>TITLE</b>	<b>Page No.</b>
Table 2.1	Bacterial Strains Used in This Study	34
Table 2.2	Chemical Additions to BG11 Media for Experimental Use with <i>Synechocystis</i> Cultures	35
Table 2.3	Plasmids Used in This Study	39
Table 2.4	Synthetic Oligonucleotides Used in This Study	40
Table 2.5	PCR Programs for the Minicycler	47
Table 3.1	<i>Synechocystis</i> Genes Contained on cs0096 in the Region of Interest for This Study	74
Table 3.2	Expected Sizes of DNA Fragments Obtained by PCR Reactions Containing the Indicated Primers and Templates	82
Table 4.1	Correlation Between the Presence of the <i>crhR</i> Transcript and the Predicted Redox State of the Plastoquinone Pool	110
Table 4.2	The Effect of Alterations in Light Intensity on the Expression of <i>crhR</i>	117
Table 5.1	Candidate Proteins for Interaction with CrhR	171

## LIST OF FIGURES

FIGURE	TITLE	Page No.
Figure 1.1	Characteristic Amino Acid Motifs Of The DEAD-box Protein Family and Comparison with CrhR	4-5
Figure 1.2	Predicted Crystal Structure of the HCV NS3 RNA Helicase	9-10
Figure 1.3	Diagram of the Major Photosynthetic and Respiratory Electron Transport Components in Cyanobacteria	20-21
Figure 2.1	Absorbance Spectra of Filters Used to Alter Actinic Light	36-37
Figure 3.1	The Region of <i>Synechocystis</i> genomic DNA Surrounding the <i>crhR</i> Gene	72-73
Figure 3.2	Detection of the Wild-Type and Mutant Copies of the <i>crhR</i> Gene	75-76
Figure 3.3	Diagram of the <i>crhR</i> Subclone as well as Derived Mutant and Over-Expression Constructs	78-79
Figure 3.4	Phenotypic Analysis of <i>Synechocystis</i> Mutant and Wild-Type Cultures as Measured by Changes in Cell Density and Chlorophyll <i>a</i> Concentration	85-86
Figure 4.1	Detection of the <i>crhR</i> Transcript by Northern Analysis	99-100
Figure 4.2	Overview of Electron Transport in Cyanobacteria and the Site of Action of Electron Transport Inhibitors	103-104
Figure 4.3	Northern Analyses of <i>crhR</i> Following Treatment with Various Electron Transport Poisons	106-107
Figure 4.4	The Quality of Actinic Light Affects the Expression of <i>crhR</i>	112-113
Figure 4.5	Northern Analyses of <i>crhR</i> Following Changes in Actinic Light or Stress Treatments	114-115
Figure 4.6	Determination of <i>crhR</i> Transcript Stability	120-121
Figure 4.7	Determination of the 5' Termini of the <i>crhR</i> Transcript in <i>Synechocystis</i>	123-124
Figure 4.8	The Region of DNA Surrounding the Putative Promoter of <i>crhR</i>	125-126
Figure 4.9	The dsDNA Fragments Used as Target and Competitor DNA for EMSA	127-128
Figure 4.10	Detection of <i>cis</i> -Elements in the Putative Promoter Region of <i>crhR</i>	131-132
Figure 4.11	EMSA Experiments Using Various Cell-Free Extract Preparations	136-137

<b>FIGURE</b>	<b>TITLE</b>	<b>Page No.</b>
Figure 5.1	Amino Acid Sequence Alignment of CrhR with Other DEAD-box Proteins	151-152
Figure 5.2	Over-Expression and Purification of CrhR Fusion Proteins	153-154
Figure 5.3	Generation and Analysis of Anti-CrhR Antiserum	158-159
Figure 5.4	Western Analysis of the CrhR Protein Expression Pattern	162-163
Figure 5.5	Potential Tertiary Associations of CrhR and HIS:CrhR with Soluble Proteins from <i>Synechocystis</i> Cell-Free Extracts	167-168
Figure 6.1	HIS:CrhR Exhibits ATPase Activity	181-182
Figure 6.2	ATP Hydrolysis by HIS:CrhR is RNA-Dependent <i>in vitro</i>	185-186
Figure 6.3	Investigation of the Requirements for <i>in vitro</i> ATP Hydrolysis by HIS:CrhR	187-188
Figure 6.4	RNA Helicase Assays	191-192
Figure 7.1	A Model for the Regulation and Physiological Role of the RNA helicase CrhR	198-199



## LIST OF ABBREVIATIONS

A <sub>x</sub>	absorbance, where "x" is the wavelength in nanometres
aa	amino acid
ADP	adenosine diphosphate
Ap	ampicillin
APS	ammonium persulfate
ATP	adenosine triphosphate
BME	β-mercaptoethanol
bp	base pair
BSA	bovine serum albumin
CBB	Coomassie Brilliant Blue
CDNB	1-chloro-2,4-dinitrobenzene
Cm	chloramphenicol
cpm	counts per minute
cyt b <sub>6</sub> f	cytochrome b <sub>6</sub> f complex
Δ	deletion
DBMIB	2,5-dibromo-3-methyl-6-isopropyl- <i>p</i> -benzoquinone
DCMU	3-(3,4-dichlorophenyl)-1,1-dimethyl urea
DEPC	diethyl-pyrocabonate
DNA	deoxyribonucleic acid
DNase	deoxyribonuclease
dNTP(s)	deoxyribonucleoside triphosphate(s)
dsDNA	double-stranded DNA
dsRNA	double-stranded RNA
DTT	dithiothreitol
e <sup>-</sup>	electron
EDTA	ethylenediaminetetraacetic acid
EMSA	electrophoretic mobility shift assay
EtBr	EtBr
EtOH	ethanol
Fd	ferredoxin
x g	x gravity
glc	glucose
GST	glutathione S-transferase
GTP	guanosine triphosphate
h	hour(s)
IMAC	immobilized metal affinity chromatography
imidazole	1,3-diaza-2,4-cyclopentadiene
IPTG	isopropyl (β)-D-thiogalactopyranoside
kb	kilobase(pair)
KCN	potassium cyanide
kDa	kiloDaltons
Km	kanamycin

LB	Luria Bertani
LHC	light-harvesting complex
M	molar
min	minute(s)
mL	millilitre ( $10^{-3}$ L)
MOPS	3-(N-Morpholino)-propane-sulphonic acid
mRNA	messenger RNA
Mv	methyl viologen (paraquat)
mV	millivolt(s)
NAD(H)	nicotinamide adenine dinucleotide
NADP(H)	nicotinamide adenine dinucleotide phosphate
nt	nucleotide(s)
NTP(s)	nucleoside triphosphate(s)
OD <sub>a</sub>	optical density, where “a” is the wavelength in nanometres
3-OMG	3- <i>O</i> -methyl-D-glucopyranose
ORF	open reading frame
PBP	phycobiliprotein
PBS	phycobilisome
PC	plastocyanin
PCC	Pasteur Culture Collection
pfu	plaque-forming units
PNK	polynucleotide kinase
poly [d(I-C)]	poly-deoxy-inosinic-deoxy-cytidylic acid
PSI and PSII	photosystem I and II
PQ	plastoquinone
PQH <sub>2</sub>	plastoquinol
RBS	ribosome binding site
RNA	ribonucleic acid
RNase	ribonuclease
RNP	ribonucleoprotein
rNTP(s)	ribonucleoside triphosphate(s)
rRNA	ribosomal RNA
rpm	revolutions per minute
r.t.	room temperature (22°C)
sarkosyl	<i>N</i> -lauroyl-sarcosine
SDS	sodium dodecyl sulfate
SDS-PAGE	SDS-polyacrylamide gel electrophoresis
s	second(s)
Sm	streptomycin
Sp	spectinomycin
sp.	species
Tc	tetracycline
Tris	Tris (hydroxymethyl) aminomethane
tRNA	transfer RNA
TSB	Trypticase Soy Broth

U	unit(s)
μL	microlitre (10 <sup>-3</sup> mL)
UTCC	University of Toronto Culture Collection
UTR	untranslated region
UV	ultraviolet
V	volt(s)
v/v	volume/volume
vol	volume(s)
W	Watt(s)
w/v	weight/volume
X-gal	5-bromo-4-chloro-3-indolyl-β-D-galactopyranoside

## **CHAPTER ONE**

### **General Introduction**

## **1.1 The Significance of RNA and RNA Metabolism**

Ribonucleic acid (RNA) is a ubiquitous and critical intermediary in cell physiology. All aspects of cell growth and division are dependent upon RNA at some level, related to its informational, structural, or enzymatic functions (de la Cruz *et al*, 1999). As messenger RNA, it determines the protein complement that can be synthesized by the cell. As ribosomal and transfer RNA, it participates in the mechanism and process of translation. As ribozyme, it catalyzes tRNA processing and mRNA splicing. While each dividing cell passes to its progeny an identical complement of DNA, the daughter cells may differ significantly from each other and from the progenitor in capacity and form. These phenotypic differences, residing in the production of various enzymes, structural, or signaling proteins, can ultimately be attributed to the RNA that is intrinsic to the utilization of the genetic information (DNA). Consequently, the regulation of any particular cellular process may be affected by altering the metabolism of RNA, whether synthesis, processing, stability, availability, or degradation.

RNA is synthesized by the cell as a single-stranded polymer of ribonucleosides that possesses the intrinsic potential for inter- and intra-molecular base-pairing, analogous to the hydrogen bonding in duplex DNA. RNA is thus predisposed to the spontaneous formation of extensive and diverse secondary structures, since regions of duplex RNA are more thermodynamically stable than the single-stranded molecule. However, the resultant base-paired conformation may render the RNA "inactive" by occluding protein binding sites or precluding interaction with other RNAs, and thereby preventing active participation in cellular metabolism. Moreover, modulating these secondary structures in order to alter the chemical and/or functional stability or availability of the RNA species is an energy-dependent process. The inherent kinetic and thermodynamic barriers are overcome by a class of proteins known as RNA chaperones that form tertiary interactions with RNA, mediated by RNA recognition and binding motifs in the protein amino acid sequence (Herschlag, 1995). RNA chaperones stabilize single-stranded regions, ensure correct folding, maintain and modify secondary or tertiary RNA structures, in short they impart the appropriate conformation for subsequent RNA and/or protein interactions that occur as the RNA performs its intended physiological role (de la Cruz *et al*, 1999; Herschlag, 1995).

### **1.1.1 The DEAD-box Family of Putative RNA Helicases**

During the late 1980s, a class of RNA chaperones known as the "DEAD-box" family was initially identified on the basis of amino acid sequence analysis by Patrick Linder and colleagues (1989). Comparison of eight cellular proteins revealed a characteristic pattern of amino acid motifs, including the tandem residues aspartic acid-

glutamic acid-alanine-aspartic acid (D-E-A-D in the single letter amino acid code), whose sequence and spacing are highly conserved. Similarly, and during the same time period, the systematic analysis of protein sequences containing the purine nucleotide-binding motif led to a classification of three superfamilies of nucleoside triphosphate phosphatases that are involved in RNA and DNA metabolism. While these proteins originate from eukaryotic, prokaryotic, and viral organisms and are grouped solely on the basis of amino acid sequence homology, biochemically they are all DNA- and/or RNA-dependent NTPases possessing helicase activity. Most RNA helicases are assigned to superfamily 2, which is further classified into the DEAD-box, DEAH-box and DExH-box families that have similar but distinct complements of conserved motifs (Gorbalenya *et al.*, 1989; Gorbalenya and Koonin, 1993; Hodgman 1988).

The DEAD-box family of RNA helicases is defined by nine characteristic amino acid motifs with intervening regions that contain a conserved number, but variable sequences, of amino acids (Fig. 1.1). This core region of homology is approximately 294-359 residues, and is flanked by carboxyl- and amino-terminal extensions specific in sequence and length for individual DEAD-box proteins. The presence of these conserved elements in the linear amino acid sequence forms the basis for assigning new members into the DEAD-box family; as well, these signature sequences can be used for the detection and prediction of new helicases in the burgeoning genome databases (Aubourg *et al.*, 1999). The prototype DEAD-box protein is the eukaryotic translation initiation factor eIF4A, represented by the core region of motifs and possessing the typical biochemical activities of an RNA helicase. By extension, DEAD-box proteins that are identified solely on the basis of amino acid sequence homology are considered to be putative RNA helicases (Pause and Sonenberg, 1993; Schmid and Linder, 1992) (for a review, see Fuller-Pace, 1994).

### **1.1.2 Characteristic Biochemical Activities of RNA Helicases**

RNA helicases are characterized by RNA-dependent ATP binding and hydrolysis as well as ATP-dependent RNA unwinding or RNA helix-destabilizing activities. As enzymes they catalyze strand separation of double-stranded RNA to yield single-stranded RNA, typically coupled with the hydrolysis of (preferentially) ATP. It is generally assumed that the energy derived from ATP hydrolysis drives the RNA unwinding reaction. Certain DEAD-box proteins have been shown to exhibit only RNA destabilizing activity, in which the removal of secondary structures does not require ATP hydrolysis, although it is generally still stimulated by ATP binding; this may be artifactual to the *in vitro* assay conditions. In turn, the ATPase activity may wholly depend on, or be stimulated to higher levels by, interaction with RNA. In keeping with the nature of RNA secondary structures

**Figure 1.1 Characteristic Amino Acid Motifs of the DEAD-box Protein Family and Comparison with CrhR**

Boxed letters indicate the DEAD-box protein consensus motifs written using the single-letter amino acid code (see Appendix A). Numbers indicate the amino acids in the variable intervening sequences between the motifs. Roman numerals indicate the commonly used designation for each motif. Assigned functions (as per Fuller Pace, 1994; Pause and Sonenberg, 1993; Schmid and Linder, 1992) are indicated in the top line. The deduced amino acid sequence of CrhR contains all the consensus motifs, with a single A to S residue alteration indicated by brackets.

**Proposed functions**

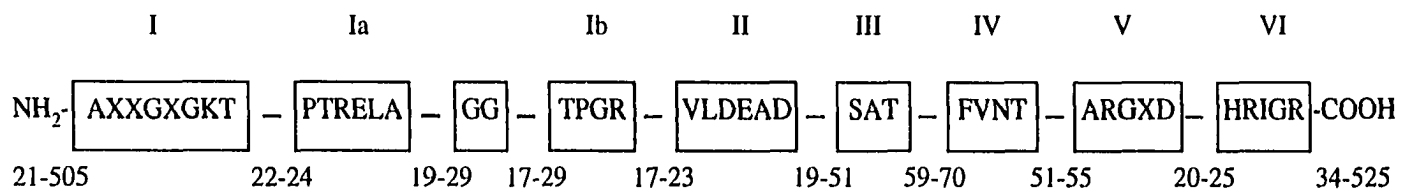
ATP binding

Coupling of  
RNA unwinding  
and ATPase

RNA unwinding

ATP hydrolysis,  
RNA binding

**Consensus  
DEAD-box  
amino acid  
sequence**



**Deduced amino  
acid sequence of  
CrhR**

50    (S)                      23                      22                      19                      18                      27                      62                      51                      20                      157



it is likely that RNA helicases act processively along short duplex regions only (Cho *et al*, 1998; de la Cruz *et al*, 1999).

In the pursuit of the mechanism of RNA unwinding, and prior to the availability of a complete tertiary structure model, researchers settled on the correlation between the conserved motifs in the primary amino acid sequence and the common *in vitro* biochemical activities of RNA helicases. Given the modular organization of DEAD-box proteins, the conserved amino acid motifs were intuitively predicted to serve as functional sites for substrate binding and catalysis within a structural framework provided by the intervening spacer sequences (Hodgman, 1988). The variable sequences at the termini are more likely to confer substrate specificity, perhaps through additional RNA binding determinants, or to influence the biological function, for example via protein-protein interactions that could influence subcellular localization (Aubourg *et al*, 1999). These predictions were investigated at the molecular level by mutational analyses of RNA helicases including murine, human, and yeast eIF4A homologues as well as Vasa from *Drosophila* (Fuller-Pace, 1994; Liang *et al*, 1994; Pause *et al*, 1993; Pause and Sonenberg, 1992, 1993; Schmid and Linder, 1992). Site-directed mutations were assessed for their biochemical effect in standard *in vitro* assays, or for the biological effect by observing the *in vivo* phenotype compared to wild-type systems.

These studies provided functional analyses of the motifs (as indicated in Fig. 1.1). The two motifs GKT and DEAD are considered to be key for ATP binding and hydrolysis since these sequences are characteristic of the catalytic sites of many enzymes that use nucleoside triphosphates (Gorbalenya *et al*, 1988). GxxGxGKT, also known as Walker Box A and found almost exclusively in ATP and GTP binding proteins, is typically AxxGxGKT in DEAD-box proteins and may be responsible for the initial ATP binding step (Linder *et al*, 1989; Rozen *et al*, 1989; Schmid and Linder, 1992). The preliminary crystal structure of an isolated NTP-binding domain indicated that GKT forms a loop that contacts the alpha phosphate of the NTP, while the gamma and beta phosphates are bound by an aspartate via a magnesium ion. This is likely the highly conserved aspartate in VLDEAD, because it is suitably located within the three-dimensional structure of the protein and strictly conserved (Hodgman, 1988). VLDEAD is a special version of the Walker Box B of NTP-binding proteins, where the DE is characteristic of DNA and RNA replication proteins (Linder *et al*, 1989). This motif is important for the ATPase activity and has been implicated in coupling ATP hydrolysis to RNA unwinding (Pause and Sonenberg, 1992). The integrity of the SAT motif was shown to be essential for RNA unwinding in eIF4A, since mutations in these amino acids affected the helicase activity but not the ability of the protein to hydrolyse ATP (Pause and Sonenberg, 1992). The region of the HRIGR motif

was similarly proposed to be involved in the ATP-dependent RNA binding and unwinding activity of eIF4A (Pause *et al*, 1993). In the *Drosophila* helicase Vasa, mutations in HRIGR abrogated helicase activity; ARGxD (particularly the G residue) was also shown to be essential for RNA unwinding (Liang *et al*, 1994). The potential importance of the GG motif is suggested by the cold-sensitive mRNA splicing phenotype obtained in the yeast RNA helicase PRP28, following a G to E amino acid alteration (Strauss and Guthrie, 1991).

The Vasa experiments further revealed the significance of the non-conserved sequences within the core region. Many of the Vasa mutants obtained by EMS treatment contained amino acid residue changes that fell outside one of the nine conserved motifs, yet still exhibited altered RNA helicase and ATP hydrolysis activity. Significantly, one class of these mutants was unaffected in helicase activity but failed to localize properly within the cells (Liang *et al*, 1994). A key conclusion from these mutational analyses is that the conserved motifs are not the only residues that affect biochemical function. Rather, it is likely that amino acid changes in the conserved residues exert their effect by altering local secondary structure and possibly the structure of the entire protein. The non-conserved intervening and terminal sequences contribute to the function as well as the structure of the RNA helicases, and may specify protein-protein or protein-RNA interactions.

Based on these functional assignments to the regions of conserved motifs, Pause and co-workers (1993) proposed a sequence of events in the biochemical functioning of eIF4A that may be extended to DEAD-box proteins in general. They postulated that initially ATP is bound by the RNA helicase via the GKT and VLDEAD motifs. This causes a conformational change in the protein that enables the HRIGR motif to bind RNA. The initial binding of RNA induces hydrolysis of the ATP, which further increases the stability of the interaction with RNA and energizes the RNA unwinding reaction. Once the reaction of dsRNA to ssRNA has been catalyzed, the RNA is released. This model satisfies the experimental observations of both productive and non-productive interactions with RNA, differentiated by the hydrolysis of ATP. It is also compatible with certain observations of competition between ATP hydrolysis and RNA binding, since the hydrolysis of ATP would result in the release of the bound RNA. The predictive value of this model is limited by the linear analysis of the conserved motifs and the speculative interactions of an RNA helicase with the RNA and ATP substrates.

### **1.1.3 Crystal Structure Predictions and a Model for RNA Unwinding**

The ternary structure of the hepatitis C virus (HCV) NS3 RNA helicase domain in the presence and absence of ssDNA has recently been solved by crystallography (Kim *et al*,

1998; Cho *et al.*, 1998; Yao *et al.*, 1997). As a viral RNA helicase NS3 belongs to the DExH family, which has an arrangement of conserved motifs similar to the DEAD-box proteins, although there are differences in the specific amino acid residues. Comparable crystal structure data for eIF4A from *Saccharomyces cerevisiae* confirms that despite sequence differences, a fold is conserved in the three-dimensional prediction for the ATPase domain (Benz *et al.*, 1999; Johnson and McKay, 1999). Therefore, the tertiary structure of NS3 provides a three-dimensional model for the common biochemical activities of RNA unwinding and ATP hydrolysis. Furthermore, it forms a structural context for the results obtained by the previous mutational analyses of DEAD-box RNA helicases.

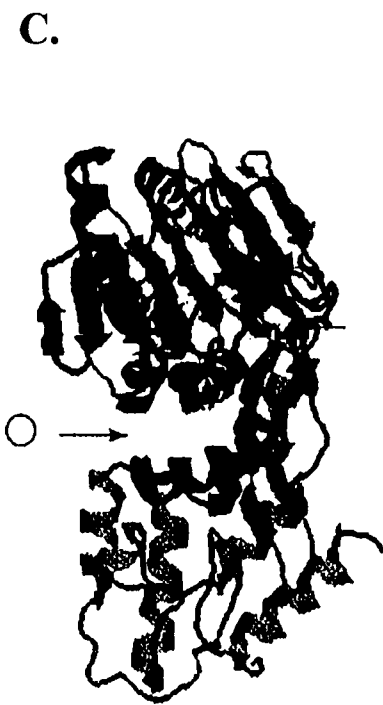
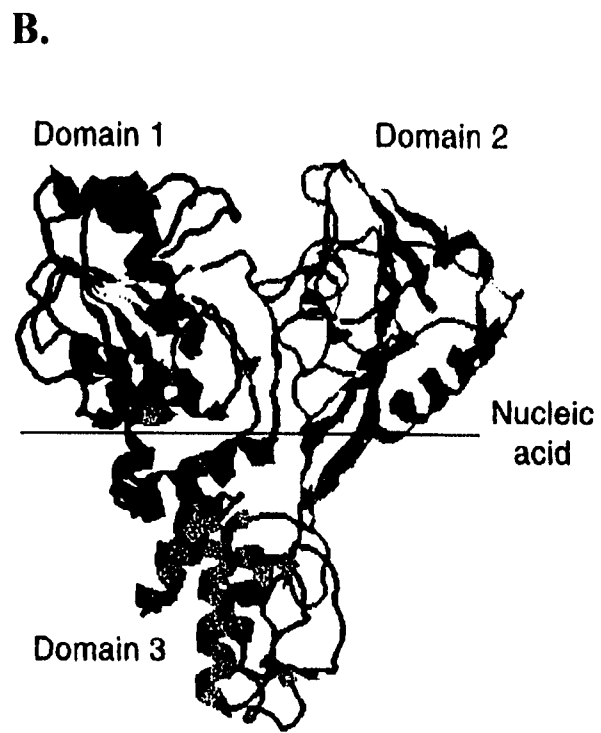
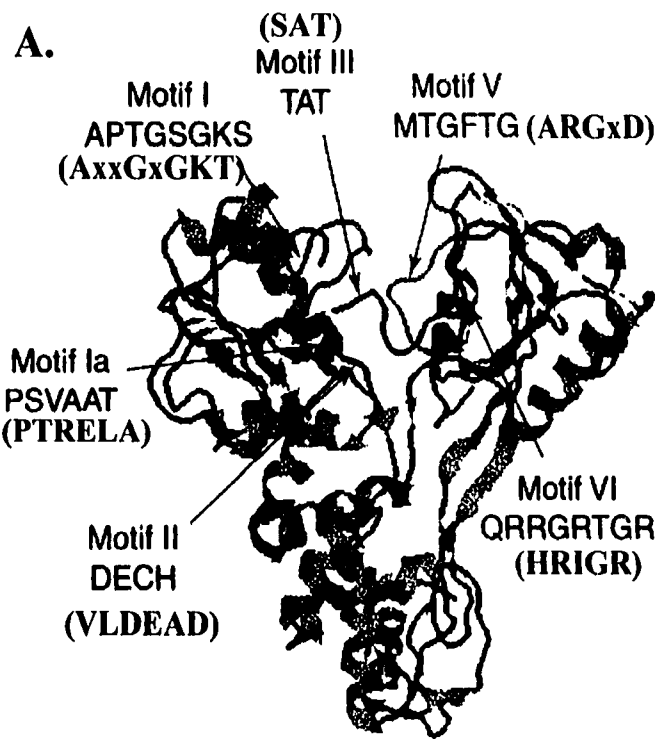
The crystal structure of HCV NS3 was determined to be a Y-shaped molecule with three domains, each formed from approximately one-third of the linear amino acid sequence (Fig. 1.2). The amino-terminus forms domain 1, and contains the GKT and DExH motifs for NTP-binding and hydrolysis. The active site cavity for NTP hydrolysis is located at the periphery of domain 1 and is partially lined by the GKT and DExH motifs that lie in close proximity to each other. Domain 3 forms from the carboxy-terminal one-third of the sequence that lacks helicase consensus motifs. The central amino acids form domain 2, and this region contains the apparent RNA recognition and binding motifs, including the equivalent of HRIGR. The first and second domains are connected by a flexible hinge region that contains the TAT (viral equivalent to SAT) motif, which would appear to enable the bending or pivoting of domain 2 relative to domains 1 and 3, such that an interdomain cleft is formed between them (Kim *et al.*, 1998; Yao *et al.*, 1997). A significant feature of the predicted tertiary structure of NS3 is the close association of the conserved helicase motifs. Rather than acting as individual domains with interdependent functions (a tacit inference in some of the previous mutational analyses), the motifs all lie along the same predicted face of the protein, and probably form a single functional domain across the interdomain cleft.

The interaction of NTPs with the GKT and DEAD motifs had been previously determined by crystallographic analysis of the NTP binding domain alone (Hodgman, 1988). The RNA-binding conformation, and its relationship to the NTP-binding residues was inferred from the crystal structure of NS3 interacting with ssDNA. Accordingly, the interdomain cleft is purported to be the site of interaction with a single strand of RNA, since it is too narrow to encompass dsRNA. Expanding upon the model of Pause and co-workers (1993), de la Cruz and colleagues (1999) have proposed a sequence of events for the interactions of the helicase with its substrates: Following an initial interaction with RNA, the binding of ATP to domain 1 causes conformational changes in domain 2. This strengthens the interactions with ssRNA within the cleft by positioning the arginine

**Figure 1.2 Predicted Crystal Structure of the HCV NS3 RNA helicase**

The sequence of the conserved motifs in NS3 (a Dexh-box helicase) are shown with the corresponding DEAD-box motifs indicated in brackets **(A)**. The domain structure and the cleft for interaction of NS3 with RNA are evident in the front **(B)** and side **(C)** views. For details see section 1.1.3.

Adapted from de la Cruz *et al*, 1999 (Figure 3).



residues of the HRIGR motif such that they interact with the strand of RNA via the phosphates of the ATP - essentially "closing" the interdomain cleft onto the RNA. Since the NS3 helicase does not exhibit sequence specificity in binding to RNA, the interaction of the helicase residues within the interdomain cleft is likely with the phosphate backbone of the RNA, and not the nucleoside bases (Kim *et al*, 1998). Subsequent hydrolysis of the bound ATP might open this cleft and cause the helicase to translocate several bases along the ssRNA.

Further to this molecular description of RNA helicase interactions with ATP and RNA, a broader model has been proposed to explain the processive unwinding of dsRNA. de la Cruz and colleagues (1999) have summarized a "descending molecular see-saw" model where the functional form of the RNA helicase is actually a dimer of two molecules of NS3. The ssRNA interacts successively with the interdomain cleft of first one, then the other, helicase monomer. Each interaction causes a conformational change in the helicase that rotates the dimer along an axis to bring the second interdomain cleft into closer contact with the ssRNA. In this way the dimer "walks" along one strand of the RNA by passing it through the interdomain channel while the other strand is forced to the outside of the dimer, thereby disrupting the pairing between the RNA strands. Accordingly, the translocation of the helicase is the active step, driven by ATP hydrolysis, whereas the RNA unwinding is a passive consequence of this movement (Kim *et al*, 1998). These (and other) models may be generally useful for predicting the mechanics of RNA unwinding by other RNA helicases, based on the assumption that similar secondary and tertiary structures are retained regardless of sequence variability outside of the common motifs.

#### **1.1.4 The Biological Significance of DEAD-box RNA Helicases**

The information derived from crystal structure and mutational analyses provides a link between the primary sequence of DEAD-box proteins, the *in vitro* biochemical activities, and the predicted tertiary interactions with the RNA and ATP substrates. Significantly, these unifying characteristics enable comparison of RNA helicases across the entire range of organisms from viruses to humans, mice, yeast, bacteria, plants, worms and fruit flies. Within these biological contexts, however, the scope of physiological functions provided by helicases is as broad and as varied as the cellular involvements of the RNA substrates they exist to modulate. Certain DEAD-box RNA helicases act post-transcriptionally during mRNA splicing, such as yeast Prp5p and Prp28p, although this is more common for DEAH-box RNA helicases (de la Cruz *et al*, 1999). Other helicases act at various points in translation. For example, eIF4A is essential for the initiation of translation, altering the secondary structure of mRNA to facilitate the binding of the

ribosome. Ded1p from yeast is also implicated in translation initiation, is distinct from the Tif homologues of eIF4A, and can be functionally replaced by the murine PL10 RNA helicase (Chuang *et al*, 1997). DEAD-box proteins may play a role in ribosome biogenesis, such as the yeast Dbp7p (Daugeron and Linder, 1998), Spb4p (de la Cruz *et al*, 1998a), and Dbp10p (Burger *et al*, 2000) proteins that are involved in pre-rRNA processing steps essential for assembly of the 60S subunit. The helicase Dob1p from *Saccharomyces cerevisiae* has been proposed to act as a cofactor for 3'-5' activity of the exosome, removing rRNA secondary structures that inhibit formation of the 3' end of the 5.8S rRNA (de la Cruz *et al*, 1998a, 1998b). RNA helicases such as RhIB aid RNA turnover by removing secondary structures that mask the recognition sites for, or inhibit the processivity of, ribonucleases in *E. coli* (Miczak *et al*, 1996; Py *et al*, 1996). Similarly, the mRNA stabilization that occurs when DeaD is over-expressed suggests that RNA helicases are capable of binding RNA in regions unprotected by ribosomes and preventing ribonucleolytic attack (Iost and Dreyfus, 1994).

The less typical reports of DEAD-box protein involvement include expression on the surface of bacterial and T-cells, where they are implicated in autoaggregation, such as AggH from *Lactobacillus*, or DNA uptake, such as with competent *Bacillus* cells (Roos *et al*, 1999, and references therein). RNA helicase A has been implicated in protein-protein interactions, mediating the association of co-activators to RNA polymerase II and thus exerting an effect on the transcription of various genes (Nakajima, *et al*, 1997). The HEL protein of *Drosophila* suppresses a white variegation phenotype and was proposed to associate with chromosomes to promote transcription during embryogenesis, possibly further affecting mitosis (Eberl *et al*, 1997). Temperature-sensitive mutations indicated that the RNA helicase Dbp5p (*S. cerevisiae*) is essential for the export of poly(A)+ RNA from the nucleus to the cytoplasm (Tseng *et al*, 1998). In contrast with the large number of nuclear helicases, this DEAD-box protein localizes to the cytoplasm and appears to associate with nuclear pore complexes; thus it is proposed to play a direct role in the nucleocytoplasmic movement of mRNA, possibly coupled to translation (Snay-Hodge *et al*, 1998). Of interest for this thesis the MgpS protein from *Rhodobacter sphaerooides*, which includes an N-terminal region of homology to RNA helicases, is able to act as an activator for transcription of the photosynthetic *puc* and *puf* gene regulons (Sabaty and Kaplan, 1996).

The direct effects of modulating an RNA substrate may have far-reaching implications for growth and differentiation. For example, the RNA helicase DDX1 plays a role in the development of human retinoblastoma (Godbout and Squire, 1993). The specific expression of the murine PL10 helicase is important for the developmental process

of spermatogenesis (Leroy *et al*, 1989). Both the localization and the RNA helicase activity of Vasa are required for proper formation of the pole cells during oogenesis in *Drosophila* (Lasko and Ashburner, 1988; Liang *et al*, 1994). For Vasa and its homologues in other organisms such as zebrafish (Knaut *et al*, 2000), the specific expression of mRNA and protein determines the fate of the germline cells. The biological functions of specific RNA helicases are illustrated by the following more detailed descriptions of the prototype eIF4A/eIF4B and five helicases from *E. coli*.

**The eukaryotic translation initiation factors eIF4A and eIF4B.** As the prototype DEAD-box protein, representative of the core region of homology in this family of proteins, significant research attention has focussed on eIF4A (Browning, 1996). While eIF4A exhibits the characteristic RNA-dependent ATPase and ATP-dependent RNA unwinding activities as an autonomous protein (Rogers *et al*, 1999), it functions more efficiently as part of the eIF4F complex, stimulated in both cases by interactions with eIF4B (Grifo *et al*, 1984; Rozen *et al*, 1990). eIF4B, which is an RNA-binding protein possessing ribosome-dependent ATPase activity, is similar to the carboxy-terminal extensions of other RNA helicases (Methot *et al*, 1994; Naranda *et al*, 1994). eIF4B may also increase the affinity of eIF4A for ATP (Bi *et al*, 2000). Mutants of eIF4A have confirmed that the RNA helicase activity is required for translation of all cellular mRNAs (Pause and Sonenberg, 1992; Schmidt and Linder, 1991). Disruption of eIF4B suggested that it is similarly required for translation of all mRNAs, especially at temperatures below 25°C when secondary structure in the 5' non-coding regions of mRNA is more stable. In all biological systems, eIF4A and eIF4B homologues cooperate with other components of the eIF4F complex to melt the secondary structure in the 5' untranslated region and facilitate ribosome attachment - specifically the 40S subunit - to the mRNA during translation initiation (Fuller-Pace, 1994; Gingras *et al*, 1999). This is considered to be the rate-limiting step in translation, therefore providing a key point for control of gene expression (Jaramillo *et al*, 1991). Subsequent to RNA unwinding, it has been postulated that eIF4A and/or eIF4B could also act as RNA chaperones, coating the newly formed ssRNA strand to prevent re-annealing (Jaramillo *et al*, 1991).

**Prokaryotic RNA helicases - examples from *E. coli*.** At least five DEAD-box proteins have been identified in *E. coli*. Of these putative RNA helicases, RhIE has not been characterized according to biochemical or biological function beyond identification of the *rhIE* gene by PCR and the lack of a discernible phenotype in the null mutant (Kalman *et al*, 1991, Ohmori, 1993). The *srmB* gene was isolated as a multi-copy suppressor of a



mutation in the ribosomal protein L24 (Nishi *et al*, 1988). The over-expression of SrmB is able to fulfill the usual binding and destabilization of 23S rRNA secondary structure that is performed by wild-type L24 during 50S ribosomal subunit assembly (Nishi *et al*, 1988). By extension, SrmB has been implicated in ribosome biogenesis, however its normal function when present at physiological levels in wild-type cells is not known. In comparison to SrmB and RhlE, more intensive research has provided information on the remaining three *E.coli* DEAD-box proteins, DbpA, RhlB and CsdA.

Significantly, biochemical characterization of DbpA yielded the first description of aspecific RNA substrate requirement for productive interactions with a DEAD-box RNA helicase (Fuller-Pace *et al*, 1993). Column-purified preparations of DbpA exhibit *in vitro* ATP hydrolysis activity that is stimulated by bacterial 23S rRNA, in particular a 93 nt region that is part of the peptidyltransferase center and that includes several of the bases that interact with the 3' terminal adenosines of both A- and P-site tRNAs (Nicol and Fuller-Pace, 1995). Subsequently, other researchers have demonstrated that ATP hydrolysis is also stimulated by other regions of the 23S rRNA, regions that all have significant secondary structure and that are closely associated within the 3-dimensional structure of the functional core of the 50S ribosomal subunit (Bodeker *et al*, 1997). These results suggest that DbpA plays a role in translation, perhaps by directly facilitating the binding of tRNAs in the peptidyltransferase reaction. Alternatively, DbpA may aid in the assembly of the functional center of the 50S ribosomal subunit by modulating the secondary structure of the 23S rRNA. In this case, the destabilization of base-paired regions by DbpA would lower the energy of activation for binding by the appropriate ribosomal proteins that maintain the structure of the peptidyltransferase center. More recently it has been proposed that DbpA may actually play a direct role in translation, rather than indirectly through ribosome biogenesis (Tsu and Uhlenbeck, 1998). The *in vitro* demonstration of ATP hydrolysis and RNA helix-destabilizing activity of DbpA indicates that the biochemical activity of certain DEAD-box proteins may exhibit a striking specificity of RNA substrate, independent of interaction with other proteins.

Western analyses localized RhlB to the degradosome, a multi-protein complex that mediates RNA turnover and that comprises enolase, polynucleotide phosphorylase and RNase E (Py *et al*, 1996; Miczak *et al*, 1996). Within this complex, the proposed RNA unwinding function of RhlB was shown to aid in the degradation of structured RNA by polynucleotide phosphorylase, presumably removing secondary structure that inhibits the processivity of this 3'-5' exoribonuclease (Py *et al*, 1996). Similarly, the unwinding of dsRNA to ssRNA by RhlB may facilitate RNA degradation by RNase E, since this endoribonuclease cleaves short stretches of ssRNA and is inhibited by stem-loops (Miczak

*et al.*, 1996). RhlB does not exhibit ATP hydrolysis apart from the degradosome, therefore protein-protein interactions are essential for its function. *In vitro* reconstitution of functional degradosomes revealed that RNase E forms a scaffold for PNPase and RhlB, but its activity is not required for the ssRNA-dependent stimulation of RhlB activity (Coburn *et al.*, 1999). Miczak and colleagues (1996) have further suggested that altering the stoichiometry of the RNA helicase within the degradosome alters the RNase activity of the entire complex. Related to this, the over-expression of certain DEAD box proteins gives an mRNA protection phenotype, attributed to binding and protection at RNase E cleavage sites (Iost and Dreyfus, 1994).

DeaD (Toone *et al.*, 1991) has been renamed CsdA (cold-shock DEAD-box protein A) following demonstration that cold shock treatment significantly induces its expression as well as its association with ribosomes (Jones *et al.*, 1996). Since the stability of secondary structures in mRNA is higher at low temperatures, CsdA is thought to act as an auxiliary ribosomal protein that increases translational efficiency following a temperature shift down. It has been proposed that the RNA-unwinding function of CsdA is aided by the subsequent ssRNA-binding activity of the RNA chaperone CspA, which is the major cold shock protein in *E. coli* (Jones *et al.*, 1996). CsdA may also regulate CspA expression during cold shock, since the over-expression of CsdA has a stabilizing effect on the *cspA* transcript (Brandi *et al.*, 1999). During the cold acclimation period that follows cold shock, CsdA is required for expression of  $\sigma^{32}$  by destabilizing the secondary structure in its mRNA; this sigma factor is responsible for the subsequent derepression of the heat shock proteins (Jones *et al.*, 1996). CsdA is therefore essential for both the initial cold shock adjustment, aided by as well as regulating CspA, and the continued survival at low temperatures via its regulation of  $\sigma^{32}$ .

### **1.1.5 Generalizations Regarding RNA Helicases**

While an exhaustive review of RNA helicases is beyond the scope of the present study, the preceding examples illustrate a number of generalizations that may be drawn regarding the biochemistry and biology of DEAD-box proteins. Given the universality of modulating RNA secondary structure it is not surprising that DEAD-box RNA helicases have been identified in all organisms investigated to date (Fuller-Pace, 1994). Many of the DEAD-box RNA helicases are required for cell viability, which implies that they perform essential functions in the cell and belies the importance of RNA metabolism. Furthermore, irrespective of genome size, both eukaryotes and prokaryotes may possess multiple, functionally non-redundant helicases, which argues for a degree of specificity toward their substrate RNAs. Often the variable sequences in the amino- and carboxy-terminal

extensions are considered to be one source of these observed distinct biological functions, related to interactions with the target RNA(s). The sequence variability, both within the core region as well as in the extensions, is also related to the interaction of DEAD-box proteins with other proteins. These protein-protein interactions may directly determine the specificity of RNA substrate and biochemical activities, or may impact these as a consequence of specifying the biological context for the RNA helicase. In fact, the observation that many RNA helicases associate with macromolecular complexes such as the degradosome, spliceosome, or ribosome is a reflection of their intermediary role within the larger scheme of RNA metabolism. The purpose of modulating RNA secondary structure by the actions of an RNA helicase is more than simply to create single-stranded RNA. By catalyzing the removal of secondary structures, RNA helicases render the RNA substrate available for participation in various physiological processes specific to its biological function. It may be said that the study of RNA helicases is a window into the world of RNA.

## **1.2 Cyanobacteria: A Model System For The Study of RNA Helicases**

### **1.2.1 General Characteristics of Cyanobacteria**

The Cyanobacteria are eubacterial photoautotrophs characterized by chlorophyll *a*-based oxygenic photosynthesis, electron flow through two distinct photosystems, and the use of phycobilisomes as the light-harvesting antennae. They are presently and historically attractive for the study of phototrophic metabolism by virtue of a photosynthetic system that is functionally and structurally analogous to that of higher plant chloroplasts, with a prokaryotic genetic organization that is highly amenable to molecular investigation. The Cyanobacteria are also interesting for study in their own right, forming the largest, most widely distributed group of photosynthetic prokaryotes, surviving and colonizing terrestrial, marine, and fresh water habitats (Madigan *et al*, 1997; Stanier and Cohen-Bazire, 1977) and even living as symbionts of water ferns, cycads, or angiosperms (Wilmotte, 1994).

United as they are by photoautotrophic metabolism and prokaryotic cell structure, the cyanobacteria exhibit a remarkable heterogeneity at both the morphological and physiological levels. According to botanical taxonomy, the Cyanobacteria have been divided into five morphological groups or Sections, reflecting their historical classification as blue-green algae under the jurisdiction of plant physiologists (Stanier and Cohen-Bazire, 1977; Madigan *et al*, 1997). Section I (Chroococcacean) comprises genera which are unicellular and divide by binary fission, such as *Synechocystis* and *Synechococcus*. Genera in Section II (Pleurocapsalean) are also unicellular, but cell division occurs by budding for

the formation of cell aggregates, and reproduction occurs via production of baeocytes. Section III genera are classified as Oscillatorian, the cells have a filamentous morphology and divide by binary fission in a single plane. Section IV cyanobacteria, or the Nostocalean genera, are filamentous and include species that produce heterocysts, such as *Anabaena* and *Calothrix*. The final group, Section V genera, form filamentous cells which divide to form branched filaments.

The diversity among cyanobacteria becomes further apparent in a brief consideration of their morphogenesis and cellular differentiation. Cyanobacterial cell "development" refers to the complete conversion of vegetative cells into one of four distinct types of specialized cells: Heterocysts are differentiated for nitrogen fixation, akinetes are resting cells equivalent to spores, hormogonia are trichomes or whole filaments possessing motility for dispersion, and baeocytes are minute reproductive cells that arise by multiple fission (Tandeau de Marsac, 1994). In terms of physiological capacities, motile species always exhibit a gliding type of motility (Stanier and Cohen-Bazire, 1977). The non-developmental synthesis of gas vesicles by planktonic species enables these cells to adjust density or buoyancy in order to maximize light-harvesting or nutritional opportunities (Madigan *et al*, 1997). Members of genera such as *Anabaena*, *Microcystis*, *Trichodesmium*, and *Synechococcus* are responsible for the phenomenon known as "red tide", the formation of massive oceanic blooms correlating with the production of ecologically significant neurotoxins. Halotolerance also varies significantly between species, which is not surprising given the spectrum of marine and freshwater habitats, and ranges from poor (species which accumulate sucrose and trehalose), to moderate (species which accumulate glucosylglycerol), or high (synthesis of glycine- and glutamate-betaine) (Hagemann *et al*, 1997).

Although historically believed to be eukaryotic "blue-green algae", the Cyanobacteria lack membrane-bound organelles and are convincingly eubacterial, hence they are presently classified according to the Bacteriological method (Rippka *et al*, 1979) as Gram negative photoautotrophs. The characteristic cyanobacterial cell wall contains both Gram negative and Gram positive elements: The protoplast is surrounded by a bilayered cell wall including the presence of a peptidoglycan layer between the outer and plasma membranes, which is similar to Gram negative bacteria in structure and function. However, the thickness and chemical composition of the peptidoglycan is more similar to that found in Gram positive bacteria, and cyanobacteria generally stain Gram positive, related to the production of a glycocalyx external to the cell wall. The glycocalyx is enriched in carbohydrate and has the appearance of a fibrous sheath or a slime layer around the cells, which provides protection against desiccation in terrestrial habitats and prevents

the loss of solutes in aqueous habitats (Gantt, 1994). A salient feature of all cyanobacteria is the presence of a third lipid bilayer known as the intracytoplasmic or thylakoid membrane, which is the site of photosynthesis as discussed below (Wolk, 1973; Schmetterer, 1994). The thylakoids have various arrangements characteristic for different cyanobacterial species and dependent upon the physiological state. Unlike the chloroplastic stacks of grana, cyanobacterial thylakoids are commonly found throughout the cytoplasm, whether in orderly concentric layers or in more irregular, dense formations (Gantt, 1994). There is electron micrograph evidence that the thylakoid membranes may contact the cell membrane, or may even be physically continuous with it in certain species (Nierzwicki-Bauer *et al.*, 1983), however the functional components and capabilities of the two membranes are definitely distinct (Omata and Murata, 1983, 1984, 1985).

Cyanobacteria share the photosynthetic limelight with two distinct groups that, despite key differences, offer insights by comparison. The first group is prokaryotic, namely the green and purple photosynthetic bacteria, in which the facultative nature of their photoautotrophic metabolism has enabled extensive investigation into the regulation of photosynthetic genes at the molecular level (Gregor and Klug, 1999). In contrast with cyanobacteria, photosynthetic light-harvesting by the green and purple photosynthetic bacteria occurs via cyclic electron flow around only one photosystem (with bacteriochlorophyll as the main light-harvesting pigment), does not result in the production of molecular oxygen by photolysis of water, and occurs solely under anaerobic conditions. The synthesis of the photosynthetic apparatus being energetically costly, expression of the corresponding genes is tightly controlled by oxygen tension; it is therefore *redox-responsive*. The transcriptional and post-transcriptional effects of various redox-regulated signal transduction pathways, as well as main components of these pathways, have been elucidated in *Rhodobacter capsulatus* and *Rhodobacter sphaeroides* (summarized in reviews by Bauer and Bird, 1996; Gregor and Klug, 1999; Pemberton *et al.*, 1998). These individual signaling circuits, which may have homologues in cyanobacteria, overlap to form a remarkably complex regulatory network that maintains homeostasis both within and between photosynthesis and the global bioenergetics. Although the redox-responsive nature of this system is primarily sensing oxygen, it offers a framework for the elucidation of redox-regulated signal transduction in other prokaryotes.

Secondly, cyanobacteria may be compared to plants and algae, the eukaryotic photoautotrophs in which photosynthesis is localized to the membrane-bound chloroplast organelles (Madigan *et al.*, 1997). Within the chloroplast, the thylakoid membrane is the site of the two photosynthetic reaction center assemblies (PSI and PSII) that are linked by a cytochrome-containing electron transport chain. The antenna complexes that capture and

funnel excitation energy towards the photosystem reaction centers are known as light harvesting complexes (LHC). LHCI and LHCII are macromolecular complexes comprising both chlorophyll *a* and *b*, organized by low molecular weight polypeptides known as chlorophyll *a/b*-binding peptides (CABs). While the *cab* genes are located in the nucleus, their expression is regulated by light via the redox state of the chloroplasts (Escoubas *et al*, 1995); the expression of the photosynthetic components that are encoded in the chloroplastic genome is similarly regulated (Pffanschmidt *et al*, 1999). Although lacking chlorophyll *b*, the cyanobacterial photosystem reaction centers and electron transport apparatus share significant homology with that of eukaryotic photoautotrophs. The structural homology includes primary sequence, subunit composition, and biochemistry of photolysis and electron transport. The antenna complexes in cyanobacteria are known as the phycobilisomes; these are structurally distinct from, but functionally identical to, LHCII and are similarly regulated by phosphorylation during state transitions (discussed below). In place of LHCI, 100-150 chlorophyll *a* molecules serve as the main light-harvesting antenna for PSI. The absence of organellar membranes within cyanobacterial cells simplifies gene regulation and protein trafficking compared to plants, but the photosynthetic apparatus is similarly assembled in thylakoid membranes.

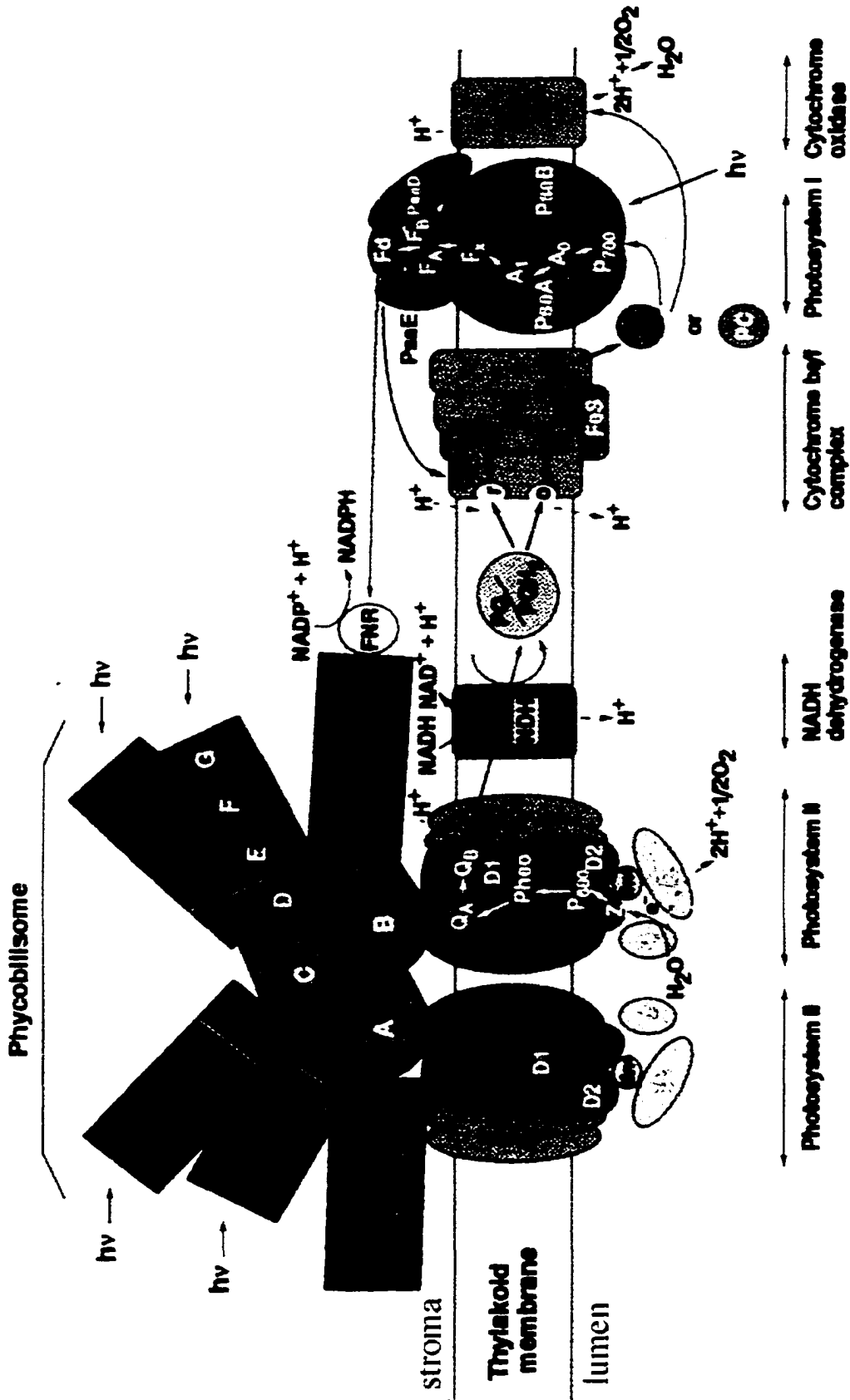
### 1.2.2 Bioenergetics

Photosynthesis is central to the bioenergetics of photoautotrophic organisms: it accomplishes the conversion of light into chemical energy for the formation of organic carbon compounds from carbon dioxide. Most cyanobacterial species are obligate photoautotrophs that are inhibited by exogenous carbon sources in the environment or the growth media. A limited number of species are reported to be capable of photomixotrophic growth, obtaining energy from light while assimilating an exogenous source of fixed carbon (Rippka *et al*, 1979). With illumination but in the absence of PSII function, which is known as photoheterotrophic growth, exogenous glucose is able to completely replace photosynthetic carbon fixation (Rippka *et al*, 1979). Exogenous carbon compounds may similarly support facultative heterotrophic growth in the dark, which is uncommon among cyanobacteria. Heterotrophic, photoheterotrophic, and photomixotrophic growth conditions do not result in loss of the cyanobacterial photosynthetic apparatus, in contrast to purple phototrophic bacteria. Localized to the thylakoid membranes, the photosynthetic apparatus comprises phycobilisomes, two photosystem complexes, and an inter-photosystem electron transport chain (Fig. 1.3). In cyanobacteria these electron carriers are shared by respiratory electron transport, as discussed below.

**Figure 1.3 Diagram of the Major Photosynthetic and Respiratory Electron Transport Components in Cyanobacteria**

Photoautotrophic growth relies on light-harvesting by the phycobilisome complex, shown here as a tricylindrical core (A, B, and C) and six peripheral rods (D to G). Allophycocyanin is the major component of the core, while phycocyanin and phycoerythrin constitute the peripheral rods (Grossman *et al*, 1993; *ibid.*, 1994). The core contacts the thylakoid membrane via the "anchor protein" that is associated with a dimer of thylakoid-bound photosystem II (PSII) reaction centers. Note  $Q_A$  and  $Q_B$  indicated on the right-hand PSII complex. Light harvesting by accessory chlorophyll molecules occurs at the PSI reaction center. Arrows indicate the direction of electron flow through plastoquinone (PQ), the cytochrome  $b_6f$  complex (cyt  $b_6f$ ), and plastocyanin (PC).  $PQH_2$ , plastoquinol. FNR, Ferredoxin-NADP reductase. Fd, Ferredoxin.

Adapted from Bryant (1994), color plate #1 (CP-1).





In the past a number of electron transport inhibitors have been used advantageously to identify the components of the photosynthetic and respiratory electron transport chains, as well as to demonstrate the interaction between these processes in cyanobacteria. Currently these inhibitors are commonly applied to the investigation of redox-mediated signaling events, including the research presented in this thesis. The physiological effects of DCMU, DBMIB, potassium cyanide (KCN), and methyl viologen (Mv) are detailed in Table 2.2, with the respective inhibition sites indicated relative to electron transport components in Figure 4.2. The following description of the individual photosynthetic and respiratory components and the overview of cyanobacterial bioenergetics are intended to provide a broader context for understanding redox-regulated RNA helicase expression.

#### **1.2.2.1 Cyanobacterial Antenna Complexes: The Phycobilisome**

The phycobilisome (PBS) functions as the cyanobacterial antenna complex, capturing light energy and preferentially transferring it to the photosystem II reaction center with 95% efficiency. The composition and function of phycobilisomes have been comprehensively reviewed by Grossman and co-workers (1993, 1994). Briefly, phycobilisomes are assembled in regular rows on the outer thylakoid surface, namely the stromal or protoplasmic side of the membrane. Each phycobilisome is a complex of phycobiliproteins (PBPs), which are soluble light-harvesting pigments formed from a low-molecular-weight apoprotein coupled to a bilin chromophore. The bilin chromophore is an open-chain tetrapyrrole, derived from a heme precursor, that exists in a number of isomeric forms which each exhibit a specific absorbance maximum ( $A_{\max}$ ). Three main classes of PBPs comprise the phycobilisome and are named according to the tetrapyrrole isomer: Allophycocyanin is encoded by the *apc* genes and is colored blue-green with an  $A_{\max}$  of 650-655 nm; phycoerythrin is encoded by the *cpe* genes, is colored red and absorbs at 565-575 nm; and phycocyanin, encoded by the *cpc* genes, has an  $A_{\max}$  of 615-640 nm such that it is a blue color. The individual PBPs associate as homodimers, which are then assembled into a fan-like complex with allophycocyanin at the core and phycoerythrin or phycocyanin in the rods, together with linker polypeptides. The phycobilisome attaches at the PSII photosynthetic reaction centers via a high-molecular-weight polypeptide known as the "anchor protein".

#### **1.2.2.2 The Photosystem Complexes (PSI and PSII)**

Photosystem I and II (PSI and PSII) are multi-subunit pigment-protein complexes embedded in the thylakoid membrane (Golbeck, 1994). Within these complexes the reaction centers are the sites where chlorophyll *a*, in conjunction with a heterodimer of

integral thylakoid proteins, donates an electron to the primary receptor moiety in response to excitation by light. P680 and P700 designate the photooxidizable chlorophyll *a* molecules in the PSII and PSI reaction centers, respectively, and differ in the spectral form of chlorophyll *a* because of the association with the polypeptide heterodimers. Carotenoids may also be present as accessory pigments, however these primarily serve a photoprotective role, namely to quench the singlet oxygen produced during the photooxidation reactions and thereby prevent the destruction of chlorophyll and the subsequent disassembly of the photosynthetic apparatus.

Photosystem II catalyzes the oxidation of water and the reduction of the plastoquinone pool in a photochemical reaction that yields charge separation across the thylakoid membrane, with reduction of the P680 chlorophyll as an intermediate step (Gantt, 1994). PSII is a pigment-protein complex of approximately 250 kDa that includes carotenoids, 35-60 chlorophyll *a*, and at least 10 polypeptides that are encoded by the *psb* genes, the most significant being *psbA* (D1 polypeptide) and *psbD* (D2 polypeptide). The D1 and D2 polypeptides form the reaction center heterodimer with sites for binding various cofactors such as the non-heme iron, and the 4Mn cluster of the water-splitting complex. The D1/D2 heterodimer also houses the primary photoreactive chlorophyll *a* (P680), and pheophytin, the chlorophyll derivative that acts as the intermediate electron acceptor. Furthermore, the D1/D2 heterodimer has receptor sites for Q<sub>A</sub> and Q<sub>B</sub>, which are the semiquinones that act as the primary and secondary acceptors for the electrons from the activated chlorophylls. Salih and Jansson (1997) have indicated these presumed interactions of various D1 residues with the other PSII reaction center components, including the non-covalent binding sites for the semiquinones in a three-dimensional model. Significant attention has focussed on the 32 kDa D1 polypeptide that is specifically damaged, cleaved, and replaced during the normal photochemical reactions involving chlorophyll *a*, resulting in a protein turnover rate that is unusually rapid relative to the other PSII subunits. This is assumed to be the result of photo-damage since D1 plays a central role in energy transformation, and is the most irradiation-sensitive component (Krieger-Liszkay and Rutherford, 1998; Minagawa *et al*, 1999). Unique to cyanobacteria is the presence of *psbA* gene families that encode at least two forms of the D1 protein, such that under conditions of light stress the alternate form(s) of D1 can be rapidly synthesized to reconstitute functional PSII units. Investigation of both the *psbA* and *psbB* gene families has revealed that their expression is regulated by light and redox conditions at the transcriptional and post-transcriptional levels.

Photosystem I is a chlorophyll-protein complex that catalyzes the light-driven transfer of electrons from plastocyanin to ferredoxin. In cyanobacteria the PSI complex is

composed of at least 12 polypeptides that are encoded by the *psa* genes, a pair of phylloquinones, three [4Fe-4S] clusters, and approximately 100-150 chlorophyll *a* that act as the light-harvesting antenna. Similar to PSII, the PSI reaction centre core comprises a heterodimer of the homologous PsaA (83 kDa) and PsaB (82 kDa) polypeptides bound to the photoreactive chlorophyll *a*, P700. The PsaA/PsaB complex also binds the primary electron acceptor  $F_x$ , which is a [4Fe-4S] cluster and which reduces the terminal PSI acceptors, ferredoxins A and B. There is evidence that the light-regulated expression of the *psaA* and *psaB* genes depends upon the redox state of either plastoquinone or cyt *b<sub>6</sub>f* in the electron transport chain. Despite the fairly rapid transcriptional responses, an increase in PSI reaction centers is not apparent until cell division and synthesis of thylakoid membranes has also occurred (Fujita *et al*, 1994). PsaA and PsaB may also be regulated at the translational level since, in barley, the addition of chlorophyll stimulates their synthesis on thylakoid-bound polysomes (Fujita *et al*, 1994).

### **1.2.2.3 The Inter-photosystem Electron Carriers and Photosynthetic Electron Transport**

Located between the two photosynthetic reaction centres is an electron transport chain comprised of both integral-membrane and soluble membrane-associated electron carriers (Fig. 1.3). Plastoquinone is quantitatively present in the highest amount of all the components, forming a pool of mobile electron carriers within the thylakoid membrane. The plastoquinone pool acts as a redox buffer, interacting with the PSII reaction center and the cytochrome *b<sub>6</sub>f* complex (cyt *b<sub>6</sub>f*) during photosynthetic electron transport, as well as participating in electron transfer reactions with other systems (Kallas, 1994). Cyt *b<sub>6</sub>f* is an integral membrane complex composed of four main subunits that are encoded by the *pet* genes, namely cytochrome *f*, cytochrome *b<sub>6</sub>*, subunit IV and the Reiske Fe-S protein. The identity of the soluble thylakoid-associated electron carrier between cyt *b<sub>6</sub>f* and PSI is plastocyanin in plants; in cyanobacteria it may be either the copper-containing plastocyanin or cytochrome *c<sub>553</sub>*, depending on the strain and the growth conditions. The stoichiometry of the various components of the electron transport chain, including PSI and PSII, is not equimolar (Nanba and Katoh, 1985). Furthermore, the mobility of the plastoquinone pool and the thylakoid associated electron carrier may allow for electron exchange between the integral membrane complexes of more than one photosynthetic electron transport chain (Nanba and Katoh, 1985).

Photosynthetic electron flow may be summarized as follows: Radiant energy captured by the phycobilisome antenna complexes is transferred to chlorophyll *a* in the PSII photosynthetic reaction center where, together with the water-splitting reaction that evolves

molecular oxygen, electron flow is initiated. Within the PSII reaction center, electrons consecutively reduce the primary and secondary electron recipient quinones  $Q_A$  and  $Q_B$ , bound to the D1 polypeptide, and then reduce the plastoquinone pool. From plastoquinone, electrons are transferred to the Reiske Fe-S center of cyt  $b_6f$  simultaneous with the translocation of protons. This proton translocation contributes to the formation of an electrochemical gradient for the synthesis of ATP, referred to as photophosphorylation. Electron flow out of the cyt  $b_6f$  complex is the rate-limiting step in the electron transport chain. While there is some evidence from *Synechocystis* sp. strain PCC 6803 that electron transfer may occur directly from cyt  $b_6f$  to PSI (Nanba and Katoh, 1985), it is generally accepted that plastocyanin or the alternate cyt  $c_{553}$  act as mobile thylakoid-associated electron carriers to transfer electrons between these two membrane-bound complexes. Subsequently, the light-dependent excitation of PSI may reduce ferredoxin for the production of NADPH; this is termed linear electron flow since the electrons to reduce PSI originate from the water-splitting reaction. Alternatively, electrons from PSI can re-enter the electron transport chain at the plastoquinone pool (or possibly at cyt  $b_6f$ ), via NADPH dehydrogenases (NADPH-DHs) such as ferredoxin-NADP<sup>+</sup> oxidoreductase; this is termed cyclic electron flow since there is no net input nor exit of electrons. While linear electron flow yields both ATP and NADPH (reducing power), cyclic electron flow generates only ATP, and these products are subsequently used during carbon fixation, nitrogen fixation or assimilation, and other anabolic processes.

#### **1.2.2.4 Bioenergetics: Respiration and Respiratory Electron Transport**

Similar to photosynthesis, but receiving decidedly less research attention, respiratory electron transport is essentially a membrane-bound process that includes several peripheral membrane proteins and that is coupled to proton translocation, which generates a proton motive force for the synthesis of ATP. This has been summarized in reviews by Schmetterer (1994) and Scherer (1990). The lack of appreciable growth in the dark, even with exogenous organic carbon substrates, suggests minimal anabolic activity and supports the assumption that the main physiological purpose of respiration is the "maintenance of an adequate energy charge during dark periods" (Scherer, 1990). Although it is often measured as the rate of consumption of molecular oxygen, the two processes are not necessarily equivalent (Schmetterer, 1994); attempts to quantify the rate of respiratory electron transport have yielded variable results, with the highest estimate being 20% that of photosynthetic electron transport (Scherer, 1990).

In cyanobacteria, respiratory metabolism of organic carbon compounds is centered on the oxidative pentose phosphate pathway for the production of NADPH, although

enzymes for glycolysis are also present. Notably, the tricarboxylic acid cycle serves a biosynthetic rather than energetic function due to the lack of the  $\alpha$ -ketoglutarate dehydrogenase and succinate dehydrogenase enzymes (Madigan *et al.*, 1997). Thus, a minor source of electrons entering the respiratory electron transport chain may occur from NADH via NADH-dehydrogenases but the ability of the cell to use NADH occurs mainly indirectly, via the activity of an NADPH-NADH transhydrogenase (Scherer, 1990). NADPH is the primary electron donor for respiratory electron transport (Sandmann and Malkin, 1983), reducing the plastoquinone pool via the activity of NADPH-dehydrogenases (NADPH-DHs). The most important of these is ferredoxin-NADP<sup>+</sup> oxidoreductase (FNR), encoded by the single *petH* gene and post-translationally modified to yield multiple isoforms that may have differing substrate specificities. Experimental evidence suggests there is a soluble form of FNR that associates with the peripheral rods of the phycobilisomes and that catalyzes reduction of NADP<sup>+</sup>, whereas a membrane-associated form of FNR catalyzes electron transfer from NADPH to quinols such as plastoquinone (Schmetterer, 1994).

Respiratory electron flow is postulated to proceed from NADPH-DH through the electron transport chain to the terminal electron acceptor, which is universally oxygen in cyanobacteria. Research has generally focused on the cytochrome *c*<sub>553</sub> oxidase, an aa<sub>3</sub>-type of terminal oxidase, although there is evidence for additional cyanide-sensitive and insensitive oxidases in most species. Present in both the cell membrane and the thylakoid membrane, cyt *c*<sub>553</sub> oxidase is a hemoprotein composed of three subunits that are encoded by the *cox* genes, and which exhibits sensitivity to azide, cyanide, and carbon monoxide. Contributing to the difficulties of respiratory research is the likelihood that the respiratory electron transport chain is branched, and no particular sequence of electron carriers is used exclusively. In other words, the electron flow from NADPH-DH via plastoquinone to one or more terminal oxidases may or may not include cyt *b*<sub>6f</sub>, plastocyanin, and/or other soluble carriers (Schmetterer, 1994).

Cyanobacteria are unique because they perform aerobic respiration and oxygenic photosynthesis in the same compartment. Coordinate regulation of these two processes is necessary in order to avoid the futile cycling that would occur if both processes were equally active in the light. While photosynthetic electron transport is restricted to the thylakoids, respiratory electron transport localizes to the cell membrane as well as the thylakoid membrane, where it utilizes the inter-photosystem electron transport carriers (Schmetterer, 1994). In the thylakoid membrane, it is well established that the plastoquinone pool is the common point of electron entry from both PSII and NADPH-dehydrogenases (Hirano *et al.*, 1980; Scherer, 1990). Similarly, the dual involvement of

the cytochrome *b<sub>f</sub>* complex is inferred from the observation that while it is oxidized by PSI in the light, in the dark it can also be oxidized by molecular oxygen. Therefore these two processes of photosynthesis and respiration impinge upon each other and are coordinated via their effects on the redox state of the shared electron transport components. This is apparent under conditions of illumination: When photosynthesis is active, endogenous respiratory processes are inhibited. The inhibition occurs firstly at the level of the terminal oxidase cyt *c<sub>553</sub>*, due to the higher turnover rate of photoenergized PSI in the competition for electrons from plastocyanin. Secondly, various respiratory enzymes are down-regulated by light, including glucose-6-phosphate dehydrogenase and 6-phosphogluconate dehydrogenase from the oxidative pentose phosphate pathway. Finally, the conformation and hence the activity of the NADPH-DHs such as FNR may be altered in response to proton extrusion and thylakoid membrane potential (Scherer, 1990).

### **1.2.3 Bioenergetics: Homeostasis**

The efficiency of photosynthesis is maximal when the excitation of the PSI and PSII reaction centers is balanced. Non-productive excitation of the chlorophylls is undesirable because it produces fluorescence as well as damaging oxygen radicals and heat in lieu of electron transport. In this respect, the intensity and/or quality of the actinic light in most environments is sub-optimal. In addition, growth conditions such as nutrient limitation or osmotic pressure will alter the total and relative requirements for the photosynthetic products ATP and NADPH. Imbalance in the light-harvesting activities may be sensed as a change in the redox state of the inter-photosystem electron transport components, such as plastoquinone and/or cyt *b<sub>f</sub>*. In particular, the redox equilibrium of the plastoquinone pool provides a sensitive indicator of any imbalance in the turnover of PSII and PSI, since it is situated between them in the photosynthetic electron transport chain (Scherer, 1990). In response to conditions that preferentially increase the excitation of one reaction center the cells induce both long- and short-term homeostatic responses; photoinhibition occurs when homeostasis can no longer be maintained.

#### **1.2.3.1 Long-Term Changes in Light-Harvesting Capacity**

Changes in the spectral quality of illumination are met with changes in both the photosystem stoichiometry and phycobilisome content (summarized by Tandeau de Marsac, 1994). Prolonged growth under PSI light - namely, wavelengths preferentially absorbed by PSI and referred to as light 1 (L1, 650 nm) - yields an increase in PSII centers relative to PSI, as well as an increase in the PBS. Conversely, preferential excitation of PSII (L2, 560 nm) will cause an increase in the PSI:PSII ratio. Furthermore, certain

cyanobacterial species are able to alter the phycobiliprotein composition of the PBS to maximize the absorption of particular wavelengths of light. Specifically, during chromatic adaptation the ratio of phycoerythrin and phycocyanin in the PBS is modulated via differential transcription of the respective genes. Certain species are able to alter the synthesis of phycoerythrin only. Other species contain both constitutive and inducible genes for the production of phycocyanin. True complementary chromatic adaptation occurs in species in which the genes for both phycocyanin and phycoerythrin are inducible and repressible (Tandeau de Marsac, 1994). The transcriptional control is likely exerted via phytochrome, and the promoter-binding factors RcaA and RcaB have been elucidated mainly in *Calothrix* sp. (Curtis and Martin, 1994, Sobczyk *et al.*, 1993). Interestingly, there are potential secondary structures in the polycistronic mRNAs for phycoerythrin and phycocyanin, which suggests translational control is also a factor.

When grown under a particular light regime for a prolonged period of time cyanobacteria will also adjust the number of photosynthetic light-harvesting complexes in a manner that is inversely proportional to the intensity of light. In comparison to conditions of high intensity of illumination, cells grown with low intensity light contain more photosystem reaction centers. The number of phycobilisomes and the length of the rods is also adjusted to augment the amount of light that can be captured by PSII. The ratio of PSI:PSII shifts in favour of PSI, related to the higher efficiency of light-harvesting by PBS compared to chlorophyll *a* antenna complexes at low light fluence.

### **1.2.3.2 Balance Of Light-Harvesting By State Transitions.**

In comparison with long-term adaptations, short-term changes in the spectral quality of light induce the phenomenon known as state transitions. Although initially described for the antenna complexes in plants, state transitions also occur in cyanobacteria despite the structural differences between LHClI and phycobilisomes. As detailed above, the PBS are associated mainly with PSII, which is known as state 1. During the transition to state 2, phosphorylation of the antenna complexes causes their dissociation from the PSII reaction centres, functionally decoupling a proportion of the light-harvesting and electron transport. As a result, the relative excitation of PSI increases, possibly due in part to a transient association of the PBS with PSI (Allen *et al.*, 1989; Allen, 1992, and references therein).

State transitions occur in both plants and cyanobacteria in response to the net redox state of the plastoquinone pool. Actinic light that is high in L2 (preferential activation of PSII) yields a net reduction of the plastoquinone pool such that plastoquinol predominates. This in turn activates a thylakoid protein kinase that phosphorylates the antenna complexes.

The resultant shift in light-harvesting activity towards PSI activation yields decreased electron flow through plastoquinone via PSII and increases the oxidation of the plastoquinone pool. As the redox equilibrium shifts towards plastoquinone, the thylakoid kinase is inactivated and a constitutive phosphatase activity dephosphorylates the antenna complexes, enabling them to re-associate with PSII reaction centers. In fact, because of the overlapping photosynthetic and respiratory electron transport chains, respiratory electron flow can effect a state 2 transition in cyanobacteria (Mullineaux and Allen, 1986). Since plastoquinone responds oppositely to increased turnover of PSII as compared to PSI, it is a sensitive mechanism for the regulation of state transitions. Whether there is a redox sensor that senses plastoquinone directly, or whether the redox signal is transduced via the quinone binding site ( $Q_O$ ) on *cyt b<sub>6</sub>f*, remains to be determined (Mullineaux and Allen, 1990; Vener *et al*, 1998; Vener *et al*, 1995).

### 1.2.3.3 Photoinhibition Due to Excess Excitation of PSII

Chromatic adaptation and state transitions permit the cell to adapt to a range of usable light wavelengths and intensity. Transfer of a low-light adapted culture into high light intensity also results in a decline in the number of antenna complexes, the number and length of the peripheral rods, and the concentration of functional PSII centers. In fact these adaptations, which decrease the efficiency of electron transport, also provide cross-protection to stresses such as lowered temperature in which electron transport processes would otherwise be overloaded. However, with prolonged exposure to conditions of excessive photoreactive illumination, photoinhibition occurs, characterized by loss of oxygen evolution and achlorosis. Photoinhibition occurs when the rate of light-harvesting exceeds the rate of conversion into metabolically useful energy (Mann, 1994). While the precise events of photoinhibition are only partially elucidated, it appears that over-reduction of the primary electron acceptor plastoquinone ( $Q_A$ ) causes a back-reduction of the photoreactive chlorophyll, which then in its highly energized state damages the D1 polypeptide (Karpinski *et al*, 1997). When the rate of degradation of the D1 polypeptide in the PSII reaction center surpasses the rate of replacement, this causes the loss of integrity of the reaction centre, releasing the chlorophylls (Krieger-Liszkay and Rutherford, 1998; Minagawa *et al*, 1999). Furthermore, in chloroplasts there is a burst of hydrogen peroxide that is thought to be associated with the damage and degradation of the D1 protein (Karpinski *et al*, 1997).



### **1.3 The Model Organism for Investigation of RNA Helicases: *Synechocystis* sp. strain PCC 6803**

*Synechocystis* sp. strain PCC 6803 (subsequently referred to as *Synechocystis* throughout this thesis) is a Section I (Chroococcales) cyanobacterium. This fresh-water isolate is moderately halotolerant due to the accumulation of glycosylglycerol and small amounts of sucrose as osmoprotectants (Hagemann *et al.*, 1997). It also possesses a constitutive, concentrative glucose transport system that is not a phosphotransferase system (Rippka *et al.*, 1979; Flores and Schmetterer, 1986). This enables *Synechocystis* to grow under photoheterotrophic or photomixotrophic conditions, a characteristic that has been used to advantage for the study of photosystem II. This species is amenable to genetic manipulation and analysis because it is unicellular and naturally competent for transformation with exogenous DNA.

Another significant advantage to using *Synechocystis* is the availability of the entire genomic sequence; it was among the initial prokaryotic genomes to be completed (Kaneko *et al.*, 1995a). The DNA sequence has been deposited in 27 entries to DDBJ, and given the accession numbers D90899 to 90917 and D63999 to D64006. Sequence data and analyses are also available at the Cyanobase site (<http://www.kazusa.or.jp/cyano/cyano.html>). The genome size is 3,573,471 bp, with a G+C content of 47.7% (Kaneko *et al.*, 1996a). Three extrachromosomal units were identified, including pSYSA which is 110 kb, and pSYSM which is 125 kb in size (Kotani *et al.*, 1995). pSYSG is 45 kb and contains the gene for PsbG2, which is a subunit of the NAD(P)H-DHs. The DNA sequence analyses have revealed open reading frames for 3168 known and putative proteins, 2 entire rRNA gene operons, and 42 putative tRNA genes. There are at least 126 genes relating to oxygenic photosynthesis (Kaneko *et al.*, 1996a), although it lacks a few of the PSI and PSII genes that are typically found in the nuclear genomes of higher plants. Notably there are a number of homologues for eukaryotic genes, including a phytochrome that is functional *in vitro* (Yeh *et al.*, 1997).

### **1.4 Summary and Research Objectives**

The present study is part of a larger research program to identify and elucidate the function of DEAD-box proteins using the Cyanobacteria as a model system. The work presented here focusses on a DEAD-box protein gene from *Synechocystis*, designated *crhR*, with the intent to characterize this putative RNA helicase on both the molecular and physiological levels. The first objective was to identify a DEAD-box gene and determine the phenotypic effects of a homozygous mutation. In chapter three the sub-cloning of the *crhR* open reading frame enabled the engineering of two mutant constructs in which this

gene is inactivated by insertion of an antibiotic resistance cassette. Transformation of the pBR*crhR*::Sp and pBR*crhR*Δ::Sp constructs into *Synechocystis* yielded gene replacement by homologous recombination at the *crhR* locus, however only heterozygous mutants were obtained.

The second objective was to elucidate the pattern of expression of the *crhR* gene at the mRNA and protein levels. In chapter four, Northern analyses indicate that the mRNA is controlled by light via redox: Transcription of *crhR* corresponds with a net reduced state of the plastoquinone pool, and the stability of the transcript increases when electron transport is inhibited between PSII and PSI. A putative promoter region is identified and electrophoretic mobility shift assays define a 228 bp region of DNA, which includes 79 bp of coding sequence, that is bound by a soluble factor present in cell-free extracts. Western analyses in chapter five reveal that CrhR is present at a constitutive basal level even when the *crhR* transcript is undetectable. Relative levels of CrhR reflect the transcriptional and post-transcriptional regulation of the *crhR* mRNA. The potential association of CrhR with other soluble factors is confirmed and should facilitate the search for a cognate ribonucleoprotein complex and/or RNA substrate(s).

The third objective was to demonstrate the biochemical activities of the CrhR protein. Expression and purification of a CrhR fusion protein preceded *in vitro* demonstration of non-specific RNA-binding, RNA-dependent ATP hydrolysis, and ATP-dependent RNA helicase abilities in chapter six. This confirms that CrhR is a true RNA helicase.

The control of an essential RNA helicase gene by light, in particular via the redox conditions that are specified by photosynthesis and respiration, places this gene within a potential signal transduction cascade and leads to a discussion on the significance of the plastoquinone pool as an integration point for coordinating various stress and metabolic signals (chapter seven). Within this context, it is hoped that this research will increase our understanding of the biological role of RNA helicases in photosynthetic cells, and the contribution that RNA secondary structure makes in the control of photosynthetic processes.

## **CHAPTER TWO**

### **Materials and Methods**

## 2.1 Bacterial Strains, Growth Conditions and Media

The bacterial strains used in this study are listed in Table 2.1.

Unless otherwise indicated, *Escherichia coli* DH5 $\alpha$  and *E. coli* JM109 were routinely cultured in liquid LB medium or on LB plates solidified with 1.2% (w/v) agar (Difco) with addition of the appropriate antibiotics according to standard procedures (Sambrook *et al*, 1989). Pure cultures were inoculated from single colonies grown on plates. Glycerol stocks of *E. coli* strains with or without plasmids were made by adding sterile glycerol to 25% (v/v) and freezing in liquid nitrogen for long-term storage at -80°C.

Stock cultures of wild-type cyanobacterial strains were obtained from the University of Toronto Culture Collection (UTCC) and maintained on BG-11 medium (Rippka *et al*, 1979) solidified with 1% (w/v) Bacto-Agar (Difco). Cells were routinely cultured in a Coldstream (Weksler) incubator at 30°C with continuous illumination at an average intensity of 300  $\mu\text{mol photons m}^{-2} \text{s}^{-1}$ . The highest intensity was obtained with 4 sets of lights (1 set = 2 fluorescent bulbs, 110 W each), 600-630  $\mu\text{mol photons m}^{-2} \text{s}^{-1}$ ; 3 sets gave 400-450  $\mu\text{mol photons m}^{-2} \text{s}^{-1}$ ; 2 sets gave 150-300  $\mu\text{mol photons m}^{-2} \text{s}^{-1}$ ; 1 set gave 60-90  $\mu\text{mol photons m}^{-2} \text{s}^{-1}$ . Liquid cultures were aerated by vigorous shaking (150-200 rpm) and bubbling with humidified air when volumes were greater than 250 mL. For *Synechocystis* sp. strain PCC 6803, photomixotrophic conditions were obtained by the addition of 5 mM glucose and buffered by addition of 10 mM TES [N-tris (hydroxymethyl) methyl-2-aminoethanesulfonic acid] pH 8.2. Other chemical additions are listed in Table 2.2. Dark conditions were obtained by wrapping individual flasks with several layers of aluminum foil. Light 1 (L1) was obtained using a medium red filter (Rosco #27) that gave 50% transmittance at 650 nm (Fig. 2.1.A). Light 2 (L2) was obtained using an orange filter (Rosco #20) that gave 50% transmittance at 560 nm (Fig. 2.1.B). These filters were chosen according to Pfannschmidt *et al* (1999). The filters were inserted between the light source and the cultures. To partially compensate for light intensity effects, experimental cultures were pre-incubated in white light for 1.5-3 h with 1 set of lights (intensity 60  $\mu\text{mol photons m}^{-2} \text{s}^{-1}$ ) immediately prior to insertion of the filters, which were used with 4 sets of lights to yield intensities of 15  $\mu\text{mol photons m}^{-2} \text{s}^{-1}$  (L1) and 240  $\mu\text{mol photons m}^{-2} \text{s}^{-1}$  (L2).

Stock cultures grown 4-10 days on solid medium served as the inoculum for liquid cultures. For experimental use, photoautotrophic cultures of cyanobacteria were inoculated at OD<sub>750</sub>=0.1 into 50 mL of BG-11 in 250 mL flasks. When these 50 mL starter cultures

**Table 2.1 Bacterial Strains Used in This Study**

PCC, Pasteur Culture Collection. UTCC, University of Toronto Culture Collection.

STRAIN	RELEVANT GENOTYPE	USE	Reference/ Source
<i>Synechocystis</i> sp. strain PCC 6803	Wild-type cyanobacterium. Capable of growth on exogenous glucose as a facultative photomixotroph or photoheterotroph	Main subject in the present study of RNA helicases in cyanobacteria.	University of Toronto Culture Collection
<i>Anabaena variabilis</i> UTCC 387 = <i>Anabaena</i> sp. strain PCC 7120	Wild-type cyanobacterium	Comparison to <i>Synechocystis</i> .	University of Toronto Culture Collection
<i>Synechococcus</i> sp. strain PCC 7942 (formerly <i>Anacystis nidulans</i> R2)	Wild-type cyanobacterium	Comparison to <i>Synechocystis</i> . Attempted isolation of a DEAD-box protein gene.	University of Toronto Culture Collection
<i>Escherichia coli</i> DH5 $\alpha$	<i>supE44</i> $\Delta$ <i>lacU169</i> ( $\phi$ 80 <i>lacZ</i> $\Delta$ <i>M15</i> ) <i>hsdR17</i> <i>recA1</i> <i>endA1</i> <i>gyrA96</i> <i>thi-1</i> <i>relA1</i>	Plasmid host during general cloning and propagation procedures. Permits $\alpha$ -complementation screening.	Hanahan 1983; Sambrook <i>et al.</i> , 1989
<i>Escherichia coli</i> JM109	<i>recA1</i> <i>supE44</i> <i>endA1</i> <i>hsdR17</i> <i>gyrA96</i> <i>relA1</i> <i>thi</i> $\Delta$ ( <i>lac-proAB</i> ) <i>F'</i> [ <i>traD36</i> <i>proAB</i> <sup>+</sup> <i>lacI</i> <sup>f</sup> <i>lacZ</i> $\phi$ <i>M15</i> ]	Plasmid host for parental and derivatives of pRSETA and pGEX-2T. Used for plasmid propagation and protein over-expression studies.	Sambrook <i>et al.</i> , 1989
<i>crhR</i> ::Sp	<i>crhR</i> / <i>crhR</i> + heterozygote	Phenotypic analysis of RNA helicase mutation.	This study
<i>crhR</i> $\Delta$ ::Sp	<i>crhR</i> / <i>crhR</i> + heterozygote	Phenotypic analysis of RNA helicase mutation.	This study

**Table 2.2 Chemical Additions to BG11 Media for Experimental Use with *Synechocystis* Cultures**

Abbr.	Full Chemical Name	Final Conc.	Physiological effect	Reference(s)
glc	glucose	5 mM	Stimulates respiration and causes an increase in electron flow from NADPH-DH into the PQ pool.	Reyes and Florencio, 1995
3-OMG	3-O-methyl-D-glucopyranose	5 mM	A glucose analogue that is transported into the cells but cannot be metabolized and therefore does not stimulate respiration or respiratory electron flow.	Reyes and Florencio, 1995
DCMU	3-(3,4-dichlorophenyl)-1,1-dimethylurea	5 $\mu$ M	Interacts with the primary acceptor (Q <sub>B</sub> ) site of the D1 polypeptide in the PSII reaction center and thereby interrupts electron flow between PSII and the PQ pool. It prevents linear electron flow but not cyclic photophosphorylation nor respiratory electron flow to PQ from the NADPH-DHs. Photosynthetic growth and CO <sub>2</sub> assimilation are inhibited.	Rippka <i>et al.</i> , 1972; Trebst, 1980; Hirano <i>et al.</i> , 1980
DBMIB	2,5-dibromo-3-methyl-6-isopropyl-p-benzoquinone (dibromothymoquinone)	20 $\mu$ M	As a PQ analog it competes for the binding site on the Reiske Fe-S center of cytb <sub>6</sub> f. At lower concentrations it strongly but incompletely inhibits the reduction of cytb <sub>6</sub> f with electrons from the PQ pool, but has no effect on the oxidation of cytb <sub>6</sub> f by PSI. It blocks the oxidation but not the reduction of the PQ pool, inhibiting linear, cyclic and respiratory electron transport. At higher concentrations it additionally suppresses electron flow from PSII into the PQ pool.	Nanba and Katoh, 1984; Trebst, 1980; Hirano <i>et al.</i> , 1980; Yu <i>et al.</i> , 1993
KCN	potassium cyanide	500 $\mu$ M	Poisons the respiratory cytochrome oxidase as well as enzymes of the pentose phosphate pathway and Calvin cycle. It prevents respiratory electron flow to the terminal oxidase but linear and cyclic photosynthetic electron flow are unaffected. However, several important enzymes for the use of reducing power are inhibited, including RuBisCo, nitrate reductase, and sulfate reductase. As well as endogenous catalase activity.	Trebst, 1980; Hirano <i>et al.</i> , 1980; Yu <i>et al.</i> , 1993
Mv	methyl viologen (paraquat)	20 $\mu$ M	Accepts electrons from the reducing site of PSI. Therefore it acts as an electron shunt that oxidizes PSI and inhibits cyclic electron flow as well as linear electron flow to Fd. However it does not prevent electron flow through the electron carriers of the respiratory and/or photosynthetic electron transport chain. Reduced Mv subsequently reduces O <sub>2</sub> to H <sub>2</sub> O <sub>2</sub> , and generates oxidative stress.	Hirano <i>et al.</i> , 1980; Yu <i>et al.</i> , 1993
Tc	Tetracycline	10 $\mu$ g/mL	Inhibits translation at the point of binding of aminoacyl tRNAs to the A-site in the ribosome (30S ribosomal subunit inhibitor.) It therefore prevents the initiation step of translation.	Mathews and van Holde, 1990
Cm	chloramphenicol	40-400 $\mu$ g/mL	Inhibits translation at the point of chain elongation, by acting as a competitive inhibitor of the peptidyltransferase complex. Blocks the peptidyl transferase reaction	Mathews and van Holde, 1990
Sp	streptomycin	2-10 $\mu$ g/mL	Interferes with translation by allowing incorrect pairing of tRNAs to the mRNA codon, which causes misreading of the mRNA to such an extent that normal proteins are not synthesized. (Aminoglycoside antibiotic) 30S ribosomal subunit is the target, grouped with Kanamycin. Prevents transition from the initiation complex to chain elongation.	Mathews and van Holde, 1990
Sm	spectinomycin	2-10 $\mu$ g/mL	Interferes with translation at the level of protein synthesis, 30S ribosomal subunit inhibitor; grouped with tet.	Madigan <i>et al.</i> , 1997
Rif	Rifampicin	400 $\mu$ g/mL	Inhibits transcription by RNA polymerase in prokaryotes; prevents the synthesis of mRNA, rRNA, and tRNA.	Mathews and van Holde, 1990

**Figure 2.1 Absorbance Spectra of Filters Used to Alter Actinic Light**

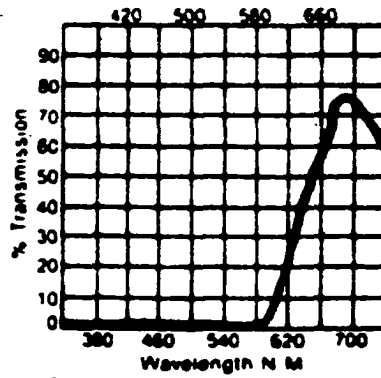
**A.** Absorbance spectrum of the L1 filter, which leads to preferential excitation of PSI reaction centres compared to white light.

**B.** Absorbance spectrum of the L2 filter, which leads to preferential excitation of PSII reaction centres compared to L1 light.

**A**

**#27**  
**Medium Red**

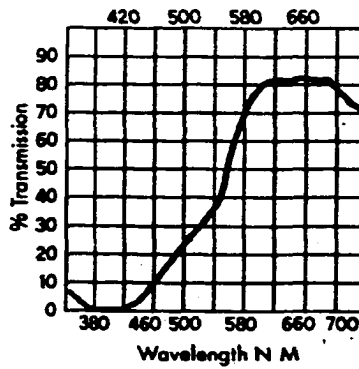
**TRANS. = 4%**



**B**

**#20**  
**Medium Amber**

**TRANS. = 54%**





had reached mid- to late- log phase they were used to inoculate larger volumes of liquid BG-11 (350-1000 mL) and grown to mid-log phase ( $OD_{750}=0.35-0.75$ ). For each experiment the large-scale culture was divided, under sterile conditions, into 40-50 mL aliquots in 250 mL flasks that were individually subjected to the desired treatment. For all liquid cyanobacterial cultures the glassware was acid-washed with 4N HCl, rinsed well with distilled water and sterile Milli-Q water, then autoclaved prior to use. The absence of contaminating heterotrophic microorganisms was routinely confirmed by lack of growth when an aliquot of the experimental cyanobacterial culture was inoculated into liquid LB medium for 2 d at 37°C. The density of cyanobacterial cultures was estimated as per LaBarre *et al* (1989) using the formula [ $1 A_{580}= 5 \times 10^7$  cells/mL]. Chlorophyll concentration was determined according to Katoh (1988) following methanol-extraction from the cyanobacterial cells, and calculated using the formula [ $A_{665} \times 13.9 = \mu\text{g/mL}$  of chlorophyll in solution].

T7 phage were obtained at  $4 \times 10^9$  pfu/mL (gift of W. Gallin, Department of Biological Sciences, University of Alberta) and stored at 4°C.

## 2.2 DNA Procedures

All routine DNA manipulations were carried out according to standard procedures for molecular biology (Sambrook *et al*, 1989) under sterile (DNase-free) conditions, including treatment of water, solutions, and equipment. All solutions containing DNA were kept on ice while in use and stored at -20°C. DNA was quantitated by visual comparison to known amounts of DNA on UV-illuminated agarose gels after EtBr staining, and/or by spectrophotometrically measuring the absorbance of a DNA-containing solution at 260 nm, where 1  $A_{260}$  unit is equivalent to 50  $\mu\text{g/mL}$  of dsDNA, 40  $\mu\text{g/mL}$  of ssDNA, or 33  $\mu\text{g/mL}$  of an oligonucleotide.

The plasmids used in this study are listed in Table 2.3. Plasmids were manipulated and propagated in *E. coli* DH5 $\alpha$ . The exceptions are pRSET:*crhR* and pGEX:*crhR*, which were maintained and used for protein over-expression in *E. coli* JM109.

Synthetic oligonucleotides (Table 2.4) were obtained from the Department of Biological Sciences Synthesis Service (University of Alberta) or from BioServe Biotechnologies, Ltd. (Laurel, MD, USA). The locations of the oligonucleotides complementary to the known *Synechocystis* genomic sequence are indicated in Figure 3.1. Chromosomal DNA from *E. coli* DH5 $\alpha$  was routinely prepared in the lab by W. Magee or D. Chamot using a modified Marmur (1961) procedure.

**Table 2.3 Plasmids Used in This Study**

Plasmid Designation (parent vector)	Use in This Study	Reference or Source
cs0096 (SuperCosI)	Gift of S. Tabata. The insert is a <i>Synechocystis</i> genomic DNA fragment that includes the entire open reading frame of slr0083 ( <i>crhR</i> ). (Genbank Accession #D64004)	Kaneko <i>et al</i> , 1995
pBluescriptKS+	General cloning vector.	Stratagene
cs0096-9 (pBluescriptKS+)	The insert is a 3.02 kb <i>Eco</i> RI fragment (bp #2887357-2890377) of <i>Synechocystis</i> genomic DNA, containing the entire open reading frames for slr0083 ( <i>crhR</i> ) and slI0080, as well as 3' sequence of slr0082.	This study
pBR322	Cloning and transformation of <i>Synechocystis</i> for inactivation of the <i>crhR</i> open reading frame.	Bolivar <i>et al</i> , 1977
pBR <i>crhR</i> ::Sp (pBR322)	Insertional inactivation of the <i>crhR</i> open reading frame	This study
pBR <i>crhRA</i> ::Sp (pBR322)	Insertional inactivation of the <i>crhR</i> open reading frame	This study
pHP45Ω	The omega fragment contains the aminoglycoside-3/adenyltransferase fusion protein gene from the R100.1 plasmid, flanked by the T4 bacteriophage promoter and termination sequences. This gene confers spectinomycin and streptomycin resistance. (Genbank Accession #M60473; PID #g207855)	Prentki and Krisch, 1984
pGEX-2T (Genbank Accession #U13850)	Vector for over-expression and affinity purification of GST fusion proteins.	Pharmacia
pGEX: <i>crhR</i> (pGEX-2T)	Over-expression and purification of recombinant GST:CrhR protein.	This study
pRSETA	Vector for over-expression and affinity purification of HIS-tagged fusion proteins.	Invitrogen
pRSETA: <i>crhR</i> (pRSETA)	Gift of D. Chamot. Over-expression and purification of recombinant HIS:CrhR protein, subsequently used as an antigen for polyclonal antibodies from rabbit and to demonstrate the biochemical activities of CrhR.	This study
pAV1100	Gift of A. Vioque. The <i>Synechocystis</i> gene <i>mnpB</i> (460 bp) encoding the RNA component of the RNase P complex is contained on a 580 bp <i>Hind</i> III/ <i>Bam</i> HI fragment. This transcript provides an internal control for RNA loading during Northern analysis.	Vioque, 1992

**Table 2.4 Synthetic Oligonucleotides Used in This Study**

All sequences correspond to the *Synechocystis* genomic locations as indicated, unless specified otherwise. Non-homologous bases are indicated in bold.

Name	Sequence (5'-3')	Origin of sequence	Use
FWD	GTAAAACGACGGCCAGT	pBluescript KS+, nt #599-616	Sequencing; Site-directed mutagenesis; S1 nuclease protection assay
REV	AACAGCTATGACCATG	pBluescript KS+, nt #826-808	Sequencing
GWO25	<b>CGAACGGATCCATGACTA</b>	bp #2887634-2887651	PCR; Site-directed mutagenesis
GWO26	<b>GCGGGATCCGAATTCGGTG</b>	bp #2889560-2889542	PCR
GWO33	GGGCTGGCAAGCCACGTTTGGTG	pGEX-2T, nt #869-891	Sequencing pGEX: <i>crhR</i>
GWO34	<b>CCGGGAGCTGCATGTGTCAGAGG</b>	pGEX-2T, nt #1020-998	Sequencing pGEX: <i>crhR</i>
GWO38	GGTTGTAGCGCTTTA	bp #2888357-2888343	PCR
GWO39	TGACGATGTGAAAACC	bp #2888142-2888157	PCR
GWO40	TGTGTGGCTTCAGGC	Internal to the omega fragment of pHP45Ω	PCR
GWO41	CCGGGGGAGGTAGAGA	bp #2889765-2889750	PCR
GWO42	AGGGGAATGGCTTCAGTTG	bp #2887763-2887744	Primer extension
GWO45	AAGCCAATGTCGGCCAAGAG	bp #2887724-2887705	S1 nuclease protection assay; Primer extension; PCR
GWO47	AGTTTGCGGGAATGGCTGGG	bp #2887580-2887560	S1 nuclease protection assay; Primer extension; PCR
GWO48	<b>AAAAAAAAAGGGGTAAAGGAATTA</b>	bp #2886738-2886761	S1 nuclease protection assay; PCR
SLK1 (Z0230)	CGCATTGACCCAGAG	bp #2887846-2887860	Sequencing
SLK2 (Z0229)	GTGGTGCTGGATGAA	bp #2888098-2888112	Sequencing
SLK3 (Z0227)	TAAAGCGCTACAACC	bp #2888343-2888357	Sequencing
SLK4 (Z0228)	AACGCTGAAACCTA	bp #2888617-2888631	Sequencing
SLK5 (Z0225)	AGCGATGAGTACGA	bp #2888875-2888888	Sequencing
SLK6 (Z0226)	TGAAAAAATAAAGCC	bp #2889146-2889160	Sequencing
SLK7	<b>CACCGAATTCGGATCCCGC</b>	bp #2889542-2889560	Site-directed mutagenesis

## **2.2.1 Isolation of DNA from Whole Cells**

### **2.2.1.1 Chromosomal DNA from Cyanobacteria**

For large-scale extraction of *Synechocystis* genomic DNA, cells from a 300 mL mid-log phase culture were harvested by 10 min centrifugation at 6700 rpm in a Beckman JA-14 rotor at r.t.. The supernatant was decanted and the cell pellet was washed once with 8 mL SE buffer (120 mM NaCl, 50 mM EDTA, pH 8) then resuspended in 8 mL of fresh SE buffer. Cell lysis, as indicated by the increasing viscosity of the solution, was obtained by addition of lyophilized lysozyme powder to a final concentration of 3 mg/mL and incubation at 37°C for 3 h. SDS was then added to a final concentration of 1% (w/v), and the solution was further incubated at 37°C for 45 min, followed by 60°C for 10 min. After addition of NaClO<sub>4</sub> to a final concentration of 0.5 M, the solution was extracted twice with an equal volume of phenol and twice with an equal volume of chloroform:isoamyl alcohol (24:1, v/v). To avoid shearing the chromosomal DNA, the extractions were performed with gentle mixing followed by low-speed centrifugation to separate the organic layer from the aqueous layer, and by transferring the aqueous layer using glass pipettes with the tips removed or blue plastic pipette tips with the ends cut off. Nucleic acid was EtOH-precipitated for 14-24 h at -20°C and pelleted by a 30 min centrifugation at 8500 rpm in a Beckman JA-20 rotor at 4°C. The pellet was gently resuspended in sterile Milli-Q water and contaminating RNA was removed by digestion with DNase-free RNase A (50 µg/mL) for 1 h at 37°C, followed by extraction once with phenol and twice with chloroform:isoamyl alcohol (24:1, v/v) as above. The DNA was again EtOH-precipitated, then resuspended in water, quantitated, and stored at -20°C.

Small scale extraction of genomic DNA from *Synechocystis* was performed by resuspending the cells in 300 µL of STE (0.1 M NaCl, 1 mM EDTA, 10 mM Tris-HCl pH 8), and mixing with equal volumes of glass beads and phenol. The cells were lysed by four repetitions of 1 min vortex followed by 1 min incubation on ice, and centrifuged to pellet cell debris. The aqueous layer containing the DNA was extracted once each with equal volumes of phenol:chloroform (1:1, v/v) and chloroform:isoamyl alcohol (24:1, v/v). The DNA was ethanol-precipitated, resuspended in sterile Milli-Q water and used without further treatment.

### **2.2.1.2 Plasmid DNA from *E. coli***

Small-scale preparations (20-40 µg) of plasmid DNA were prepared from *E. coli* by the TENS alkaline lysis mini-prep procedure as described (Zhou *et al*, 1990). The nucleic acid was resuspended in an appropriate volume of water and used directly without further treatment. Contaminating RNA was removed by digestion with DNase-free RNase A as necessary.

Large-scale preparations (0.3-0.5 mg) of plasmid DNA were prepared from *E. coli* using QIAGEN Midi-prep or Maxi-prep columns according to the manufacturer's instructions. The purified plasmid DNA was resuspended in an appropriate volume of sterile Milli-Q water, quantitated and stored at -20°C.

## **2.2.2 DNA Manipulation**

### **2.2.2.1 Restriction Enzymes, Agarose Gel Electrophoresis, and Isolation of DNA Fragments**

DNA fragments were generated by digestion of chromosomal or plasmid DNA with restriction enzymes obtained from Amersham Pharmacia Biotech, Roche, Promega and New England Biolabs. The enzymes were used according to manufacturers' specifications with the buffers supplied. In reactions containing moderate amounts of plasmid DNA, 1-3 h incubation was generally sufficient for complete digestion. In reactions containing chromosomal DNA or large quantities of plasmid DNA, the digestion was carried out for 20-30 h, with fresh enzyme added to the reaction after 8 h. When it was desirable to remove the 5' phosphate moieties, fragments were treated with 1 U calf intestine alkaline phosphatase (Roche) for 1 h at 37°C prior to purification.

DNA fragments were separated according to size by electrophoresis through 0.7-1.2% (w/v) agarose (ICN) gels with either 0.5X TBE (10X TBE is 1M Tris-HCl, 1 M Boric acid, 20 mM EDTA) or 1X TAE (25 mM Tris pH 7.8, 5 mM NaOAc, 1 mM EDTA) as the buffer system. The DNA was prepared in 1X loading dye (6% [w/v] sucrose, 0.025% [w/v] bromophenol blue, 1 mM EDTA) and briefly heated to 90°C prior to loading onto the gels. Following electrophoresis, fragment sizes were determined by comparison to a standard curve of the migration of known size standards, run simultaneously on the gel. The standards used were 1 kb ladder (GIBCO-BRL), *Hind* III digest of lambda phage genomic DNA (Roche), or *Bst*NI digest of pBR322.

For isolation of specific DNA fragments from agarose gels, 1X TAE was used as the buffer system, and the appropriate band of DNA was sliced out of the gel after

electrophoresis. The GENECLAN<sup>®II</sup> (BIO 101, Inc.) procedure [initially described by Vogelstein and Gillespie (1979)] was carried out according to the manufacturer's instructions, as appropriate for different sizes of DNA fragments. The procedure was modified as suggested by Smith *et al* (1995), specifically, incubation at 55°C instead of r.t.. The DNA was eluted from the glassmilk with sterile Milli-Q water, quantitated by EtBr fluorescence quantitation, and stored at -20°C.

### **2.2.2.2 Ligation of DNA Fragments**

DNA fragments, generated by PCR or restriction digests, were purified for ligation by the GENECLAN<sup>®II</sup> procedure, or by phenol:chloroform (1:1, v/v) extraction and EtOH precipitation. In general, for ligating fragments that had complementary 5' or 3' single-stranded overhangs, the DNA was added in a 3:1 molar ratio of insert:vector, in a 20 µL final reaction volume containing 1 U of T4 DNA Ligase (Roche or Amersham Pharmacia Biotech), and 1X manufacturer's buffer. For blunt end ligations, the DNA was added in a 5:1 molar ratio of insert:vector, in a 10 µL final reaction volume with 1 U of ligase and 1X manufacturer's buffer. Ligation reactions were incubated at 15°C for 14-24 h in a MiniCycler (MJ Research).

### **2.2.2.3 Transformation and Electroporation of *E. coli***

Competent *E. coli* DH5α was routinely generated by rubidium chloride/calcium chloride treatment essentially as described (Sambrook *et al*, 1989). Single-use aliquots containing 7% (v/v) DMSO were frozen in liquid nitrogen and stored at -80°C. Competent cells were thawed on ice for at least 30 min, and 200 µL of cells were transformed by incubation with 1-2 µg of the appropriate plasmid DNA or ligation reaction (section 2.2.2.2). Cells were incubated on ice for 20 min, heat shocked for 2 min in a 42°C water-bath, and incubated in 1 mL LB broth without selection for 1 h at 37°C.

Electrocompetent *E. coli* JM109 cells were prepared in TSB (Trypticase Soy Broth) (Becton Dickenson) essentially as described (Sambrook *et al*, 1989). For each electroporation, 40 µL of chilled cells were mixed with 1 µg of DNA and added to a pre-chilled cuvette [BTX Electroporation Cuvettes Plus (TM)]. Electroporation was performed in a Bio-Rad Gene Pulser II set at 2500 V, 200 ohms resistance, and 25 microfarads

capacitance. TSB (1 mL) was added immediately, and the cells were incubated at 37°C for 1 h without shaking.

Following transformation or electroporation, cell aliquots (25-200 µL) were plated onto solid media containing the appropriate antibiotic(s). For cloning strategies that included blue-white colour selection, 50 µL of a solution of 2% (w/v) X-gal (in dimethyl formamide)/20 mM IPTG was spread onto the surface of the media prior to plating.

#### **2.2.2.4 Transformation of *Synechocystis* sp. strain PCC 6803**

*Synechocystis* is naturally competent for DNA uptake, therefore no chemical treatment was used to prepare them for transformation as previously described (Grigorieva and Shestakov, 1982). Cells were cultured in liquid BG-11 to a density of approximately  $10^7$  cells/mL. For each transformation,  $10^8$  cells were pelleted by 5 min r.t. centrifugation at the highest speed in a clinical centrifuge (International Equipment Co.). The pellet was gently resuspended in the residual liquid before adding 1-2 mL of fresh BG-11. Transformation was achieved by incubating the cells with 1 µg of DNA at 30°C, shaking at 150 rpm, for 6 h under dark conditions. The cells were then incubated with illumination for a further 12-18 h at 30°C with agitation. Aliquots of 100-200 µl were spread onto BG-11 plates containing the appropriate antibiotic, and incubated for 10-14 days with illumination. When the individual *Synechocystis* colonies were approximate 0.5 mm in diameter they were re-streaked onto fresh selective BG-11 plates. Mutants were maintained in this manner and transferred at least 6 times before extraction of genomic DNA for analysis by Southern hybridization or by whole-cell PCR using a method modified from Howitt (1996).

### **2.2.3 DNA Analysis**

#### **2.2.3.1 Southern Transfer and Hybridization**

Following agarose gel electrophoresis, capillary transfer of DNA onto Hybond™-N (Amersham) 0.45 micron nylon membrane was performed as previously described with 20X SSC (3 M NaCl, 0.3 M sodium citrate) as the transfer solution (Sambrook *et al*, 1989). After 12-24 h, the transfer was disassembled and a soft pencil was used to mark the top of the lanes and the orientation of the gel on the membrane. The transferred DNA was secured to the membrane by UV crosslinking at 150 J in a Bio-Rad GS GeneLinker™. Prehybridization and hybridization were carried out in sealed plastic bags containing 100

$\mu\text{g/mL}$  sheared herring sperm DNA (Sigma type XIV DNA) in hybridization solution {6X SSC, 0.5% [w/v] SDS, 5X Denhardt's solution [0.1% (w/v) BSA, 0.1% (w/v) Ficoll, 0.1% (w/v) polyvinylpyrrolidone]} using 1 mL hybridization solution per 10 cm<sup>2</sup> of membrane. The membrane was prehybridized at 65°C for at least 3 hours. For hybridization, radioactively labeled DNA probe (section 2.2.6.2) was added to fresh hybridization solution at a final concentration of 10<sup>6</sup> cpm/mL. Both the probe DNA and the herring sperm DNA were denatured by incubation for 5 min at 95°C followed by 5 min on ice immediately prior to addition. After 14-24 h of hybridization the membrane was washed first at low stringency [2X SSC, 0.1% (w/v) SDS] and r.t., then at higher stringency [0.2X SSC, 0.1% (w/v) SDS] with increasing temperature (from r.t. up to 65°C), as appropriate for the probe being used. The radioactive signal from bound probe was detected by autoradiography using Kodak X-OMAT™ AR X-ray film at -80°C with intensifying screens, and/or captured using a Phosphor-Screen (Molecular Dynamics). Prior to storing or reprobing, the membranes were stripped by immersion in boiling 0.5% (w/v) SDS and slow cooling to r.t..

### **2.2.3.2 Sequencing**

Single-stranded templates (1-3  $\mu\text{g}$ ) were prepared by denaturing in fresh 0.2 N NaOH/0.2 mM EDTA for 5 min at 50°C followed by addition of 2 M NH<sub>4</sub>OAc and EtOH-precipitation for 5 min at -80°C. The DNA pellet was resuspended in water and annealed with the appropriate oligonucleotide (0.1  $\mu\text{g}$ ) in 1X Sequenase Reaction Buffer (Amersham Life Sciences) by incubating at 37°C for 12 min, then allowing the mixture to stand at r.t. for at least 10 min prior to incubation on ice. DNA sequence was generated by the dideoxy method, using [ $\alpha$ -<sup>35</sup>S]dATP (Mandel Scientific) and the Sequenase v.2 sequencing kit (Amersham Life Sciences) according to manufacturer's instructions. Reactions were denatured for 2 min at 95°C prior to electrophoresis using the Sequi-Gen sequencing apparatus (Bio-Rad). The DNA fragments were separated on a denaturing (6 M urea) 6% polyacrylamide gel (19:1, acrylamide:bisacrylamide; Bio-Rad), with 1X TBE buffer, at constant wattage of 40-50 W for 1.5-8 h. The gels were fixed in 5% (v/v) acetic acid/5% (v/v) methanol for 20 min and dried under vacuum using a Slab Gel Dryer and Gel Pump (Savant). Radioactive signals were detected by autoradiography at r.t. as described above (section 2.2.3.1).



#### 2.2.4 PCR

DNA fragments were generated by the Polymerase Chain Reaction (PCR) using various DNA templates and combinations of oligonucleotide primers (Table 2.3). In control reactions each primer was tested individually. Furthermore, all solutions and equipment for PCR were treated to minimize contaminating DNA; gloves were worn at all times, UV illumination was used for surface sterilization as appropriate, and reaction tubes were prepared in a sterile flowhood using appropriate aseptic technique.

Routine PCR reactions where the sequence fidelity of the products was not essential were carried out using Taq polymerase (gift from M.A. Picard, University of Alberta). In a final volume of 50  $\mu$ L, reactions contained 1X PCR buffer [70 mM Tris-HCl pH 8.8, 4 mM MgCl<sub>2</sub>, 0.1% (v/v) Triton X-100, 100  $\mu$ g/mL BSA], 100  $\mu$ M of each dNTP (dATP, dCTP, dGTP, dTTP), 50 ng of each primer, 2.5  $\mu$ L of Taq polymerase diluted 1/10 in 1X PCR buffer, and up to 20 ng of template DNA as the final addition.

For generating PCR products with high sequence fidelity, as necessary for applications such as cloning or S1 nuclease mapping, the Expand™ Long Template PCR System (Roche) was used. In a final volume of 50  $\mu$ L each reaction contained 1X buffer #1 (completely thawed and mixed before use), 50 ng of each primer, 350  $\mu$ M of each dNTP, 0.5  $\mu$ L of Expand™ enzyme, and 20 ng of template DNA as the final addition.

The reactions were quickly mixed, briefly centrifuged, and overlaid with 75  $\mu$ L of sterile mineral oil. PCR was performed in a MiniCycler (MJ Research) according to preset PCR programs (Table 2.5), using a “hotstart” method whereby the reaction tubes were placed into the machine once it had reached the initial denaturing temperature.

#### 2.2.5 Site-Directed Mutagenesis

Site-directed mutagenesis was performed as described by Zoller and Smith (1987) with the detailed modifications described by Magee (1997), to produce a specific DNA fragment that contained the *crhR*. Briefly, template DNA (cs0096-9) was denatured to single-stranded for 5 min at 95°C, and three 5'-phosphorylated oligonucleotides were annealed to the same strand of the DNA. Two mutagenic oligonucleotides, GWO25 and SLK7 (Table 2.4), were used to engineer a *Bam* HI site immediately preceding the ATG initiator codon in the *crhR* ORF and a downstream *Eco* RI site, respectively. A third primer, FWD, anneals to pBluescriptKS+ sequence a short distance upstream of GWO25, and is purported to have a stabilizing effect. Klenow enzyme was added to synthesize the intervening DNA, followed by DNA ligase to ligate the single-stranded breaks that would

**Table 2.5 PCR Programs for the Minicycler**

Program Name	Denature	Anneal	Elongation	No. of Cycles	Finish
S1NUC	95°C, 2 min	40°C, 30 sec	68°C, 2 min	1	
	94°C, 30 sec	40°C, 30 sec	68°C, 1 min	29	68°C, 4 min; 4°C hold
S1NUC2	95°C, 2 min	35°C, 30 sec	68°C, 2 min	1	
	94°C, 30 sec	35°C, 30 sec	68°C, 2 min	1	
	94°C, 30 sec	48°C, 30 sec	68°C, 1 min	29	68°C, 5 min; 4°C hold
SLK	95°C, 5 min	31°C, 30 sec	72°C, 1 min	1	
	95°C, 30 sec	50°C, 30 sec	72°C, 1 min	19	72°C, 5 min; 4°C hold
3-STEP	94°C, 1 min			1	
	92°C, 40 sec	60°C, 40 sec	75°C, 90 sec	29	75°C, 5 min; 4°C hold

remain at the 5' end of each primer. The DNA was transformed into *E. coli* DH5 $\alpha$ , and used to inoculate 5 mL LB(Ap) cultures directly. Miniprep DNA from these cultures was then analyzed for the presence of a 1907 bp DNA fragment after digestion with *Bam* HI/*Eco* RI. This fragment was purified for subcloning into the *Bam* HI/*Eco* RI site of pGEX-2T (Amersham Pharmacia Biotech) (see section 2.4.3.1.1).

## **2.2.6 Radioactive Labeling of DNA**

### **2.2.6.1 End-labeling**

Radioactive labeling of the 5' end(s) of oligonucleotides or dsDNA fragments was performed with polynucleotide kinase (PNK) (Roche). In a final volume of 10  $\mu$ L, each reaction contained 25 pmol of DNA, 30  $\mu$ Ci of [ $\gamma$ -<sup>32</sup>P]dATP (Amersham), 1 U of PNK, 1X manufacturer's PNK buffer. The mixture was incubated for 1 h at 37°C, with an additional 1 U of PNK added after 30 min.

### **2.2.6.2 Random Primer Labeling**

Radioactive label was incorporated into ssDNA fragments according to the procedure of Feinberg and Vogelstein (1983). Approximately 25-100 pmol of dsDNA, in nuclease-free water, was denatured for 5 min at 95°C followed by 5 min incubation on ice. Synthesis of the complementary strands of DNA was carried out in a 50  $\mu$ L reaction containing 1X hexanucleotide mix (Roche), 60  $\mu$ M of each of dATP, dGTP, and dTTP, 50  $\mu$ Ci [ $\alpha$ -<sup>32</sup>P]dCTP (Amersham) and 2 U Klenow fragment (Roche). The reaction was incubated at r.t. for 14-24 h, or alternatively at 37°C for 1 h with an additional 2 U of Klenow added after 30 min. 15  $\mu$ L of stop solution (2% (w/v) blue dextran in TE) was added and the radioactive dsDNA was separated from the unincorporated nucleotides using a Sephadex G-50 (Amersham Pharmacia Biotech) column with 50/100 TE (50 mM Tris-HCl, 100 mM EDTA, pH 8) as the elution buffer. Radioactivity was quantitated by Cerenkov counting.

## **2.3 RNA Procedures**

All equipment and solutions were treated to remove and prevent RNase contamination. Solutions were made with Milli-Q water that had been sterilized in pre-baked flasks by 40 min autoclaving. All glassware and metal was sterilized by baking at

450°C for at least 4 h. Other equipment and tools were sterilized by soaking in either (i) 3% (v/v) H<sub>2</sub>O<sub>2</sub>, (ii) 1% (w/v) SDS, (iii) 100% ethanol or (iv) chloroform, followed by thorough rinsing with sterile Milli-Q water, and autoclaving as appropriate. Furthermore, these solutions and equipment were set apart for RNA use only, and clean gloves were worn at all times.

### **2.3.1 RNA Extraction**

Unless otherwise noted all steps were carried out on ice, with pre-chilled solutions and labware.

#### **2.3.1.1 Cyanobacterial RNA Extraction**

Total RNA was extracted by mechanical lysis using glass beads as previously described (Sato, 1995) with modifications. Cyanobacterial cells were harvested by mixing with an equal volume of ice-cold 5% (v/v) phenol in EtOH, followed by 10 min centrifugation at 4 °C and 5000-7000 rpm in a Beckman JA-14 rotor. The supernatant was decanted and the cell pellet was resuspended in 1 mL of ice-cold 50/100 TE (50 mM Tris-HCl, 100 mM EDTA, pH 8) by pipetting. Cells were transferred into a pre-cooled Eppendorf tube and microcentrifuged at r.t. for 1 min at 5000 rpm in order to obtain a soft pellet. After decanting this TE wash, the cell pellet was quickly resuspended in 250 µL of ice-cold lysis buffer [50/100 TE, 0.5% (v/v) Triton X-100, 0.5% (w/v) sarkosyl, 0.4% (w/v) SDS], and transferred into an Eppendorf tube containing 400 µL of Dyno-mill glass beads (0.2-0.3 mm; Impandex, Inc.), 400 µL of phenol, and 40 µL of 10% (w/v) SDS. The cells were lysed by 10 repetitions of vortexing at full speed for 1 min, followed by incubation in an ice-water bath for 1 min. Following 5 min r.t. microcentrifugation, the pink aqueous layer was extracted once each with phenol, phenol:chloroform (1:1, v/v), and chloroform:isoamyl alcohol (24:1, v/v). RNA was selectively precipitated with 2 M LiCl at -20°C for 12-24 h, and pelleted by 30 min microcentrifugation at 4°C. The RNA was re-precipitated and stored in EtOH at -80°C. Prior to use, the RNA was pelleted and resuspended in an appropriate volume of water to yield 1-3 µg/µL final concentration as determined by spectrophotometric quantitation.

#### **2.3.1.2 RNA Extraction from *E. coli***

Total RNA from *E. coli* was extracted with hot phenol. For each sample, a pellet of *E. coli* cells was resuspended in 750 µL of extraction buffer [1% (w/v) SDS, 10 mM

NaOAc pH 4.5, 150 mM sucrose] that had been preheated to 65°C. An equal volume of phenol, also preheated to 65°C, was added and RNA was extracted for 5 min by alternately vortexing and heating in a 65°C waterbath. Following a 5 min r.t. microcentrifugation, the aqueous layer was extracted once each with phenol, phenol:chloroform (1:1, v/v), and chloroform:isoamyl alcohol (24:1, v/v). The RNA was precipitated with 2 M LiCl and treated as described for cyanobacterial RNA extraction (section 2.3.1.1).

### 2.3.2 Northern Analysis

Northern analysis was performed according to standard procedures (Ausebel *et al*, 1995; Sambrook *et al*, 1989). For formaldehyde gels, 5-8 µg of total RNA was denatured in 25-30 µL of 1X formaldehyde loading buffer [50% (v/v) deionized formamide, 17% (v/v) formaldehyde, 7% (v/v) glycerol, 0.2% (w/v) bromphenol blue in 1X MOPS (20 mM MOPS, 5 mM NaOAc, 1 mM EDTA, pH 7)] for 15 min at 65°C, then the samples were cooled to r.t. and 0.05% (w/v) EtBr was added. RNA species were resolved by electrophoresis of a 10% (v/v) formaldehyde/1% (w/v) agarose gel with 1X MOPS as the buffer system. For glyoxal gels, 5-8 µg of RNA was mixed 1:9 (v/v) with GFP [0.93 M glyoxal, 78% (v/v) deionized formamide, 11.1 mM sodium phosphate pH 7] and denatured for 20 min at 56°C. Glyoxal loading buffer [2% (w/v) Ficoll 400, 0.5 mM EDTA, 0.02% (w/v) bromphenol blue] was added to each sample on ice and the RNA species were resolved by electrophoresis through a 1% (w/v) agarose gel, with 1X TAE as the buffer system. Electrophoresis was performed at r.t. for formaldehyde gels, or 4°C for glyoxal gels, with a current of 80-100 V. In lieu of recirculating the buffer, the electrode connections and gel orientation were reversed every 30-45 min.

The RNA was transferred by capillary action from the agarose gel onto a Hybond-N<sup>+</sup> or Hybond-XL (Amersham) 0.45 micron nylon membrane according to the manufacturer's instructions with 20X SSC as the transfer buffer. RNA was anchored to the membrane by UV-crosslinking at 150 J in the Bio-Rad GS GeneLinker™, or by baking 2 h under vacuum at 80°C. The membrane was washed twice for 30 min at 65°C in 0.1% (w/v) SDS, 0.1X SSPE (1X SSPE is 0.18 M NaCl, 10 mM NaH<sub>2</sub>PO<sub>4</sub>, 1 mM EDTA, pH 8) in order to remove excess salt that was found to interfere with hybridization. Using sealed plastic bags, the membrane was prehybridized for at least 2 h then hybridized 14-24 h with the appropriate labeled DNA probe (section 2.2.6.2) at 65°C in aqueous RNA

hybridization solution [100 µg/mL ssDNA in 5X SSPE, 5X Denhardt's, 0.5% (w/v) SDS]. RNA hybridization solution was used at 1 mL per 10 cm<sup>2</sup> of membrane, and probe was added at a final concentration of 10<sup>6</sup> cpm/mL. Consecutive washes were routinely performed at low stringency [0.1% (w/v) SDS, 1X SSPE] and r.t., then at high stringency [0.1% (w/v) SDS, 0.1X SSPE] and r.t., with the final wash at high stringency and 60°C. Radioactive signals from the bound probe were detected by autoradiography at -80°C using an intensifying screen. The probe for the *crhR* mRNA generally required exposure times of 24-96 h, whereas the probe for the RNase P RNA was detected in 1-4 h. Prior to re-probing membranes were stripped as described above (section 2.2.3.1).

The *crhR* probe is a 325 bp internal *Sma*I fragment that includes the PTRELA, DEAD and SAT motifs. As a control for RNA loading, filters were stripped and re-probed with a 580 bp *Hind* III-*Bam* HI DNA fragment from pAV1100 (gift of A. Vioque, Spain) that carries the 460 bp RNase P RNA gene (subsequently referred to as RNase P) from *Synechocystis*.

### **2.3.3 Determination of 5' Transcript Ends and Preliminary Promoter Analysis**

#### **2.3.3.1 Primer Extension**

Primer extension was performed as previously described (Ausebel *et al*, 1995) using AMV-RTase to synthesize radioactively-labeled DNA fragments complementary to the sample mRNA. Template RNA was total RNA from *Synechocystis* that had been analyzed for the presence of *crhR* mRNA by Northern analysis (section 2.3.2). Oligonucleotide primers were designed to hybridize to the mRNA sequence in a region that was predicted to be within 100 nt downstream of (i.e., 3' relative to) the 5' end of the *crhR* transcript. The oligonucleotide primer (25 pmol) was radioactively end-labeled as described above (section 2.2.6.1) and purified with a Nucletrap (Stratagene) column according to the manufacturer's instructions, using STE as the elution buffer. The radioactivity was quantitated by Cerenkov counting.

The annealing reaction was carried out in a final volume of 30 µL that contained the radioactively labeled oligonucleotide primer (6x10<sup>5</sup> cpm), 30 µg RNA, and 0.5 µL (20U) of RNase Inhibitor (Roche) in 1X aqueous hybridization buffer (1 M NaCl, 0.167 M HEPES-KOH pH 7.5, 0.33 mM EDTA). The nucleic acids were heat-denatured for 10 min at 85°C in a heating block, centrifuged briefly and replaced in the heating block, which was allowed to cool to 50°C over 2.5 h. The primer was then annealed for a further 1 h at

50°C. The solution was EtOH-precipitated, and the pellet was completely resuspended in 25.5 µL of ice-cold RT mix (20U of RNase Inhibitor, 560 µM of each dNTP, and 2X manufacturer's RT buffer). Following the addition of 25 U of AMV Reverse Transcriptase (Roche), DNA synthesis proceeded for 1 h at 44°C. To stop the reaction, the RNA template was digested by incubation with 1 µg DNase-free RNase A for 10 min at 37°C. Glycogen (Roche) (20 µg) was added and the ssDNA fragments synthesized by RT were EtOH-precipitated for 30 min at -80°C. The pellet was washed once with 100% EtOH, airdried briefly and resuspended in 8 µL of Sequenase Stop Solution (Amersham). The DNA was denatured for 2 min at 95°C and separated by electrophoresis on a denaturing (6 M urea) 6% polyacrylamide gel for 2.5-3 h at 50 W (section 2.2.3.2). Sequencing reactions were performed using the primer extension oligonucleotide as the sequencing primer and cs0096-9 as the template, and were electrophoresed simultaneously with the primer extension reactions. Radioactive products were visualized by autoradiography at -80°C using an intensifying screen.

### **2.3.3.2 S1 Nuclease Protection Assay**

The dsDNA fragments used in S1 nuclease mapping are diagrammed in Figures 4.8 and 4.9. The S1 nuclease protection assay was carried out according to standard procedures (Ausebel *et al*, 1995) with modifications as follows. The probe was specifically designed with non-homologous sequence at the 5' end of the non-hybridizing strand, which would be susceptible to S1 nuclease digestion and would not produce a protected end-labeled fragment; therefore, further purification of the strand complementary to the mRNA was not necessary (Leskiw *et al*, 1993). Template RNA was total RNA from *Synechocystis* that had been assessed for the presence of *crhR* by Northern analysis.

For use as probe, one pmol (100 ng) of the appropriate DNA fragment was radioactively end-labeled as described above (section 2.2.6.1), and EtOH-precipitated with 0.5 M NH<sub>4</sub>OAc and 20 µg glycogen. Total radioactivity in the pellet was determined by Cerenkov counting, and the pellet was resuspended in water to yield 10<sup>4</sup> cpm/µL. The annealing reaction was carried out with 10<sup>5</sup> cpm dsDNA probe, 15-30 µg RNA, and 0.5 µL (20U) RNase Inhibitor (Roche) in 1X aqueous hybridization buffer (1M NaCl, 0.33 mM EDTA, 0.167 M HEPES-KOH pH 7.5) in a final volume of 30 µL. After denaturation at 85°C for 10 min in a heating block, the samples were centrifuged briefly,

returned to the heating block, allowed to cool to 37°C over 1 h, and hybridization was performed for a further 1 h at 37°C. S1 nuclease digestion was performed in a final volume of 330 µL with 33 U of *Aspergillus oryzae* S1 nuclease (Amersham Pharmacia Biotech) in 1X S1 buffer [20 µg/mL ssDNA (Sigma type XIV DNA), 4.5 mM ZnSO<sub>4</sub>, 0.28 M NaCl, 50 mM NaOAc, pH 4.5]. The reaction was incubated for 30 min at 37°C and stopped by addition of S1 stop solution (0.8 M NH<sub>4</sub>OAc, 8 µg/mL tRNA, 4 mM EDTA pH 8). The resultant RNA-protected DNA fragments were EtOH-precipitated, washed once with 100% EtOH, airdried and resuspended in 10 µL of Sequenase Stop Solution (Amersham). DNA samples were denatured at 95°C for 2 min, incubated on ice for at least 2 min and resolved by electrophoresis. Sequencing reactions were performed using the PCR oligonucleotide as primer and cs0096-9 as template, and were electrophoresed simultaneously with the S1 nuclease reactions as described above (section 2.2.3.2). Radioactive signals were detected by autoradiography for 3-5 d at -80°C with an intensifying screen.

### 2.3.3.3 Electrophoretic Mobility Shift Assay (EMSA)

DNA fragments used for EMSA (Fig. 4.9) were generated by restriction digests of the appropriate PCR product, dephosphorylated, and gel-purified as described above (section 2.2.2.1). Protein samples (cell-free extracts) were prepared without addition of detergents as described below (section 2.4.1)

For use in EMSA 1-2 pmol (50-100 ng) of dsDNA fragment was end-labeled (section 2.2.6.1) and EtOH-precipitated with 20 µg glycogen and 0.5 M NH<sub>4</sub>OAc for 30 min at -80°C. The DNA was pelleted by microcentrifugation, washed with 100% EtOH and airdried briefly. Total radioactivity in the pellet was determined by Cerenkov counting, and the pellet was resuspended in water to a concentration of 10<sup>4</sup> cpm/µL. 5000 cpm (approximately 0.3 ng) of this target DNA was added to a 50 µL reaction containing 0.5 µg poly dI-dC (Amersham Pharmacia Biotech), 10 mM Tris-HCl pH 7.5, 50 mM NaCl, 1 mM EDTA, 5% (v/v) glycerol, 1 mM DTT, and the indicated amount of cell-free extracts. The mixture was incubated 20 min at 37°C and electrophoresed without addition of loading buffer. A non-denaturing gel was prepared according to standard procedures (Ausebel *et al*, 1995) by addition of 100 µL 30% (w/v) APS (Sigma) and 60 µL TEMED (Sigma) to a 40 mL solution of 5% polyacrylamide [acrylamide:bisacrylamide, 37.5:1(Bio-Rad)] in 1X



TBE. Electrophoresis was carried out with 1X TBE at 4°C for 3-4 h at 200 V, or 14-18 h at 40-50 V, and the radioactive signals were detected by autoradiography at -80°C using an intensifying screen.

## **2.4 Manipulation of Protein**

Protease inhibitors used were PMSF (Sigma) or Complete Mini, EDTA-free Protease Inhibitor Cocktail Tablets (Roche) prepared according to manufacturer's instructions. As appropriate, proteins were precipitated on ice with addition of 1% (w/v) sodium deoxycholate/10% (v/v) TCA, and the pellet was washed with 100% cold acetone, airdried and resuspended in 0.1 M Na<sub>2</sub>CO<sub>3</sub>/0.1 M DTT.

### **2.4.1 Preparation of Cell-Free Extracts Containing Soluble Protein from *Synechocystis***

Following centrifugation at 7000 rpm for 10 min at 4°C, the cell pellet from 40-50 mL of a *Synechocystis* culture was resuspended in 1 mL ice-cold 50/100 TE, transferred to a 1.5 mL pre-chilled Eppendorf tube and microcentrifuged 1 min at 5000 rpm. The cell pellet was lysed by one of three methods: (A) After resuspension in cyanobacterial protein extraction buffer (20 mM Tris-HCl pH 8, 10 mM NaCl, 1 mM EDTA, 5 mM DTT, 1 mM PMSF) the cells were lysed by 4 consecutive cycles of one min sonication at a frequency of -077 using a Braun-Sonic 2000 Sonicator, followed by one min incubation in an ice-water bath, or 8 cycles of 30 seconds each. (B) Alternatively, the cells were resuspended in cyanobacterial protein extraction buffer and lysed by mechanical lysis with glass beads as described for RNA extraction but in the absence of phenol. (C) To increase membrane solubilization and cell lysis, cells were resuspended in RNA breakage buffer and lysed by mechanical lysis with beads as described for RNA extraction (section 2.3.1.1) but in the absence of phenol. Insoluble cell debris was pelleted by microcentrifugation at 4°C for 15 min at 14,000 rpm. The supernatant was removed without further treatment and protein concentration was determined by the Bradford Assay (Bio-Rad reagent) with BSA as the standard. Aliquots were stored at -20°C or -80°C, or used immediately. The proteins in cyanobacterial cell-free extracts tended to precipitate if stored at -20°C in the absence of detergents. Method (C) yielded the highest concentration of soluble protein in the cell-free extracts, however the presence of detergents prevented their use in applications that require native protein conditions, and so were limited to Western or FarWestern analyses.

## **2.4.2 Electrophoresis of Proteins**

### **2.4.2.1 SDS-Polyacrylamide Gel Electrophoresis (SDS-PAGE)**

For electrophoresis of denaturing polyacrylamide gels, the MiniProtean (Bio-Rad) apparatus was used according to manufacturer's instructions. Gels were prepared with acrylamide:bisacrylamide (37.5:1) (Bio-Rad). Resolving gels were prepared by addition of 750  $\mu\text{L}$  1.5% (w/v) APS (Sigma) and 7.5  $\mu\text{L}$  TEMED (Sigma) to a 15 mL solution of 10% (w/v) polyacrylamide, 0.1% (w/v) SDS, 0.375 M Tris-HCl, pH 8.8. Stacking gels were prepared by addition of 250  $\mu\text{L}$  1.5% (w/v) APS (Sigma) and 7.5  $\mu\text{L}$  TEMED (Sigma) to a 5 mL solution of 4% (w/v) polyacrylamide, 0.1% SDS, 0.125 M Tris-HCl, pH 6.8. To facilitate size estimation of experimental protein samples, protein standards were included on each gel: either unstained Molecular Weight Standards (Low range; Bio-Rad), Kaleidoscope Prestained Standards (Bio-Rad), or Rainbow High Molecular Weight Range Standards (Amersham Pharmacia Biotech). All samples, including protein markers, were prepared in a final volume of less than 25  $\mu\text{L}$  in 1X loading dye [31.25 mM Tris-HCl, pH 6.8, 1% (w/v) SDS, 5% (v/v) glycerol, 2.5% (v/v) BME, 0.005% (w/v) bromphenol blue]. Samples were vortexed well prior to and following heat-denaturation for 2 min at 95°C, then centrifuged briefly and loaded onto the gel. Electrophoresis was performed with 1X Reservoir Running Buffer [25 mM Tris, 192 mM glycine, 0.1% (w/v) SDS] at 100 V for 1-2 h.

### **2.4.2.2 Non-denaturing Polyacrylamide Gel Electrophoresis**

Native polyacrylamide gels were prepared from a stock solution of polyacrylamide (Life Technologies):bisacrylamide (Aldrich Chemical Company) (30:0.5). Resolving gels were prepared by addition of 30  $\mu\text{L}$  10% (w/v) APS (Sigma) and 30  $\mu\text{L}$  TEMED (Sigma) to a 10 mL solution of 10% (w/v) polyacrylamide, 0.12% (v/v) glycerol, 0.375 M Tris-HCl, pH 8.7. Stacking gels were prepared by addition of 40  $\mu\text{L}$  10% (w/v) APS (Sigma) and 8  $\mu\text{L}$  TEMED (Sigma) to a 10 mL solution of 4% (w/v) polyacrylamide, 0.12% (v/v) glycerol, 0.125 M Tris-HCl, pH 6.8. Samples were prepared in 0.02% (v/v) BME, 10% (v/v) glycerol, 0.016% (w/v) Bromphenol blue, 10 mM Tris-HCl pH 6.8. Electrophoresis was performed with 7.7 mM glycine/1 mM Tris-HCl pH 8.3 as the running buffer, at 100 V for 2-3 h.

### **2.4.2.3 Staining of Polyacrylamide Gels**

Following electrophoresis, proteins were visualized by fixing and removal of SDS for 30 min in destain solution [30% (v/v) methanol, 10% (v/v) acetic acid], staining with Coomassie Brilliant Blue Stain [45% (v/v) methanol, 10% (v/v) acetic acid, 0.25% (w/v) Coomassie Brilliant Blue R250] and destaining with fresh destain solution until the desired contrast between the bands and the background was obtained. Gels were then soaked in sterile 2% (v/v) glycerol for at least 30 min. Alternatively, to visualize small amounts of protein, Silver Stain Plus (Bio-Rad) was used according to manufacturer's instructions for polyacrylamide gels, with glassware and equipment that had been washed with 50% (v/v) nitric acid and rinsed with water. Gels were dried under vacuum using a Slab Gel Dryer and Gel Pump (Savant).

## **2.4.3 Over-Expression and Purification of Recombinant CrhR Proteins**

### **2.4.3.1 pGEX-2T, GST Fusion Protein System (Amersham Pharmacia Biotech)**

#### **2.4.3.1.1 Cloning**

A 1927 bp dsDNA fragment containing the entire *crhR* ORF was obtained by Taq polymerase PCR using GWO25/GWO26 as primers (Table 2.4) and cs0096-9 as the template with the program SLK (Table 2.5). This dsDNA fragment was cloned into the pGEX-2T Glutathione S-transferase Gene Fusion Vector (Amersham Pharmacia Biotech) after digestion of both insert and vector with *Bam* HI/*Eco* R1. The resultant 6.88 kb clone is designated pGEX:*crhR*, and the fusion protein obtained is GST:CrhR (Table 2.3 and Fig. 3.5). Screening of ligation products was aided by Rosa Spencer (Wisest student, 1996). Potential pGEX:*crhR* clones were identified by restriction analysis with *Bam* HI, *Eco* RI, and *Bst* EII; selected clones were confirmed by DNA sequencing with the oligonucleotide primers GWO33, GWO34, and SLK1 through SLK7 (Table 2.4).

#### **2.4.3.1.2 Over-Expression and Purification of GST:CrhR**

Since the pGEX:*crhR* clone was constructed in *E. coli* DH5 $\alpha$ , initial over-expression and analyses were performed with this host. The construct was subsequently electroporated into *E. coli* JM109. Cells were grown in LB, TSB or 2XYT with Ap (100  $\mu$ g/mL) selection, and 2% (w/v) glucose for repression of the pGEX-2T tac promoter as necessary.

Typically, a 5 mL culture was inoculated from a single colony and grown to OD<sub>600</sub>>1. This was diluted 1/100 into fresh medium and grown at 37°C to OD<sub>600</sub>=0.6, at

which point an aliquot was removed for analysis as the "uninduced" control. The remaining cells were induced by addition of 0.4 mM IPTG and grown at 37°C for a further 3 h, then harvested by centrifugation at 4°C, frozen in liquid N<sub>2</sub> and stored at -80°C. For preliminary analysis of whole cell extracts by SDS-PAGE, an aliquot equivalent to 0.1 OD<sub>600</sub> was resuspended in 400 µL of 0.1 M DTT/ 0.1 M NaCO<sub>3</sub> and loading dye was added. Samples were boiled 1 min, vortexed vigorously and microcentrifuged 5 min at 14000 rpm to pellet the cell debris and nucleic acids. Alternatively, the cells were lysed by 1 min sonication or by single passage through a French press, and the lysate was clarified by 15 min microcentrifugation prior to addition of loading dye.

The procedures for preparation of Glutathione Sepharose 4B, batch purification of the fusion protein GST:CrhR, cleavage of GST:CrhR into the constituent polypeptides by digestion with thrombin, and CDB Assay for GST activity in various cell extracts were performed according to the manufacturer's instructions. Various modifications suggested by Frangione and Neel (1993) were also adapted to GST:CrhR purification, specifically the use of lysozyme in STE to increase cell lysis. Following incubation with Glutathione-Sepharose 4B, GST:CrhR was eluted with 10 mM reduced glutathione in either: (a) 75 mM HEPES-KOH pH 7.4, 150 mM NaCl, 5 mM DTT, 0.1% (v/v) Triton X-100 (Frangione and Neel, 1993); (b) 50 mM Tris-HCl pH 8 (Amersham Pharmacia Biotech protocol); (c) 50 mM Tris-HCl pH 8, 150 mM NaCl; (d) 50 mM Tris-HCl pH 8, 150 mM NaCl, 5 mM DTT; (e) 50 mM Tris-HCl pH 8, 150 mM NaCl, 5 mM DTT, 0.1% (v/v) Triton X-100; or (f) 5 mM DTT, 50 mM Tris-HCl pH 8. Thrombin cleavage was performed by addition of 10 cleavage units or 2 NIH units of thrombin (Sigma) per mg of fusion protein estimated to be in the solution.

#### **2.4.3.2 pRSETA, HIS-Tagged Fusion Protein System (Invitrogen)**

##### **2.4.3.2.1 Cloning**

The *crhR* ORF was cloned into pRSETA by Dr. D. Chamot (University of Alberta). The 2.1 kb DNA fragment from bp#2888247-2890397, which contains the 3' sequence of *crhR* and x bp downstream sequence, was generated by *Dra I/Eco RI* digestion of cs0096-9. The 610 bp *crhR* fragment from bp#2887644-2888246 was generated by *Dra I/Bam HI* digest of the 1907 bp fragment that had been amplified by PCR using the Expand enzyme with the primers GWO25+GWO26 and cs0096-9 as the template. pRSETA was digested with *Bam HI/Eco RI*, purified and ligated to the 2.1 kb *Dra I/Eco RI* fragment containing *crhR*. The desired product from this initial ligation was mixed with the purified 610 bp *Bam HI/Dra I* fragment in a second ligation reaction, and transformed into *E. coli*

DH5 $\alpha$ . The resultant clone was confirmed by sequencing and electroporated into *E. coli* JM109. This clone is designated pRSET:*crhR* and the recombinant protein obtained following over-expression and purification is designated HIS:CrhR (Fig. 3.5).

#### 2.4.3.2.2 Over-Expression and Purification of HIS:CrhR

Over-expression and purification of HIS:CrhR was performed according to manufacturer's specifications. Briefly, a 5 mL culture of *E. coli* JM109(pRSETA:*crhR*) was inoculated from a single colony and grown to OD<sub>600</sub>>1. This was diluted 1/50 into fresh LB containing Ap (100  $\mu$ g/mL), and grown at 37°C with shaking for 2 h, or until the culture reached OD<sub>600</sub>=0.6-0.8. For synthesis of HIS:CrhR from the T7 phage promoter, 400  $\mu$ L of T7 phage and 1 mM IPTG were added and the culture was incubated a further 1.5-2 h at 37°C with shaking. The cells were harvested by 10 min centrifugation at 5000 rpm in a JA-20 rotor at 4°C. The supernatant was decanted and the pellet was frozen in liquid N<sub>2</sub> for long-term storage at -80°C. Alternatively, the pellet was resuspended in salt buffer (300 mM NaCl, 50 mM NaH<sub>2</sub>PO<sub>4</sub> pH 8) or lysis buffer (10 mM imidazole in salt buffer) at 1/10 of the original culture volume, and 1 mL aliquots were used immediately or frozen in liquid N<sub>2</sub> for storage at -80°C. Cells were lysed by mechanical lysis with beads or sonication as described above (section 2.4.1). Best results were obtained with sonication for 4 repetitions of (30 s sonication, 30 s cooling) performed while cells were in an ice-water bath. Following a 15 min microcentrifuge at full speed at 4°C, the supernatant was removed; where appropriate, the pellet was resuspended in the original volume of lysis buffer with addition of 0.2% (w/v) sarkosyl, and solubilized at r.t. for 20 min with shaking. The remaining insoluble debris was pelleted by 1 min microcentrifugation at 1000 rpm (82 x g). Meanwhile, Ni-NTA agarose matrix (Qiagen) was prepared as a 50% slurry following two washes with lysis buffer.

To allow binding of HIS:CrhR, the solubilized and/or clarified supernatant was incubated with 1/4 volume of prepared Ni-NTA agarose in lysis buffer for 1 h at 4°C with gentle agitation. This mixture was transferred to a Poly-Prep Chromatography Column (Bio-Rad) either before or after the binding reaction. All further procedures were carried out at 4°C with ice-cold solutions. Column wash and elution solutions were prepared as salt buffer with addition of imidazole as follows: Wash I, 20 mM imidazole; Wash II, 50 mM imidazole; Wash III, 100 mM imidazole; Wash IV, 150 mM imidazole; Elution buffer,

250 mM imidazole. Wash and elution volumes were altered as appropriate for the intended use of the eluate. During the lysis and purification procedure, samples of each fraction were collected for subsequent SDS-PAGE and Western analysis.

Eluate containing HIS:CrhR for use in the RNA helicase and ATPase assays was prepared as described above, with the following modifications: 1.5  $\mu\text{g}/\text{mL}$  RNase A was added to the clarified supernatant during the binding reaction. The column was washed with 5X 1 vol Wash I, 2X 0.5 vol Wash II, 0.5 vol Wash III, 0.1 vol Wash IV and 50  $\mu\text{L}$  of elution buffer. HIS:CrhR was eluted with 75  $\mu\text{L}$  of elution buffer, and the protein concentration of the eluate was determined by Bradford assay.

Columns that were incubated with the supernatant that was obtained following solubilization of the initial lysis pellet yielded large amounts of denatured HIS:CrhR. Due to the presence of sarkosyl this eluate was useful only for preparation of HIS:CrhR as antigen as described below (section 2.4.4).

## **2.4.4 Generation of Rabbit Polyclonal Anti-CrhR Antiserum**

### **2.4.4.1 Large-Scale Preparation and Purification of HIS:CrhR**

Eluates obtained from multiple large-scale preparations of HIS:CrhR were TCA precipitated, pooled, and loaded onto a preparative gel for separation by SDS-PAGE. Following electrophoresis, the protein bands were visualized by incubating the polyacrylamide gel in a solution of 0.25 M KCl/2 mM DTT, with gentle shaking at 4°C for 5 min. A significant band of protein corresponding to the expected size of the HIS:CrhR fusion protein was apparent and this narrow region of the gel was excised with a sterile scalpel.

### **2.4.4.2 Electroelution of Proteins from Polyacrylamide Gel**

Electroelution of HIS:CrhR from the polyacrylamide gel was carried out using the Electrophoretic Elution System EE-04 (Tyler Research Instruments) according to the manufacturer's instructions. The bottoms of the large and small wells of the electrophoretic elution cell were fitted with 2-inch squares of prepared dialysis membrane (SPECTRA/POR molecularporous membrane tubing, 10 mm wide, Fisher Scientific, 12-14 kDa molecular weight cut off) secured with 3 rubber O-rings for each well. The dialysis membrane had been previously prepared by successive 1 h, 60°C incubations first in 1% (w/v)  $\text{NaHCO}_3$ , then in 0.1% (w/v) SDS, with distilled water rinses after each incubation; the membrane was stored at r.t. in 0.1% (w/v) SDS/0.1% (w/v)  $\text{NaN}_3$  until needed. The gel slice containing HIS:CrhR (prepared according to section 2.4.4.1) was rinsed with

water, and further sliced into 1 mm<sup>2</sup> pieces that were soaked in elution buffer [0.1% (w/v) SDS, 0.05 M NH<sub>4</sub>HCO<sub>3</sub>] for 5 min. The gel pieces were transferred into the large well of the electrophoretic elution cell, where they were covered with 1 mL soaking buffer [0.1% (w/v) DTT, 2% (w/v) SDS, 0.4 M NH<sub>4</sub>HCO<sub>3</sub>] and then gently overlaid with enough elution buffer to fill both wells of the elution cell, taking care to remove all bubbles from the cross passage. The elution cell was fitted into the elution tank and air bubbles were removed from underneath the dialysis membrane that was covering the elution cell caps. The gel pieces were soaked for 3-5 h prior to electroelution at 50 V for 12-18 h with the polyacrylamide gel pieces at the anode. Then the elution buffer in the tank and mixing chamber was replaced with dialysis buffer [0.2% (w/v) SDS, 0.01 M NH<sub>4</sub>HCO<sub>3</sub>], bubbles were again removed from underneath the elution cell caps, and elution-dialysis was performed for a further 4-6 h at 80 V. During electrophoresis, the buffers were slowly recirculated from the mixing chamber into the electrode chambers of the tank by a peristaltic pump (Watson Marlon-503S) at a rate of 3 mL/min. Once electroelution was complete, the buffer was removed from the elution cell, and HIS:CrhR was recovered from the sample collection well at the cathode side, in a total volume of approximately 250 µL (pooled from 200 µL in the initial collection, and 50 µL after rinsing the well with fresh dialysis buffer).

#### **2.4.4.3 Preparation of Anti-CrhR Polyclonal Antiserum**

For generation of polyclonal antiserum in rabbits, BioSciences Animal Service was responsible for care of the animals, including injections, bleedings, and final harvesting. The anti-CrhR antiserum was generated by injecting two rabbits with antigen, namely HIS:CrhR fusion protein that had been purified and concentrated as described above (sections 2.4.4.1 and 2.4.4.2). Approximately 250 µg of the antigen was added to an equal volume of Freund's Complete Adjuvant (Serva) in a maximum total volume of 1.8 mL, and mixed well to obtain a milky emulsion. Prior to the first injection, 5 mL of blood was collected, allowed to coagulate for 1 h at r.t, and centrifuged 15 min at 5000 rpm. This supernatant, referred to as the pre-immune serum, was collected and stored in small aliquots in Eppendorf tubes at -80°C, for comparison with anti-CrhR antiserum and for use as a control. Unfortunately, one of the rabbits died of a bacterial infection within 24 hours of the first injection, but the remaining rabbit was boosted 3 times at 4 week intervals, with 250 µg of protein in Freund's Incomplete Adjuvant (Serva). Test-bleeds (5 mL) were taken ten days after each boost, and antiserum was prepared as described above for the pre-immune serum. Following the third and final boost, the anti-CrhR antiserum was prepared

as described for the pre-immune serum and dispensed in small aliquots that were kept at -80°C for long-term storage or 4°C for regular use.

#### **2.4.5 Western Analysis**

Cell-free extracts (section 2.4.1) were separated on SDS-PAGE gels as described (section 2.4.2.2), using equivalent total protein (generally 15-30 µg) in each sample as determined by the Bradford assay and confirmed by CBB staining (section 2.4.2.3) of a duplicate gel or Ponceau S staining of the nitrocellulose membrane after electroblotting.

Proteins in unstained polyacrylamide gels were transferred onto 0.45 micron nitrocellulose membrane (Bio-Rad) by semi-dry electroblotting, using an Electrophoretic Transfer System ET-10 (Tyler Research Instruments). The nitrocellulose membrane, Whatmann 3MM and polyacrylamide gel components were soaked at least 10 min in 1X transfer buffer [25 mM Tris, 192 mM glycine, 20% (v/v) methanol] and assembled on the bottom plate of the transfer apparatus in the following order: two pieces of Whatmann 3MM paper; polyacrylamide resolving gel; nitrocellulose membrane cut to size and marked for orientation; two pieces of Whatmann 3MM paper. During assembly all air bubbles were removed from between the layers. The top plate of the transfer apparatus was screwed in place tightly, and transfer was carried out for 1 h at 52 mA, with the gel at the cathode side and the nitrocellulose membrane at the anode side. Following transfer proteins were visualized on the nitrocellulose membrane by staining with Ponceau S for 5 min; progressive rinsing with distilled water was used to completely remove the dye before proceeding.

For the purpose of microsequencing, proteins in unstained polyacrylamide gels were transferred onto Sequi-blot PVDF (polyvinylidene difluoride) membrane (Bio-Rad) by tank electroblotting using the Trans-Blot Cell (Bio-Rad) according to manufacturer's instructions. The transfer components were assembled as described above and electrophoresed at 4°C with 100 V for 30 min, using a solution of [10% (v/v) methanol, 10 mM CAPS (3-[cyclohexamino]-1-propanesulfonic acid), pH 11] as the transfer buffer. Following transfer the PVDF membrane was washed 3X with distilled water for 5 min each, stained for 15 min by soaking in a solution of [0.025% (w/v) Coomassie Blue R-250, 40% (v/v) methanol], and destained by soaking for 5 min in 50% (v/v) methanol. The appropriate band of protein was excised and submitted to the Protein Microchemistry Centre, c/o Department of Biochemistry and Microbiology, University of Victoria, Victoria BC.



Western analysis was carried out as described (Harlow and Lane, 1988). The unstained nitrocellulose membrane was incubated in 1X Blotto [5% (w/v) skim milk powder (Difco), 0.02% (v/v)  $\text{NaN}_3$ , in 1X TBS (150 mM NaCl, 10 mM Tris-HCl pH 8)] for 15-30 min at r.t. with gentle agitation. Rabbit pre-immune serum or anti-CrhR antiserum (section 2.4.4.3) was subsequently added at a dilution of 1/2000 to 1/200 (v/v) and incubated for 14-20 h. Three consecutive washes were performed for at least 5 min each with 1X TBS, 1X TBST [0.05% (v/v) Tween-20 in 1X TBS], and 1X TBS. The membrane was then incubated with peroxidase-conjugated goat anti-rabbit IgG (Sigma) at 1/1000 dilution in fresh 1X TBS at r.t. for at least 3 h. The three consecutive washes were repeated and bands were visualized with Western Color Developer [0.02% (v/v)  $\text{H}_2\text{O}_2$  (BDH), 0.5 mg/mL chloro-naphthol (dissolved in methanol), in 1X TBS] in darkness for 5-60 min. Developed blots were rinsed well in distilled water, dried, and stored airtight at 4°C.

#### 2.4.6 FarWestern Analysis

FarWestern analysis was performed as previously described (Ausebel *et al*, 1995). Cell-free extracts were separated by SDS-PAGE and transferred onto nitrocellulose membrane by electro-blotting as described above (section 2.4.5). The membrane-immobilized proteins were denatured by 10 min incubation in a solution of 8 M urea in 1X HBB (2.5 mM HEPES-KOH pH 7.5, 25 mM NaCl, 5 mM  $\text{MgCl}_2$ , 1 mM DTT) and renatured by successive 10 min incubations in 4 M, 2 M, 1 M, and 0.5 M urea in 1X HBB. Finally, the membrane was incubated 5 min in 1X HBB without urea prior to 30 min incubation in a solution of 5% (w/v) skim milk in 1X HBB.

Meanwhile, HIS:CrhR was column purified using the following wash volumes: 4X 1 ml of Wash I; 2X 500  $\mu\text{l}$  of Wash II; 500  $\mu\text{l}$  of Wash III; 100  $\mu\text{L}$  of Wash IV. Purified HIS:CrhR was obtained in a final volume of 250  $\mu\text{L}$  of elution buffer, in order to maximize recovery of the fusion protein from the column.

The membrane was then incubated with the column-purified HIS:CrhR at a final concentration of 2  $\mu\text{g}/\text{mL}$  in buffer D [20 mM HEPES-KOH pH 7.5, 75 mM KCl, 25 mM  $\text{MgCl}_2$ , 0.1 mM EDTA, 1 mM DTT, 0.1% (v/v) nonidet P40, 1% (w/v) skim milk powder]. Following 14-24 h of incubation at r.t. with gentle shaking, the membrane was washed by 5 consecutive 10 min incubations in 1X TBST/1 mM DTT and incubated a further 3 h with addition of anti-CrhR antiserum at 1/100 (v/v) dilution. Immobilized proteins that interact with HIS:CrhR were visualized on the membrane as described for Western analysis (section 2.4.5) with the addition of 1 mM DTT to all solutions and very

gentle agitation; developing was performed for 55 min in darkness. A duplicate membrane was subjected to Western analysis for comparison.

#### **2.4.7 Biosynthetic Labeling of Proteins**

Biosynthetic labeling of cells was performed as described (Ausebel *et al.*, 1995) with modifications. Sulfate-free liquid BG11 medium was prepared by replacing the sulfate-containing constituents  $\text{MgSO}_4$ ,  $\text{ZnSO}_4$ , and  $\text{CuSO}_4$  with an equal molarity of  $\text{MgCl}_2$ ,  $\text{ZnCl}_2$ , and  $\text{Cu}(\text{NO}_3)_2$ , respectively, and 10 mM HEPES-KOH pH 7.5 was added to increase the efficiency of incorporation. 50 mL cyanobacterial cultures were grown to mid-log phase ( $\text{OD}_{750}=0.4-0.8$ ) and pelleted by 5 min r.t. centrifugation at 300xg (2000 rpm in the JA-20 rotor). Meanwhile, sulfate-free liquid BG11 medium was pre-warmed to 30°C. The supernatant was decanted carefully, the soft cell pellet was washed twice (20-30 mL pre-warmed medium) and gently resuspended in 75 mL of pre-warmed sulfate-free BG11. Cells were incubated at 30°C with illumination (2 sets of lights) and shaking at 150 rpm for 5-10 min prior to further incubation in the presence of 1  $\mu\text{Ci/mL}$  [ $^{35}\text{S}$ ]-Methionine (Amersham) for 1.5-2 h. Alternatively, the cells were labeled at 20°C for 2 h, or at 30°C for 1 h followed by 20°C for 1 h.

#### **2.4.8 Immunoprecipitation**

Immunoprecipitation was performed as described (Ausebel *et al.*, 1995) with modifications. To prepare the protein A-Sepharose (Sigma), 0.025 g of lyophilized powder was swollen in 1 mL of a solution of 1 mg/mL BSA in 120 mM NaCl/20 mM sodium phosphate pH 8 and stored at 4°C. For use in the immunoprecipitation reaction, an aliquot of swollen protein A-Sepharose was washed 3X with dilution buffer {0.1% (v/v) Triton X-100, 0.1% (w/v) BSA in TSA [140 mM NaCl, 0.025% (w/v)  $\text{NaN}_3$ , 10 mM Tris-HCl pH 8]}. Cell-free extracts were prepared from a biosynthetically labeled culture by mechanical lysis with beads as described above (section 2.4.1), except that the lysis buffer was replaced with a solution of 1% (w/v) BSA in TSA. The cell lysate was clarified by 15 min microcentrifugation at 4°C, and incubated for 1.5 h with 1/20 (v/v) dilution of prepared protein A-Sepharose. Following 1 min microcentrifugation at 80xg and 4°C, the protein A-Sepharose pellet was washed and eluted as described below. The supernatant, referred to as the pre-treated clarified lysate, was stored in 200  $\mu\text{L}$  aliquots at -80°C or used

immediately. For immunoprecipitation, an aliquot of pre-treated clarified lysate was diluted 1:3 with dilution buffer and antiserum was added at 1/200 (v/v) dilution. The mixture was incubated on ice for 1.5 h with occasional gentle mixing by inversion. Prepared protein A-Sepharose was added at 1/20 (v/v) dilution and the mixture was further incubated with gentle shaking for 1.5 h in an ice-water bath. The protein A-Sepharose::immunoprecipitate complexes were pelleted by 5 sec full-speed microcentrifugation at 4°C and the supernatant was carefully removed by pipetting. The pellet was washed with 2X 1 mL dilution buffer, 1X 500 µL TSA, and 1X 25 µL 0.05 M Tris-HCl pH 6.8, and 50 µL SDS-PAGE loading dye (section 2.4.2.3) was added without mixing. The immunoprecipitation complexes were solubilized and denatured by heating for 15 min at 50°C followed by 5 min at 90°C, and resolved by SDS-PAGE (section 2.4.2.1). Following electrophoresis, the gel was stained with Coomassie Brilliant blue, dried under vacuum, and the radioactive signals from <sup>35</sup>S-labeled proteins were visualized by autoradiography at r.t. for 5 weeks.

Alternatively, the immunoprecipitation procedure was modified by replacing TSA with a solution of (50 mM NaCl, 0.025% (w/v) sodium azide, 10 mM Tris-HCl pH 8).

## **2.5 *In vitro* Biochemical Analyses**

### **2.5.1 ATPase Assays**

Standard *in vitro* ATP hydrolysis assays were carried out as previously described (Rodriguez and Carrasco, 1993) in a 20 µL final reaction volume that contained 20 mM HEPES-KOH pH 7.5, 1 mM DTT, and 3 µCi [ $\gamma$ -<sup>32</sup>P]ATP, with the addition of 5 mM MgOAc, 40 µM ATP, and 5-10 ng/µL total RNA from *Synechocystis* as appropriate. Unlabelled dATP, CTP, GTP, and UTP (Roche) were tested at 3 mM, and unlabeled ATP (Roche) was tested at 40 µM to 6 mM. Reactions were prepared on ice. Meanwhile, HIS:CrhR was prepared as described above (section 2.4.3.2.2), the concentration of the eluate was determined by the Bradford assay and subsequently confirmed by SDS-PAGE and Western analysis. HIS:CrhR was routinely added in a volume of 2.5 µL, to yield 25 ng/µL protein and 31.25 mM imidazole. The reaction was mixed gently, incubated at 37°C for 30 min, and stopped by addition of 5 µL 0.5 M EDTA pH 8. From each reaction, 2 µL was spotted in an asymmetric pattern onto a pencil line drawn 1 cm from the bottom of a 10 cm high thin layer chromatography (TLC) plate [flexible TLC plates, cellulose PEI, 100 micron, Selecto Scientific (Georgia, USA)]. The plates were developed with 0.15 M formic acid/0.15 M LiCl as the mobile phase for 20 min or until the mobile phase reached the top of the plate, allowed to air-dry briefly, and covered with plastic wrap.

Radioactive signals were detected by autoradiography with intensifying screens at r.t. for 20-60 min, or with a Phosphor Screen.

### 2.5.2 RNA Helicase Assays

RNA helicase assays were performed according to the method of Pause and Sonenberg (1995). All solutions and labware were kept free from RNase contamination as described above (section 2.3). RNA substrate, RNA II, was generated using pGEM3 (Promega) and pGEM-MO1/2 vectors. pGEM3 was linearized with *Bam* HI and transcribed with SP6 polymerase (Promega), yielding a 41 nt transcript with the sequence GAAUACAAGCUUGCAUGCCUGCAGGUCGACUCUAGAGGAUC. pGEM-MO1/2 was linearized with *Hinc* II and transcribed with T7 polymerase (Promega), yielding a 68 nt transcript with the sequence GGGAGACCGGAAUUCCCAUGGCUGACUAAUUU UUUUUAUUUAUGCAGAGGGGGGAUCCUCUAGAGUC. Underlined nts indicate the 14 bp region of complementary sequence. Transcriptions were performed using a Riboprobe *in vitro* Transcription System kit (Promega) according to the manufacturer's protocol. The 41 nt strand was synthesized with addition of [ $\alpha$ -<sup>32</sup>P]UTP (Amersham Pharmacia Biotech), while the 68 nt strand was synthesized using unlabelled nucleotides. The transcripts were resolved on a denaturing (8 M urea) 6% polyacrylamide (30:0.5 acrylamide:bisacrylamide) gel with 1X TBE as the buffer system. The labeled strand was visualized by autoradiography for 2 min at r.t. and the non-radioactive strand was visualized by UV shadowing. The transcripts were excised and eluted in RNA elution buffer (0.5 M NH<sub>4</sub>OAc, 1 mM EDTA, 0.1% SDS) overnight at 4°C, then extracted once with phenol:chloroform (1:1, v/v) and once with chloroform:isoamyl alcohol (24:1, v/v) before EtOH-precipitation for 30 min at -80°C. The transcripts were washed, airdried, and resuspended in 15  $\mu$ L RNA annealing buffer (150 mM NaCl, 1 mM EDTA, 20 mM HEPES-KOH pH 7.2). Hybridization was performed by mixing the two transcripts, heating at 95°C for 2 min, then cooling to 37°C over 1 h with further 2 h incubation at 37°C. Duplex RNA was purified on a native 8% polyacrylamide gel, visualized, excised, eluted, extracted and precipitated as described for the ssRNA transcripts.

Standard RNA helicase assays were performed with column-purified HIS:CrhR (30 ng/ $\mu$ L) in a 20  $\mu$ L reaction mixture containing 100 cpm/ $\mu$ L dsRNA substrate, 3 mM MgCl<sub>2</sub>, 3 mM ATP, 200  $\mu$ g/mL BSA, 1 mM DTT, 20 mM HEPES-KOH, pH 8.5. Reactions were mixed gently, incubated at 37°C for 15 min, and stopped by addition of 5

$\mu$ L RNA helicase stop solution [150 mM EDTA, 3% (w/v) SDS, 0.25% (w/v) Bromophenol blue, and 15% (w/v) Ficoll]. Aliquots (12.5  $\mu$ L) were resolved by SDS-PAGE using a 10% polyacrylamide gel (section 2.4.2.1). Electrophoresis was carried out at 100 V for 1.5-2 h or until the bromophenol blue was 2 cm from the bottom of the gel. Radioactive signals were detected overnight by autoradiography with an intensifying screen at -80°C or by exposure to a Phosphor Screen (Molecular Dynamics).

## 2.6 Computer Analyses and Graphic Images

This thesis was produced using Microsoft Office 97-98 software except as indicated. Graphic images were generated by scanning original autoradiograms and Western blot membranes. The originals were scanned at an optical resolution of 300-1000 dpi, most commonly at 800 dpi, using a Color One scanner and Ofoto software (version 2) (Light Source Computer Images Inc.), or the SNAPSCAN 310 (AGFA) and Photoshop LE software (Adobe Products). Alternatively, the signal from radioactive decay was captured by exposure of a Phosphor Screen (Molecular Dynamics) that was subsequently scanned at 176 microns using the Phosphor Imager 445SI and ImageQuant™ v. 4.1 image analysis software (Molecular Dynamics). No alterations were made to the computer images other than improving the brightness and contrast of the entire image, and cropping to the appropriate size. Images were saved as .tif files, transferred into Microsoft Powerpoint for labeling and printed using a LaserJet 4Plus (Hewlett Packard) laser printer. For quantitation of various autoradiograph signals, NIH Image software (version 1.61) (Scientific Computing Resource Center, National Institutes of Health) was used to perform densitometric analysis of the scanned images. Linear regression analysis and graphic representations were performed in Microsoft Excel.

*Synechocystis* genomic sequence and additional information on the genome are available at the Cyanobase site address <http://www.kazusa.or.jp/cyano/cyano.html>.

The National Centre for Biotechnical Information (NCBI) search engine BLASTN was used to search GenBank, EMBL, DDBJ, and PDB sequences for comparison to the unknown sequences obtained during cloning, including those obtained from a genomic library of *Synechococcus* sp. strain PCC 7942 (section 3.2.1). The oligonucleotides used for primer extension analysis were designed by the Genetics Computer Group (GCG) v. 8 program (Wisconsin Sequence Analysis Package) using the PRIME command after entering the stretch of DNA sequence downstream of the predicted 5' end of the *crhR* transcript. As appropriate, the GeneTool™ and PepTool™ (BioTools Inc.) were used for DNA and protein analyses.

## **CHAPTER THREE**

### **Genetic Analysis of a Putative RNA Helicase Gene in the Cyanobacterium *Synechocystis* sp. strain PCC 6803**

### 3.1 Introduction

Implicit in the study of genes are a number of general assumptions. Perhaps the most unconscious and yet the most fundamental of these is the expectation that a particular gene is present in the genome of a particular organism for a purpose. In other words, the gene product is designed to provide an essential function or a useful (albeit non-essential) growth advantage at some point in the cell cycle. The initial identification and cloning of the open reading frame for a gene of interest enables further phenotypic and physiological analyses, as well as preliminary sequence analysis for nucleotide and/or deduced amino acid motifs, including homology to proteins whose structure or function has been previously established. Construction and analysis of gene disruption and gene replacement mutants with a discernible and distinct phenotype may also provide key information on the biological function of the gene product.

The investigation of gene function in cyanobacteria is generally complicated by their characteristic polyploidy, where each cell contains multiple copies of the genome. The degree of ploidy depends on growth rate, which in turn is influenced by the availability of light and carbon dioxide, these being the key nutrients for growth. In *Synechocystis* this has been estimated as an average of 12 genomes per cell (Labarre *et al*, 1989). Polyploidy has several implications for the study of mutants. Following an initial mutational event in one chromosome, cells that are homozygous for the mutation (all genomic copies of the gene carry the mutation) are obtained by a procedure of serial transfers. For example, if the cells contain ten chromosomes, a homozygote cannot appear before at least four cell generations if the chromosomes segregate randomly (Haselkorn, 1991) and more generations would be necessary in order to obtain an entire population of homozygous cells. If the mutation is recessive, the phenotype will be masked by wild-type copies of the gene in heterozygous cells. Where the gene is essential for cell viability, non-random segregation of the chromosomes occurs and homozygous mutants cannot be generated. Instead, the population of cells will always be heterozygous at that locus, detected as incomplete inactivants that maintain both wild-type and mutant copies of the gene in the same cell. Thus a homozygous genotype must be confirmed by an adequately sensitive technique that can detect the non-mutated copies of the gene. A homozygous mutation is considered to be stable if it is maintained in the absence of selection (LaBarre *et al*, 1989).

As in other systems, gene-specific mutations can be generated in cyanobacteria by inserting a selectable marker into a subclone of the open reading frame at a point that will disrupt transcription and translation, and then transforming wild-type cells with this construct. To obtain homologous recombination between the construct and the

chromosome, the selectable marker must be flanked by sufficient genomic DNA (Golden *et al*, 1987), at least 0.9 kb to 2.3 kb in *Synechocystis* (LaBarre *et al*, 1989). Occurrence of a single (or odd number of) cross-over event(s) between the homologous regions results in insertion of the entire transforming plasmid. The mutants will be merodiploids containing wild-type and mutant copies of the locus in tandem in the chromosome (Golden *et al*, 1987; Haselkorn, 1991; Thiel, 1994). In contrast, a double crossover event leads to gene conversion by replacement of wild-type sequences with the transforming selectable marker, with subsequent loss of the vector sequence. While single crossovers are favoured in some species, double crossovers preferentially occur in *Synechocystis* (Golden *et al*, 1987; Thiel, 1994).

Transformation of many cyanobacterial species is complicated by difficulties in introducing foreign DNA into the cells. Various tri-parental mating schemes are employed and relatively few vectors have been engineered specifically for use in cyanobacteria (Ferino and Chauvat, 1989; Thiel, 1994). Transformation is facilitated by a suitable suicide-type vector such as pBR322, which lacks a cyanobacterial origin of replication such that heterologous sequences are lost following recombination. *Synechocystis* is an excellent choice for genetic engineering, being naturally competent for transformation by exogenous DNA. DNA uptake is due to a Ca<sup>2+</sup>-dependent nuclease that is located in the cytoplasmic membrane (Scharnagl *et al*, 1998). Furthermore, while *Synechocystis* possesses three different sequence-specific methylation recognition sites for chromosomal DNA, neither restriction endonuclease activities nor the respective endonuclease genes are present (Scharnagl *et al*, 1998).

In the present study the isolation of a DEAD-box protein gene was pursued in two unicellular cyanobacterial species belonging to the family Chroococcales. In *Synechocystis*, the subcloned open reading frame is designated *crhR*, and has been disrupted by insertion of a selectable marker. The mutants were assessed for homozygosity at the *crhR* locus as well as qualitative and quantitative growth phenotypes under various conditions of aeration, illumination, and/or exogenous glucose.

## **3.2 Results**

### **3.2.1 Initial Attempts to Isolate a DEAD-box Gene from *Synechococcus* sp. strain PCC 7942**

The unicellular *Synechococcus* sp. strain PCC 7942 (hereafter referred to as *Synechococcus*) is widely used as a model cyanobacterium, including significant research in the areas of photosynthesis and gene regulation, hence stock cultures are routinely



maintained in the laboratory. The availability of a *Synechococcus* genomic library (gift of S. Golden, Texas A&M University, USA) facilitated screening for a DEAD-box RNA helicase gene. The library was digested with *Eco* RI and Southern analysis was performed using random-primer-labeled DNA probes from two putative RNA helicase genes from *Anabaena* sp. strain PCC 7120: A 348 bp fragment of *crhB*, containing the VLDEAD and SAT motifs; and a 780 bp fragment of *crhC*, containing the VLDEAD, FAT, DIAA, and HRIGR motifs (Chamot *et al*, 1999). The “8C12” clone from the *Synechococcus* library hybridized to both probes and was partially sequenced. A BLASTN search indicated 97% identity with the *E. coli kdpABC* operon encoding the Kdp-ATPase proteins -A, -B, and -C. Since 97% identity would be unusually high homology between homologues for any cyanobacterial and *E. coli* gene, this clone likely originated from *E. coli* DNA contamination of the original *Synechococcus* library, therefore this line of research was not continued. Hybridization of the DEAD-box probes to this region of *E. coli* DNA is likely due to sequence homology with the NTP binding motif (VLDEAD). Although the DNA that was cloned is not the desired DEAD-box gene from *Synechococcus*, these results confirm the validity of *crhB* and *crhC* gene fragments as probes for detecting genes with NTP binding and hydrolysis motifs.

### 3.2.2 Subcloning of the *crhR* Open Reading Frame

A web-based search was performed of the 1.1 Mbp of *Synechocystis* sp. strain PCC 6803 genomic sequence available at Cyanobase (<http://www.kazusa.or.jp/cyano/cyano.html>) (G.W. Owtrim, personal communication). This search and the published genomic sequence analyses performed by Kaneko *et al* (1995a, 1995b, 1996a, 1996b) identified a single open reading frame whose deduced amino acid sequence contains the consensus motifs characteristic of the family of DEAD-box RNA helicases (Fig. 1.1). The entire *Synechocystis* genomic sequence has been deposited in 27 Genbank entries and each base pair of DNA has been assigned a reference number according to its relative position in the linear sequence of the chromosome (Kaneko *et al*, 1996a, 1996b). These reference numbers are used throughout this thesis, indicated by “bp #” immediately preceding the seven-digit number. As well, the genome has been cloned into a cosmid library (SupercosI-derived) that has been made available to other researchers upon request. The predicted open reading frame of the putative DEAD-box gene corresponds to bp #2887644 to #2889122 as recorded in DDBJ accession number D64004; this open reading frame was obtained on the cosmid cs0096 (gift of S. Tabata, Kazusa DNA Research Institute, Japan).

Figure 3.1 presents a diagrammatic representation of the region of genomic DNA immediately surrounding the *crhR* ORF in the cs0096 and cs0096-9 constructs, according to Kaneko *et al* (1995a, 1995b, 1996a, 1996b). The similarity of these open reading frames to genes found in other organisms is presented in Table 3.1. It is significant that there are putative proteins for RNA metabolism and signal transduction located upstream of *crhR*; since the genes are transcribed in the same direction they may be expressed as an operon.

For subcloning of the putative RNA helicase gene, the cs0096 cosmid DNA was digested with *Eco* RI and subjected to Southern analysis using the *crhB* fragment (Chamot *et al*, 1999) as probe, with hybridization at 55°C. In agreement with the predicted *Eco* RI recognition sites at bp #2887357 and #2890377, a 3.02 kb *Eco* RI fragment hybridized strongly to the DEAD-box gene probe. This fragment was subcloned into pBluescriptKS+ (Stratagene) and confirmed by Southern analysis (Fig. 3.2.A, lane 1). The identity and orientation of the resultant subclone, designated cs0096-9, was confirmed by sequencing using oligonucleotide primers (Table 2.4). The coding strand of the DEAD-box gene open reading frame is oriented 5' to 3' on the same strand as the M13-20 primer sequence in pBluescriptKS+ (equivalent to FWD in Table 2.4). Based on subsequent experimental evidence for redox regulation of the expression of this gene, as presented in chapters four and five, this gene is designated *crhR* for cyanobacterial RNA helicase - Redox.

The presence of the *crhR* open reading frame in the genome of the laboratory-maintained *Synechocystis* sp. strain PCC 6803 was confirmed by Southern analysis of chromosomal DNA following *Bam* HI and *Eco* RI single- and double-digests. In addition to the *Eco* RI sites listed above, there are predicted *Bam* HI endonuclease recognition sites at bp #2882746 and #2889552. Southern hybridization was performed at 55°C using a 325 bp *Sma* I fragment of *crhR*, followed by low stringency washes at r.t. This probe corresponds to bp #2887892 to #2888217, sequence which is internal to the predicted ORF and includes the coding region for the PTRELA, SAT, and DEAD motifs (Fig 3.1). The probe hybridizes with the expected 6.8 kb *Bam* HI, 2.195 kb *Eco* RI/*Bam* HI, and 3.02 kb *Eco* RI fragments (Fig 3.2.A, lanes 2-4). These results confirm that the *crhR* gene that was subcloned from cs0096 into cs0096-9 (Fig. 3.2A, lane 1) is present in the experimental cultures of *Synechocystis*. The absence of additional hybridizing fragments in the chromosomal DNA is in agreement with published sequence information (Kaneko *et al*, 1995a, 1995b, 1996a, 1996b) indicating this gene exists as a single copy in the *Synechocystis* genome.

**Figure 3.1 The Region of *Synechocystis* Genomic DNA Surrounding the *crhR* Gene**

Numerical designations for the *Synechocystis* genomic sequence are as described in the text. Thick arrows with open arrowheads indicate putative open reading frames (refer to Table 3.1 for details).

**(A) The region of interest from the *Synechocystis* genome.** This sequence is included in the SuperCosI-derived cs0096 construct. Gene designations are indicated in brackets above the appropriate open reading frame. Two *Eco* RI (E) sites indicate the boundaries of the fragment cloned into cs0096-9. Drawn to scale, where 0.5 inch=500 bp.

**(B) The 3.02 kb subclone contained in cs0096-9.** Genomic sequences are indicated by a solid line, thick arrows with open arrowheads indicate open reading frames, and vector sequences are indicated by the dashed line. Key restriction sites are indicated as follows: B, *Bam* HI; BI, *Bgl* I; D, *Dra* I; E, *Eco* RI; EV, *Eco* RV; H, *Hinc* II; HI, *Hpa* I; HIII, *Hind* III; P, *Pml* I; S, *Sma* I. Synthetic oligonucleotides are indicated below the line by small arrows with closed arrowheads (refer to Table 2.4 for details), at the site of complementary sequence. The grey rectangle indicates the *Sma* I probe used for routine Northern and Southern analyses. Roman numerals indicate DEAD-box protein consensus motifs: I, GKT box; Ia, PTRELA; II, DEAD; III, SAT; VI, HRIGR. Drawn to scale, where 1 inch=500 bp.

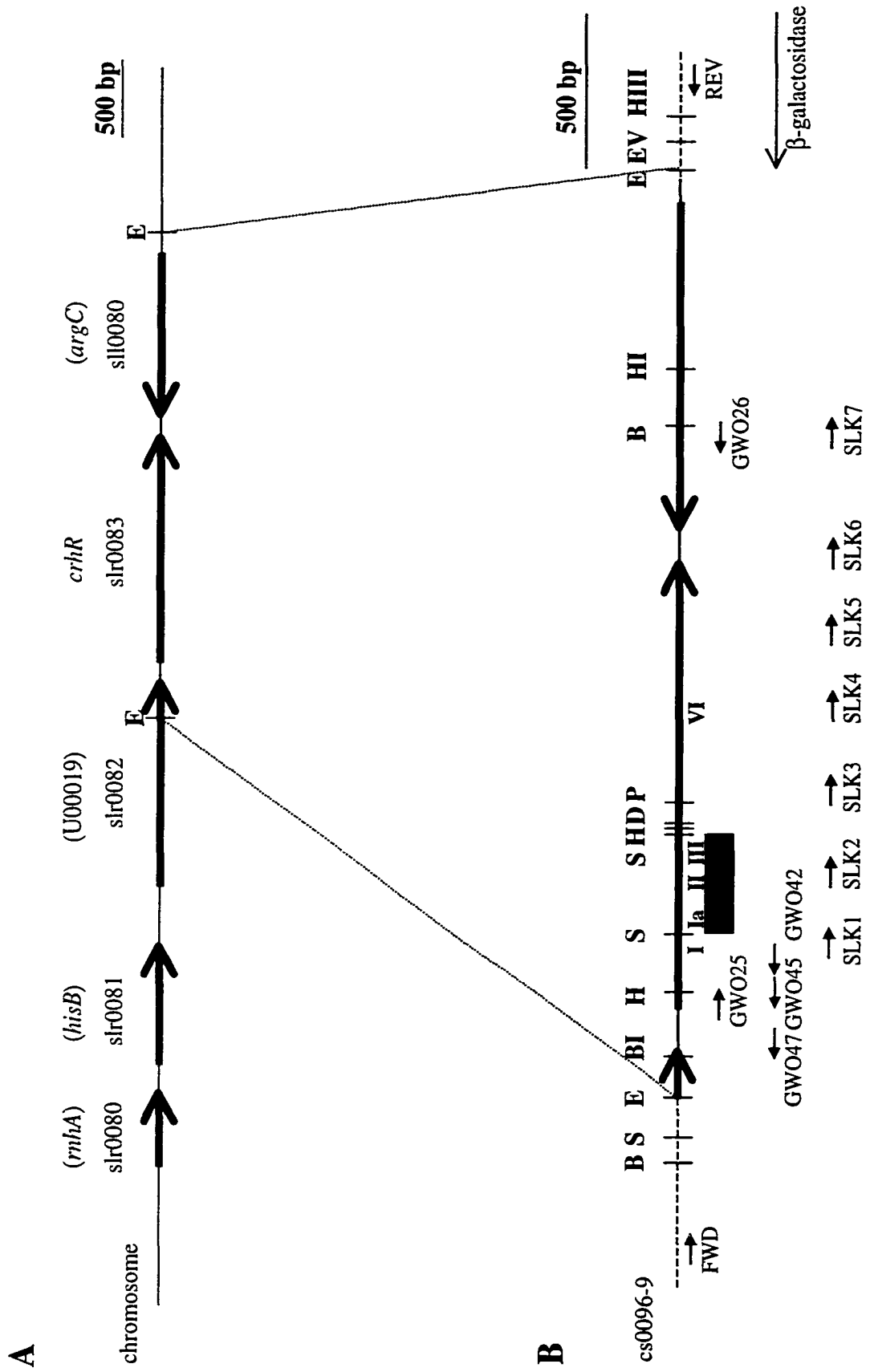


**Table 3.1 *Synechocystis* Genes Contained on cs0096 in the Region of Interest for the Present Study**

Summary information as per Kaneko *et al* (1995a, 1995b).

ORF (Location in the genome)	Homologous Gene (% DNA similarity)	Predicted protein product and % amino acid identity (overlap/total)
slr0080 (bp #2884358-2884840)	<i>rnhA</i> ( <i>E. coli</i> ) (37.3%)	Ribonuclease H ( <i>E. coli</i> ) 50% (150/160)
slr0081 (bp #2885023-2885811)	<i>hisB</i> (51.4%)	Phosphate regulon transcriptional regulatory protein PhoB; N-terminal region is similar to that of other regulatory components of sensory transduction systems. 35.6% (239/262)
slr0082 (bp #2886183-2887514)	Genbank Accession #U00019 (17%)	Unknown gene product
slr0083 (bp #2887645-2889123)	<i>deaD</i> ( <i>E. coli</i> ) (32.8%)	DEAD box family of RNA-dependent RNA helicases. 41.3% (477/492)
slr0080 (bp #2890321-2889266)	<i>argC</i> ( <i>Bacillus subtilis</i> ) (36%)	N-acetyl- $\gamma$ -glutamyl-phosphate reductase; third step in arginine biosynthesis. 44.3% (345/351)

**Figure 3.2 Detection of Wild-type and Mutant Copies of the *crhR* Gene.** For Southern and Northern analyses, *crhR* was detected by hybridization with a 325 bp *Sma* I fragment internal to the *crhR* open reading frame and containing the PTRELA and DEAD motifs. The antibiotic resistance cassette was probed with the omega fragment of pHP45Ω.

**A. Confirmation of subcloned and genomic copies of the *crhR* open reading frame.** Southern analysis was performed on cs0096-9 (2 μg) digested with *Eco* RI (lane 1), and *Synechocystis* chromosomal DNA (20 μg) digested with *Bam* HI (lane 2), *Eco* RI and *Bam* HI (lane 3), or *Eco* RI (lane 4). Hybridization was performed at 55°C.

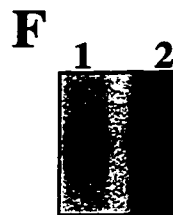
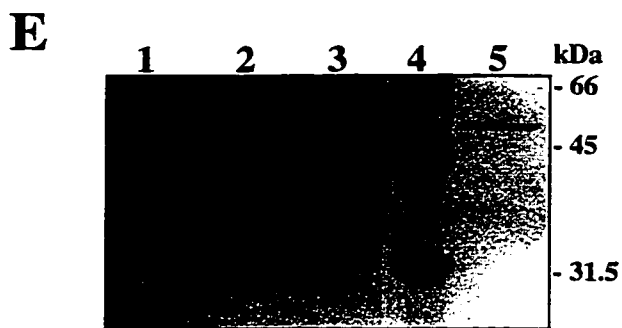
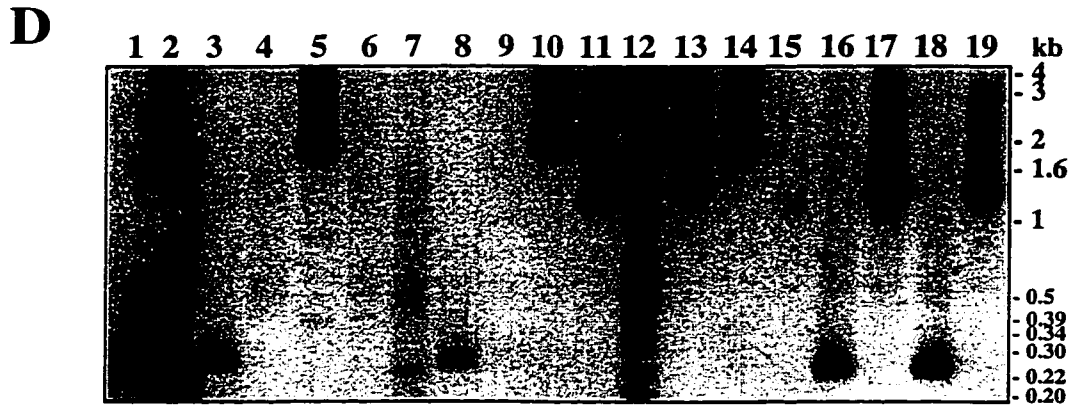
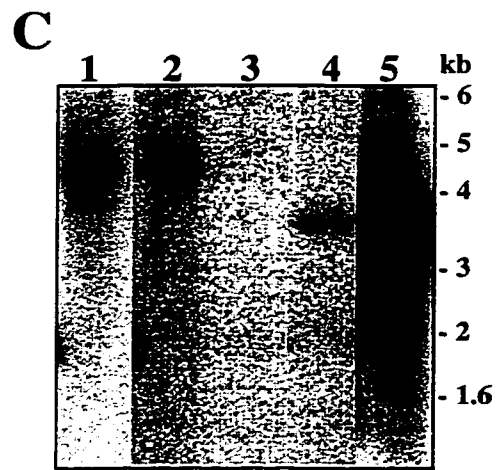
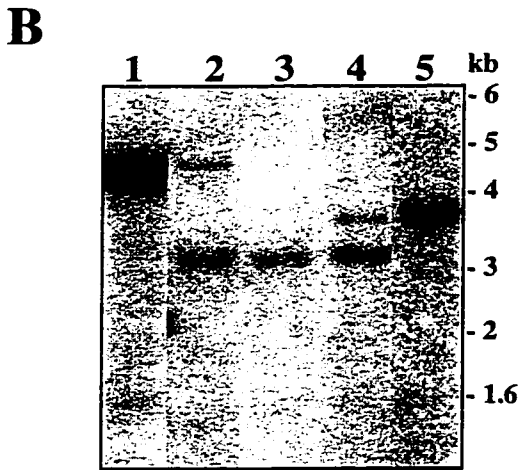
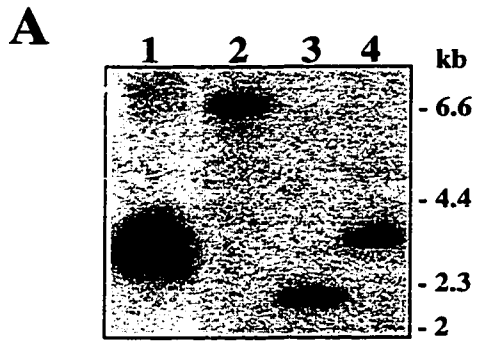
**B. Detection of *crhR* in various plasmid and genomic DNA preparations.** Southern analysis was performed following *Eco* RI digestion of the plasmids pBR*crhR*::Sp (lane 1) or pBR*crhRΔ*::Sp (lane 5), or of genomic DNA from *crhR*::Sp (lane 2), wild-type (lane 3), or *crhRΔ*::Sp (lane 4) cultures of *Synechocystis*.

**C. Detection of the omega fragment sequences in wild-type and mutant plasmids or genomic DNA.** Southern analysis was performed following *Eco* RI digestion of the plasmids pBR*crhR*:Sp (lane 1) or pBR*crhRΔ*:Sp (lane 5), or of genomic DNA from *crhR*:Sp (lane 2), wild-type (lane 3), or *crhRΔ*:Sp (lane 4) cultures of *Synechocystis*.

**D. Detection of wild-type and mutant copies of *crhR* by PCR.** PCR reactions were performed with combinations of the following template DNA with primers as indicated within brackets: cs0096-9 (GWO38+GWO39) (lane 1), cs0096-9 (GWO39+GWO41) (lane 2), wild-type chromosomal DNA (GWO38+GWO39) (lane 3), wild-type chromosomal DNA (GWO39+GWO40) (lane 4), wild-type chromosomal DNA (GWO39+GWO41) (lane 5), wild-type chromosomal DNA (GWO38+GWO40) (lane 6), wild-type chromosomal DNA (GWO40+GWO41) (lane 7), *crhR*:Sp (GWC38+GWO39) (lane 8), *crhR*:Sp (GWO39+GWO40) (lane 9), *crhR*:Sp (GWO39+GWO41) (lane 10), *crhR*:Sp (GWO38+GWO40) (lane 11), *crhRΔ*:Sp (GWO39+GWO40) (lane 13), *crhRΔ*:Sp (GWO39+GWO41) (lane 14), *crhRΔ*:Sp (GWO40+GWO41) (lane 15), cs0096-9+*crhR*:Sp (GWO38+GWO39) (lane 16), cs0096-9+*crhR*:Sp (GWO39+GWO40) (lane 17), cs0096-9+*crhRΔ*:Sp (GWO38+GWO39) (lane 18), cs0096-9+*crhRΔ*:Sp (GWO39+GWO40) (lane 19). 1 kb ladder (Bio101) was included on the agarose gel as DNA size markers (lane 12). Refer to Table 3.2 for expected sizes of the PCR products.

**E. Western analysis of wild-type *Synechocystis* cultures and *E. coli* transformed with various plasmid constructs.** Western analysis was performed on cell-free extracts of *E. coli* DH5α (cs0096-9) (lane 1), *E. coli* DH5α (pBR*crhR*::Sp) (lane 2), *E. coli* DH5α (pBR*crhRΔ*::Sp) (lane 3), and wild-type *Synechocystis* (lane 5). Kaleidoscope protein standards were run simultaneously (lane 4).

**F. *crhR* transcripts are detected in both mutant and wild-type cultures.** Northern analysis was performed on RNA extracted from a wild-type *Synechocystis* culture (lane 1) and a *crhR*::Sp mutant culture grown with illumination and static conditions (lane 2).



### 3.2.3 Construction and Analysis of *crhR*<sup>-</sup> Mutants

Since the *crhR* gene appears to encode the sole DEAD-box protein in *Synechocystis*, mutants in the *crhR* coding region were expected to yield a detectable phenotype and possibly provide insight into the physiological function performed by CrhR. To investigate this, the chromosomal *crhR* gene was inactivated through gene conversion with engineered constructs that contain a selectable marker interrupting or replacing part of the coding sequence of *crhR* (Fig. 3.3).

#### 3.2.3.1 Inactivation of *crhR* by Insertion of a Selectable Marker into the Coding Region

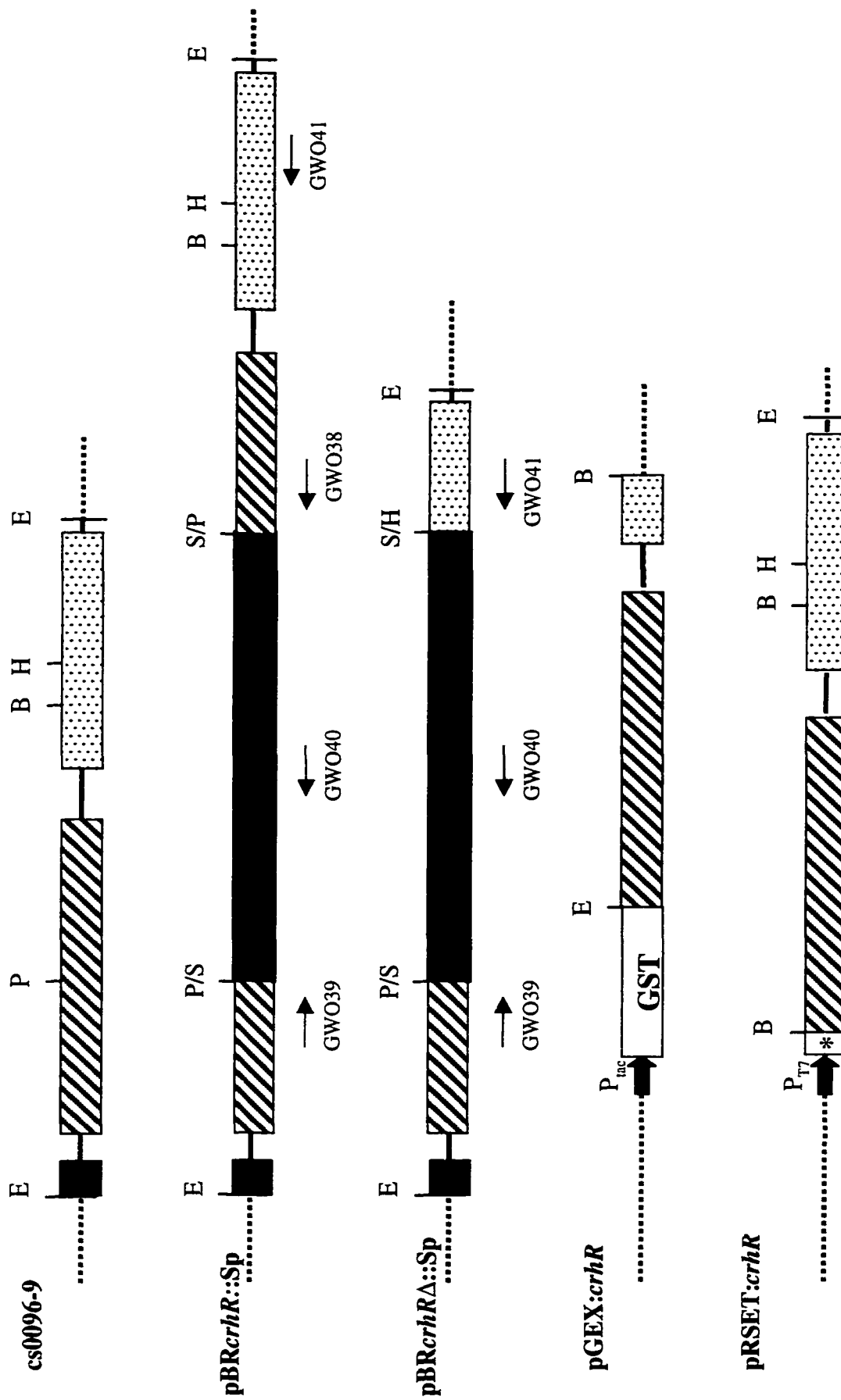
The *crhR* mutant constructs (Fig. 3.3) are derived from the 3.02 kb *Eco* RI fragment of cs0096-9. The *crhR* open reading frame was mutated by insertion of the 1.98 kb omega fragment of pHP45Ω carrying the aminoglycoside-3/adenyltransferase fusion protein (*aadA*) gene that confers resistance to the antibiotics spectinomycin (Sp) and streptomycin (Sm) (Prentki and Krisch, 1984). This antibiotic resistance cassette is flanked by strong transcription/translation termination signals to prevent read-through into adjoining sequences. Two *crhR* gene inactivation constructs were engineered in pBR322, which was chosen as vector since it is suitable for transformation of *Synechocystis* (Thiel, 1994). In pBR*crhR*::Sp, the omega fragment is inserted at the *Pml* I site (bp #2888318) that lies between the DEAD and SAT motifs. In pBR*crhR*Δ::Sp, the 1.42 kb *Pml* I/*Hpa* I (bp# 2889738) fragment was replaced by the omega fragment. This deletion removes 805 bp of *crhR* coding sequence, as well as 472 bp from the 3' end of the downstream open reading frame sll0080 (*argC* homologue) and 143 bp of intervening sequence. These constructs retain sufficient genomic sequences flanking the omega fragment to enable efficient homologous recombination between the transforming plasmid and the chromosome.

The constructs were confirmed by restriction digests using *Eco* RI, *Bam* HI, *Hind* III and *Bst* EII, then sequenced across the junctions between the antibiotic resistance cassette and the *crhR* coding sequence. The *Eco* RI digests were subjected to Southern analysis using probes for *crhR* and the omega fragment. As expected, both probes hybridized to a 5 kb fragment of the pBR*crhR*::Sp construct (Fig 3.2.B and C, lane 1) and a 3.6 kb fragment of the pBR*crhR*Δ::Sp construct (Fig 3.2.B and C, lane 5). These results confirm the insertional inactivation of *crhR* in the engineered plasmids.



### Figure 3.3 Diagram of the *crhR* Subclone, as well as Derived Mutant and Over-Expression Constructs

cs0096-9 is the pBluescriptKS+ subclone containing the wild-type *crhR* sequence. pBR*crhR*Δ::Sp and pBR*crhR*::Sp indicate the insertional inactivation of *crhR* in the pBR322 vector. pRSET:*crhR* and pGEX:*crhR* indicate the protein over-expression constructs (refer to chapter 5). Restriction sites are indicated by single letters. E, *EcoRI*. H, *HpaI*. P, *PmlI*. S, *SmaI*. B, *BamHI*. P<sub>tac</sub> and P<sub>T7</sub> indicate promoters. GST, Glutathione-*S*-transferase. \* indicates the 6XHIS tag of pRSETA, with the amino acid sequence MRGSHHHHHHGMASMTGGQQMGRDLYDDDDK (in single-letter code, with histidine residues underlined). The *crhR* coding region is striped, slr0082 is grey, slI0080 coding region is dotted, and the omega fragment containing the Sp<sup>R</sup>/Sm<sup>R</sup> gene is solid black. All vector sequences are indicated by dotted lines. pBluescriptKS+ is 2.96 kb, pBR322 is 4.36 kb, pGEX-2T is 4.9 kb, and pRSETA is 2.9 kb. The PCR primers GWO38, GWO39, GWO40 and GWO41 are indicated at the position of complementary sequence by small arrows. Drawn to scale where 1.5 inches = 1 kb of DNA sequence.



### 3.2.3.2 Transformation of *Synechocystis* to Obtain Homozygous *crhR*<sup>-</sup> Mutants

The *crhR*<sup>-</sup> constructs from Section 3.2.3.1 were transformed into *Synechocystis* in order to generate chromosomal *crhR*<sup>-</sup> mutants by gene replacement as described in the introduction (section 3.1). *Synechocystis* cultures were transformed with pBR*crhR*::Sp or pBR*crhRΔ*::Sp, plated onto solid selective medium and incubated with illumination at 30°C. The mutant cultures are designated *crhR*::Sp or *crhRΔ*::Sp, respectively. After 7 d of growth with antibiotic selection (2 μg/mL each of spectinomycin and streptomycin) it was possible to detect pinprick-sized green colonies. Once the colonies reached a characteristic size of approximately 1 mm in diameter, single colonies were restreaked onto fresh media; this was repeated every 14 d. To ensure a sufficient number of generations for homozygous mutants to appear by random segregation of the chromosomes, the re-streaking of individual colonies was repeated for 5-8 serial transfers on solid medium in the presence of antibiotic selection prior to analysis of the DNA or growth characteristics.

An interesting although unexplained observation was made during long-term culturing of the mutants by serial transfer. Occasionally two different types of colony morphologies arose from a single restreaked colony, namely, smaller (~0.75 mm diameter) pale green colonies and larger (up to 1.5 mm diameter) darker green colonies. This did not occur with every transfer; furthermore, restreaking colonies of either morphology could give rise to both types of morphology in subsequent transfers. The basis for this unstable phenotype was not investigated.

pBR322 contains an ampicillin (Ap) resistance gene, therefore to minimize selective pressure for the undesirable insertion of the entire plasmid by single crossover, only spectinomycin and streptomycin were added to the selective media. The occurrence of single crossover progeny, which would be Sp<sup>R</sup>/Sm<sup>R</sup>/Ap<sup>R</sup>, was subsequently tested by replica plating Sp<sup>R</sup>/Sm<sup>R</sup> colonies onto BG11 containing 2 μg/mL ampicillin. No growth was observed, providing evidence that the transforming vector sequences have been lost from the cells rather than being maintained by recombination either into the chromosome or into a resident *Synechocystis* plasmid. This is also consistent with the desired gene conversion event due to homologous recombination in the sequences flanking the omega fragment, rather than the undesirable random recombination of the *crhR*<sup>-</sup> constructs into the chromosome.

It was necessary to confirm the specific replacement of wild-type *crhR* in the genome with the inactivated copy, as well as to determine whether the mutants were homozygous for the *crhR*<sup>-</sup> genotype. Therefore, genomic DNA was isolated from mutants cultured on solid medium, digested with *Eco* RI and subjected to Southern

analyses. As expected, the *crhR* probe hybridizes to a 3.02 kb fragment in wild-type cells (Fig. 3.2.B, lane 3), a 5 kb fragment in the *crhR::Sp* mutant (Fig. 3.2.B, lane 2) and a 3.6 kb fragment in the *crhRΔ::Sp* mutant (Fig. 3.2.B, lane 4). Also as expected, probing with the omega fragment yields no hybridization with wild-type DNA (Fig. 3.2.C, lane 3), while the *crhR::Sp* (Fig. 3.2.C, lane 2) and *crhRΔ::Sp* (Fig. 3.2.C, lane 4) contain 5 kb and 3.6 kb hybridizing fragments, respectively. Detection of the *crhR* and omega fragment sequences on the same *Eco* RI fragments in the mutants is interpreted as successful transformation and gene conversion in *Synechocystis*. Significantly, *crhR::Sp* and *crhRΔ::Sp* also contain the 3.02 kb fragment that hybridizes with the *crhR* probe (Fig. 3.2.B, lanes 2 and 4, respectively), indicating that wild-type copies of the gene are present in addition to the inactivated copies.

PCR analysis was routinely performed to check the progress of random segregation since it is a rapid method of identifying wild-type and mutant copies of *crhR* with a relatively small amount of genomic DNA. For this purpose, four oligonucleotide primers (Table 2.4) were synthesized, the relative priming locations of which are indicated in Figure 3.3. GWO39 and GWO41 are complementary to sequence outside of the deleted region, hybridizing just upstream from the *Pml* I and downstream from the *Hpa* I deletion endpoints, respectively. GWO38 is complementary to sequence internal to the *crhR* deletion, and GWO40 is complementary to sequence internal to the omega fragment. Amplification of the indicated size of DNA fragments (Table 3.2) is expected with both plasmid and chromosomal DNA templates, whereas there are no expected products from control reactions using other primer pairs. Optimal PCR conditions were determined empirically in conjunction with the 3-STEP program (Table 2.5).

PCR generates the expected fragments from cs0096-9 using the GWO38+GWO39 (Fig. 3.2.D, lane 1) and GWO 39+GWO41 (Fig. 3.2.D, lane 2) primer pairs. These fragments are also obtained using wild-type chromosomal DNA as the template (Fig. 3.2.D, lanes 3 and 5), whereas no products are observed in control reactions containing GWO40 as one of the primers (Fig. 3.2.D, lanes 4, 6, and 7). When *crhR::Sp* DNA is the template, the amplification of the 230 bp (Fig. 3.2.D, lane 8) and 1630 bp fragments (Fig. 3.2.D, lane 10) indicates that wild-type copies of the *crhR* gene are present, while the 1100 bp fragment amplified by GWO38+GWO40 (Fig. 3.2.D, lane 11) confirms that inactivated copies are also present. Similarly, reactions containing *crhRΔ::Sp* as the template DNA show amplification of the wild-type *crhR* sequences with GWO39+GWO41 (Fig. 3.2.D, lane 14), and amplification of the inactivated *crhR* sequence with GWO39+GWO40 (Fig. 3.2.D, lane 13). As expected, there are no PCR

**Table 3.2 Expected Sizes of DNA Fragments Obtained by PCR Reactions Containing the Indicated Primers and Templates**

N/A, no products expected due to lack of one or more priming sites.

Primers	Template		
	Wild-type	pBR <i>crhR</i> ::Sp or <i>crhR</i> ::Sp	pBR <i>crhRA</i> ::Sp or <i>crhRA</i> ::Sp
GWO38 + GWO39	230 bp	2200	2200
GWO39 + GWO41	1630 bp	3600	n/a
GWO39 + GWO40	n/a	1200	1200

products in the control reaction GWO40+GWO41 (Fig. 3.2.D, lane 15). These results agree with the Southern analyses detailed above.

Interestingly, although both wild-type and inactivated copies of the *crhR* gene are present in chromosomal DNA from the mutants, only one of these is apparent in any particular PCR reaction, suggesting that the primer pairs preferentially amplify either the wild-type or the mutant sequence. This was confirmed in PCR reactions that contain mixtures of the plasmids cs0096-9 (wild-type *crhR*) with either pBR*crhR*::Sp or pBR*crhR*Δ::Sp. In both cases the 230 bp fragment (wild-type) was preferentially amplified with GWO38+GWO39 (Fig. 3.2.D, lanes 16 and 18), and the 1200 bp fragment (*crhR*<sup>-</sup>) was preferentially amplified with GWO39+GWO40 (Fig. 3.2.D, lanes 17 and 19).

Both the PCR and Southern hybridization results agree with the Ap<sup>S</sup> phenotype and confirm the expected mutant genotypes, namely gene replacement at the *crhR* locus rather than integration of the transforming vector. They also lead to the conclusion that wild-type *crhR* copies are present in both mutants, which are therefore heterozygotic at the *crhR* locus. The extent of segregation, determined as the ratio of wild-type to inactivated copies of *crhR* in the genome, could not be accurately quantified nor estimated because of difficulties in obtaining uniform cultures of the mutants.

### 3.2.3.3 Expression of Mutant Constructs in a Heterologous System - *E. coli*

Subsequent production of anti-CrhR antiserum (section 2.4.4; see also section 5.2.2) permitted Western analysis of cell-free extracts from wild-type *Synechocystis* compared to *E. coli* DH5α carrying one of the following plasmids: cs0096-9, pBR*crhR*::Sp, or pBR*crhR*Δ::Sp. The cell-free extracts from wild-type *E. coli* DH5α (cs0096-9) (Fig 3.2.E, lane 1) and *Synechocystis* (Fig. 3.2.E, lane 5) contain an approximately 55 kDa peptide that is absent in *E. coli* containing either of the *crhR*<sup>-</sup> constructs (Fig. 3.2.E, lanes 2 and 3). This confirms that insertional inactivation of the *crhR* open reading frame prevents synthesis of full-length wild-type CrhR protein. Interestingly, a 28-30 kDa peptide that reacts with the antiserum is found only in the cell-free extracts from *E. coli* DH5α (pBR*crhR*::Sp) (Fig. 3.2.E, lane 2) and *E. coli* DH5α (pBR*crhR*Δ::Sp) (Fig. 3.2.E, lane 3). This peptide is likely a truncated form of CrhR, since the 224 amino acids N-terminal to the insertion of the omega cassette have a predicted molecular weight of approximately 25 kDa. With respect to the detection of CrhR in cell-free extracts from *E. coli* DH5α (cs0096-9), it is significant that the orientation of *crhR* in the cs0096-9 subclone would not enable *crhR* expression to occur from the B-galactosidase promoter in the vector, because this implies that the *crhR* transcription and translation signals are recognized and functional in *E. coli*.

#### 3.2.3.4 Phenotypic Comparison of Wild-type and *crhR*<sup>-</sup> Mutants Of *Synechocystis*

While growth was relatively reliable on solid medium, a number of qualitative observations were recorded during attempts to culture the *crhR::Sp* or *crhRA::Sp* mutants in liquid medium. The mutants exhibited rapid achlorosis (the loss of green pigmentation) compared to wild-type cultures when grown under identical conditions of illumination and aeration; both types of mutants seemed to survive longer under reduced light intensity and mixing. Furthermore, the likelihood of survival was increased by using a higher inoculum ( $OD_{750} > 0.2$ ) compared to the wild-type cultures. While conditions of ambient light intensity, darkness, or reduced agitation increased the apparent survival of mutant cultures, this did not prevent one or more replicates from succumbing to achlorosis in any particular experiment. In terms of colour, the wild-type cultures were a brighter green than the mutants, which were often a darker greyish-green that is more typical of older, stationary phase wild-type cultures. The *crhR::Sp* cultures appeared more grey-blue in colour compared to the grey-green of *crhRA::Sp* cultures that occasionally also formed small pellets of cells during growth in liquid medium. Finally, the addition of 0.1% glucose and buffering with 10 mM TES produced the most reliable conditions for maintaining the mutant cultures, which then survived under low light intensities at both 30°C and r.t.

The previous results and observations (section 3.2.3.2) indicated that the *crhR* gene is important for cell viability, since wild-type copies are maintained in both types of mutants. It was therefore desirable to quantify the lack of growth in liquid medium by the mutants compared to wild-type. For this purpose, a growth experiment was performed with duplicate cultures of wild-type, *crhR::Sp* mutants and *crhRA::Sp* mutants treated to three conditions, either (a) illumination with shaking at 150 rpm, (b) darkness with shaking at 150 rpm, or (c) illumination and static (i.e. no shaking) conditions. All six cultures of a particular wild-type or mutant construct were inoculated as 50 mL cultures in 250 mL flasks, from a single concentrated cell suspension to give the same initial cell density and chlorophyll concentration. At regular intervals samples were withdrawn from the cultures and assessed for cell density by  $OD_{750}$  measurements (Fig. 3.4.A, C, and E), followed by methanol extraction and chlorophyll *a* quantitation using  $A_{665}$  (Fig. 3.4.B, D, and F), as described (section 2.1.1). It is important to note that all cultures were cultured with addition of 5 mM glucose, which would permit photomixotrophic growth. Furthermore, possible effects of cell size on the optical density of the cultures was not determined.

**Figure 3.4 Phenotypic Analysis of *Synechocystis* Mutant and Wild-type Cultures as Measured by Changes in Cell Density and Chlorophyll *a* Concentration**

For all graphs, circle indicates illuminated, aerated cultures; square indicates aerated cultures grown with darkness; triangle indicates static cultures grown with illumination. All cultures were grown with addition of 5 mM glucose to the medium.

**A. Growth of wild-type (wT) cultures as measured by changes in cell density over time.**

**B. Growth of *crhR*Δ::Sp mutants as measured by changes in cell density over time.**

**C. Growth of *crhR*::Sp mutants as measured by changes in cell density over time.**

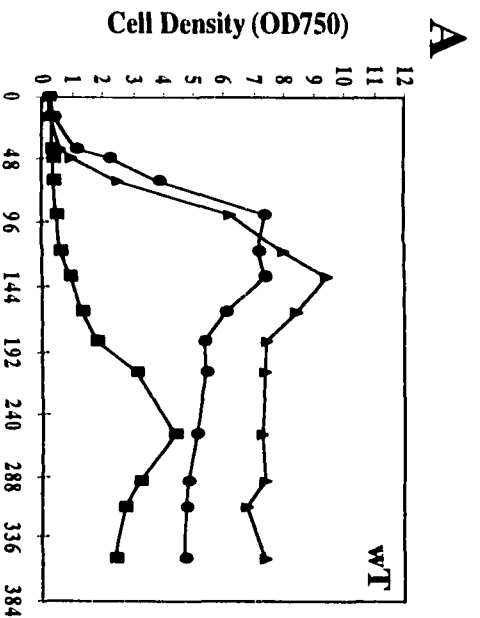
**D. Growth of wild-type (wT) cultures as measured by changes in chlorophyll *a* concentration over time.**

**E. Growth of *crhR*Δ::Sp mutants as measured by changes in chlorophyll *a* concentration over time.**

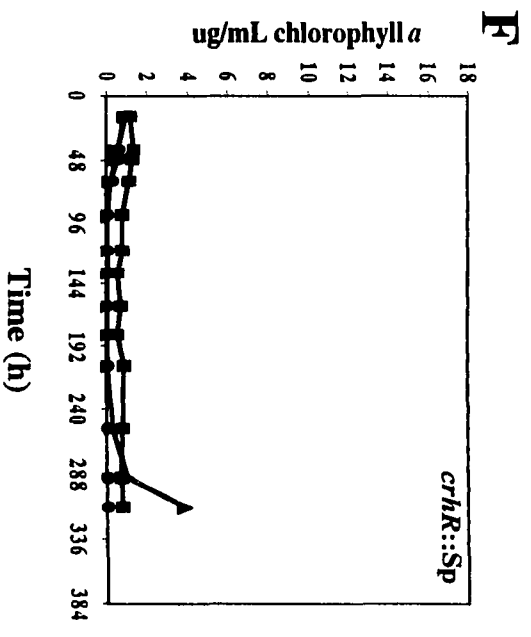
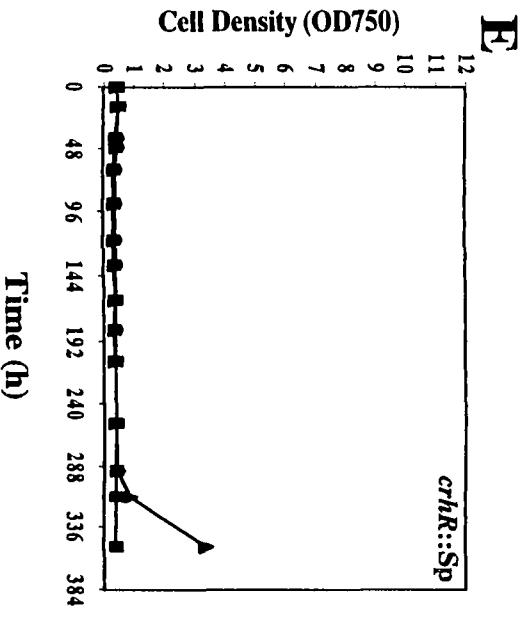
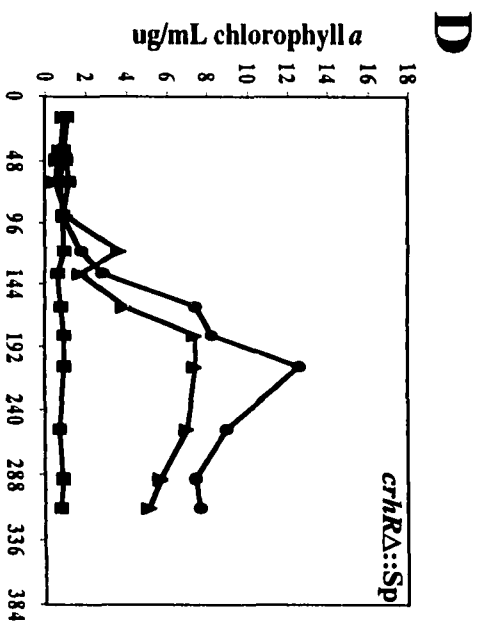
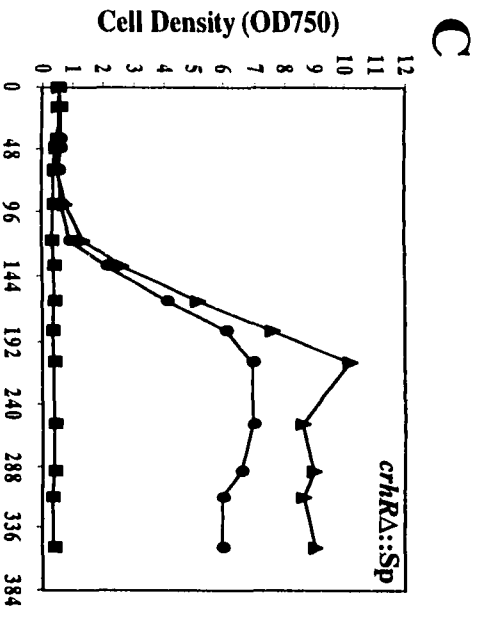
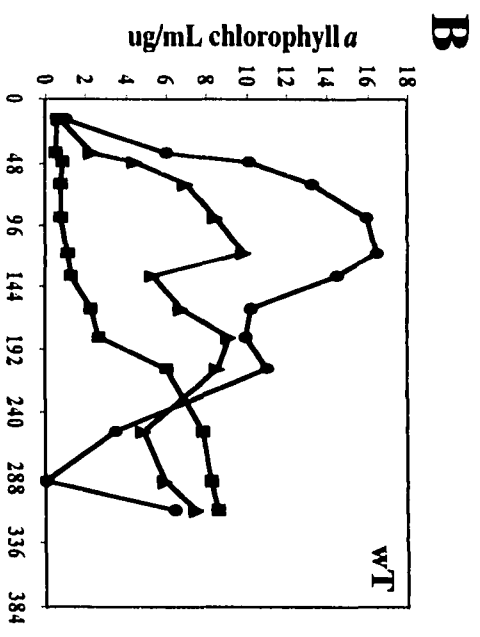
**F. Growth of *crhR*::Sp mutants as measured by changes in chlorophyll *a* concentration over time.**



### Growth Curve



### Chlorophyll Assay



Analysis of wild-type *Synechocystis* cultures (Fig. 3.4.A and B) indicates that during the first 4-5 days cell density increases faster and reaches a higher density with illumination as compared to darkness. Conditions of low aeration with illumination yielded a higher cell density in stationary phase as compared to shaken cultures, with a corresponding increase and peak in chlorophyll *a* concentration. Wild-type cultures that were grown in darkness took approximately twice as long to reach stationary phase, with approximately half the cell density compared to illuminated cultures. With darkness the chlorophyll *a* concentration showed a similar initial lag period, but continued to increase even after cell density began to decline.

With illumination, cultures of the *crhRΔ::Sp* mutant (Fig. 3.4.C and D) showed a lag period prior to increasing in cell density and chlorophyll *a* concentration that is approximately twice as long as the lag period seen in wild-type cultures (compare Fig. 3.4.A and B). Similar to wild-type cultures, static cultures of *crhRΔ::Sp* maintained a higher cell density in stationary phase compared to aerated cultures. The cultures grown in darkness did not increase in cell density nor chlorophyll concentration over the course of the experiment, suggesting a metabolic defect such that they are unable to grow on exogenous glucose in the dark.

Under all three growth conditions there was no increase in cell density or chlorophyll *a* in the *crhR::Sp* cultures (Fig. 3.4.E and F) during the sampling period. Illuminated cultures rapidly became achlorotic whereas the dark-incubated culture showed neither loss nor accumulation of chlorophyll *a*. The notable exception to this pattern occurred with one of the static illuminated cultures, which began to increase in chlorophyll concentration at approximately 200 h, and cell density at approximately 288 h; the duplicate culture for this treatment remained white with no change in cell density.

At the conclusion of these growth curve experiments, the RNA was extracted from the remaining cells and subjected to Northern analyses. Significant quantities of intact RNA were recovered from only two samples, namely, one of the wild-type cultures (Fig 3.2.F, lane 2) and the static *crhR::Sp* culture that suddenly showed growth around 200 h (Fig. 3.2.F, lane 1). Both of these cultures contained a *crhR* transcript of the appropriate size (section 4.2.1).

Due to the pleiotropic phenotype of the *Synechocystis crhR<sup>-</sup>* mutants and the inability to obtain cultures that were homozygous at the *crhR* locus, this research was not pursued further.

### 3.3 Discussion

The sequencing of the 3.5 Mbp *Synechocystis* genome revealed a single DEAD-box protein gene (Kaneko *et al*, 1996a, 1996b). In this study the open reading frame for this DEAD-box protein (slr0083), subcloned from the cosmid cs0096, is designated *crhR* and shown to be present in the laboratory strain of *Synechocystis*. If this gene is part of an operon, it may be co-transcribed with any or all of the genes immediately upstream. If so, the expression of this putative RNA helicase may be coordinately regulated with other genes for RNA metabolism and/or signal transduction.

Two lines of evidence suggest that the putative RNA helicase CrhR provides an essential physiological function. First, there is only one DEAD-box RNA helicase gene and neither DEAH- nor DExH-box genes were identified in *Synechocystis* (Kaneko *et al*, 1996a, 1996b). This is unexpected, given the complexity of RNA metabolism and the multiplicity of DEAD-box proteins in all cellular organisms, including other prokaryotes (de la Cruz *et al*, 1999). The possibility of RNA helicase activity by proteins lacking the typical SF1 family motifs remains to be investigated. Second, both *crhR::Sp* and *crhRA::Sp* mutants retain wild-type copies of the gene, therefore homozygous *crhR*<sup>-</sup> mutants are assumed to be lethal under the growth conditions tested here. This is similar to the essential function postulated for the RNA helicase RhlB based on the inability to obtain viable *rhlB*<sup>-</sup> cells (Py *et al*, 1996). Furthermore, despite the presence of wild-type copies of the *crhR* gene, heterozygotes exhibit reduced viability compared to wild-type cultures. This may be related to the potential expression of the 25 kDa N-terminal region of CrhR. By contrast, other researchers have reported isolation of *crhR*<sup>-</sup> homozygotes lacking a detectable phenotype (J. Vinnemeier, personal communication), achieved by replacement of a 363 bp *Dra* I/*Hinc* II fragment corresponding to bp #2888246-2888598, with a 1.25 kb kanamycin resistance cassette. Their results may be due to differences in mutational protocols or growth conditions, since this lab has similarly constructed homozygous *dnaA*<sup>-</sup> mutants with a wild-type cell division phenotype, despite the fact that *dnaA* is an essential gene in other organisms (Richter *et al*, 1998).

In this study, both *crhR::Sp* and *crhRA::Sp* mutants exhibit loss of the photosynthetic pigment chlorophyll *a*, sensitivity to aeration, and lack of growth on glucose in the dark. The pleiotropic nature of this phenotype precludes precise identification of the link between *crhR*<sup>-</sup> and physiological effects. The mutants may be stressed by the increased rate of metabolism that occurs in the presence of higher illumination and carbon dioxide levels (i.e. aeration by agitation), possibly deficient in light-harvesting or Calvin cycle function(s). The loss of chlorophyll *a* is reminiscent of photoinhibition but occurs at lower light fluence levels compared to wild-type, implying

that *crhR* may be important for the integrity of the photosystem reaction centers and the light-harvesting capacity. Perhaps efficient translation of certain transcripts for PSI or PSII components, such as the D1 polypeptide, is dependent upon or aided by the RNA unwinding activity of CrhR. The achlorosis of the cells may also be a symptom of macronutrient limitation, which induces the breakdown of phycobilisomes (Grossman *et al.*, 1992, 1993).

It appears that the *crhR*<sup>-</sup> cells experience low photosynthetic efficiency and are therefore impaired in the processes required for photoautotrophic growth. Interestingly, the addition of glucose seems to increase the viability of the mutants in liquid culture with illumination but did not support growth in the dark. A simple explanation could be that CrhR is not required during metabolism of exogenous glucose; this is unlikely in view of the transcriptional induction of *crhR* that occurs in response to the addition of glucose, as described in chapter four. One possible scenario is that conditions of low aeration and illumination (low metabolic rate) decrease the requirement for CrhR activity, hence a mutation in *crhR* is less deleterious. In fact a lower level of expression of *crhR* is noted under these conditions (section 4.2.1.5). Under these same conditions, however, the cells may not be able to obtain sufficient energy for long-term photosynthetic growth, whereas the addition of glucose supplies ATP by glycolysis and carbon intermediates for assimilation via the TCA cycle. In other words, exogenous glucose may indirectly compensate for the *crhR*<sup>-</sup> mutation by enabling the cells to survive under the growth conditions that minimize the deleterious effects of the mutation. The inability to grow on glucose in the dark, and the longer lag period observed for the *crhR*Δ::Sp mutant with illumination support the hypothesis that the mutants are able to incorporate the carbon skeletons but have reduced photosynthetic efficiency at the level of either light-harvesting, electron transport, or carbon fixation via the Calvin cycle.

The phenotypic effects observed even in heterozygous mutants indicate that the *crhR*<sup>-</sup> mutation exerts a dominant negative effect on cellular metabolism. This could occur if expression of the 224 amino acids upstream of the inserted omega cassette generates a correctly folded N-terminal portion of CrhR. In fact this sequence would correspond to the expected "domain 1" predicted from the crystal structure of HCV NS3, containing the GKT and DEAD motifs and the putative NTP hydrolysis cleft. Western analysis suggests that a truncated peptide of the correct molecular weight is produced from the mutant constructs in *E. coli*. Although highly speculative, it is possible to envision that a functional CrhR "domain 1" could disrupt the normal metabolism by interacting with ATP even in the absence of further hydrolysis.

Further speculation that the CrhR carboxy-terminus might be expressed in the *crhR::Sp*, but not the *crhRΔ::Sp*, cells could explain the observation that the simple insertion mutant is significantly less viable than the deletion mutant for increases in both cell density and chlorophyll concentration. However, the expression of the CrhR carboxy-terminus should not occur by read-through from the omega fragment since there are strong transcription-translation termination signals engineered into this cassette (Prentki and Krisch, 1984; experimental evidence in Li and Golden, 1993). Alternatively, since the deletion in *crhRΔ::Sp* is almost the same size as the inserted antibiotic resistance cassette, the more severe *crhR::Sp* phenotype may be due to a disruption of spacing of enhancer sequences for the surrounding genes. Furthermore, it is impossible to discern the effects of simultaneously deleting the carboxy-terminus of the putative *argC* gene, *sll0080*; this gene would also be a heterozygous mutant. Related to the ability of other workers to obtain *crhR*<sup>-</sup> homozygotes, it is possible that the present *crhR*<sup>-</sup> constructs are maintained as heterozygotes simply as a consequence of deleting *sll0080* or disrupting the transcriptional controls for this gene. It is not known if *sll0080* is an essential gene in *Synechocystis*.

The present results do not permit unequivocal identification of a single physiological target or process that depends upon the RNA helicase activity of CrhR. Rather, the observation that *crhR* is the sole *Synechocystis* DEAD-box gene and the pleiotropic effects of *crhR*<sup>-</sup> mutants are compatible with a general role for *crhR* in RNA metabolism, as discussed further in chapter seven.

## **CHAPTER FOUR**

### **Expression of the *crhR* Transcript: Regulation by Redox**

**A version of this chapter has been published.**

**Kujat, S. L., and G. W. Owtrim. 2000. *Plant Physiology* 124: 703-713.**

## 4.1 Introduction

Along with the assumption that a gene exists because it is used by the cell is the expectation that the gene will be uniquely expressed when the cognate (m)RNA and/or protein are required. The physiological conditions that elicit transcription and translation may therefore provide contextual information for predicting or confirming the biological significance of the gene. Given the essential role of light in photoautotrophic bioenergetics, conditions of illumination or darkness are expected to specify global and dramatic changes in cyanobacterial gene expression.

The most obvious effect of light for photoautotrophs is regulation of the cell cycle. Cell division and initiation of DNA replication are blocked when an exponentially growing culture is transferred into darkness, and these processes resume immediately upon re-illumination (Richter *et al*, 1998). The *dnaA* gene, which encodes the protein regulator for initiation of chromosomal replication, mimics this pattern: the *dnaA* transcript decays to undetectable levels during incubation in the dark, but expression increases dramatically following a return to illumination (Richter *et al*, 1998). With continuous illumination the generation time of *Synechocystis* has been estimated to be 8-12 h (Williams, 1988); following transfer into darkness the growth rate slows and after 48 h the cells stop dividing (Smart and McIntosh, 1991) unless provided with supplemental glucose in the medium (Anderson and McIntosh, 1991). This reflects the change in energy status during photoautotrophic metabolism in the dark, due to the depletion of reductive pentose phosphate pathway intermediates, which are generated only in the light (Mullineaux and Allen, 1986).

### 4.1.1 Redox-Responsive mRNA Expression Patterns

In the past, research has focussed on phytochrome and other light sensors as mediators of light-responsive transcription in plants (Fankhauser and Chory, 1997; Mustilli and Bowler, 1997). More recent is the recognition that changes in illumination may be sensed as a shift in the cellular redox status. Specifically, the redox equilibrium of the plastoquinone pool (i.e. the ratio of plastoquinone to plastoquinol) in the thylakoid membrane modulates the activity of thylakoid protein kinases and phosphatases (Gal *et al*, 1997; Vener *et al*, 1998), with two potential outcomes. The first is state transitions, described previously (section 1.2.3.2). The second is a postulated signal transduction cascade that activates transcription factors for the expression of redox-responsive genes.

Evidence for a redox-responsive signal transduction cascade in eukaryotes comes from the elucidation of nuclear and chloroplastic expression of photosynthetic genes. Transcription of the nuclear-encoded *cab* genes in *Dunaliella tertiolecta* was proposed to

be coupled to light intensity via the redox state of plastoquinone in the thylakoid membranes, indicating that redox signals in the chloroplast indirectly control nuclear gene expression (Escoubas *et al*, 1995; Maxwell *et al*, 1995). Similar conclusions were derived from manipulation of the redox status of the plastoquinone pool by addition of electron transport inhibitors, which simulates the light intensity-dependent regulation of the cytosolic *apx* (ascorbate peroxidase) genes in *Arabidopsis* (Karpinski *et al*, 1997). Transcriptional control of chloroplast genes is also regulated by the plastoquinone-plastoquinol equilibrium as evidenced by changes in transcription rates of the *psaA* and *psbAB* genes in mustard seedling, alterations that result in relatively rapid adjustment of the stoichiometry of the PSI and PSII reaction centers (Pfannschmidt *et al*, 1999). These effects are generally attributed to a cytosolic phosphorylation cascade potentially initiated by the redox-modulated thylakoid membrane-bound kinase known to participate in state transitions (Allen *et al*, 1995; Baginsky *et al*, 1997; Escoubas *et al*, 1995; Pfannschmidt *et al*, 1999). This hypothesis is supported by reports that *psbA* expression is differentially regulated by two sigma-like transcription factors. *In vivo*, the phosphorylation of these transcription factors is light-dependent (Tiller and Link, 1993) and *in vitro* the phosphorylation is effected by a protein kinase activity that is associated with RNA polymerase (Baginsky *et al*, 1997). Indeed, it has been suggested that state transitions are not the most important outcome of the protein phosphorylation changes that stem from cellular redox-sensing events via plastoquinol (Vener *et al*, 1998).

Cyanobacterial transcriptional responses to light are also well-documented (Golden, 1995), with similar evidence accumulating that gene regulation may be redox-responsive. In *Synechocystis* this is generally demonstrated by the use of photoheterotrophic or photomixotrophic growth conditions, with or without electron transport inhibitors. Regulation of the *secA* gene, which encodes part of the protein translocation apparatus, responds to the availability of reducing power that occurs with high intensity of illumination (Mazouni *et al*, 1998). The *glnA* transcript for glutamine synthetase and the *rbcLS* operon, encoding the Calvin cycle enzyme RuBisCO, are redox-responsive as shown by the dramatic decrease that occurs in darkness unless a metabolizable form of glucose is present (Mohamed and Jansson, 1989; Reyes and Florencio, 1995). Furthermore, *glnA* transcript levels fully recover within 5 minutes of re-illumination, except in the presence of DCMU and DBMIB (Reyes and Florencio, 1995). Similarly, inhibition of photosynthetic electron flow prevents the light-dependent expression of *desA*, *desB* and *desD*, encoding fatty acid desaturases (Kis *et al*, 1998).

Since the plastoquinol-induced protein phosphorylation that accompanies state transitions in eukaryotes is also implicated in cyanobacterial state transitions (Harrison *et*



*al*, 1991, Mullineaux and Allen, 1986; Mullineaux and Allen, 1990), there is likely a corresponding cyanobacterial signal transduction pathway for transcription of redox-responsive genes. Supporting evidence for this includes the demonstration that phosphorylation signal transduction cascades are not limited to eukaryotes but are employed within a wide range of prokaryotic systems (Cozzone, 1993; Kennelly and Potts, 1996; Saier Jr., 1993; Shi *et al*, 1998). It is well-documented that *trans*-acting factors and two-component signal transduction systems are redox-modulated in the purple and green phototrophic bacteria (Pemberton *et al*, 1998). Within cyanobacteria, changes in protein phosphorylation patterns have been observed in total cell extracts as well as specifically in thylakoid membrane preparations (Mann, 1994), correlating with alterations in nutrient, stress, or energy status. A link to the thylakoid kinase responsible for state transitions is suggested by altered protein phosphorylation profiles following addition of glucose (Mann, 1994; Bloye *et al*, 1992), which stimulates respiratory electron transport and causes state transitions (Mullineaux and Allen, 1990), and during adaptation to salt stress, which resembles state transitions by virtue of causing a decrease in energy transfer between the phycobilisomes and PSII (Hagemann *et al*, 1993). Integration with carbon metabolism is suggested by observations that the transfer of bicarbonate limited cultures into darkness or into photomixotrophic conditions yields changes in protein phosphorylation patterns that resemble those following transfer into bicarbonate sufficient conditions (Bloye *et al*, 1992). Finally, protein kinase and phosphatase activities respond to changes in the concentration of metabolites and, significantly, the redox state of plastoquinone and/or cyt *b<sub>6</sub>f*, even in cell-free systems (Mann *et al*, 1991; Mann, 1994). These observations support the hypothesis that phosphorylation cascades and signal transduction networks are important for regulating cyanobacterial bioenergetics.

#### **4.1.2 Light-Responsive Promoter Elements: *cis*- and *trans*-Acting Factors**

Light-regulated promoters in plants have a complex organization with overlapping *cis*-elements that integrate tissue- and/or development-specific signals (Gilmartin *et al*, 1990; Marraccini *et al*, 1994). Similar elements may modulate cyanobacterial gene expression. While cyanobacterial promoters often contain a -10 element typical of *E. coli*  $\sigma$ 70 consensus promoter sequences, the apparent lack of a corresponding -35 element (Curtis and Martin, 1994; Mohamed *et al*, 1993) has been presented as circumstantial evidence that additional activator proteins are required during initiation of transcription (Curtis and Martin, 1994). Preliminary identification of five putative promoter regions from *Synechocystis* has revealed potential *cis*-elements, but lacks positional information.

Despite the absence of typical *E. coli*-like promoter motifs, these genomic fragments confer light-responsive expression of downstream genes in a promoter search vector, related to the CCGATG and G(G/A)N<sub>5</sub>AAC elements identified by sequence analysis and confirmed by mutation (Marraccini *et al*, 1994). The validity of these generalizations had been limited by the small size of the available cyanobacterial promoter sequences database (Curtis and Martin, 1994), but should expand as new cyanobacterial genome sequences become available.

A more detailed analysis of the transcription of *psbA* and *psbD* genes in *Synechococcus* sp. strain PCC 7942 (subsequently referred to as *Synechococcus*) demonstrates the regulatory role of positive and negative *cis*-elements in the region of DNA that extends both downstream and upstream of the transcript initiation site. The differential expression of the three *psbA* transcripts is due to the presence of basal promoters (of the *E. coli* type) that confer constitutive expression; superimposed upon this are additional *cis* elements in *psbA-2* and *psbA-3* that modulate transcription in response to high intensity illumination (Bustos *et al*, 1990; Kulkarni *et al*, 1992). Upstream elements present at -52 to -39 in *psbA-2* negatively affect gene expression whereas downstream elements, located at +1 to +41/+39 in *psbA-2/3*, positively regulate expression (Li and Golden, 1993). Electrophoretic mobility shift assays indicate that the regions surrounding these *cis*-elements are constitutively bound by soluble proteins from cell-free extracts obtained under both high- and low-light conditions (Li *et al*, 1995). Since sequence similarity between these regions is low, Li and co-workers (1995) speculated that DNA conformation rather than primary sequence is important for the general DNA-effector interactions. In conjunction with this, *in vivo* DNase protection assays revealed that only the cell-free extracts from high-light conditions exhibit sequence-specific binding to the downstream enhancer element of *psbA-2* and *psbA-3* (Li *et al*, 1995). The promoter and untranslated leader regions of *psbD-2* produce three protected sites in *in vivo* footprinting assays, corresponding with light-responsive expression of the gene (Bustos and Golden, 1991). Further investigation of *psbD-2* expression by deletion analysis indicated that the light-responsive regulation extends from -38 to +160, a region that includes 52 bp of the open reading frame (Anandan and Golden, 1997).

In *Synechocystis* the investigation of the non-photosynthetic *secA* gene revealed three *cis*-elements that control its expression in response to light (Mazouni *et al*, 1998). The basal promoter region from -71 to +47, which includes *E. coli*  $\sigma^{70}$  motifs, is flanked by an upstream element (-71 to -361) that increases expression, and a downstream negative element extending from +47 to +104. Interestingly, the sequence from +104 to

+175, which corresponds to the coding region of *secA*, harbours a positive element that overcomes the down-regulation imposed by the negative element. Alterations in the spacing of the -35 box relative to the -10 box were shown to influence the promoter strength and regulation by illumination. The effector binding sites and identity have not been characterized further.

#### **4.1.3 Light-Responsive Differential mRNA Stability**

Since the levels of mRNA detected by Northern analysis are the product of both the rate of transcription and the stability of the transcript, post-transcriptional regulation may contribute to differential gene expression. In *E. coli* calculated mRNA half-lives range from 30 seconds to greater than 20 minutes, with an estimated average of 2-4 minutes (Reyes *et al*, 1997). By comparison the average mRNA half-life in cyanobacteria has been estimated to be between 12-20 minutes (Leach and Carr, 1974; Reyes *et al*, 1997). This may reflect the relatively longer generation time of cyanobacteria compared to enterobacterial species (12 hours compared to 30 minutes). Similar to transcription, in photoautotrophic cells the conditions of illumination or darkness also influence mRNA stability, in a transcript-specific manner. For example, in *Synechocystis* the *glnA* mRNA is equally stable in light and dark, with a half-life of approximately 2.5 minutes (Reyes and Florencio, 1995), and levels of the *dnaK* mRNA remain elevated even after a 12 hour dark period, whereas the *dnaA* transcript is highly unstable in darkness and is likely degraded from the 3' end (Richter *et al*, 1998). The *Synechocystis psbA-2* and *psbA-3* transcripts have half-lives of 15 minutes in the light but the stability increases to 7 hours in darkness and is accompanied by production of a specific degradation intermediate that lacks 200-300 nucleotides of 5' sequence. Since this effect is mimicked by addition of electron transport inhibitors, the cellular redox state is implicated in this post-transcriptional regulation of gene expression (Mohamed and Jansson, 1991; Mohamed *et al*, 1993; Tryystjarvi *et al*, 1998). It has been suggested that thylakoid phosphatases or kinases may be involved in coupling mRNA stability to photosynthetic electron transport (Mohamed *et al*, 1993).

#### **4.1.4 Post-Transcriptional Modulation of Gene Expression: A Role for RNA Helicases**

There is evidence that the secondary structure of mRNA is important during the light- and redox-responsive post-transcriptional regulation of gene expression. For example, the abundance of the pea *Fed-1* transcript that encodes ferredoxin is dependent upon the association of polyribosomes for efficient translation. Under conditions of

darkness the increased instability of the mRNA is due to loss of protection by polyribosomes, influenced by a CATT repeat element in the 5' UTR (Dickey *et al.*, 1998). In chloroplasts of the unicellular algae *Chlamydomonas reinhardtii*, light-dependent translation of *psbA* requires a multi-protein complex that associates with secondary structures in the 5' untranslated region of the mRNA. Although this multi-protein complex is constitutively present under conditions of both illumination and darkness, there is an ADP-stimulated phosphorylation that attenuates the association with mRNA in the dark. When this RNA-protein complex is artificially subjected to oxidizing conditions the binding capacity is abolished, whereas the addition of reducing agents such as DTT restores the interactions; this provides evidence that redox conditions may regulate translation (Danon and Mayfield, 1994; Mayfield *et al.*, 1994). In *Synechococcus* the mRNA stability determinants that localize to the 5' UTR of the *psbA* and *psbD-1* transcripts mediate turnover in response to light intensity, and are postulated to act by recruiting RNA-binding proteins for translation or degradation (Li and Golden, 1997). The presence of stabilizer elements in these regions of the mRNA may also cause ribosome pausing and lead to the protective accumulation of ribosomes upstream of the pause site (Anandan and Golden, 1997; Kulkarni and Golden, 1997). This demonstrates the importance of RNA secondary structure and therefore implicates RNA helicase involvement during post-transcriptional regulation. It is conceivable that the translation or degradation of redox-regulated mRNAs could be controlled in part through the coordinated, redox-regulated expression of an RNA helicase.

In the present study the *crhR* gene is examined at the level of mRNA accumulation to elucidate both transcriptional and post-transcriptional regulation. Determination of the conditions that elicit detectable levels of the *crhR* transcript and/or influence transcript stability is accomplished by Northern analysis. The putative 5' ends of the *crhR* transcript(s) are determined by primer extension and S1 nuclease protection assays. The DNA sequence in the region surrounding a putative (+1) site is subjected to electrophoretic mobility shift assays (EMSA) in pursuit of a DNA-binding protein that could be responsible for altering the transcription of *crhR*.

## 4.2 Results

### 4.2.1 Northern Analyses

#### 4.2.1.1 Preliminary Screen for Transcript(s) from the *crhR* Open Reading Frame

As the primary investigation into the expression of the RNA helicase gene *crhR*, Northern analyses were performed with a randomly labelled DNA probe consisting of the 325 bp *Sma* I fragment described in chapter 3 (section 3.2.2). The size of the predominant *crhR* transcript, determined using a glyoxal gel with 1 kb DNA ladder as the size standards, is 1400-1600 nt. Relative to the ribosomal RNA transcripts, *crhR* mRNA migrates electrophoretically slower than the 1500 nt rRNA (Fig. 4.1.A). Hybridizing bands of 1100 nt and 1900 nt may also be present. Total RNA from photoautotrophic cultures of *Synechocystis* sp. strain PCC 6803 (Fig. 4.1.A, lanes 1-4), *E. coli* DH5 $\alpha$ (cs0096-9) (Fig. 4.1.A, lane 6) and photoautotrophic *Anabaena* sp. strain PCC 7120 (gift of D. Chamot, University of Alberta) (Fig. 4.1.A, lane 7) were assessed for the presence of transcripts that are homologous to the 325 bp *crhR* gene probe under high stringency conditions (hybridization and final wash at 60°C and 0.1X SSC). In comparison to the putative *crhR* transcript from *Synechocystis*, RNA from *Anabaena* does not contain a hybridizing mRNA species, while there are three strongly hybridizing transcripts in the RNA from *E. coli* DH5 $\alpha$ (cs0096-9). In the absence of size standards, the sizes of the hybridizing species in *E. coli* are estimated to be greater than 2900 nt and may correspond to *E. coli* DEAD-box genes. Since low levels of the CrhR protein were detected by Western analysis of cell-free extracts of *E. coli* DH5 $\alpha$ (cs0096-9) (refer to Fig. 3.3.F), the presence of the *crhR* transcript is likely, although it is not detected under these conditions.

Differential expression of the *crhR* transcript was predicted to reflect the involvement of this putative RNA helicase in cellular processes specific to conditions under which *crhR* is present and/or highly expressed. Therefore, total RNA was isolated from photoautotrophic *Synechocystis* cultures following various treatments (gift of Ian Le, University of Alberta), and screened for the presence or absence of the *crhR* transcript by Northern analysis, using the entire *crhR* ORF as probe. Following this screen, only the 4 h dark treatment was considered for further investigation because the single *crhR* transcript that is present in the light was conspicuously absent. The RNA component of the RNase P ribonucleoprotein complex (*mpB* gene, gift of A. Vioque, Spain) was chosen as an internal control for the amount of total cellular RNA loaded in each lane, since it is a structural RNA that has a long half-life (Alfonso *et al*, 2000; Reyes and Florencio, 1995). An untreated, illuminated control culture is included in each

#### **Figure 4.1 Detection of the *crhR* Transcript by Northern Analysis**

Northern analysis was performed with 6 µg of total RNA extracted from *Synechocystis*, except as indicated.

**A. Preliminary screen for *crhR* transcripts.** Northern analysis was performed with 8 µg total RNA extracted from *Synechocystis* sp. strain PCC 6803 grown photoautotrophically with illumination (lane 1), or after 3 hours in dark (lane 2), and from *E. coli* DH5α(cs0096-9) (lane 3), and *Anabaena* sp. strain PCC 7120 (lane 4).

**B. Differential expression of *crhR* in response to illumination.** Photoautotrophic *Synechocystis* cultures were grown with illumination (lane 1) prior to transfer into darkness for 3 h (lane 2) or 24 h (lane 3).

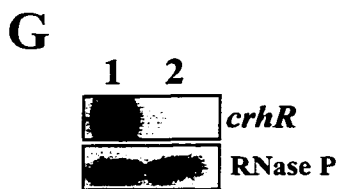
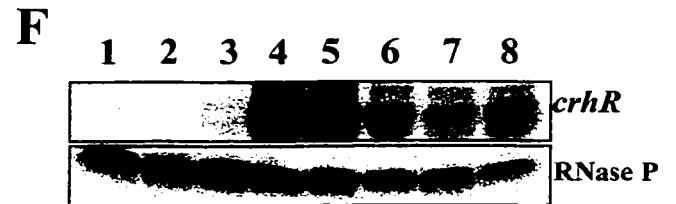
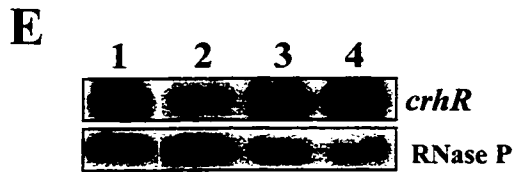
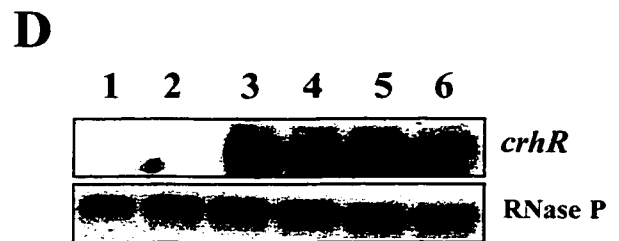
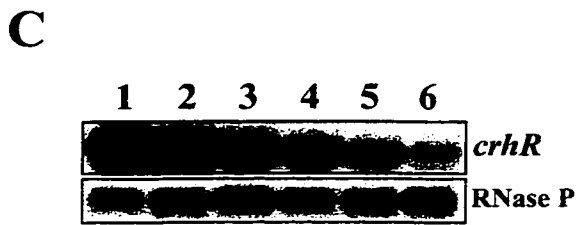
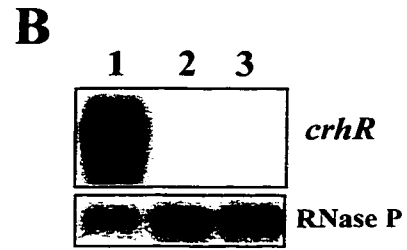
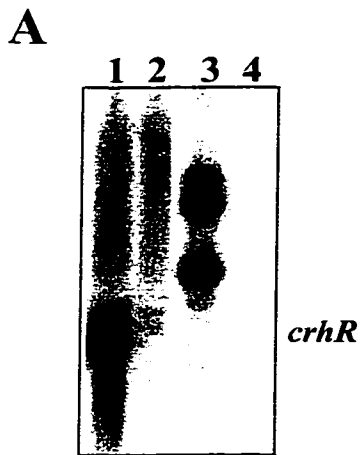
**C. Decay of the *crhR* transcript following transfer into darkness.** Photoautotrophic *Synechocystis* cultures were grown with illumination (lane 1) prior to transfer into darkness for 5 min (lane 2), 10 min (lane 3), 15 min (lane 4), 20 min (lane 5) or 25 min (lane 6).

**D. *crhR* levels following re-illumination of photoautotrophic cultures.** Photoautotrophic *Synechocystis* cultures were treated to 3 h dark (lane 1) prior to re-illumination for 1 min (lane 2), 5 min (lane 3), 15 min (lane 4), 30 min (lane 5) or 60 min (lane 6).

**E. *crhR* levels in photomixotrophic cultures.** *Synechocystis* was cultured with addition of 5 mM glucose and illumination (lane 1) prior to incubation in the dark for 1 h (lane 2), 3 h (lane 3), or 24 h (lane 4).

**F. Addition of glucose to photoautotrophic cultures in the dark.** Photoautotrophic *Synechocystis* cultures were treated to 3 h dark (lane 1) prior to addition of 5 mM glucose and further incubation in the dark for 15 min (lane 2), 30 min (lane 3), 60 min (lane 4), 2 h (lane 5), 3 h (lane 6), 6 h (lane 7), or 24 h (lane 8).

**G. *crhR* levels in cultures grown with 3-OMG.** *Synechocystis* that had been cultured with addition of 5 mM 3-OMG and illumination (lane 1) was subsequently treated to 3 h darkness (lane 2).



experiment as the internal standard of steady-state levels of the *crhR* transcript. Furthermore, valid comparison of relative levels of *crhR* is restricted to samples from the same autoradiogram following Northern analysis.

#### **4.2.1.2 *crhR* Exhibits a Light-Responsive Pattern of Expression That is Altered in Response to Glucose Metabolism**

The transcription of an RNA helicase gene during growth with illumination suggests that CrhR plays a role in photosynthetically-dependent metabolism, a role that is inferred to be less or not important during growth in the dark. Further investigation revealed that the *crhR* transcript (Fig. 4.1.B, lane 1) is no longer detectable at three hours after onset of the dark treatment (Fig. 4.1.B, lane 2), and is still absent at 24 hours (Fig. 4.1.B, lane 3). A time-course of *crhR* transcript levels during dark treatment of photoautotrophic cultures indicates that the transcript levels decrease significantly during the first 30 min (Fig. 4.1.C) and are undetectable at any time point tested beyond 2 h of darkness, even with long autoradiography exposure times. Therefore, in all subsequent experiments a minimum 2 h dark incubation was considered sufficient to obtain undetectable levels of *crhR*. Re-illumination of a culture, following a 3 h dark treatment (Fig. 4.1.D, lane 1), results in detectable levels of the *crhR* transcript within 5 min (Fig. 4.1.D, lane 3), although not after 1 min (Fig. 4.1.D, lane 2). *crhR* levels peak at 15-30 min (Fig. 4.1.D, lanes 4 and 5) and return to a more basal level by 60 min (Fig. 4.1.D, lane 6) and beyond; *crhR* transcripts are consistently present in illuminated cultures. This demonstrates that *crhR* expression requires light to initiate and maintain transcription.

While most cyanobacteria are obligate photoautotrophs, *Synechocystis* can be cultured photomixotrophically, since it has the ability to import and respire appropriate exogenously-supplied organic carbon compounds (Flores and Schmetterer, 1986). The presence of exogenous glucose stimulates respiration and may affect photosynthetic activity, therefore *crhR* expression was determined in cultures that had been grown with the addition of 5 mM glucose and illumination (Fig. 4.1.E, lane 1) prior to transfer into darkness. Significantly, *crhR* transcript accumulation is not altered by 1 h, 3 h, and 24 h of dark incubation (Fig. 4.1.E, lanes 2-4), which is in stark contrast to cultures grown in the absence of glucose. Since the photomixotrophic cultures were grown in the presence of both continuous illumination and glucose prior to the dark treatment, it was important to determine whether the addition of glucose is sufficient to induce *crhR* expression, or whether a synergistic interaction with light is required for the induction. For this purpose a photoautotrophic culture was incubated in the dark for 3 h, at which point the *crhR* transcript is no longer detectable (Fig. 4.1.F, lane 1). Subsequent glucose addition (5



mM) was carried out in a darkroom under a red safelight that does not induce *crhR* transcription. At 30 min following glucose addition, low levels of the *crhR* transcript may be detected with prolonged autoradiogram exposures (Fig. 4.1.F, lane 3). Levels of *crhR* mRNA peak approximately 1-2 h after glucose addition (Fig. 4.1.F, lanes 4 and 5), and are subsequently maintained for at least 48 h in darkness. It is apparent that dark-treated cultures induce *crhR* transcription more slowly in response to addition of glucose compared to re-illumination (30-60 min vs. 5 min); this suggests that the *crhR* induction occurs following metabolism of the exogenous glucose.

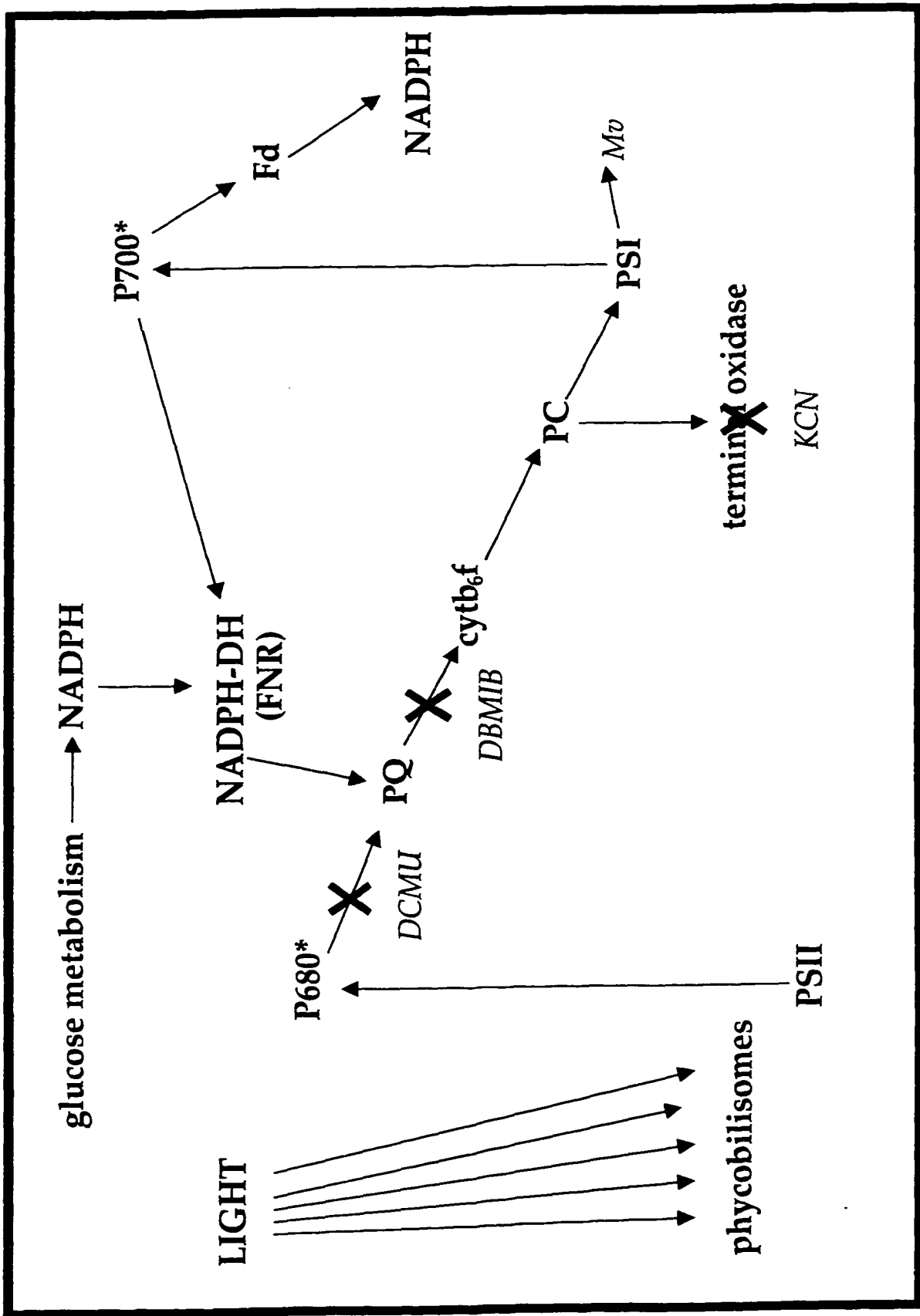
To confirm that respiration of the exogenous glucose is a prerequisite for induction of *crhR* expression, cells were grown in the presence of 3-*O*-methyl-D-glucose (3-OMG) (5 mM), which is a glucose analogue that is transported into, but not metabolized by, *Synechocystis* (Flores and Schmetterer, 1986). In the presence of 3-OMG the *crhR* transcript (Fig. 4.1.G, lane 1) degrades to undetectable levels after a 3 h dark treatment (Fig. 4.1.G, lane 2), results identical to the observed degradation of *crhR* in dark-treated photoautotrophic cells. However, this is in stark contrast to continued expression of *crhR* in dark-treated cultures in the presence of glucose. These results demonstrate that the exogenous carbon substrate must be metabolized in order to induce *crhR* transcription in the absence of light, and suggests that glucose metabolism mimics some aspect of the light-generated intracellular signal for transcription of *crhR*. A similar pattern of expression has been noted for the *glnA* transcript where the regulatory signal was attributed to the redox state of electron transport components (Reyes and Florencio, 1995). Therefore the significance of electron transport for the transcription of *crhR* was investigated further.

#### **4.2.1.3 Alterations in the Net Redox Status of the Plastoquinone Pool Correlate with Differential Expression of the *crhR* Transcript**

The most apparent activity that is common to conditions of illumination and metabolism of exogenous glucose is the overlapping photosynthetic and respiratory electron transport in the cyanobacterial thylakoid membrane. Therefore, treatment with the electron transport inhibitors DCMU, DBMIB, KCN, and Mv was used to investigate the possibility that *crhR* transcription responds to redox-generated signals. DCMU and DBMIB act at defined transfer points in the electron transport chain while KCN and Mv have additional secondary metabolic effects on the cells; all four inhibitors affect electron transport that is driven by either photosynthesis or respiration, or both. This is summarized in Table 2.4 and represented in Figure 4.2.

### **Figure 4.2 Overview of Electron Transport in Cyanobacteria and the Site of Action of Electron Transport Inhibitors**

The inter-photosystem electron transport carriers are shared by photosynthetic and respiratory electron transport. The PQ pool has an established role as an intermediary electron carrier for both photosynthetic and respiratory electron flow. The balance between electron entry from PSII and/or NADPH-dehydrogenase, and electron exit to cyt *b<sub>6</sub>f* determines the overall redox state of the PQ pool. The sites of action of the electron transport inhibitors DCMU, DBMIB, KCN, and Mv are as indicated (see also Table 2.2). The electron transport inhibitors DCMU and DBMIB interrupt linear electron flow: DCMU prevents electron transfer from PSII to PQ, which leads to oxidization of the PQ pool. DBMIB, acting as a PQ analogue, binds the cyt *b<sub>6</sub>f* complex and inhibits oxidation of the PQ pool. During photomixotrophic growth conditions, NADPH generated by respiration of glucose (through the pentose phosphate pathway) reduces the PQ pool via NADPH-dehydrogenases (NADPH-DH), and these electrons therefore enter the electron transport chain below the interruption by DCMU but above the DBMIB inhibition site. KCN affects respiratory electron flow by inhibiting the terminal cytochrome oxidase; KCN also inactivates G6P-DH and enzymes of the Calvin cycle. Mv acts as an electron shunt on the acceptor side of PSI, thus affecting both linear and cyclic electron flow without preventing turnover of the inter-photosystem carriers.



Compared to untreated illuminated photoautotrophic cultures (Fig. 4.3.A, lane 1), the levels of the *crhR* mRNA decline significantly as a result of treatment with DCMU for 1 h (Fig. 4.3.A, lane 2) or 2 h (Fig. 4.3.A, lane 3). Since the addition of DCMU blocks electron transfer from PSII to plastoquinone - preventing its reduction but not its oxidation - the decline in *crhR* levels correlates with net oxidation of the plastoquinone pool. Under conditions of darkness there is no reduction of plastoquinone via PSII. The observation that *crhR* does not decline to the undetectable levels seen with 2 h dark treatment (Fig. 4.3, lane 4) may indicate that a low level of electron donation from PSII to plastoquinone is DCMU-insensitive, or may reflect the transient reduction of plastoquinone via cyclic electron flow from PSI or via respiratory electron flow, both of which are unaffected by DCMU. Similarly, addition of DCMU prior to (Fig. 4.3.A, lane 5) or simultaneously with (Fig. 4.3.A, lane 6) illumination of a previously dark-incubated culture does not prevent the *crhR* transcriptional response but does dampen or impair it, seen as a lower magnitude of *crhR* induction compared with re-illumination in the absence of DCMU (compare with Fig. 4.1.D).

Treatment of cultures with glucose and DCMU is commonly referred to as photoheterotrophic conditions, and it is well-established that the block imposed by DCMU is rescued by respiratory electron transport due to electron donation from NADPH-DH to plastoquinone. Thus, under these conditions electron flow into the plastoquinone pool continues both in the light and in the dark, and this correlates with continued expression of *crhR* (Fig. 4.3.B). In fact, in the presence of glucose and light the addition of DCMU results in a significant increase in *crhR* transcript levels (Fig. 4.3.B, lanes 1-3). Since this is not seen in the dark with DCMU and glucose (Fig. 4.3.B, lanes 4-6), the previous speculations about the involvement of cyclic electron flow or incomplete blockage by DCMU may similarly explain these results.

In parallel experiments DBMIB was added to photoautotrophic and photomixotrophic cultures. DBMIB inhibits plastoquinone oxidation by the *cyt b<sub>6</sub>f* complex and yields a net reduction of the plastoquinone pool. In photoautotrophic conditions the increase in *crhR* levels following a 1 h DBMIB treatment (Fig. 4.3.C, lane 2) is in striking contrast to the 1 h treatment with DCMU (Fig. 4.3.A, lane 2). Furthermore, simultaneous addition of DBMIB and re-illumination (Fig. 4.3.C, lane 5) of a dark-incubated culture (Fig. 4.3.C, lane 4) yields *crhR* transcript levels that are elevated by comparison with the corresponding DCMU treatment (Fig. 4.3.A, lanes 5 and 6). Illuminated photomixotrophic cultures treated with DBMIB would experience the same block in plastoquinone oxidation as photoautotrophic cultures, and similar results of increased *crhR* levels are observed (Fig. 4.3.D, lane 2). Both in the presence and

### **Figure 4.3 Northern Analysis of *crhR* Expression Following Treatment with Electron Transport Inhibitors**

Northern analysis was performed with 6  $\mu$ g total RNA extracted from *Synechocystis*.

**A. DCMU addition to photoautotrophic cultures.** *Synechocystis* was cultured with illumination (lane 1) prior to treatment with DCMU for 1 h (lane 2) or 2 h (lane 3). Alternatively, the cultures were incubated in darkness for 2 h (lane 4) then DCMU was added for 10 min in the dark prior to re-illumination for 15 min (lane 5), or DCMU was added simultaneously with re-illumination for 15 min (lane 6).

**B. DCMU addition to photomixotrophic cultures.** *Synechocystis* was cultured with glucose and illumination (lane 1) prior to treatment with DCMU for 1 h (lane 2) or 2 h (lane 3). Alternatively, the cultures were incubated in darkness for 2 h (lane 4) or treated with DCMU and darkness for 1 h (lane 5) or 2 h (lane 6).

**C. DBMIB addition to photoautotrophic cultures.** *Synechocystis* was cultured with illumination (lane 1) prior to treatment with DBMIB for 1 h (lane 2), or 2 h (lane 3). Alternatively, the cultures were incubated in darkness for 2 h (lane 4) prior to re-illumination with addition of DBMIB for 15 min (lane 5).

**D. DBMIB addition to photomixotrophic cultures.** *Synechocystis* was cultured with glucose and illumination (lane 1) prior to treatment with DBMIB for 1 h (lane 2) or 2 h (lane 3). Alternatively the cultures were incubated in darkness for 2 h (lane 4) or treated with DBMIB and darkness for 1 h (lane 5) or 2 h (lane 6).

**E. KCN addition to photoautotrophic cultures.** *Synechocystis* was cultured with illumination (lane 1) prior to treatment with KCN for 1 h with illumination (lane 2). Alternatively, the cultures were incubated in darkness for 3 h followed by addition of KCN for 1 h in darkness (lane 3) or 1 h with illumination (lane 4).

**F. KCN addition to photomixotrophic cultures.** *Synechocystis* was cultured with glucose and illumination (lane 1) prior to treatment with KCN for 1 h with illumination (lane 2), or in the dark (lane 3).

**G. Mv addition to photoautotrophic cultures.** *Synechocystis* was cultured with illumination (lane 1) prior to treatment with Mv for 30 min (lane 2) or 1 h (lane 3).

**H. Mv addition to photoautotrophic cultures.** *Synechocystis* was cultured with glucose and illumination (lane 1) prior to treatment with Mv for 30 min (lane 3), or 1 h (lane 4). Alternatively, the cultures were incubated in darkness for 2 h (lane 2) or treated with Mv and darkness for 30 min (lane 5) or 1 h (lane 6).



absence of glucose, the decline in *crhR* transcript levels seen after a 2 h DBMIB treatment (Fig. 4.3.C, lane 3 and Fig. 4.3.D, lane 3, respectively) is attributed to long-term or subsidiary effects of the blockage at the *cyt b<sub>6</sub>f* complex. In control experiments to eliminate possible side-effects of the ethanol solvent used for the stock solutions of DCMU and DBMIB, photoautotrophic cultures were treated with a final concentration of 1% ethanol; this did not alter the expression of *crhR* compared to untreated cultures with either illumination or darkness.

The effects of DCMU and DBMIB are revealing because these two inhibitors act at opposite sides of plastoquinone in the electron transport chain. While both inhibitors interrupt light-dependent linear electron flow, they exert opposite effects on the redox state of the plastoquinone pool; furthermore, the metabolism of exogenous glucose is able to compensate for the block imposed by DCMU but not by DBMIB. The effects of these two inhibitors on *crhR* transcript levels is noticeably different in photoautotrophic cultures, and is altered by the metabolism of exogenously supplied glucose in agreement with the expected effects on the redox equilibrium of the plastoquinone pool.

KCN and Mv inhibit electron flow to cytochrome oxidase and to the PSI electron acceptors, respectively. Therefore these treatments were performed to assess the contributions of respiratory and cyclic electron flow. In photoautotrophic cultures treated with KCN and illumination for 1 h (Fig. 4.3.E, lane 2), the *crhR* transcript levels are elevated compared to untreated illuminated cultures (Fig. 4.3.E, lane 1). Furthermore, KCN does not prevent nor impair the *crhR* transcriptional response that normally occurs following re-illumination of a dark-incubated culture (Fig. 4.3.E, lane 4). These results agree with the expectation that *crhR* transcript levels will not decrease as a result of KCN addition since KCN does not prevent the reduction of the plastoquinone pool by PSII, which is the main reductant in the light. Also as expected, the addition of KCN to a dark-incubated photoautotrophic culture does not induce *crhR* transcription in the absence of light (Fig. 4.3.E, lane 3). In contrast, the addition of KCN to photomixotrophic cultures corresponds with a decrease in transcript levels both with illumination (Fig. 4.3.F, lane 2) and in darkness (Fig. 4.3.F, lane 3), as compared to the untreated control (Fig. 4.3.F, lane 1). This would be expected if the contribution of respiration to the total electron flow is much higher in cells that are utilizing exogenous glucose. In this case, the reduction of plastoquinone via NADPH-DHs would decrease due to the inhibitory effects of cyanide on enzymes of the pentose phosphate pathway for the production of NADPH; these effects are in addition to, and separate from, the blockage at the terminal cytochrome oxidase.

Mv acts as an artificial electron acceptor from PSI, thereby decreasing cyclic electron flow and/or ferredoxin reduction without preventing the oxidation or reduction of the inter-photosystem electron carriers. Compared to illuminated, untreated photoautotrophic cultures (Fig. 4.3.G, lane 1), initial *crhR* mRNA levels are relatively unaffected by the addition of Mv (Fig. 4.3.G, lane 2), but decrease after a 1 h treatment (Fig. 4.3.G, lane 3). Similarly, the *crhR* levels in illuminated photomixotrophic cultures are relatively unchanged after a 30 min Mv treatment (Fig. 4.3.H, lane 4) compared to the untreated control (Fig. 4.3.H, lane 1). The degradation of the *crhR* transcript observed in photomixotrophic cultures treated with Mv and illumination for 1 h (Fig. 4.3.H, lane 5) is attributed to general degradation of RNA, since it also occurs in the RNase P transcript. This is also representative of the non-specific RNA degradation that was observed in photoautotrophic cultures at higher Mv concentrations (200  $\mu$ M), and is presumed to be a consequence of the hydrogen peroxide and free oxygen radicals formed by the reduction of oxygen by Mv. Since this RNA degradation is not observed during incubation with Mv in the dark, Mv and DCMU, or Mv and DBMIB, it is ascribed to Mv-mediated oxidative stress that occurs as a result of the higher influx of electrons through PSI from PSII. The addition of Mv to photomixotrophic cultures grown in the dark for 30 min (Fig. 4.3.H, lane 6) or 1 h (Fig. 4.3.H, lane 7) yields a slight decrease in *crhR* levels compared to untreated dark-incubated cultures (Fig. 4.3.H, lane 2). Overall, the lack of significant effect on *crhR* levels is not unexpected, since Mv does not exert direct redox control over the plastoquinone pool.

The evidence obtained from DCMU or DBMIB treatment of cultures grown with or without exogenous glucose clearly indicates that *crhR* transcription increases when the redox equilibrium of the plastoquinone pool shifts towards a more reduced state (plastoquinol predominates). The inhibition of respiratory or cyclic electron flow with KCN or Mv treatments, respectively, also yields results that are compatible with this conclusion. Further to the individual treatments, *crhR* levels were assessed by Northern analysis following treatment of photoautotrophic and photomixotrophic cultures with various combinations of inhibitors, with or without illumination. These results indicate that conditions of plastoquinone oxidation correlate with a decrease in *crhR* levels, whereas conditions of net reduction of the plastoquinone pool correlate with the presence or increase in *crhR* transcript levels (Table 4.1).



**Table 4.1 Correlation Between the Presence of the *crhR* Transcript and the Predicted Redox State of the Plastoquinone Pool** All treatments were carried out with illumination at 400-450  $\mu\text{mol photons m}^{-2} \text{s}^{-1}$  unless otherwise specified. D, the culture was transferred into darkness simultaneous with addition of the poison. PQ, plastoquinone. glc, exogenous glucose added to medium (photomixotrophic culture conditions). Relative levels of the *crhR* transcript are indicated by: +, equivalent to control (untreated) levels; ++ or +++, increase compared to the control; +/- or +/- -, decrease; -, no transcript detected.

Treatment	<i>crhR</i> levels	Predicted net redox state of PQ	Brief explanation
DCMU	+/- -	oxidized	; cyclic electron flow continues
glc + DCMU	+++	reduced	electrons from NADPH-DHs and PSI reduce PQ in the absence of electrons from PSII
glc + DCMU + D	+	reduced	electrons from NADPH-DHs reduce PQ, independent of illumination
DBMIB	++	reduced	electrons prevented from exiting PQ pool
glc + DBMIB	++	reduced	electrons from PSII and NADPH-DHs reduce PQ, oxidation by cyt b6f is inhibited
glc + DBMIB + D	+	reduced	electrons from NADPH-DHs reduce PQ, oxidation by cyt b6f is inhibited
KCN	++	reduced	fewer electron sinks due to inhibition of cyt oxidase and Calvin cycle enzymes.
glc + KCN	-	oxidized	respiration of the exogenous glc is inhibited by KCN
glc + KCN + D	-	oxidized	respiration of the exogenous glc is inhibited by KCN
Mv	+	reduced	lowers the rate of PQ reduction by cyclic electron flow; general RNA degradation observed
glc + Mv	+	reduced	electrons from PSII and NADPH-DHs reduce PQ; no electron donation via PSI
glc + Mv + D	+	reduced	electrons from NADPH-DHs reduce PQ; no electron donation via PSI
DCMU + DBMIB	+	reduced	electron donation from PSII to PQ is inhibited; DBMIB prevents electron exit from PQ pool
DCMU + Mv	-	oxidized	both cyclic and linear electron flow through PQ are inhibited
glc + DCMU + Mv	++	reduced	PQ reduction by NADPH-DHs
glc + DCMU + Mv + D	+/-	reduced	PQ reduction by NADPH-DHs
DBMIB + Mv	+/- -	reduced	expected dominance of DBMIB-mediated effects masked by interaction of DBMIB and Mv?
glc + DBMIB + Mv	+	reduced	PQ reduction by NADPH-DHs; interaction of DBMIB and Mv
glc + DBMIB + Mv + D	+/-	reduced	PQ reduction by NADPH-DHs; interaction of DBMIB and Mv
DCMU + DBMIB + Mv	+/-	reduced	electron donation from PSII to PQ is inhibited; interaction of DBMIB and Mv
glc + DCMU + DBMIB + Mv	+	reduced	PQ reduction by NADPH-DHs; interaction of DBMIB and Mv
glc + DCMU + DBMIB + Mv + D	+/-	reduced	PQ reduction by NADPH-DHs; interaction of DBMIB and Mv
DBMIB + KCN + Mv	+++	reduced	observed effects of KCN alone?; interaction of DBMIB and Mv
glc + KCN + Mv	?	oxidized	general RNA degradation observed
KCN + Mv	-	oxidized	Mv provides alternative electron sinks, counteracts the effect of KCN alone

#### 4.2.1.4 Actinic Light-Induced Shifts in the Redox Equilibrium of the Plastoquinone Pool Yield a Corresponding Change in *crhR* Transcript Accumulation

To confirm that plastoquinol is the key mediator of *crhR* expression under physiological conditions, filters were used to alter the wavelengths of actinic light. Photoautotrophic cultures were grown to mid-log phase in a 30°C incubator with white light, then subjected to filtered illumination for 15, 30, and 60 min by inserting the appropriate filter between the cultures and the light source. The L1 filter, with a transmittance spectrum that gives 50% transmittance at 650 nm and 0% below 580 nm, was used to provide light which preferentially excites PSI and is predicted to shift the redox equilibrium of the plastoquinone pool to the oxidized (plastoquinone) form. The L2 filter, yielding 50% transmittance at 560 nm, preferentially excites PSII and is predicted to shift the redox equilibrium to the reduced (plastoquinol) form. The filters were used with higher intensity source light to compensate for reduced light transmission through the filters. Northern analysis and quantitation of *crhR* levels following each treatment indicates that at all time points *crhR* levels are significantly higher during incubation in L2 light compared to L1 light (Fig. 4.4), namely when plastoquinone-reducing conditions predominate. Transfer of a white light-adapted culture into L1 (Fig. 4.4, open bars) results in a significant decrease in the levels of *crhR* mRNA. In contrast, *crhR* transcript levels do not change significantly following transfer from white light into L2 (Fig. 4.4, filled bars). These results are also seen in representative Northern analyses obtained following transfer of white light-adapted cultures into L1 (Fig. 4.5.A, lanes 1-3) or L2 (Fig. 4.5.B, lanes 1-3). The correlation between plastoquinol and *crhR* that was apparent following the artificial alteration of electron transport (section 4.2.1.3) is therefore physiologically relevant in terms of light-harvesting conditions.

Subsequently, the effect of treating dark-incubated cultures with DCMU or DBMIB during re-illumination with L1 or L2 light was investigated. Interestingly, *crhR* transcripts levels are similar in cells transferred into L1 from white light (Fig. 4.5.A, lane 3) as from darkness (Fig. 4.5.A, lane 5). *crhR* levels are not significantly altered by DCMU treatment during re-illumination with L1 (Fig. 4.5.A, lane 6) but increase noticeably with L1 and DBMIB treatment (Fig. 4.5.A, lane 7). The level of cyclic electron occurring with L1 illumination transiently reduces plastoquinone via PSI, and this would be unchanged by addition of DCMU. Treatment with DBMIB, however, would prevent the oxidation of the plastoquinone pool by cyt *b<sub>6</sub>f*, thus shifting the redox equilibrium towards plastoquinol.

As observed for transfer into L1, *crhR* transcript accumulation is similar for cells transferred into L2 from white light (Fig. 4.5.B, lanes 2 and 3) as from darkness (Fig.

#### **Figure 4.4 The Quality of Actinic Light Affects the Expression of *crhR***

Photoautotrophic *Synechocystis* cells cultured in white light were transferred into L1 (open bars) or L2 (solid black bars) filtered illumination for the time indicated. Quantitation of the *crhR* transcript levels determined by Northern analysis was expressed as percentage of transcript in white light. L1 preferentially excites PSI and oxidizes the plastoquinone pool. L2 preferentially excites PSII and reduces the plastoquinone pool. \*, values are significantly different from L1.

Source: Kujat and Owttrim (2000).

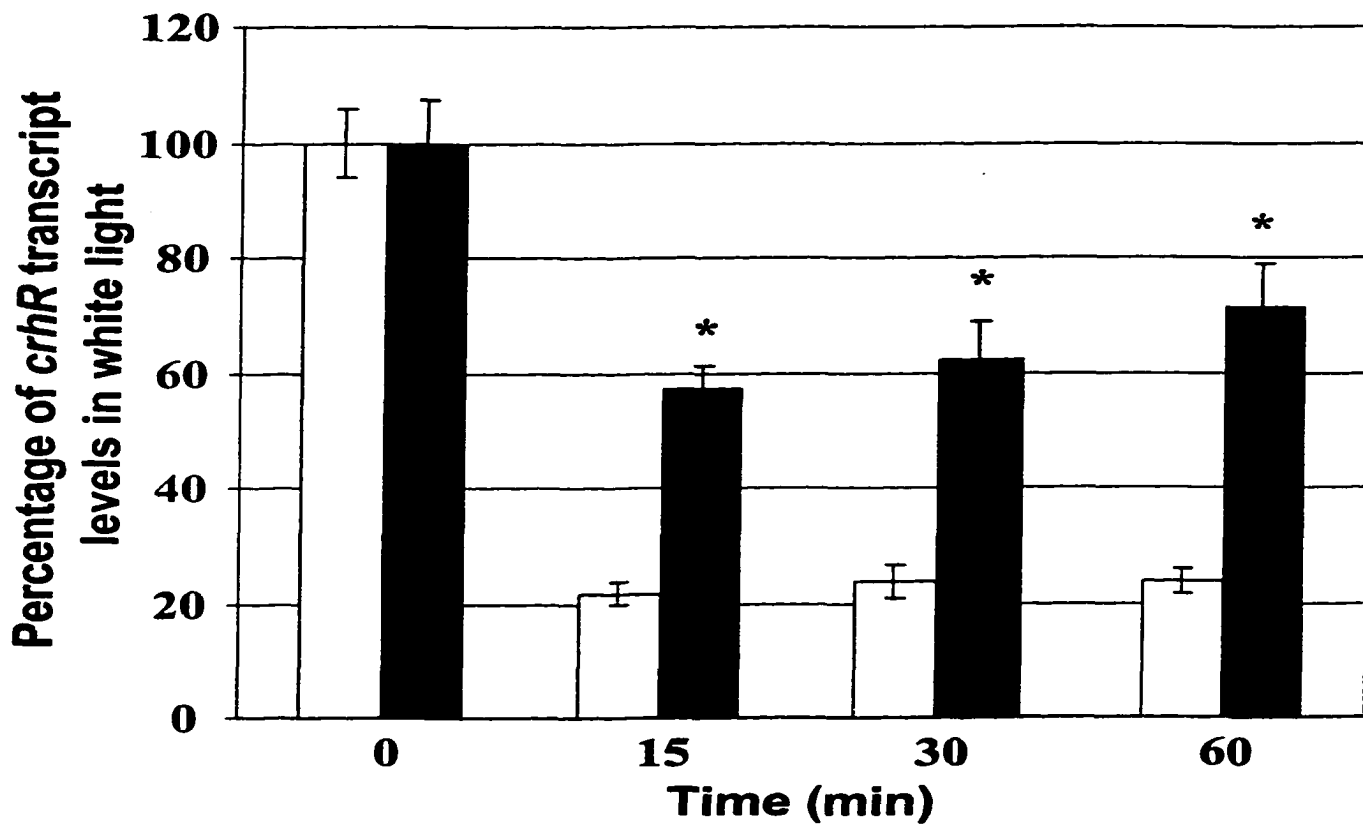


#### **Figure 4.5 Northern Analysis of *crhR* Transcript Accumulation Following Changes in Actinic Light or Stress Treatments**

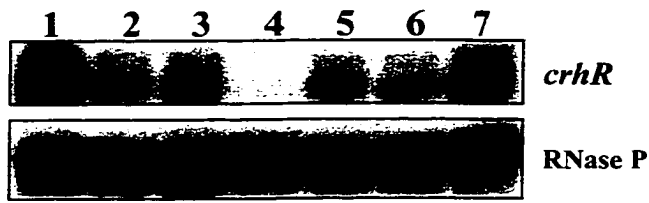
*Synechocystis* cultures were cultured at 30°C with white light at intensity of 400-450  $\mu\text{E m}^{-2} \text{s}^{-1}$ , except as indicated. The intensity of L1 illumination was 15  $\mu\text{E m}^{-2} \text{s}^{-1}$ , and of L2 illumination was 240  $\mu\text{E m}^{-2} \text{s}^{-1}$  (L2).

**A. Transfer into light that preferentially energizes PSI.** Cultures were grown with white light (lane 1), then transferred into L1 light for 1 h (lane 2) or 2 h (lane 3). Alternatively, cultures were incubated in darkness for 2 h (lane 4) prior to illumination for 1 h with L1 (lane 5), L1 and DCMU (lane 6), or L1 and DBMIB (lane 7).

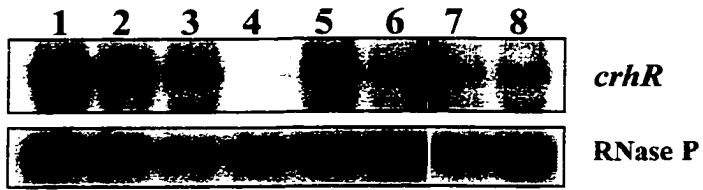
**B. Transfer into light that preferentially energizes PSII.** Cultures were grown with white light (lane 1), then transferred into L2 for 30 min (lane 2) or 60 min (lane 3). Alternatively, cultures were pre-incubated in darkness for 2 h (lane 4) prior to re-illumination with L2 for 30 min (lane 5) or 60 min (lane 6), or 60 min of L2 plus DCMU (lane 7) or DBMIB (lane 8).

**C. Treatment of *Synechocystis* with various stresses.** Illuminated photoautotrophic cultures at 30°C (lane 1), were subjected to the following 1 h treatments: 20°C (lane 2), 44°C (lane 3), 0.5 M NaCl (lane 4), 5 mM glucose (lane 5), 80  $\mu\text{g/mL}$  naladixic acid (lane 6), 80  $\mu\text{g/mL}$  naladixic acid and darkness (lane 7), 10  $\mu\text{g/mL}$  tetracycline (lane 8), 40  $\mu\text{g/mL}$  chloramphenicol (lane 9). Alternatively, cultures were incubated for 2 h in darkness prior to the following 1 h treatments with continued darkness: 20°C (lane 10), 44°C (lane 11), 0.5 M NaCl (lane 12), 5 mM glucose (lane 13), 80  $\mu\text{g/mL}$  naladixic acid (lane 14), 40  $\mu\text{g/mL}$  chloramphenicol (lane 15), re-illumination (lane 16). Alternatively, illuminated photoautotrophic cultures (lane 17) were subjected to the following 1 h treatments: 20°C and illumination of 300  $\mu\text{E m}^{-2} \text{s}^{-1}$  intensity (lane 18), 20°C and illumination of 60-90  $\mu\text{E m}^{-2} \text{s}^{-1}$  intensity (lane 19), 37°C (lane 20).

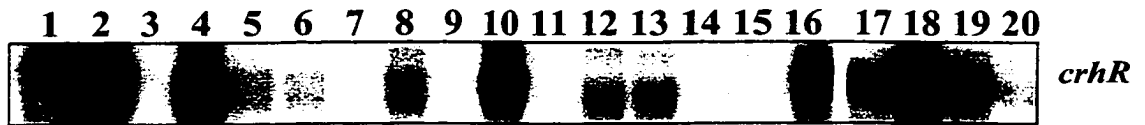
**A**



**B**



**C**



4.5.B, lanes 5 and 6). A similar level of *crhR* mRNA is also apparent following re-illumination with L2 light in the presence of DCMU (Fig. 4.5.B, lane 7). By comparison with L1, L2 illumination generates an increased rate of linear electron flow, which would be inhibited by addition of DCMU. Also in L2, relative levels of PSI turnover and cyclic electron flow are higher than in white light; since these are unaffected by DCMU transient plastoquinone reduction would continue following transfer from white light into L2. The expression of *crhR* with L2 and DCMU would thus correspond with the plastoquinone reduction resulting from cyclic electron flow. Accordingly, DBMIB treatment with L2 light is expected to yield an increase in *crhR* transcript accumulation, since plastoquinone oxidation is inhibited essentially as described for L1. Unexpectedly, *crhR* levels are not significantly affected by this treatment (Fig. 4.5.B, lane 8). These results are possibly influenced by light intensity (investigated below), and by the manner in which the filters modulate the actinic light to yield *preferential* excitation of one photosystem without preventing general light-harvesting and photosynthesis, as discussed in section 4.3.1.

#### **4.2.1.5 *crhR* Transcript Levels Respond to the Intensity of Actinic Light**

During the course of the previous experiments (section 4.2.1.4) the presence of the L1 and L2 filters may have simultaneously affected the intensity as well as the quality of the actinic light, although every effort was taken to minimize these differences relative to white light. Therefore, the influence of illumination intensity on *crhR* transcript accumulation was investigated. For this purpose RNA was isolated from duplicate photoautotrophic and photomixotrophic cultures following changes in the intensity of illumination, and subjected to Northern analysis (Table 4.2). For each experiment the levels of *crhR* were quantitated and converted to percent of transcript levels in high intensity illumination; calculations are based upon comparisons restricted to samples from the same experiment. From these results it is apparent that *crhR* levels decline following a transfer from high to low intensity light, unless exogenous glucose is present. Conversely, the expression of *crhR* increases following a transfer from low to higher intensity illumination. Interestingly, this correlation is only seen when cells are transferred from 60-90  $\mu\text{mol photon m}^{-2} \text{s}^{-1}$  into 150-300  $\mu\text{mol photon m}^{-2} \text{s}^{-1}$ , whereas further increases do not induce a corresponding increase in *crhR* transcript levels. Thus it appears that there is a certain threshold of light intensity that causes alterations in *crhR* expression. Compared to the higher levels of *crhR* seen with addition of DBMIB, the addition of DCMU dampens the response to increasing intensity of actinic light. These results are in agreement with the previously observed effects of DCMU and DBMIB

**Table 4.2 The Effect of Alterations in Light Intensity on the Expression of *crhR***  
*Synechocystis* was cultured at 400-450  $\mu\text{mol photons m}^{-2} \text{s}^{-1}$  prior to treatments unless otherwise indicated. For details see text, section 4.2.1.

Experiment	Treatment	Relative <i>crhR</i> transcript levels (%)
1. Transfer of photoautotrophic cultures from high to low intensity illumination	(a) growth at 600-650 $\mu\text{mol photons m}^{-2} \text{s}^{-1}$	100 $\pm$ 2.3
	(b) 30 min at 60-90 $\mu\text{mol photons m}^{-2} \text{s}^{-1}$	38.6 $\pm$ 11.6
	(c) 60 min at 60-90 $\mu\text{mol photons m}^{-2} \text{s}^{-1}$	28.6 $\pm$ 10.3
	(d) 2 h at 60-90 $\mu\text{mol photons m}^{-2} \text{s}^{-1}$	35.3 $\pm$ 12.5
2. Transfer of photomixotrophic cultures from high to low intensity illumination	(a) growth at 600-650 $\mu\text{mol photons m}^{-2} \text{s}^{-1}$	100
	(b) 30 min at 60-90 $\mu\text{mol photons m}^{-2} \text{s}^{-1}$	87.7 $\pm$ 9.8
	(c) 60 min at 60-90 $\mu\text{mol photons m}^{-2} \text{s}^{-1}$	91.4 $\pm$ 11.0
3. Transfer of photoautotrophic cultures from low to high intensity illumination	(a) 3 h at 60-90 $\mu\text{mol photons m}^{-2} \text{s}^{-1}$	38.4 $\pm$ 4.9
	(b) a + 30 min at 150-300 $\mu\text{mol photons m}^{-2} \text{s}^{-1}$	96.4 $\pm$ 3.8
	(c) b + 30 min at 400-450 $\mu\text{mol photons m}^{-2} \text{s}^{-1}$	110.8 $\pm$ 4.3
	(d) c + 30 min at 600-650 $\mu\text{mol photons m}^{-2} \text{s}^{-1}$	100 $\pm$ 5.1
4. Transfer of photoautotrophic cultures from low to high intensity of illumination with addition of electron transport inhibitors	(a) growth at 400-450 $\mu\text{mol photons m}^{-2} \text{s}^{-1}$	100 $\pm$ 1.3
	(b) a + 60 min at 60-90 $\mu\text{mol photons m}^{-2} \text{s}^{-1}$	46.3 $\pm$ 7.1
	(c) b + 60 min at 400-450 $\mu\text{mol photons m}^{-2} \text{s}^{-1}$ with DCMU	70.9 $\pm$ 11.6
	(d) b + 60 min at 400-450 $\mu\text{mol photons m}^{-2} \text{s}^{-1}$ with DBMIB	106 $\pm$ 0.6



when added simultaneous with re-illumination and are compatible with the higher rate of plastoquinone reduction via PSII that occurs at higher light intensities.

#### 4.2.1.6 Re-examination of the Effects of Various Stresses on *crhR* Expression

Since redox conditions are altered by treatments other than illumination it was hypothesized that *crhR* expression would also be affected, therefore the initial investigation into stress-induced *crhR* expression was reviewed and expanded (Fig. 4.5.C). All treatments were performed with photoautotrophic *Synechocystis* cultures. Representative results of Northern analysis indicate that the *crhR* transcript is not detected following heat-shock induced by transfer from 30°C (Fig. 4.5.C, lane 1) to 44°C (Fig. 4.5.C, lane 3) or 37°C (Fig. 4.5.C, lane 20). Neither is *crhR* expression induced by transfer to 44°C in darkness (Fig. 4.5.C, lane 11). In stark contrast, when *Synechocystis* cultures are cold-shocked by transfer from 30°C (Fig. 4.5.C, lane 17) to 20°C and the intensity of illumination remains constant (Fig. 4.5.C, lane 18) *crhR* levels are significantly higher than in cultures transferred to 20°C with a simultaneous decrease in light intensity (Fig. 4.5.C, lane 19). In cultures that have been pre-incubated in darkness, transfer to 20°C induces expression of the *crhR* transcript (Fig. 4.5.C, lane 10). These effects of temperature on *crhR* expression clearly indicate that it is a cold-induced gene, and that illumination conditions modulate the transcriptional response. Northern analysis following treatment with 0.5 M NaCl and illumination (Fig. 4.5.C, lane 4) or darkness (Fig. 4.5.C, lane 12) confirm that expression of *crhR* is induced by salt. Similar to the effects of cold-shock, the *crhR* transcriptional response to increasing osmolarity is higher with illumination than with darkness, suggesting a synergistic interaction that may localize to the thylakoid membrane.

To determine the effect of DNA damage on *crhR* transcription, cultures were treated with naladixic acid and illumination (Fig. 4.5.C, lane 6), which yields a decrease in *crhR* levels. Addition of naladixic acid simultaneous with darkness (Fig. 4.5.C, lane 7) or following a 2 h pre-incubation in darkness (Fig. 4.5.C, lane 14) does not induce *crhR* expression. Inhibition of the elongation step of translation by addition of the antibiotic tetracycline (Fig. 4.5.C, lane 8) has no effect on *crhR* levels. In contrast, chloramphenicol treatment, which also inhibits translation but does so at the initiation stage, correlates with lack of accumulation of the *crhR* transcript during illumination (Fig. 4.5.C, lane 9) as well as darkness (Fig. 4.5.C, lane 15). The significance of these results is integrated into a model of *crhR* expression as presented in chapter seven.

## **4.2.2 The Post-Transcriptional Regulation of *crhR* is Mediated by Cellular Redox State**

Since differential effects of light on mRNA stability may affect transcript levels in cyanobacteria, it was important to determine the *crhR* transcript half-life. The transcriptional inhibitor rifampicin was added simultaneously with light or dark treatments to photoautotrophic and photomixotrophic cultures. Experiments were repeated in duplicate using independent large-scale cultures. *crhR* levels were determined by Northern analysis, quantified from autoradiograms, and expressed as a percentage of the *crhR* transcript level in untreated illuminated cultures. Transcript half-lives were calculated by linear regression analysis. These results indicate that under photoautotrophic conditions the *crhR* transcript half-life is significantly shorter in the light than in the dark, with values of 6 min and 36 min, respectively (Fig. 4.6.A). When the cultures are grown with addition of 5 mM glucose, the *crhR* transcript half-life is again shorter in the light than in the dark, with values of 6 min and 38 min, respectively (Fig. 4.6.B). Evidently, *crhR* transcript stability is affected by illumination but not by the presence of glucose, in contrast to transcription.

When rifampicin is added simultaneously with DCMU or DBMIB to illuminated cultures grown with and without glucose, the transcript half-lives increase significantly. Addition of DCMU to photoautotrophic cultures causes the *crhR* half-life to increase to 22 min, while DBMIB causes an increase to greater than 5 h. Similarly, DCMU and DBMIB treatment of photomixotrophic cultures increases the *crhR* half-life to greater than 5 h. Since DCMU and DBMIB both interrupt linear electron flow, the observation that they exert the same effect on the *crhR* half-life suggests that the transcript stability responds to redox conditions. Unlike the transcriptional regulation that is mediated via redox state of the plastoquinone pool, the post-transcriptional regulation appears to be responsive to a separate aspect of the changes in photosynthetic electron transport.

## **4.2.3 Mapping of the Putative 5' Transcription Initiation Site of the *crhR* mRNA, and Sequence Analysis in the Surrounding Region**

### **4.2.3.1 Primer Extension to Determine 5' Ends of the *crhR* Transcript**

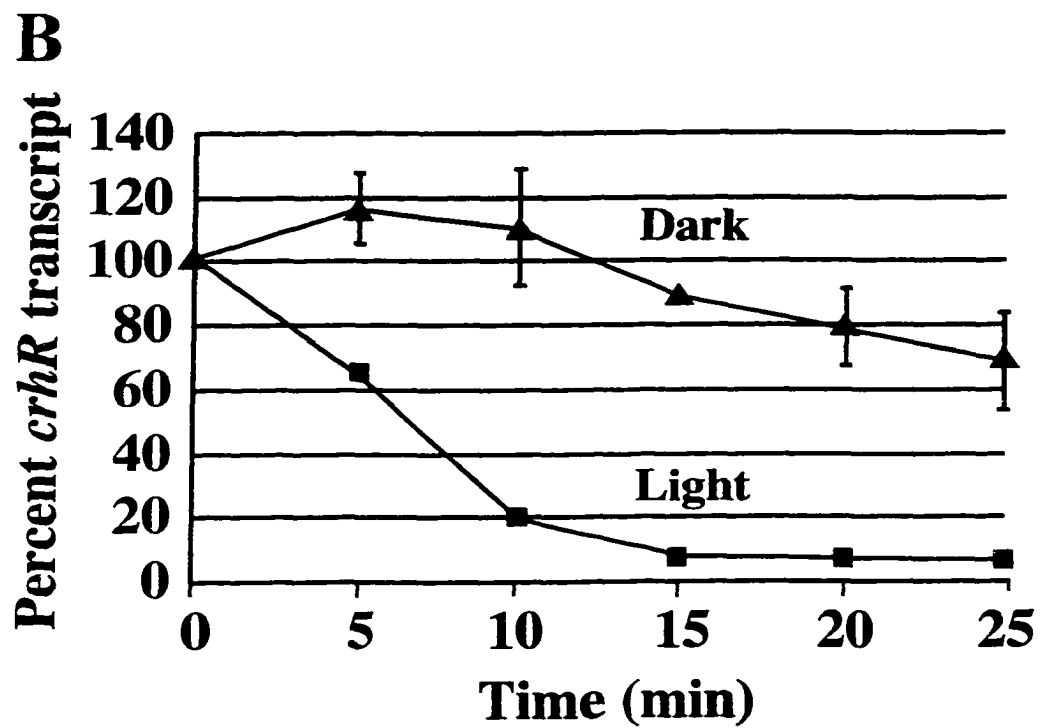
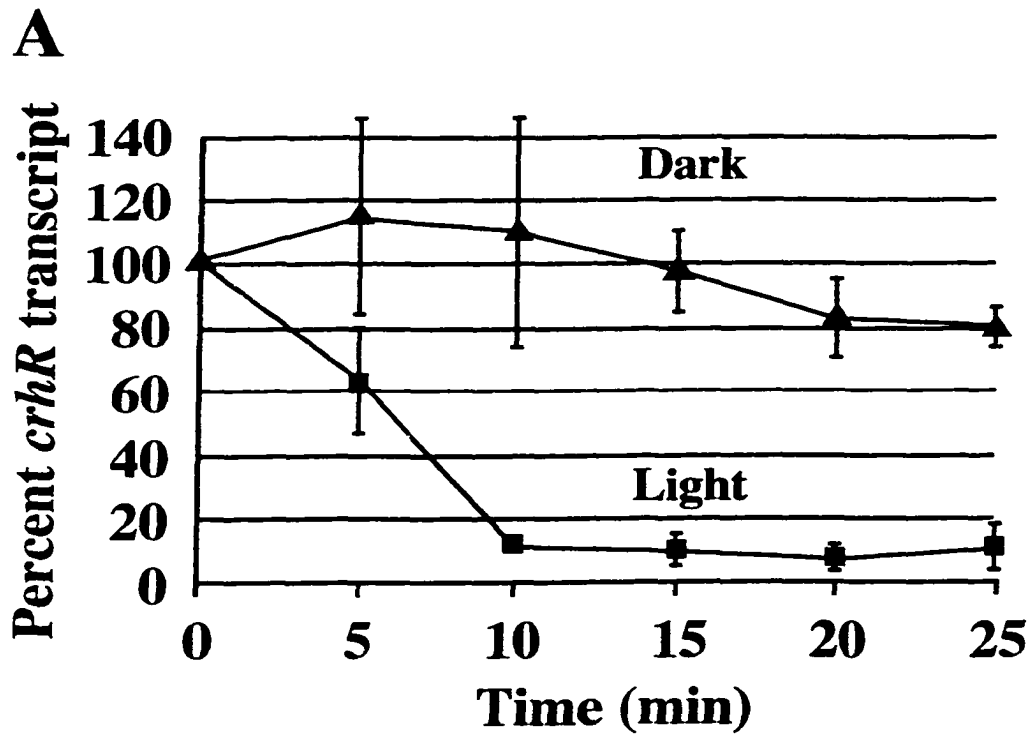
Primer extension was carried out with GWO42 and GWO45 end-labeled oligonucleotides as the primers (Table 2.4). The template RNA was total RNA from photoautotrophic or photomixotrophic cultures treated to light or darkness, in which the presence or absence of the *crhR* transcript had been confirmed by Northern analysis. The resultant autoradiographs showed significant background, seen as variable numbers of signals due to non-specific termination by Reverse Transcriptase. These signals were not

## Figure 4.6 Determination of *crhR* Transcript Stability

**A. *crhR* half-life under photoautotrophic conditions.** Photoautotrophic *Synechocystis* cultures were treated with rifampicin (400 µg/mL) and white light or darkness for the time indicated. Following Northern analysis, the signals for *crhR* were quantitated and expressed as a percentage of *crhR* mRNA in untreated illuminated cultures.

**B. *crhR* half-life in the presence of exogenous glucose.** Photomixotrophic cultures were treated with rifampicin (400 µg/mL) and white light or darkness for the time indicated. Following Northern analysis, the signals for *crhR* were quantitated and expressed as a percentage of *crhR* mRNA in untreated illuminated cultures.

Source: Kujat and Owttrim (2000).



consistent between experiments, were not limited to the samples that contained *crhR* by Northern analysis, and were observed at positions both upstream and downstream of the signal indicated by an asterisk in Fig. 4.7.A and Fig. 4.7.B. The indicated band is consistently observed with both primers and correlates with the presence or absence of the *crhR* transcript. This signal indicates the presence of a transcript whose 5' end corresponds to bp #2887535 in the DNA sequence, which is an A residue 109 bp upstream of the ATG initiator codon of the *crhR* gene.

#### **4.2.3.2 S1 Nuclease Mapping of the 5' Ends of the *crhR* Transcript: The *crhR* Gene Has Two Redox-Regulated Transcripts**

To confirm the results obtained by primer extension, a high resolution S1 nuclease protection assay was used to map the 5' end(s) of the *crhR* transcript and thereby identify possible promoter regions. Template RNA is as described for the primer extension assays. The ssDNA probes were generated as dsDNA fragments by PCR amplification using pairs of synthetic oligonucleotide primers where one primer is internal to the *crhR* transcript and complementary to the coding strand, and the second primer is complementary to the non-coding strand but includes sequence that is not complementary to the genome. With cs0096-9 as the template DNA, the primer pair (GWO45 + FWD) yields a 478 bp fragment that includes 157 bp of the 3' end of *slr0082* and 111 bp of vector sequence (Fig. 4.8). With cs0096 as template, the primer pair (GWO47 + GWO48) yields an 842 bp fragment that includes 770 bp of sequence homologous to *slr0082*, and 7 bp of non-homologous residues included in GWO48 (Fig. 4.9). Although these dsDNA PCR fragments were end-labeled on both 5' termini, the non-homologous sequence at the 5' end of the non-hybridizing strand would be susceptible to S1 nuclease digestion and would not produce a labeled protected fragment, thus further purification of the strand complementary to the mRNA is unnecessary.

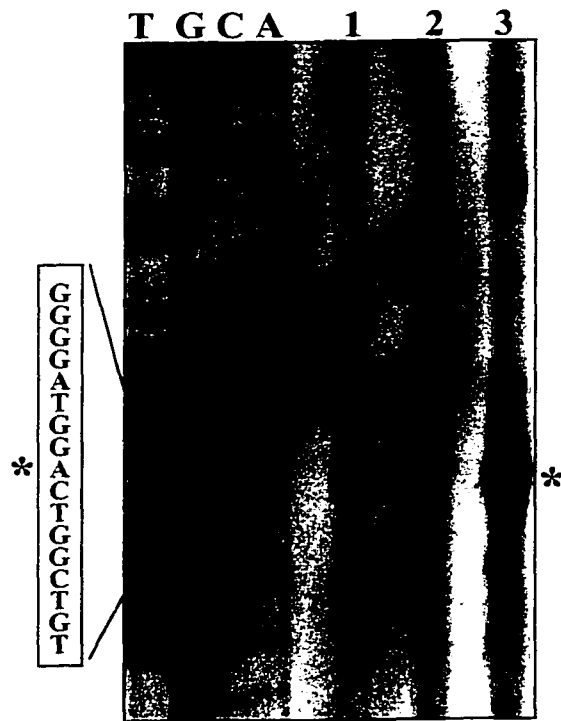
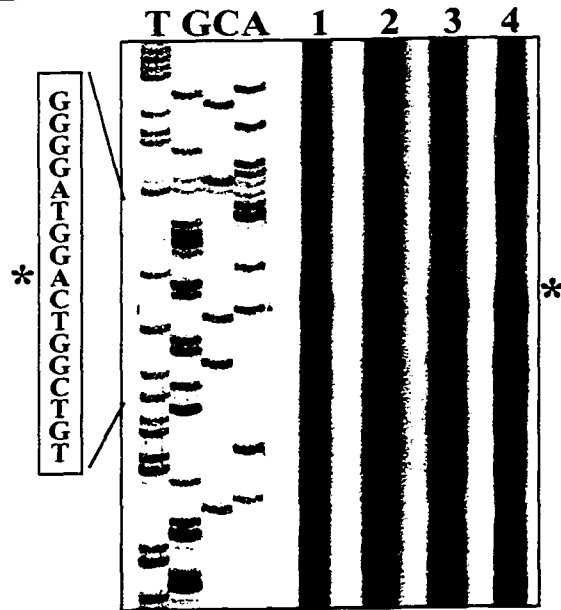
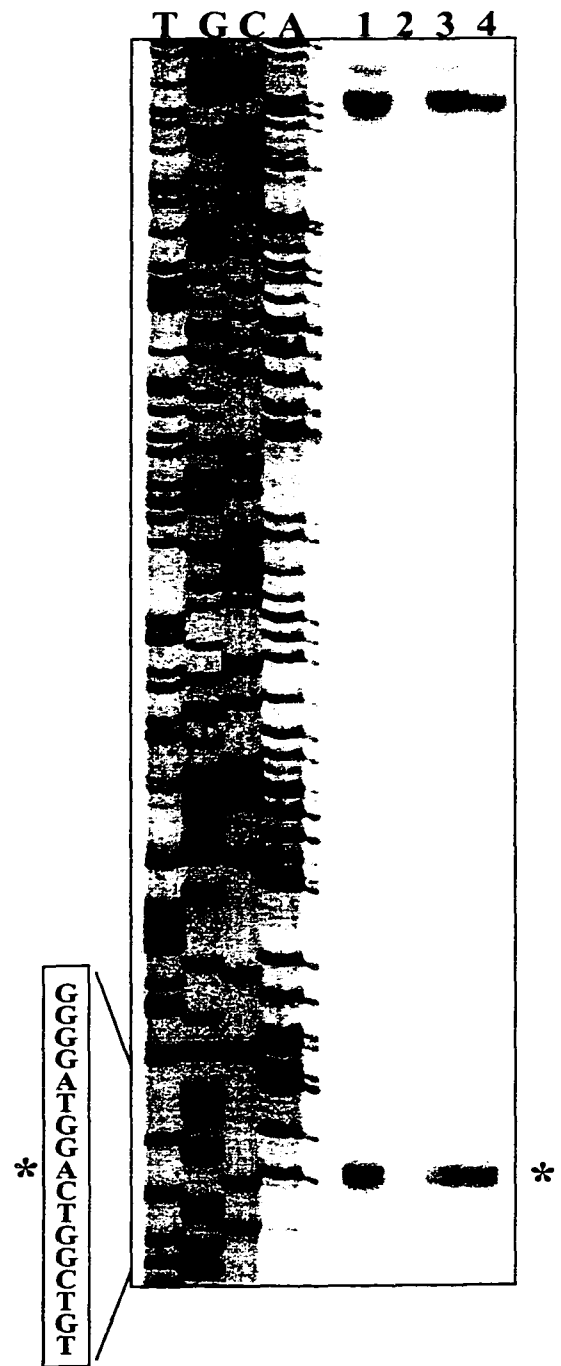
S1 nuclease protection assays performed with the DNA fragments 47/48 and 45/FWD (diagrammed in Fig. 4.9) yielded cleaner results than the primer extension assays. The data obtained using 47/48 is not shown since the results are identical. In agreement with Northern analyses, RNA extracted from dark-treated photoautotrophic cultures (Fig. 4.7 C, lane 2) does not generate protected fragments of the 45/FWD probe. Also in agreement with Northern analysis, protected fragments are detected in reactions containing RNA extracted from cultures grown under illuminated photoautotrophic (Fig. 4.7 C, lane 1), illuminated photomixotrophic (Fig. 4.7 C, lane 3), and dark-incubated photomixotrophic (Fig. 4.7 C, lane 4) conditions. Two protected fragments are obtained: The fragment of size 188 nt (indicated in Fig. 4.7 by "\*") indicates the presence of a

### **Figure 4.7 Determination of the 5' Termini of the *crhR* Transcript**

**A. Primer extension using GWO42 as the primer.** The oligonucleotide primer GWO42 was end-labeled and annealed to total RNA extracted from photoautotrophic cells grown with illumination (lane 1) or treated to 3 h darkness (lane 2), or from illuminated photomixotrophic cultures (lane 3).

**B. Primer extension using GWO45 as the primer.** The oligonucleotide primer GWO45 was end-labeled and annealed to total RNA extracted from photoautotrophic cultures that had been grown with illumination (lane 1) or treated to 3 h darkness (lane 2), or from photomixotrophic cultures grown with illumination (lane 3) or treated to 3 h darkness (lane 4).

**C. S1 nuclease protection assay.** The dsDNA PCR fragment 45/FWD was annealed to total RNA extracted from photoautotrophic cultures that had been grown with illumination (lane 1) or treated to 3 h darkness (lane 2), or from photomixotrophic cultures grown with illumination (lane 3) or treated to 3 h darkness (lane 4).

**A****B****C**

**Figure 4.8 The Region of DNA Surrounding the Putative Promoter of *crhR***

The top line represents the DNA probe used for S1 nuclease mapping of the 5' termini of the *crhR* transcript, where the dashed portion indicates pBluescriptKS+ vector sequence. The small thicker arrows labeled GWO45 and FWD indicate the position of the PCR primers used to generate the fragment. E, *Eco* RI site. The lower line represents the region of genomic DNA comprising the 5' region of the *crhR* gene. The DNA sequence given below the two lines extends from the *Eco* RI site to the putative translation initiation codon, indicated by the boxed ATG. The A residue that is indicated as the +1 site, is the proximal 5' terminus of the *crhR* mRNA as determined by primer extension and S1 nuclease mapping. Relative to this site, the -10 (extended -10) and -35 regions are indicated in bold. Two copies of the putative photoregulatory element (Marraccini *et al*, 1994) are also indicated on the sequence. The diagram is drawn to scale, except for the arrows indicating primer homology sites.



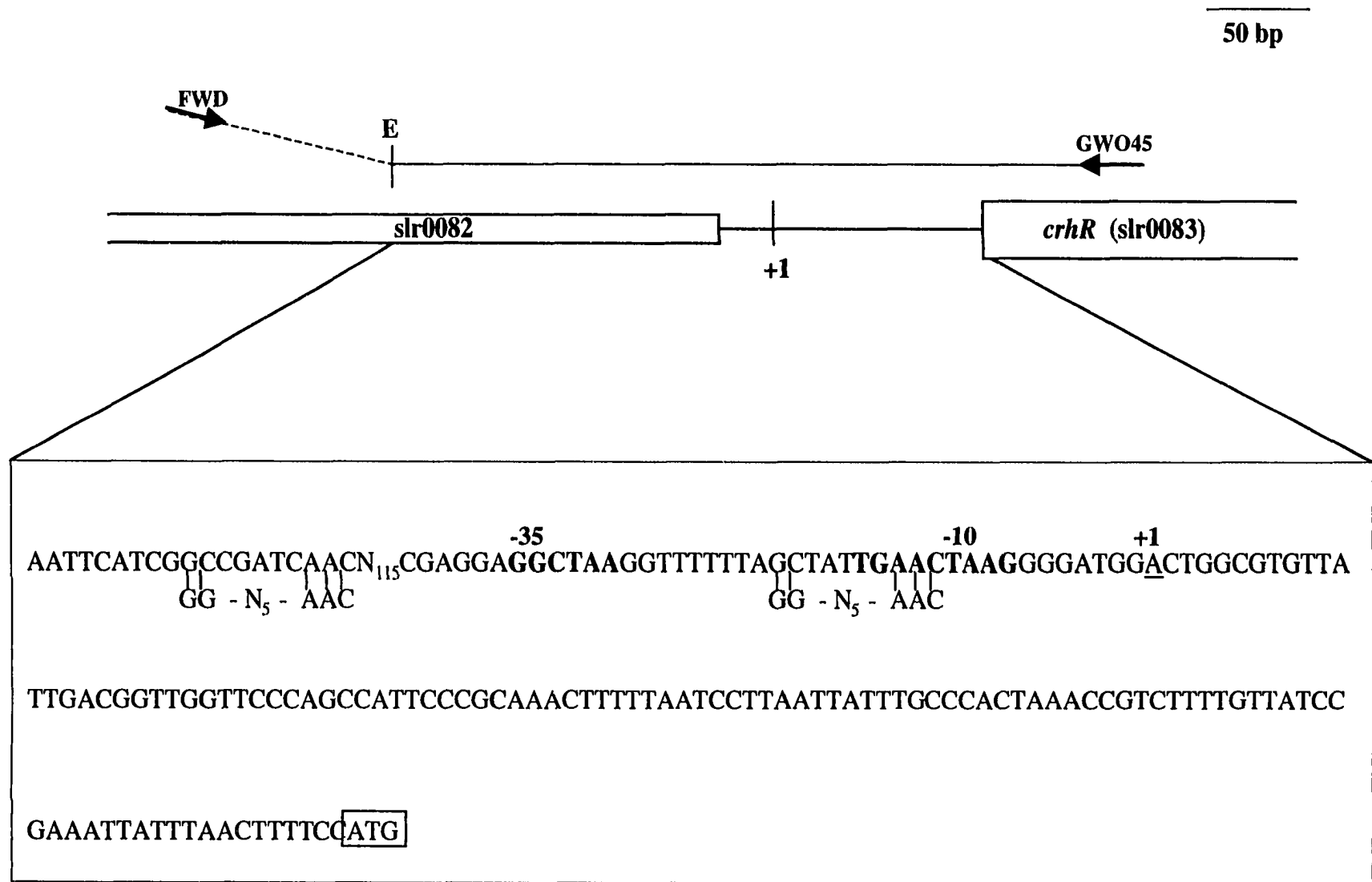
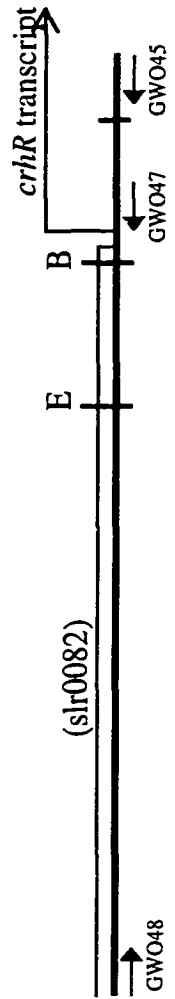


**Figure 4.9 dsDNA Fragments Used in EMSA Experiments, as Target and as Competitor DNAs**

Top line is a map of the region, showing the putative promoter region as determined by S1 nuclease mapping. Fragments are named according to the primer(s) and/or enzyme sites at the termini, to indicated how they were generated. For each fragment the size in bp is indicated in brackets. The diagram is drawn to scale, except for the arrows indicating primer homology sites. The *crhR* transcript is indicated as starting from the +1 site identified by S1 nuclease. Boxes indicate fragments that show reduced mobility when incubated with cell-free extract from *Synechocystis*. E, *Eco* RI. B, *Bgl*I.

100 bp



(slr0082)

(986 bp)

(842 bp)

(620 bp)

(224 bp)

(140 bp)

(367 bp)

(228 bp)

45/48

47/48

48E

47E

B-E

45E

45B

transcript whose 5' terminus maps to bp #2887535 in the DNA. This is identical to the results obtained by primer extension analyses.

The 367 nt protected fragment indicates the presence of a second redox-regulated transcript. The 5' end of this fragment corresponds to the *Eco* RI site (bp #2887277) that forms the boundary between *Synechocystis* genomic sequence and pBluescriptKS+ vector sequence. This indicates that the 111 nt of pBluescript sequence has been removed leaving only the region of the probe derived from *Synechocystis* genomic sequence. Therefore the 5' end of the second transcript must be upstream of the *Eco* RI site, such that the transcription initiation site and the location of the distal promoter will require further investigation. The 367 nt protected fragment is not the result of genomic DNA contamination in the RNA samples, since it (as well as the 188 nt fragment) is not detected when the RNA samples are pre-treated with DNase-free RNase A.

#### **4.2.3.3 Identification of Potential *cis*-Elements Proximal to the Putative Transcript Initiation Site**

The S1 nuclease and primer extension results identify a transcript whose 5' end is an A residue 109 bp upstream of the putative ATG translation initiation codon. Relative to this site, the sequence 5'-ACTAAG-3' occurs in the -10 region and 5'-GGCTAA-3' occurs in the -35 region (Fig. 4.8). When these sequences are compared to the consensus promoter motifs recognized by *E. coli*  $\sigma^{70}$ , the *crhR* -35 sequence lacks homology to the *E. coli* 5'-TTGACA-3' consensus and the -10 region has weak homology to the *E. coli* 5'-TATAAT-3'. In fact the -10 region may contain an "extended -10" motif, since the sequence 5'-TGA ACTAAG-3' has significant homology to the consensus sequence 5'-TGnTATAAT-3' (Barne *et al*, 1997).

Various promoter regions have been analyzed in the literature, and specifically in unicellular cyanobacteria different light-regulated promoter elements have been identified, conferring both negative and positive regulatory control. Interestingly, in agreement with the light-responsive expression of *crhR* there are two copies of the 10 nt motif GCN<sub>5</sub>AAC, which has significant homology to a GGN<sub>5</sub>AAC putative photoregulatory promoter element from *Synechocystis* (Marracini *et al*, 1994) (Fig. 4.8).

#### **4.2.4 Analysis of the Putative Promoter Region by Electrophoretic Mobility Shift Assays (EMSA)**

The putative photoregulatory motifs in the proximal promoter region and the observation of light-responsive *crhR* expression suggested an interaction between *cis*-elements in the DNA and *trans*-acting factors from the cytosol. As well, the

circumstantial evidence for a signal transduction pathway leading from light-sensing via plastoquinone to *crhR* transcription implies that any DNA-binding proteins isolated would be candidate transcription or accessory factors. This was pursued by electrophoretic mobility shift assays (EMSA) in which various end-labeled dsDNA fragments were incubated with cell-free extracts from *Synechocystis* and resolved by native polyacrylamide gel electrophoresis. If the target dsDNA is bound by an effector moiety from the extracts, the formation of a complex causes a reduction in the mobility of the DNA fragment compared to the unbound DNA, visualized by autoradiography.

#### **4.2.4.1 Formation of a Complex Between the dsDNA Fragment 45E and a Soluble Effector**

The dsDNA fragments that were employed as target or competitor DNA are diagrammed in Figure 4.9. These were incubated with cell-free extracts obtained from illuminated photoautotrophic cultures of *Synechocystis*, since the *crhR* transcript is detected under these conditions. Initially the assays were performed with the PCR products 47/48 (842 bp) and 45/48 (985 bp) as target DNA; DNA-effector complexes were not detected presumably due to the large size of the fragments that prevents resolution of the bound versus free DNA. Subsequently, the 45/48 dsDNA fragment was digested with *Eco* RI to yield a 367 bp fragment, designated 45E. The control reaction lacking cell-free extracts indicates the migration position of the unbound 45E dsDNA (Fig. 4.10.A, lane 1; Fig. 4.10.B, lane 1), and the addition of cell-free extracts corresponds with a shift in the mobility of 45E, interpreted as the formation of DNA-effector complexes (Fig. 4.10.A, lanes 2-5). This confirms that the *in vitro* assay conditions are conducive to interactions between the target dsDNA fragment and an unidentified factor(s) or complex in the cell-free extracts. Since the amount of DNA that shifts correlates with an increase in the amount of cell-free extracts added, this implies the interaction has a stoichiometric relationship. The bound DNA fragment is consistently detected following incubation with extracts prepared under non-denaturing conditions regardless of storage at -20°C or -80°C. Furthermore, cell-free extracts prepared by sonication are equally competent for inducing the shift as extracts prepared by mechanical lysis with glass beads.

When 45E is incubated with an equivalent amount of BSA in place of cell-free extracts no shift occurs (Fig. 4.10.B, lane 2), which shows that the binding is not the result of non-specific DNA-protein interactions. Pre-treating the cell-free extract by heating (Fig. 4.10.B, lane 4), or by addition of detergent (Fig. 4.10.B, lane 5) abolished the shift, indicating that the interaction between the target DNA and the effector is

**Figure 4.10 EMSA for the Detection of Protein Binding to the Putative Promoter Region of *crhR***

Unless otherwise indicated, cell free extracts were prepared from photoautotrophic *Synechocystis* cultures grown with continuous illumination.

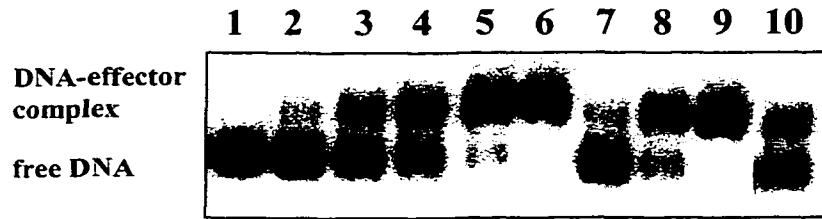
**A. EMSA performed with 45E as the target DNA.** The dsDNA fragment 45E was incubated without additions (lane 1), or with 1  $\mu\text{g}$  (lane 2), 5  $\mu\text{g}$  (lane 3), 10  $\mu\text{g}$  (lane 4), 20  $\mu\text{g}$  (lane 5) or 35  $\mu\text{g}$  (lane 6) of cell-free extract. Alternatively, 45E was incubated with 1  $\mu\text{g}$  (lane 7), 10  $\mu\text{g}$  (lane 8), or 35  $\mu\text{g}$  (lane 9) of cell-free extract prepared after 24 h dark treatment of photoautotrophic *Synechocystis* cultures. All reactions were incubated at 37°C for 30 minutes (lanes 1-9). For comparison, 45E was incubated with 10  $\mu\text{g}$  of cell-free extract from light-grown cells on ice for 30 minutes (lane 10).

**B. EMSA performed with 45E as the target DNA.** The dsDNA fragment 45E was incubated without additions (lane 1), with 20  $\mu\text{g}$  BSA (lane 2), or with 20  $\mu\text{g}$  untreated cell-free extract (lane 3). Alternatively, the cell-free extract (20  $\mu\text{g}$ ) was pre-treated as follows: 1 min at 95 °C (lane 4), 0.1% SDS (lane 5), 2 U proteinase K (30 min, 37°C) (lane 6), 0.5  $\mu\text{g}$  DNase (30 min, 37°C) (lane 7), or 0.5  $\mu\text{g}$  RNase (30 min, 37°C) (lane 8). 45E was incubated with 20  $\mu\text{g}$  untreated cell-free extract with addition of the following competitor DNA: 5  $\mu\text{g}$  poly[d(I-C)] (lane 9), 1.25  $\mu\text{g}$  *Synechocystis* chromosomal DNA (lane 10), 0.5  $\mu\text{g}$  325 bp *Sma* I fragment internal to *crhR* gene (lane 11), 0.5  $\mu\text{g}$  48E (lane 12), 0.5  $\mu\text{g}$  47E (lane 13), or 0.5  $\mu\text{g}$  B-E (lane 14).

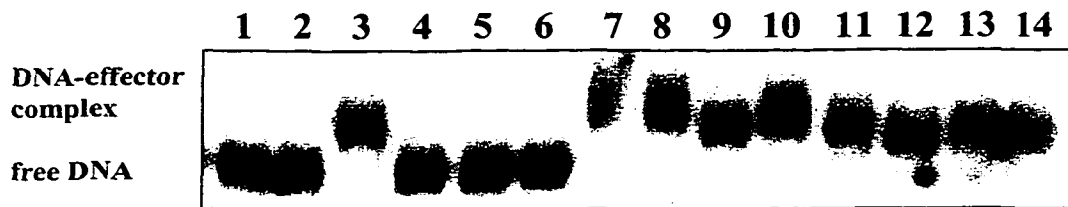
**C. EMSA performed with 45B as the target DNA.** The dsDNA fragment 45B was incubated without additions (lane 1), or with 2  $\mu\text{g}$  (lane 2), 10  $\mu\text{g}$  (lane 3), 20  $\mu\text{g}$  (lane 4), or 30  $\mu\text{g}$  (lane 5) of cell-free extract.

**D. EMSA performed with 45B as the target DNA.** The dsDNA fragment 45B was incubated without additions (lane 1), with 20  $\mu\text{g}$  of untreated cell-free extract (lane 2), or with 20  $\mu\text{g}$  BSA (lane 3). Alternatively, EMSA reactions with the target DNA 45B were performed as detailed above for part (B) (lanes 4-14).

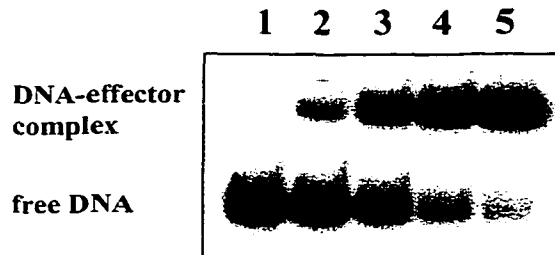
**A**



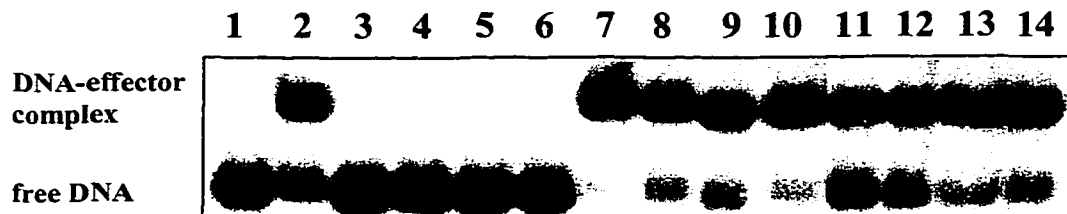
**B**



**C**



**D**



sensitive to denaturation of the effector. In contrast, the ability of the effector to recognize and bind the DNA does not degrade during long-term storage at  $-20^{\circ}\text{C}$  or  $-80^{\circ}\text{C}$ . Following proteinase K pre-treatment of the cell-free extract the DNA-effector complex is no longer detected (Fig. 4.10.B, lane 6), whereas treatments with DNase (Fig. 4.10.B, lane 7) or RNase A (Fig. 4.10.B, lane 8) do not affect complex formation. These results indicate that the observed shift in the mobility of the dsDNA is due to interactions with a DNA-binding protein, rather than with cellular DNA or RNA that are potential contaminants of the cell-free extracts. While the EMSA reactions were routinely incubated at  $37^{\circ}\text{C}$ , DNA-effector complexes also form during incubation on ice, although the intensity of the shifted band is lighter. This is interpreted to mean that less DNA is bound and suggests that the binding is less efficient at  $4^{\circ}\text{C}$  (Fig. 4.10.A, lane 10).

The formation of DNA-effector complexes was tested in the presence of unlabeled dsDNA fragments to confirm the specificity of the interaction. A 10-fold molar excess of the competitor DNA is expected to titrate out the effector protein and abolish or decrease the formation of complexes with the target DNA. When poly [d(I-C)], a non-specific DNA (Fig. 4.10.B, lane 9), or *Synechocystis* genomic DNA (Fig. 4.10.B, lane 10) are added in excess, the intensity of the shifted band representing DNA-effector complexes is not affected. Therefore, neither of these high molecular weight DNAs interferes with binding of the protein factor to the target DNA. Similarly, pre-incubation of the extract with an excess of either the 325 bp *Sma* I fragment of *crhR* (described in Section 3.2.2) (Fig. 4.10.B, lane 11), or the 620 bp 48E DNA fragment (Fig. 4.10.B, lane 12), does not interfere with the formation of DNA-effector complexes containing 45E. These fragments are of similar size as 45E and are derived from the sequence surrounding or including the *crhR* gene, but they do not compete with the radioactively labeled 45E target DNA for binding by the protein effector. Similarly, the 224 bp 47E fragment (Fig. 4.10.B, lane 13) and the 140 bp B-E fragment (Fig. 4.10.B, lane 14) do not compete with 45E for binding of the protein effector, which was unexpected since these fragments have overlapping sequence with 45E. Ideally, competition with unlabelled 45E should have been performed as a control. Overall, the results from these competition experiments indicate that the protein effector interacts specifically with the DNA sequence contained in 45E and suggest that the key recognition sequences lie downstream of the putative transcription start site.



#### 4.2.4.2. Formation of a Complex Between dsDNA Fragment 45B and a Soluble Effector

It was desirable to identify a smaller fragment of dsDNA that retains the ability to form DNA-effector complexes in order to delimit a region that contains the *cis*-elements that are necessary and sufficient for recognition and binding of the cytosolic factor. To this end, EMSA experiments were performed with the 224 bp fragment 47E (Fig. 4.9). The results consistently indicated that incubation of 47E with cell-free extracts prepared from both light-grown and dark-treated *Synechocystis* cultures does not yield DNA-effector complexes. This is consistent with the previous observation that the 47E and B-E fragments do not compete with 45E for binding to the effector. These results led to the hypothesis that the DNA sequences required for the recognition and stability of the binding are contained within the region between the GWO45 and GWO47 oligonucleotide endpoints.

Consequently the 228 bp fragment 45B, which includes the region between GWO45 and GWO47 but lacks the more distal sequence between the *Bgl* I and *Eco* RI sites, was chosen as the target DNA for further investigation. The control reaction lacking cell-free extracts indicates the migration position of the unbound 45B dsDNA (Fig. 4.10.C, lane 1), and the progressive addition of 2-30  $\mu$ g cell-free extracts corresponds with an increase in the amount of shifted 45B DNA (Fig. 4.10.C, lanes 2-5). Identical results are obtained with 45B as previously shown with 45E: The DNA-effector complexes do not form following incubation of 45B with BSA (Fig. 4.10.D, lane 3) nor with cell-free extracts that have been pre-treated with heat (Fig. 4.10.D, lane 4), detergent (Fig. 4.10.D, lane 5), or proteinase K (Fig. 4.10.D, lane 6), whereas DNase (Fig. 4.10.D, lane 7) or RNase (Fig. 4.10.D, lane 8) treatments had no effect. Incubation of the cell-free extracts with an excess of the various unlabeled competitor DNAs (Fig. 4.10.D, lanes 9-14) does not interfere with the formation of DNA-effector complexes as compared to incubation of the same amount of cell-free extracts with 45B alone (Fig. 4.10.D, lane 2). Interestingly, the addition of excess poly[d(I-C)], genomic DNA, 47E fragment, or B-E fragment seems to increase the amount of 45B that is bound by the protein effector, since the intensity of the unbound band appears to decrease. This unusual result was consistently observed only with addition of *Synechocystis* genomic DNA, and may be due to stabilization of the complexes by ions present in the DNA preparation(s).

Since *crhR* transcripts are detected specifically in illuminated photoautotrophic *Synechocystis* cultures, the *in vitro* EMSA reactions were routinely performed with cell-free extract obtained from these growth conditions. To determine if the pattern of effector binding to 45E and 45B correlates with the conditions that elicit transcription of

*crhR*, extracts from cells grown under a variety of conditions were tested. Incubation with extracts from dark-treated photoautotrophic cultures (conditions where the *crhR* transcript is not detected) consistently yielded the same DNA mobility shift as incubation with the cell-free extracts from light-grown cells for both 45E (Fig. 4.10.A, lanes 7-9, compare lanes 2-6) and 45B (Fig. 4.11.A, lane 3, compare lane 2). This shift is of the same magnitude with both extracts and exhibits similar correlations with the concentration of the cell-free extracts. Incubation of 45B with extracts from illuminated photomixotrophic cultures (Fig. 4.11.A, lane 4), or from illuminated photoautotrophic cultures treated with DCMU (data not shown), DBMIB (Fig. 4.11.A, lane 6), Mv (Fig. 4.11.A, lane 5) or chloramphenicol (Fig. 4.11.A, lane 7) indicates that the DNA-binding protein is present under all conditions. While the same quantity of protein was added to each reaction, it is apparent that incubation with extracts from cells treated with chloramphenicol causes a shift in relatively less of the target DNA. This may be interpreted as a lower concentration of the DNA-binding factor in these extracts, and since chloramphenicol inhibits protein synthesis this observation agrees with the previous conclusion that the factor binding to the DNA is composed of protein(s). The extracts from cells grown with glucose also appear to contain relatively less of the DNA-binding protein, for which there is no simple explanation. The main conclusion from these results is that the DNA-binding protein is constitutively present, in contrast with detection of *crhR* mRNA by Northern analyses.

This apparent lack of correlation between the formation of DNA-effector complexes and detection of the *crhR* mRNA has been noted for the promoters of other genes (for examples refer to section 4.1.2). Therefore, it is possible that post-translational modifications such as phosphorylation may alter the ability of the effector protein to bind to the target DNA. In an attempt to test this hypothesis, the cell-free extracts were pre-treated with calf intestine alkaline phosphatase (CIP) immediately prior to incubation with 45B, followed by addition of sodium phosphate buffer to inhibit further CIP enzyme activity. The results are inconclusive due to the undesirable dephosphorylation of the end-labeled target DNA in the experimental reactions. However, the control reaction containing sodium phosphate in the absence of CIP (Fig. 4.11.B, lane 3) is interesting because it shows an increase in the formation of DNA-effector complexes. By comparison, the addition of potassium phosphate (Fig. 4.11.B, lane 4) does not yield the same magnitude of increase in DNA-effector complexes. While the basis for these observations was not investigated further, one possible explanation is that the increased ionic strength of the reaction buffer stabilizes the DNA-effector interaction. Another interpretation, although it remains highly speculative, is that the addition of

### **Figure 4.11 EMSA Experiments Using Various Cell-free Extract Preparations**

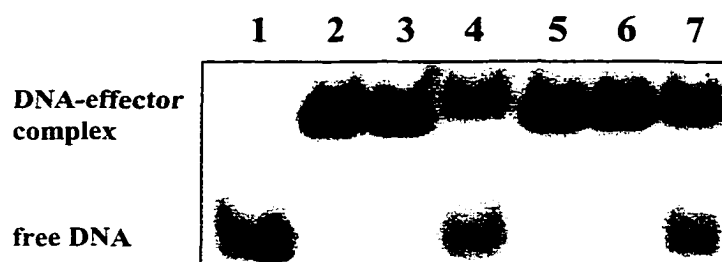
**A. EMSA performed with 45B.** The dsDNA fragment 45B was incubated without additions (lane 1) or with 20 µg of cell-free extracts prepared from *Synechocystis* cultures that were grown photoautotrophically either with continuous illumination (lane 2), with 24 h darkness (lane 3), with light and glucose (lane 4), with light and methyl viologen for 3 h (lane 5), with light and DBMIB for 3 h (lane 6) or with light and chloramphenicol for 6 h (lane 7).

**B. EMSA performed with 45B.** The dsDNA fragment 45B was incubated without additions (lane 1) or with 20 µg of *Synechocystis* cell-free extracts (lane 2) and addition of 20 mM sodium phosphate (lane 3) or 20 mM potassium phosphate (lane 4). Similarly, 45B was incubated with the supernatant (lane 5) or pellet fraction (lane 6) following precipitation of the cell-free extract at -20°C.

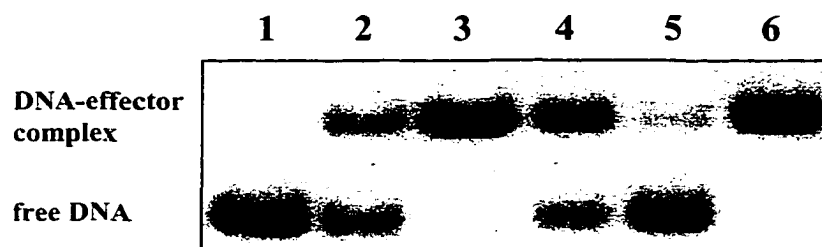
**C. EMSA performed with 45E and cyanobacterial extracts.** The dsDNA fragment 45E was incubated without cell-free extract (lane 1) or with 35 µg of cell-free extract prepared from photoautotrophically grown cells of *Synechococcus* sp. strain PCC 7942 (lane 2), *Anabaena* sp. strain PCC 7120 (lane 3), or *Synechocystis* sp. strain PCC 6803 (lane 4).

**D. EMSA performed with 45B and cyanobacterial extracts.** The dsDNA fragment 45B was incubated without cell-free extract (lane 1) or with 35 µg of cell-free extract prepared from photoautotrophically grown cells of *Synechococcus* sp. strain PCC 7942 (lane 2), *Anabaena* sp. strain PCC 7120 (lane 3), or *Synechocystis* sp. strain PCC 6803 (lane 4).

**A**



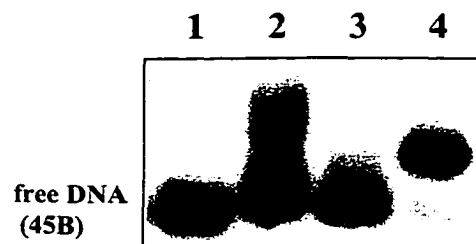
**B**



**C**



**D**



phosphate inhibits protein phosphatases in the cell-free extracts, decreasing the dephosphorylation of the DNA-binding protein that would otherwise lower its affinity for the target DNA.

Additionally, cell-free extracts from two other cyanobacterial species were tested by incubation with 45E and 45B, to determine if the *cis*-element(s) in this region of the DNA are recognized and bound by a protein that is specific to *Synechocystis*. Interestingly, extracts from the unicellular *Synechococcus* (Fig. 4.11.C and D, lane 2) and the filamentous *Anabaena* (Fig. 4.11.C and D, lane 3) species show unique patterns of shifting the target DNAs. It appears that the DNA sequence elements present in 45E and 45B are bound by soluble effector moieties present in the other cyanobacterial species, but these results do not indicate whether these effectors are homologous to the DNA-binding protein from *Synechocystis* (Fig. 4.11.C and D, lane 4).

During the course of the EMSA experiments, cell-free extracts prepared without detergents were observed to precipitate when stored at -20°C. Incubation of 45B with the resultant supernatant (Fig. 4.11.B, lane 5) and pellet (Fig. 4.11.B, lane 6) fractions indicate that the DNA-binding protein is present in the pellet fraction, and retains the ability to form complexes with the target DNA. Since this proved to be a simple method for concentrating the cell-free extracts, it was hoped that this would also provide a means of concentrating the DNA-binding protein for subsequent purification. Following native gel electrophoresis, the DNA-effector complex was excised and subjected to SDS-PAGE; a 31 kDa polypeptide was visualized by silver-staining of the gel. N-terminal microsequencing of the first 23 a.a. of this polypeptide (Protein Microchemistry Centre, University of Victoria) yielded the sequence MFDVFTRVVSQADARGEYLSGSQ, which shares 100% homology with the sequence of the C-phycocyanin beta chain. Although this polypeptide is assumed to be a contaminant, these results suggest that it should be possible to isolate the DNA-binding effector and obtain amino acid sequence data for comparison with *Synechocystis* genomic sequence, leading to identification of the protein.

### 4.3 Discussion

A number of *Synechocystis* genes have been shown to be regulated transcriptionally and/or post-transcriptionally by redox conditions. The results presented here indicate that *crhR* belongs to this group of redox-regulated genes: The transcriptional regulation of *crhR* responds to the net redox state of the plastoquinone pool, while the mRNA stability effects are attributable to changes in photosynthetic

electron transport. A putative promoter region was identified by mapping the 5' termini of the *crhR* transcripts and suggests that *crhR* expression is influenced by *cis*-elements in the DNA as well as potential *trans*-acting accessory or transcription factors from the cytosol.

In preparations of total *Synechocystis* RNA a transcript of 1500 nt is the main species detected by Northern analysis; according to S1 mapping and primer extension, the predicted size is 1529 nt (1420 nt of coding sequence and 109 nt of 5' UTR). The 5' ends of the *crhR* transcript(s) as determined by the S1 nuclease analysis may be the result of either transcription initiation or transcript processing. The speculation that *crhR* could be part of an operon stems from (i) the gene organization in the surrounding region (section 3.2.2), (ii) the presence of a distal, unidentified 5' transcript end indicated by S1 nuclease mapping, and (iii) the presence of additional hybridizing species. Interestingly, this would provide coordinate regulation of *crhR* with the putative signal transduction response regulator encoded upstream (slr0081). The predicted size of a polycistronic transcript containing slr0082 and slr0083 is at least 2800 nt, and a transcript spanning the entire sequence from slr0080 to slr0083 would be at least 4765 nt. If *crhR* is co-transcribed with other genes, the processing of the 5' end(s) must occur relatively quickly, since transcripts larger than 1900 nt are not detected; furthermore, Vinnemeier and Hagemann (1999) have identified separate promoters for slr0082 and *crhR*. However, if the 5' ends represent processing sites, this could be related to the observed differences in mRNA stability, since processing could be regulated separately from transcription. For example, if processing was a prerequisite for degradation of the *crhR* transcript, then decreasing the rate of processing in the dark (or in the absence of photosynthetic electron transport) would increase the half-life of the mRNA.

#### **4.3.1 Plastoquinol-Mediated Transcription of *crhR***

Northern analysis revealed that *crhR* transcripts accumulate during growth in the light but are undetectable following incubation in the dark unless exogenous glucose is present. Two observations suggested that the difference in *crhR* expression between photoautotrophic and photomixotrophic cultures in the dark is related to the overlap of respiratory and photosynthetic electron transport: First, detectable levels of *crhR* mRNA are restored much faster in response to re-illumination compared to addition of glucose in the dark. Secondly, this effect is conspicuously absent under identical light/dark treatments in the presence of a non-metabolizable glucose analogue, 3-OMG. Subsequently, experimental treatment of *Synechocystis* cultures with electron transport

inhibitors and/or wavelength-specific light filters confirms that there is a correlation between the (predicted) net reduction of the plastoquinone pool and transcription of *crhR*.

Interpretation of the experimental evidence for plastoquinol-mediated *crhR* transcription is influenced by a number of factors that pertain to the *in vivo* system. Of primary significance is the complexity of the bioenergetic processes that are being experimentally manipulated. Due to the overlapping respiratory and photosynthetic electron transport chains, the relative contributions of linear, cyclic, and respiratory electron flow within the thylakoid membrane are neither well-defined nor static. According to one estimate, 92% of the electrons flowing through PSI initiate at PSII, 2.6% are due to cyclic flow, and 5% are donated by respiratory NADPH-DHs (Yu *et al*, 1993; Myers, 1986). In fact this may underestimate cyclic electron flow which, by driving the formation of ATP, is essential for energizing the Calvin cycle and bicarbonate concentrating mechanisms (Li and Canvin, 1998). Similarly, the level of respiratory electron flow is altered by depletion of endogenous organic carbon compounds (during dark incubation) and/or by the addition of exogenous carbon substrates. Attempts to isolate respiratory effects are further complicated by the branched nature of the respiratory chain as well as possible interactions between cell membrane- and thylakoid membrane-localized respiratory chains. Competition between respiratory and photosynthetic electron transport is implied by the difficulty of culturing *Synechocystis* under photomixotrophic conditions, where the toxicity of exogenous glucose appears to be dependent upon the activity of PSII since it is reversed by PSII mutations or addition of DCMU (Marraccini *et al*, 1994; Rippka, 1979; personal observation). It is difficult to estimate or predict the contributions or influence from other redox reactions such as succinate:quinol oxidoreductases and sulfide-quinone reductase that impinge upon electron transport at the point of plastoquinone (Cooley *et al*, 2000; Kallas, 1994).

Another consideration concerns the use of the electron transport inhibitors. Whereas *in vitro* it may be possible to specifically isolate the inhibition of electron transport, *in vivo* these chemicals exert secondary or multiple effects on other metabolic processes that may indirectly alter electron flow and induce homeostatic adjustments (refer to Table 2.4). Prolonged treatments are more likely to obscure the electron transport-specific effects. In the present study inhibitor treatments were performed according to the current literature and were adjusted to minimize any noticeable short-term toxicity, particularly with Mv. When added in combination, the inhibitors may interact with each other in a manner that interferes with the expected electron transport effects.

Finally, experimental manipulations must be understood in terms of their *net* redox effects. At the level of individual photosynthetic units - where each unit consists of PSII, PSI and the inter-photosystem electron carriers - changes in electron flow cause a *shift* in the redox equilibrium of the plastoquinone pool. Furthermore, it is the sum of these redox changes to the individual photosynthetic units that ultimately determines the overall cellular redox state and specifies downstream effects such as changes in gene expression. To the extent that a particular treatment directly alters electron transport, it is expected to yield a corresponding alteration in redox-responsive signaling pathways. Where the correlation between redox conditions and gene expression is weak, this may reflect the involvement of unidentified factors that alter the activity of the thylakoid kinases and phosphatases. A weak correlation may also result from complex interactions between various signaling pathways within the global bioenergetic signal transduction network.

These considerations enable clarification of certain unexpected results. For example, the decrease in *crhR* levels after the 2 h DBMIB treatment, compared to the 1 h treatment, is attributed to secondary effects of the prolonged inhibition at *cyt b<sub>6</sub>f*. Since DBMIB inhibits linear, cyclic, and respiratory electron flow, the deleterious effects on cellular metabolism would be quickly apparent. Another unexpected observation is the increase in *crhR* mRNA with addition of KCN to photoautotrophic cultures. While KCN has no direct effects on plastoquinone, it inhibits a variety of enzymes that derive energy from the products of linear electron flow (i.e. NADPH and ferredoxin). This would decrease the pool of electron acceptors after PSI, thereby increasing cyclic electron flow while decreasing the rate of oxidation of the inter-photosystem carriers and effectively shifting the plastoquinone pool towards plastoquinol. The treatment of cultures simultaneously with DBMIB and Mv does not yield informative results because Mv continuously oxidizes DBMIB, which must be in the reduced form to inhibit *cyt b<sub>6</sub>f* (Nanba and Katoh, 1984; Trebst, 1980).

The treatments with L1 or L2 illumination differ from the addition of the inhibitors by the magnitude of the changes in *crhR* expression. This is attributed to the modulation, rather than the inhibition, of inter-photosystem electron transport. With both filters, the preferential excitation of one reaction centre does not preclude light-harvesting activity by the other. Rather, the relative excitation of PSII, and hence plastoquinone reduction, is higher under L2 than under L1 illumination. Furthermore, the L2-driven state 2 transition functionally uncouples only a proportion of the phycobilisome-PSII associations. Under L1 illumination, preferential excitation of PSI yields a relative increase in cyclic electron flow compared to linear electron flow, such that the turnover



of plastoquinone is maintained but there is a lower net reduction of the plastoquinone pool. In addition, light captured by accessory pigments may contribute to PSII or PSI activation despite illumination that is deficient in PSII- or PSI-specific wavelengths. Overall, in L1 versus L2 the relative *crhR* levels correlate with the predictions of the shift in the redox equilibrium of the plastoquinone pool.

The magnitude of *crhR* induction following addition of DCMU or DBMIB simultaneous with re-illumination using L1 or L2 filtered illumination differs from similar treatments using white light. It was expected that the addition of DCMU would correlate with a decrease in transcript levels in L2 compared to L1, whereas addition of DBMIB would cause an increase in *crhR* mRNA with both types of illumination; these predictions were only partially fulfilled. The level of *crhR* expression seen with DCMU treatments is attributed to cyclic electron flow through plastoquinone via PSI. With DBMIB and L2 illumination the lack of significant increase in *crhR* mRNA is an indication that either the predictions regarding electron flow through plastoquinone are not entirely correct, and/or that the signal transduction pathway leading to *crhR* expression is influenced by factors that are not immediately apparent. It may be related to the lower intensity of illumination that occurs with use of the filters, since *crhR* levels respond to alterations in light intensity. It may also be significant that, irrespective of the quality of actinic light, DCMU treatment does not correspond with complete loss of the *crhR* transcript, although the plastoquinone pool is predicted to be in a net oxidized state. Hypothetically, the transient reduction of plastoquinone due to cyclic electron flow may be sufficient to trigger initiation of the putative signal transduction pathways for gene expression.

The experimental manipulation of light intensity reveals that *crhR* expression increases as the intensity of illumination increases, as expected with the higher level of plastoquinone reduction due to increased electron flow from PSII. Interestingly, treatments with translational inhibitors affect the accumulation of the *crhR* transcript, as do changes in temperature and salinity. The results presented here are in agreement with previous research by Vinnemeier and Hagemann (1999) in which *crhR* mRNA gave a positive result during a screen for *Synechocystis* transcripts that are highly expressed in response to increases in salt concentration and cold-shock and by Suzuki and co-workers (2000) who noted a cold-induced increase in *crhR* mRNA levels. These observations are integrated into the model presented in chapter seven, where they are discussed in more detail.

### 4.3.2 Redox Effects on *crhR* mRNA Stability

Interestingly, in addition to the plastoquinol-induced transcriptional effects, the levels of *crhR* mRNA are also influenced by redox-induced changes in stability. The transcript half-life differs only in response to light versus darkness, independent of the presence of respiratory substrates. While the specific mechanism for controlling stability remains to be determined, it correlates with changes in photosynthetic electron transport and cellular redox state but not specifically plastoquinol, since the effects of DCMU and DBMIB are equivalent in stabilizing the transcript. Therefore *crhR* transcription and mRNA stability are regulated separately. Since there is a high rate of *crhR* mRNA turnover in the light, it follows that transcription must also be occurring at elevated rates in order to maintain detectable levels of the transcript. Furthermore, the longer half-life of *crhR* mRNA in the dark or with the addition of the inhibitors, suggests that mRNA stability contributes significantly to the accumulation of the transcript seen in the absence of rifampicin. Thus, the influence of mRNA stability must be taken into account when interpreting the Northern analysis results.

### 4.3.3 *cis*-Elements and *trans*-Acting Factors in the Expression of *crhR*

S1 nuclease mapping detected the 5' ends of two transcripts, one of which was also detected by primer extension assays as well as by other researchers (Vinnemeier and Hagemann, 1999). While these protected fragments may represent either transcription initiation sites or RNA processing sites, it is apparent that both transcripts are present under the plastoquinone-reducing conditions as indicated by Northern analyses. The distal terminus remains to be determined. The proximal terminus is an A residue 109 bp upstream of the presumed translational initiation site (ATG codon). If this site is a transcriptional initiation site, the surrounding region of DNA is hypothesized to contain promoter elements. Comparison of this region to promoter sequences recognized by the *E. coli*  $\sigma^{70}$  sigma factor indicates the -35 element is absent. This may be compensated by the presence of an "extended -10" promoter motif and two putative photoregulatory elements. Extended -10 motifs have been described in heterotrophic bacteria for promoters lacking the -35 element, including the redox-regulated *secA* gene from *Synechocystis* (Mazouni et al, 1998). The functional confirmation of *crhR* promoter activity will require further analysis such as the use of vectors containing promoter-less reporter genes.

It has been suggested that transcription from cyanobacterial promoters lacking the typical *E. coli* -35 sequences requires *trans*-acting factors. Therefore, the proximal *crhR* promoter region was expected to contain binding sites for soluble transcription factors or

complexes. EMSA results indicate that the dsDNA fragments 45E (-180 to +188) and 45B (-39 to +188) form DNA-effector complexes when incubated with soluble cell-free extracts from *Synechocystis*. Surprisingly, 47E (comprising -180 to +44) does not form these complexes. Therefore the GWO45 and GWO47 oligonucleotide endpoints may define a region (+44 to +188) that is necessary for the DNA recognition and/or binding; this region includes 79 bp of coding sequence and 65 bp corresponding with the 5' UTR in the putative *crhR* mRNA. 45B is the smallest dsDNA fragment that was demonstrated to contain all *cis*-elements that are both necessary and sufficient for the formation of DNA-effector complexes; whether these are confined to the region from +44 to +188 remains to be determined. 45B comprises 79 bp of the *crhR* open reading frame, 129 bp of non-coding sequence and 20 bp of slr0082. Interestingly, upstream of the putative +1 site there are two copies of a GCN<sub>5</sub>AAC motif that was originally hypothesized to be a light-responsive promoter element; one copy is included in 45B but both are excluded from the key region of DNA between +44 and +188. These results are similar to the observation that promoter elements for the *Synechococcus psbD* and *psbA* genes and the *Synechocystis secA* genes are located downstream of the putative transcription start site and may include sequence that corresponds to the open reading frame (Anandan and Golden, 1997; Mazouni *et al.*, 1998).

The DNA-effector complexes formed following incubation of 45B or 45E with cell-free extracts from *Synechocystis* contain protein(s), as shown by various treatments including proteinase K digestion. *In vitro* the formation of complexes is favoured at higher incubation temperatures compared to lower temperatures, and at higher concentrations of phosphate buffer although the significance of this latter observation requires further experiments. The interaction is specific for the target DNA fragments, since excess unlabelled dsDNAs do not interfere with the formation of complexes when included in the binding reaction. Interestingly, the 45E and 45B dsDNA fragments also form complexes with soluble factors from the cyanobacterial *Anabaena* and *Synechococcus* species. Since the magnitude and the appearance of the shifts differs between extracts from different species, it is likely that the *trans*-acting factors are different. Further investigation may reveal common *cis*-elements and homologous *trans*-acting factors in the modulation of cyanobacterial gene expression by redox-regulated signal pathways.

Identifying the DNA-binding protein(s) and elucidating the effect on expression of *crhR* is an exciting direction for future research efforts. If the DNA-binding protein acts as a transcription factor, its activity is hypothesized to be modified by a signal transduction pathway that senses changes in the redox state. This leads to the expectation

that it will be present or active uniquely under conditions when *crhR* is expressed. Significantly, under the *in vitro* assay conditions employed here, DNA-effector complexes form with cell-free extracts obtained both from inducing (illumination) and non-inducing (darkness or electron transport inhibitors) conditions, and result in similar magnitudes of the DNA mobility shift. Therefore it appears that the DNA-binding protein is constitutively present, in contrast with detection of *crhR* by Northern analyses. This may be reconciled by the likelihood that the *in vitro* reaction does not completely reflect *in vivo* conditions, thereby masking the differences between light- and dark-derived extracts. For example DTT, which was used by Mayfield and co-workers (1994) to demonstrate the redox-responsive nature of RNA-protein interactions, is commonly included in the EMSA reaction buffer used in the present study. Additionally, the method of preparing cell-free extracts may also mask the difference between *in vivo* and *in vitro* conditions: Immediately prior to lysis the cells from both illuminated and dark-treated cultures were harvested for 10 minutes in the dark. Finally, it is conceivable that regulation of the activity of the DNA-binding factor could be due to specific localization within the cells, and this would be lost during preparation of a homogenous cell lysate.

Regardless of the distinctions between *in vitro* and *in vivo* conditions, the DNA-binding protein is constitutively present. Therefore, if it is a transcription factor, differential expression of *crhR* could be achieved by post-translational modification of this effector to yield active versus inactive states. This modification could affect the binding reaction, either to prevent or enhance the formation of DNA-effector complexes. Alternatively, following the binding reaction the modification may differentiate between productive and non-productive interactions with the DNA. Such an alteration would not likely be detected by EMSA because the magnitude of the change in mobility of the target DNA would be below the resolution of the gel. This is observed with *Synechococcus psbA* and *psbD* promoters, where *in vivo* footprinting assays were able to detect differences in protein-DNA interactions that were not apparent during EMSA (Bustos *et al*, 1991; Li *et al*, 1995). Furthermore, as noted for the interaction between downstream elements in the *secA* gene (Mazouni *et al*, 1998), it is possible that the transcriptional effect of the DNA-binding protein is modulated by other *cis*-elements that may be absent on the target dsDNAs. Finally, it is possible that the effects of these DNA-effector complexes is coupled to translation, similar to the situation described for *psbD-2* (Anandan and Golden, 1997). Since the preceding speculations regarding transcriptional regulation of *crhR* are based on the assumption that the present research has identified the essential *cis*-acting sequences and *trans*-acting factors, further

investigation will be required to establish the physiological significance of these *in vitro* DNA-effector complexes.

The implications for a regulating an RNA helicase transcript in response to alterations in electron transport and cellular redox conditions are explored in chapter seven.

## **CHAPTER FIVE**

### **Investigation of the CrhR Protein: Over-Expression, Purification and Western Analyses**

**A version of this chapter has been published.  
Kujat, S. L., and G. W. Owttrim. 2000. Plant Physiology 124: 703-713.**

## 5.1 Introduction

Complementary to the study of gene expression at the transcriptional level is the elucidation of the protein expression pattern. The implicit expectation in such research is that the coordinate effects of transcription and mRNA stability directly influence the detectable level of the cognate protein. Discrepancy between accumulation of the mRNA versus protein is an indication of post-transcriptional regulation or alterations in protein stability. Furthermore, detection by Western analysis does not indicate the level of biochemical or biological activity.

Research into the temporal and spatial patterns of expression of various DEAD-box proteins has been performed as a means of determining the particular physiological role. Protein localization within a cell may be essential for the biological function. This is apparent for *Vasa* (*Drosophila*), where mutations that disrupted the protein localization determinants led to aberrant oocyte formation in the same manner as mutations abolishing the biochemical properties (Liang *et al.*, 1994). With regards to the pattern of expression, the discovery that CsdA and CrhC are highly expressed following cold-shock treatment directed the initial research to determine their respective roles in *E. coli* and *Anabaena* during acclimation to temperature down-shift (Jones *et al.*, 1996; Chamot *et al.*, 1999).

Identification of tertiary interactions between a DEAD-box protein and a particular multimeric complex may also provide valuable insight into the biological role of the RNA helicase. Co-sedimentation was employed to demonstrate an association of CsdA with the ribosomal fraction, which occurs preferentially at 15°C compared to 37°C. CsdA is postulated to act as an auxiliary ribosomal protein since it forms ionic interactions with both subunits of the ribosome (Brandi *et al.*, 1999; Jones *et al.*, 1996). Western analyses and immunoprecipitation indicated the presence of RhlB (*E. coli*) in the degradosome, which suggested a role in RNA turnover (Miczak *et al.*, 1996; Py *et al.*, 1996). The eukaryotic translation initiation factor eIF4A functions within a multi-subunit complex designated eIF4F, interacting with eIF4G and eIF4E to effect ribosomal attachment to mRNA (Browning, 1996; Fuller-Pace, 1994). The human eIF4AIII isoform exhibits different protein-protein interactions with eIF4G compared to the eIF4AI isoform: eIF4AIII binds to the central region but not the carboxy-terminus (Li *et al.*, 1999). The three isoforms of eIF4A, which all possess the characteristic RNA helicase activities, may have different biological functions since eIF4AIII cannot substitute for eIF4AI *in vitro* and appears to inhibit, rather than promote, translation; these differences may stem from the altered protein-protein interactions within the eIF4F

complex (Li *et al*, 1999). Finally, certain helicases may be regulated by post-translational protein modifications. For example, the RNA-dependent ATPase activity of p68 is inhibited by protein kinase C-mediated phosphorylation *in vitro*, as well as by binding to calmodulin; these observations suggest that the biochemical and hence the biological activity may be regulated by dual calcium signal transduction pathways (Buelte *et al*, 1994; Hirling *et al*, 1989). Cumulatively, these observations highlight the importance of determining the physiological context for each DEAD-box RNA helicase.

The investigation of a particular protein requires appropriate methods for detection and manipulation. Therefore, it is limited by the availability and specificity of antiserum. Furthermore, it may be difficult or time-consuming to isolate sufficient quantity of proteins that are expressed at low levels. For these purposes several purification systems are commercially available for the routine over-expression of recombinant proteins. These permit the protein of interest to be engineered with amino- or carboxy-terminal peptide tags that facilitate efficient purification via affinity interactions with a specific ligand. Recombinant DEAD-box proteins have been successfully synthesized using these systems, including a HIS-tagged CrhC (*Anabaena variabilis*) (Yu and Owtrim, 2000) and an MBP fusion protein of Rok1p (yeast) (Oh and Kim, 1999).

The present study includes a description of native CrhR as well as the production of recombinant GST:CrhR and HIS:CrhR proteins. Analysis of rabbit anti-CrhR antiserum validates its use in Western analysis to determine the pattern of expression of CrhR in *Synechocystis*. A potential tertiary association of CrhR with soluble proteins is investigated by incubating *Synechocystis* cell-free extracts either with anti-CrhR antiserum (i.e. immunoprecipitations) or with HIS:CrhR.

## 5.2 Results

Based on the nucleotide sequence of the putative open reading frame, the *crhR* gene encodes a 492 a.a. protein, with a predicted molecular weight of 55122 Daltons (approximately 55 kDa) and an estimated pI of 9.10 as determined using the Peptool program (BioTools, Inc). The deduced amino acid sequence contains all characteristic motifs of the DEAD-box protein family, with a single residue difference in the GKT box (serine rather than alanine) (Fig 1.1). Blast search indicates NeIF4A2 (Genbank X61205) is presently the most homologous protein in the database while CsdA (formerly DeaD) (Accession # PIR A42357) is the most homologous of the *E. coli* DEAD-box proteins.



As shown in Figure 5.1, a sequence alignment of CrhR with various DEAD-box putative RNA helicases indicates significant regions of homology.

### 5.2.1 Construction and Purification of Recombinant CrhR Proteins

It was desirable to obtain CrhR fusion protein constructs for two applications: First, for the generation of anti-CrhR antiserum to be used in Western and FarWestern analyses as well as immunoprecipitations. Second, for use in *in vitro* assays to confirm and characterize the biochemical activities of this putative RNA helicase, as described in chapter six. The constructs were engineered, propagated, and expressed using *E. coli* hosts.

#### 5.2.1.1 The pGEX-2T System (Pharmacia)

The over-expression and purification of recombinant CrhR was initially pursued by cloning the *crhR* gene as a *Bam* HI/*Eco* RI fragment into the corresponding site in the pGEX-2T vector (section 2.4.3.1.1). As confirmed by sequencing across the vector-insert junctions, this produces an in-frame fusion of *crhR* with the glutathione-S-transferase (GST) gene transcribed from an IPTG-inducible promoter  $P_{tac}$  (Fig. 3.3). Following over-expression of GST:CrhR it is possible to separate the GST moiety from the N-terminus of CrhR by thrombin cleavage. Detection of GST activity using the CDNB assay, as suggested by the manufacturer, may serve as an indicator of the relative success of over-expression.

**Over-Expression of GST:CrhR.** Two *E. coli* strains were used as hosts for the pGEX:*crhR* construct. Initial experiments employed *E. coli* DH5 $\alpha$ . Subsequently, the pGEX:*crhR* plasmid was electroporated into *E. coli* JM109 as the preferred host for over-expression of foreign proteins. Cultures of *E. coli* DH5 $\alpha$ , *E. coli* DH5 $\alpha$ (pGEX-2T), *E. coli* DH5 $\alpha$ (pBluescriptKS+), and *E. coli* DH5 $\alpha$ (cs0096-9) were treated appropriately as controls.

The expression of GST:CrhR was analyzed by Coomassie Brilliant Blue (CBB) staining of SDS-PAGE gels. Compared to whole cell preparations of uninduced *E. coli* JM109(pGEX:*crhR*) (Fig. 5.2.A, lane 2), *E. coli* JM109(pGEX:*crhR*) treated with IPTG (Fig. 5.2.A, lane 1) contains a protein that is present at noticeably higher levels and that migrates at approximately the same position as the 78 kDa size standard (Fig. 5.2.A, lane 3). This is compatible with the predicted 81 kDa size of GST:CrhR, where the GST moiety has a molecular weight of 26 kDa and CrhR has a molecular weight of 55 kDa.

**Figure 5.1 Amino Acid Sequence Alignment of CrhR with Other DEAD-box Proteins**

The deduced amino acid sequence of CrhR (slr0083, Genbank D64004), as compared to CrhC from *Anabaena* sp. strain PCC 7120 (Genbank AF040045), CsdA from *E. coli* (Genbank P23304) and N4A2, NeIF4A2 from tobacco (Genbank X61205). Amino acid sequence is written in the one-letter code. The DEAD-box consensus motifs are indicated in the top line. Dashes indicate residues that are identical to the corresponding position in CrhR. Periods (.) indicate spaces introduced by the University of Wisconsin Genetics Computer Group Sequence Analysis Software (GCG) program v. 8.1.

1 50  
**CrhR** .....MINTLTS TFADLGLSEK  
**CrhC** .....M S-SH----NE  
**CsdA** .....MMS YVDWPPILLR HTYYMAEFET --AD---KAP  
**N4A2** MAGSAPEGSQ FDARQFDAKM TELLGTEQEE FFTSYDEVYD S-DAM--Q-N

51 AxxGxGK T 100  
**CrhR** RCQLLADIGF EAPTQIQTEA IPLLLSGRDM LAQSQTGTGK TAAFALPLMD  
**CrhC** IINAVTEL-Y TK--P--MQS --AV-----L -RGA----- --SFTLPLLH  
**CsdA** ILEA-N-L-Y -K-SP--A-C --H--N---V -GMA----- --S---LQ  
**N4A2** LLRGIYAY-- -K-SA--QRG -VPFCK-L-V IQ-A-S---- --T-CSGVLQ

101 PITRELA 150  
**CrhR** RIDPE.....GDLQAL ILTPTRELAQ QVAEAMKDFS HERRLFILNV  
**CrhC** YYPKIVLKA. LQCFLTIR-- -----A --ESSVR-YG KYLK-NSMVM  
**CsdA** NL---LKA.. .....P-I- V-A-----V -----T--- KHM-GVN.V-  
**N4A2** QL-YSLVEC. ....V-A----- -IEKV-RALG DYI.GVK.VH

151GG TPGR VLDE  
**CrhR** ..YGGQSIER QIRSLERGVQ IVVGTTPGRVI DLIDRKKLKL ETIQWVVLDE  
**CrhC** ..F--V--NP -KQR-KGR-D -L-A----LL -HVQQGTVN- SQ-EIL----  
**CsdA** AL---RYDV -LRA-RQ-P- -----LL -HLK-GT-D- SKLSGL----  
**N4A2** ACV--T-VRE DQRI-QS--H V-----F -MLR-QS-RP DH-KMF----

AD S AT 250  
**CrhR** ADEMLSMGFI DDVKTILRKT PPTRQTACFS ATM.PREIKE LVNQFLNDPA  
**CrhC** --R--D---- R-IRR--SLL -KQ--NLL-F --FS.DK--- -AAGL--R-Q  
**CsdA** -----R---- E--E--MAQI -EGH---L-- ---.-EA-RR ITRR-MKE-Q  
**N4A2** -----R--K -QIYD-FQLL --KI-VGV-- ---P-EAL.- ITRK-M-K-V

251 300  
**CrhR** LVTIVKQTQST PTRIEQQLYH VPRGWSKAK. .ALQPILEME DPESAIIFVR  
**CrhC** MIE-ARRNV- A.DTVT-KVY KIERDR-RD. .L-AHLIRKD NWYQVLV-T-  
**CsdA** E-RIQSSVT- RPD-S-SYWT -WG.MR-NE. ALVRF.--A- -FDA-----  
**N4A2** RIL--RDEL- LEG-K-FYVN -DKEEW-LET .LCDLYETLA ITQ-.V---N

301 350  
**CrhR** TKQTAADLTS RLQEAGHSVD .EYHCNLSQS QRERLVHR.F RDGKIKLVVA  
**CrhC** --YG-DR-VK Q-GHERIQ.A LAI---K--- A-THALAK.- KN-SLQVL--  
**CsdA** --NATLEVAE A-ERN-YN.S AALN-DMN-A L--QTL-.L K--RLDILI-  
**N4A2** -RRKVDW--D KMRSRD-T-S .AT--DMD-N T-D.IIM-E- -S-SSRVLIT

351 ARGxD H RIGR 400  
**CrhR** TDIAARGLDV NNLSHVVNFD LPDNAETYIH RIGRTGRACK TGKAIALVEP  
**CrhC** -----I SE-PY----- --YVP-D-V- -----A S-E-VS--SA  
**CsdA** --V----- ERI-L---Y- I-MDS-S-V- -----R A-R-LLF--N  
**N4A2** --LL---I --QQV-L-I-Y- --TQP-N-L- ----S--F-R K-V--NS-TK

401 450  
**CrhR** IDRRLLRSIE NRLKQIEVC TIPNRSQ... VEAKRIEKLQ EQLKEALTGE  
**CrhC** DEYH--AD-- KLIEKRLPFE LVAGIGANSQ .--P.-PT- DER-QKPKDS  
**CsdA** RE-----N-- RTM-LT-PEV EL--AELLGK RRLEKFAAKV Q-QL-SSDLD  
**N4A2** D-E-M-FD-Q KFYNVV--EL PANVADLL\* . . . . .

451 500  
**CrhR** RMAFLPLVR ELSDEYDAQA IAAAALQMIY DQSCPHWMKS DWEVPEVDFN  
**CrhC** QHQPRSAAG VPKKSGKKRL TNSGKR\*... . . . . .  
**CsdA** QYRAL-SKIQ PTAEGEELDL ETL--ALLKM A-GERTLIVP PDGPMRPKRE

501 550  
**CrhR** KPVLRRGRNA GGGQNKSGGG YQKPGKPRR SSGRRPAYS DRQQ\*.....  
**CsdA** FRDRDDRGR DRNDRGPR-D REDR-RRE-- DV-DMQLYRI EVGRDDGVEV

551 603  
**CsdA** RHIVGAIANE GDISSRYIGN IKLFASHSTI ELPKVCRVKC CNTLRALAFS TSR\*

## Figure 5.2 Over-Expression and Purification of CrhR Fusion Proteins

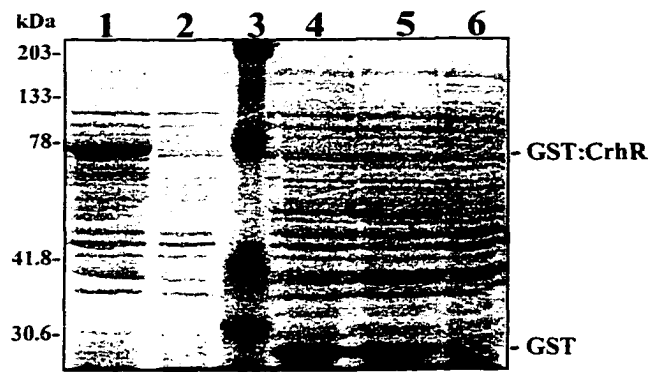
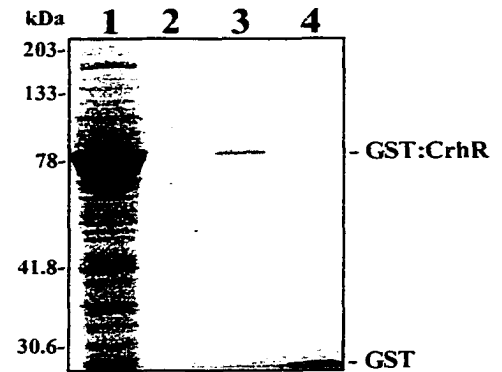
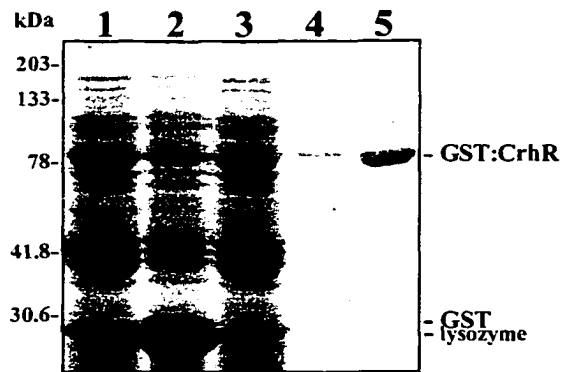
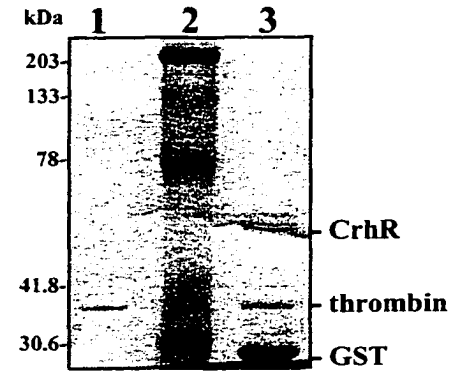
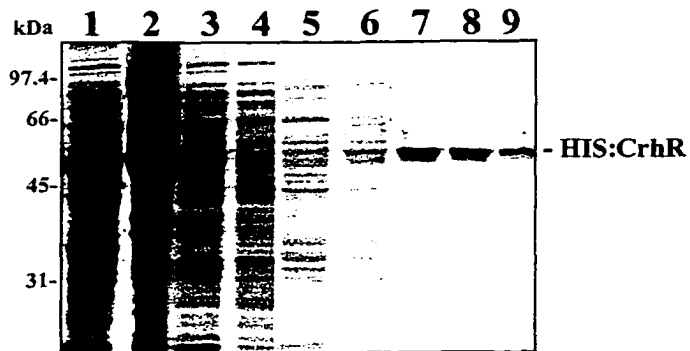
**A. Identification of GST:CrhR in whole cell lysates.** Equivalent amounts of whole cell lysates of IPTG-induced *E. coli* JM109(pGEX:crhR) (lane 1), *E. coli* JM109(pGEX:crhR) (lane 2), IPTG-induced *E. coli* DH5 $\alpha$ (pGEX-2T) (lane 4), *E. coli* DH5 $\alpha$ (pGEX-2T) (lane 5), and IPTG-induced *E. coli* DH5 $\alpha$  (lane 6) were resolved by SDS-PAGE and visualized by staining with CBB. Kaleidoscope (Bio-Rad) prestained standards (lane 3) are included.

**B. Purification of GST:CrhR.** Analysis by SDS-PAGE of the pellet (lane 1) and supernatant (lane 2) fractions from *E. coli* JM109(pGEX:crhR) following sonication, as well as the glutathione-eluted fractions from *E. coli* DH5 $\alpha$ (pGEX:crhR) (lane 3) and *E. coli* DH5 $\alpha$ (pGEX-2T) (lane 4) following incubation with Glutathione-Sepharose 4B.

**C. Optimization of lysis and elution procedures during production of GST:CrhR.** *E. coli* JM109(pGEX:crhR) was grown in LB(Ap) broth overnight at 30°C without IPTG and with agitation (lane 1) prior to lysis by passage through a French press. Following centrifugation, the pellet (lane 2) and supernatant (lane 3) fractions were collected, and the supernatant was incubated with Glutathione-Sepharose 4B. GST:CrhR was eluted on ice for 30 min with 10 mM glutathione in buffer “E” containing 5 mM DTT, 150 mM NaCl, 0.1% (v/v) Triton X-100, and 50 mM Tris-HCl pH 8 (lane 4), or overnight at 4°C with 10 mM glutathione in buffer “F” containing 5 mM DTT, 50 mM Tris-HCl pH 8 (lane 5).

**D. Thrombin cleavage separates the CrhR and GST moieties.** One unit of thrombin (Sigma) (lane 1) was added to the elution fraction obtained with buffer “F” (lane 3), to release CrhR from GST. Kaleidoscope (Bio-Rad) prestained standards (lane 2) are included.

**E. Analysis of HIS:CrhR purification procedure.** Whole cell preparations (lane 1) of *E. coli* JM109(pRSET:crhR) were sonicated and centrifuged to obtain pellet (lane 2) and supernatant (lane 3) fractions. Following incubation of the supernatant with Ni-NTA agarose, the flow-through (lane 4), 20 mM imidazole wash (lane 5), 50 mM wash (lane 6) and 150 mM wash (lane 7) fractions were collected. The recombinant HIS:CrhR was collected in tandem 250 mM elution fractions (lanes 8 and 9), the second of which is generally used for *in vitro* activity assays (see chapter 6). All buffers contain 300 mM NaCl, 50 mM sodium phosphate pH 8.

**A****B****C****D****E**

This highly expressed protein was similarly apparent in preparations of *E. coli* DH5 $\alpha$ (pGEX:crhR) but is noticeably absent in *E. coli* DH5 $\alpha$  (Fig. 5.2.A, lane 6) and *E. coli* DH5 $\alpha$ (pGEX-2T) with or without addition of IPTG (Fig. 5.2.A, lanes 4 and 5, respectively). Based on these observations, the over-expressed protein was presumed to be GST:CrhR. The unconjugated 26 kDa GST polypeptide is evidently over-expressed in *E. coli* DH5 $\alpha$ (pGEX-2T) both in the presence and absence of inducer (Fig. 5.2.A, lanes 4 and 5, respectively).

Following cell lysis by sonication, the majority of the GST:CrhR protein is present in the pellet (Fig. 5.2.B, lane 1) rather than the supernatant fraction (Fig. 5.2.B, lane 2). This agrees with results obtained from qualitative use of the CDNB assay: GST activity is present in both the supernatant and the resuspended pellet of sonicated cultures of *E. coli* DH5 $\alpha$ (pGEX:crhR) and *E. coli* DH5 $\alpha$ (pGEX-2T), but absent in similar preparations of control cells that contain either no plasmid, pBluescriptKS+, or cs0096-9. Higher levels of GST activity were detected in the pellets compared to the supernatants, suggesting that most of the GST and GST:CrhR proteins remain in the insoluble fraction. These observations could result from incomplete cell lysis and/or the formation of inclusion bodies. The first possibility was addressed by modifying the cell lysis procedures, including mechanical lysis with beads, increasing the number of sonication cycles with or without lysozyme pre-treatment, and use of the French press. While French press yields the most complete cell lysis (Fig. 5.2.C, lanes 2 and 3), sonication provides the most reproducible results for small culture volumes with the advantage of shorter preparation times. Relative insolubility of highly expressed proteins in *E. coli* may also occur as a result of deposition into inclusion bodies. Although extraction and solubilization is possible through extensive use of detergents and longer pre-purification and purification steps, this is undesirable during the production of GST:CrhR because it would contribute to loss of the biochemical activity of CrhR. Hence, optimal conditions for maximizing the proportion of soluble GST:CrhR were determined empirically: The *E. coli* host should be cultured at 30°C until it reaches late log phase or early stationary phase ( $OD_{600} > 1$ ), prior to or in lieu of a 1-2 h induction period with addition of 0.4 mM IPTG. Comparison of various IPTG concentrations, from 0.05 mM to 0.8 mM, did not yield significant differences in the relative production of soluble GST:CrhR. Various media such as TSB or 2XYT were also tested, with or without addition of glucose and/or IPTG to control the expression from  $P_{lac}$ , but these provided no significant advantages to the routine use of LB medium.

**Purification and elution of GST:CrhR using Glutathione-Sepharose 4B.** Column purification was performed based on the affinity of GST for reduced glutathione. This yielded variable but relatively low quantities of GST:CrhR from both *E. coli* DH5 $\alpha$ (pGEX:*crhR*) and *E. coli* JM109(pGEX:*crhR*) (Fig. 5.2.B, lane 3). In comparison, column purification of GST alone from *E. coli* DH5 $\alpha$ (pGEX-2T) (Fig. 5.2.B, lane 4) was more successful. Attempts to optimize elution buffer conditions indicate that overnight incubation with 10 mM glutathione in 5 mM DTT/50 mM Tris-HCl pH 8 (Fig. 5.2.C, lane 5) increases the recovery of GST:CrhR compared to 30 min incubation in this elution buffer with 0.1% (v/v) Triton X-100/150 mM NaCl (Fig. 5.2.C, lane 4).

For use as an antigen or for the *in vitro* biochemical characterization, it is desirable to separate the CrhR protein from the GST moiety. Therefore 1 U of thrombin (Fig. 5.2.D, lane 1) was added to the GST:CrhR elution fraction. This results in three protein bands, corresponding to CrhR, thrombin and GST (Fig. 5.2.D, lane 3). It appears that the relative amount of protein in the GST band is higher than the amount of CrhR present, which is unexpected if the original eluate contains only the GST:CrhR fusion protein. This may indicate that CrhR has precipitated following cleavage. It is also possible that additional, internal thrombin cleavage sites could decrease the yield of full-length CrhR. Alternatively, the non-stoichiometric relationship may indicate that a proportion of GST expression occurs without concomitant transcription or translation of CrhR.

#### **5.2.1.2 The pRSETA System (Invitrogen)**

As an alternative to the pGEX-2T system, recombinant CrhR was synthesized with a 31 amino acid peptide (approximately 3.5 kDa) fused to the N-terminus, with a predicted total molecular weight of 58.5 kDa. This peptide includes six histidine (HIS) residues in tandem, which confers affinity for divalent cations and permits purification using Ni-NTA agarose. Elution is obtained by chelating Ni<sup>2+</sup> via progressively increasing the imidazole concentration, although other divalent ion chelators such as EDTA serve the same purpose. The pRSET:*crhR* construct (gift of D. Chamot, University of Alberta) is diagrammed in Figure 3.3. *E. coli* JM109 was employed as the host for propagation and over-expression of this construct.

**Over-expression and purification of HIS:CrhR.** HIS:CrhR was routinely prepared according to the manufacturer's protocol, with minor modifications determined

empirically as indicated (section 2.4.3.2.2). At various steps in the procedure, samples were analyzed by CBB staining of SDS-PAGE gels. A highly expressed 59 kDa protein is present in whole cell preparations of *E. coli* JM109(pRSET:*crhR*) (Fig. 5.2.E, lane 1), as well as in the pellet and supernatant fractions following sonication (Fig. 5.2.E, lanes 2 and 3, respectively). By comparison, this polypeptide was not observed in control preparations of *E. coli* JM109, and is therefore presumed to constitute the 58.5 kDa HIS:CrhR fusion protein. Following incubation of the supernatant fraction with Ni-NTA agarose the intensity of the HIS:CrhR band decreases to background levels in the column flow-through (Fig. 5.2.E, lane 4), which is interpreted as affinity binding to the Ni-NTA agarose column. The subsequent 20 mM and 50 mM imidazole washes remove most of the contaminating *E. coli* proteins from the column (Fig. 5.2.E, lanes 5 and 6, respectively). While the 20 mM wash does not appear to contain HIS:CrhR, a certain amount is eluted from the affinity column by the 50 mM (Fig. 5.2.E, lane 6), 100 mM, and 150 mM imidazole washes (Fig. 5.2.E, lane 7). This loss is acceptable because the wash steps also increase the purity of the final 250 mM eluate containing HIS:CrhR (Fig. 5.2.E, lanes 8 and 9). These results confirm that sufficient quantities of soluble HIS:CrhR protein are readily obtained at a satisfactory level of homogeneity.

### 5.2.2 Analysis of the Polyclonal Anti-CrhR Antiserum

Following large-scale synthesis of recombinant HIS:CrhR, the 250 mM elution fraction was further purified by SDS-PAGE and electro-elution, then injected into rabbits to elicit production of polyclonal anti-CrhR antibodies. Analysis of the pre-immune serum indicates that at a 1/200 (v/v) dilution there is no apparent reaction with purified HIS:CrhR (Fig. 5.3.A, lane 5), nor with any peptides in cell-free extracts of *Synechocystis* (Fig. 5.3.B, lane 9). In contrast, the antiserum obtained from the first test bleed reacts with the column-purified HIS:CrhR at all dilutions tested (Fig. 5.3.A, lanes 1-4). Similarly, the antiserum obtained following the fourth injection reacts at all dilutions with a 55 kDa protein, presumed to be CrhR, in *Synechocystis* cell-free extracts (Fig. 5.3.B, lanes 1, 3, 5, and 7). This antiserum is able to detect CrhR at a 1/2000 (v/v) dilution, which was considered to be sufficient and was used for Western analyses.



### Figure 5.3 Analysis of Anti-CrhR Antiserum

**A. Detection of HIS:CrhR by anti-serum obtained from the first test bleed.** HIS:CrhR was routinely purified and 0.5 µg aliquots were separated by SDS-PAGE. Western analysis was performed using the anti-serum prepared from the first test-bleed. This anti-CrhR anti-serum was added at 1/200 vol (lane 2), 1/500 vol (lane 3), 1/1000 vol (lane 4), or 1/2000 vol (lane 5). Alternatively, pre-immune serum was added at 1/200 vol (lane 6). Rainbow (Amersham Pharmacia Biotech) molecular weight markers are included (lane 1).

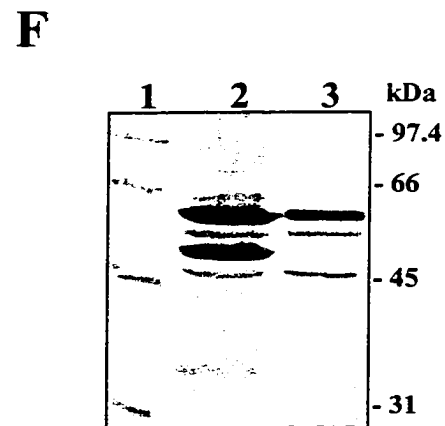
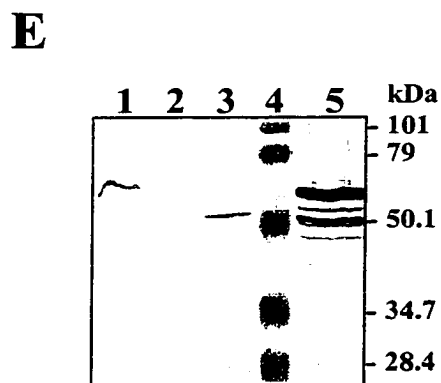
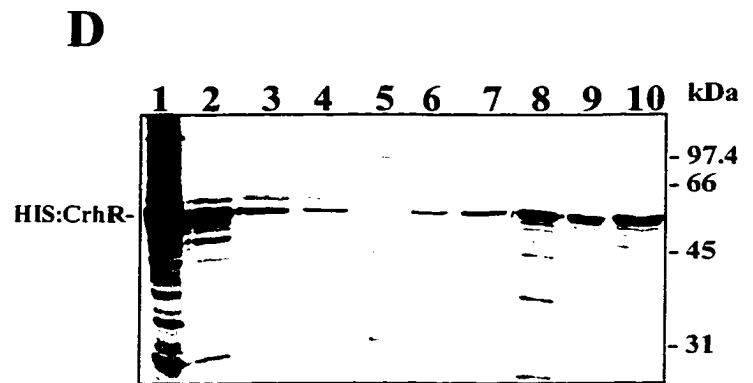
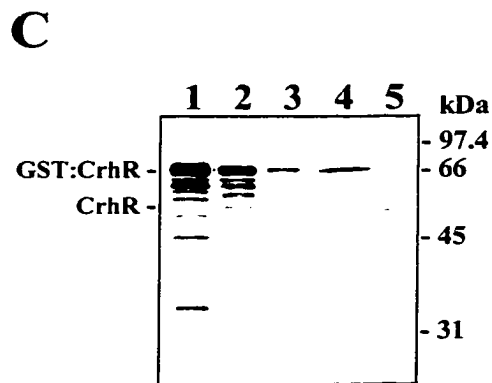
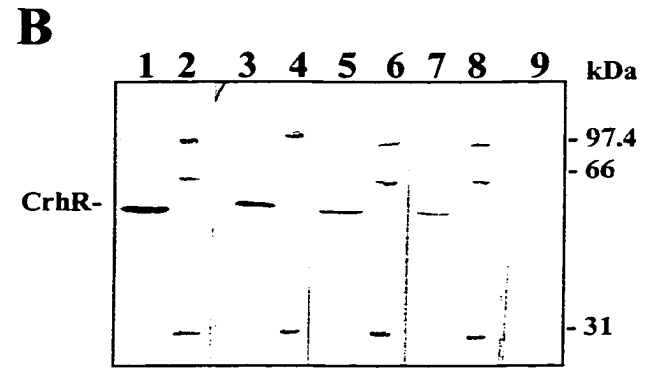
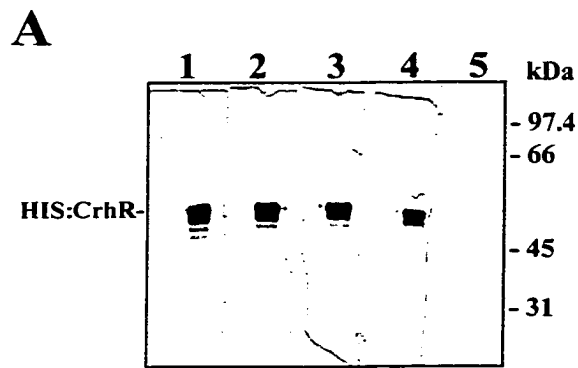
**B. Detection of CrhR in cell-free extracts of *Synechocystis*.** Aliquots containing 35 µg of cell-free extracts from illuminated photoautotrophic cultures of *Synechocystis* were separated by SDS-PAGE. Western analysis was performed using anti-CrhR antiserum at 1/200 vol (lane 1), 1/500 vol (lane 3), 1/1000 vol (lane 5), or 1/2000 vol (lane 7) or using pre-immune serum at 1/200 vol (lane 9). Low molecular weight standards (Bio-Rad) are included (lanes 2, 4, 6, and 8).

**C. Western analysis of GST:CrhR purification samples.** Western analysis was performed using anti-CrhR antiserum with the following samples: Whole cells of *E. coli* DH5α(pGEX:crhR) (lane 1), flow-through from Glutathione Sepharose 4B column (lane 2), wash fraction (lane 3), elution fraction (lane 4), and elution fraction following digestion with thrombin (lane 5).

**D. Western analysis of HIS:CrhR purification samples.** Western analysis was performed using anti-CrhR antiserum with the following samples: *E. coli* JM109 (pRSET:crhR) cell lysis pellet (lane 1), pre-Ni-NTA supernatant (lane 2), column flow-through (lane 3), 20 mM wash (lane 4), 50 mM wash (lane 6), 100 mM wash (lane 7), 150 mM wash (lane 8), and 250 mM elution (lane 9) fractions. Finally, loading dye was added with heating to elute the remaining HIS:CrhR from the column (lane 10). Low molecular weight standards (Bio-Rad) (lane 5) are included.

**E. Detection of immunologically related proteins in cyanobacteria and *E. coli*.** Western analysis was performed using anti-CrhR antiserum with 22.5 µg of cell-free extracts from *Synechococcus* sp. strain PCC 7942 (lane 1), *Anabaena* sp. strain 7120 (lane 2), and *Synechocystis* sp. strain PCC 6803 (lane 3), or from *E. coli* JM109 (lane 5). Prestained SDS-PAGE standards (low-range) (Bio-Rad) are included (lane 4).

**F. *E. coli* JM109 peptides that cross-react with anti-CrhR antiserum.** The pellet (lane 2) and supernatant (lane 3) fractions were subjected to Western analysis following lysis and centrifugation of *E. coli* JM109 cells. Low molecular weight standards (Bio-Rad) are included (lane 1).



### 5.2.3 Western Analysis of CrhR Expression Patterns

#### 5.2.3.1. Evaluation of CrhR Expressed from Recombinant and Mutant Plasmid Constructs

Fractions collected during the production of GST:CrhR were subjected to Western analysis. The results indicate that the highly expressed protein present in *E. coli* JM109(pGEX:*crhR*) and visible on CBB stained gels also reacts with the anti-CrhR antiserum (Fig. 5.3.C). Whole cell lysates (Fig. 5.3.C, lane 2), the column flow-through (Fig. 5.3.C, lane 3) and the elution fraction (Fig. 5.3.C, lane 4) contain GST:CrhR as well as smaller peptides that may be products of proteolytic degradation or may result from truncation during synthesis. These smaller peptides are more frequently observed following long-term storage of the samples. Thrombin cleavage yields a protein of approximately 55 kDa, as expected for CrhR alone (Fig. 5.3.C, lane 5). As expected, the control fractions obtained during the purification of GST from *E. coli* JM109(pGEX-2T) do not react with the anti-CrhR antiserum.

Similarly, Western analysis was performed for the fractions collected during over-expression and purification of the recombinant protein HIS:CrhR (Fig. 5.3.D). These results indicate that HIS:CrhR is present in all fractions including the 20 mM imidazole wash (Fig. 5.3.D, lane 4), in which it was not obvious after staining with CBB (Fig. 5.2.E, lane 5). In this particular example the 150 mM wash fraction (Fig. 5.3.D, lane 8) contains a relatively large number of peptides which, since they react with the anti-CrhR antiserum, are assumed to be products of CrhR degradation. Similar peptides were rarely observed in other samples, and could be attributed to improper storage. The 250 mM elution step (Fig. 5.3.D, lane 9) does not remove all of the HIS:CrhR bound to the nickel column, since it is possible to recover further HIS:CrhR by subsequently boiling the remaining Ni-NTA agarose in SDS-PAGE loading buffer (Fig. 5.3.D, lane 10). Thus, Western analysis confirms HIS:CrhR is the main component of the column eluate that is applied to the *in vitro* biochemical assays (section 6.2).

Western analysis of the *crhR*::Sp and *crhR*Δ::Sp mutant constructs expressed in *E. coli* is presented in chapter three (section 3.2.3.3). In brief, those results confirm the presence of truncated CrhR (Fig. 3.2.E, lanes 2 and 3) following insertional inactivation of the *crhR* coding region.

### **5.2.3.2 Western Analysis Detects Proteins in Other Cyanobacteria and in *E. coli* that Cross-React with Anti-CrhR Antiserum**

Cell-free extracts were prepared from photoautotrophic cultures of *Synechococcus* sp. strain PCC 7942 and *Anabaena* sp. strain PCC 7120 that had been grown at 30°C with continuous illumination. Western analysis identifies a protein of approximately 65 kDa in *Synechococcus* extracts (Fig. 5.3.E, lane 1) that cross-reacts with anti-CrhR antiserum, however no such proteins are identified in *Anabaena* extracts (Fig. 5.3.E, lane 2). Extracts from wild-type *Synechocystis* contain the 55 kDa CrhR protein (Fig. 5.3.E, lane 3). By comparison, preparations of *E. coli* JM109 (Fig. 5.3.E, lane 5) and *E. coli* DH5 (Fig. 3.2.E) contain multiple proteins that react with the anti-CrhR antiserum. In *E. coli* JM109 a minimum of six peptides cross-react with the anti-CrhR antiserum; these have apparent molecular weights of 34, 46, 51, 56, 63, and 65 kDa. All six proteins are apparent in whole cell preparations (Fig 5.2.E, lane 5) and in the pellet fraction following sonication and centrifugation (Fig. 5.3.F, lane 2). Interestingly, only the 46, 56 and 63 kDa polypeptides remain in the corresponding supernatant fraction (Fig. 5.3.F, lane 3). It is significant that none of these *E. coli* bands migrates at the identical position as CrhR in *Synechocystis* extracts (Fig. 5.3.E, lane 3) or in *E. coli* DH5 $\alpha$ (cs0096-9), which carries a wild-type copy of the *crhR* gene (Fig. 3.2.E, lane 1). This supports the assumption that the HIS:CrhR antigen preparation was not contaminated by *E. coli* peptides of identical molecular weight.

### **5.2.3.3 Relative CrhR Protein Levels Reflect the mRNA Accumulation Patterns Determined by Northern Analysis**

The levels of CrhR were examined by Western analysis for comparison with the transcriptional effects identified by Northern analysis (see chapter four and figures therein). Since CrhR is detected under all growth conditions tested, alterations in protein expression are observed as differences in the relative level of CrhR, and are evident only when samples containing equivalent amounts of total soluble protein are compared. In the absence of a reliable internal standard to normalize the amount of protein loaded per lane, this was assessed by Ponceau S staining after semi-dry transfer onto nitrocellulose filters. Therefore, caution is applied towards interpreting minor fluctuations in the apparent levels of CrhR.

In photoautotrophic cultures, CrhR levels decline during dark incubation (Fig. 5.4.A, lanes 2 and 3) compared with illumination (Fig. 5.4.A, lane 1). While the dark-dependent decrease and apparent absence of the *crhR* mRNA is already obvious at 2 h

## **Figure 5.4 Western Analysis of the CrhR Protein Expression Pattern**

Samples were prepared as cell-free extracts by mechanical lysis of *Synechocystis* and total soluble protein (30 µg) was subjected to Western analysis.

### **A. The CrhR expression pattern responds to alterations in growth conditions.**

*Synechocystis* was cultured photoautotrophically with illumination (lane 1), then treated with 4 h darkness (lane 2), 24 h darkness (lane 3), or 4 h dark followed by 30 min of re-illumination (lane 4). Photomixotrophic cultures were grown with illumination prior to treatment in darkness for 3 h (lane 5) or 24 h (lane 6). Alternatively, photoautotrophic cultures were pre-incubated for 4 h in darkness prior to addition of glucose and further incubation in darkness for 30 min (lane 7), or 2 h (lane 8), or addition of 3-OMG and further incubation in darkness for 3 h (lane 9).

### **B. CrhR levels decline in photoautotrophic cultures transferred into darkness.**

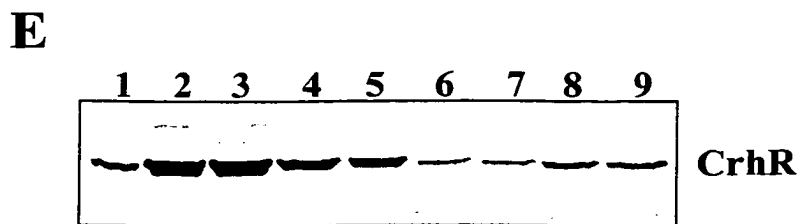
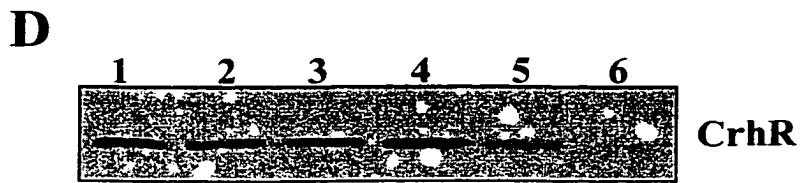
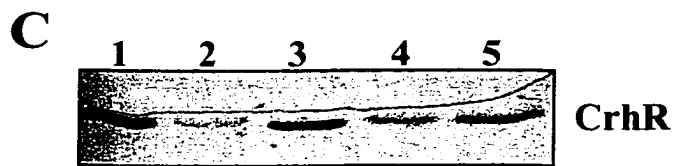
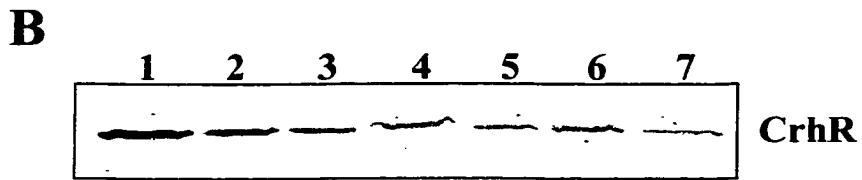
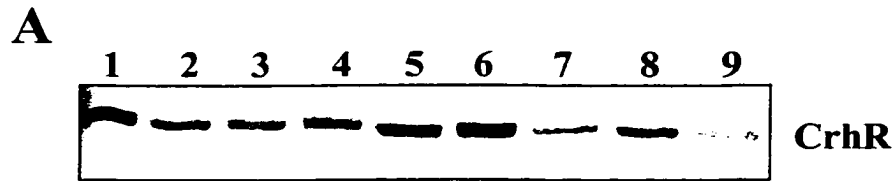
Photoautotrophic cultures were grown with continuous illumination (lane 1) and transferred into darkness for 15 min (lane 2), 30 min (lane 3), 2 h (lane 4), 4 h (lane 5), 16.5 h (lane 6), or 22 h (lane 7).

**C. Addition of poisons to photoautotrophic cultures.** *Synechocystis* was cultured with illumination (lane 1) then subjected to 3 h treatments with DCMU (lane 2), DBMIB (lane 3), KCN (lane 4), or Mv (lane 5).

**D. Addition of poisons to photomixotrophic cultures.** *Synechocystis* was cultured with glucose and illumination (lane 1) then subjected to 4 h in darkness (lane 2), or 3 h treatments with DCMU (lane 3), DBMIB (lane 4), KCN (lane 5), or Mv (lane 6).

### **E. Alterations in CrhR levels following various stress treatments.**

Photoautotrophic cultures were grown with illumination (lane 1) prior to 2 h treatment in duplicate at 20°C (lanes 2 and 3), or at 30°C with addition of 0.5 M salt (lanes 4 and 5), tetracycline (lanes 6 and 7), or chloramphenicol (lanes 8 and 9).



following transfer out of the light, the decline in CrhR protein levels first becomes evident at the 2 h time-point and then continues to progressively decline (Fig. 5.4.B, lanes 2-7). Significantly, even after 24 h in the dark CrhR remains at detectable levels (Fig. 5.4.A, lane 3). Following a 4 h incubation in darkness (Fig. 5.4.A, lane 2) re-illumination of photoautotrophic cultures for 30 min is not sufficient to restore the level of CrhR protein (Fig. 5.4.A, lane 4), in contrast with the rapid transcriptional response that enables detection of the mRNA within 5 min.

The level of CrhR in photomixotrophic cultures incubated in darkness for 3 h (Fig. 5.4.A, lane 5), and 24 h (Fig. 5.4.A, lane 6) is similar to that of illuminated photoautotrophic cultures (Fig. 5.4.A, lane 1). Glucose addition to photoautotrophic cultures following a 4 h dark treatment restores CrhR levels to that observed in illuminated cultures within 2 h (Fig. 5.4.A, lanes 7 and 8). In contrast, 3-OMG does not induce CrhR accumulation in the dark (Fig. 5.4.A, lane 9). Photomixotrophic cultures differ from photoautotrophic conditions in that they maintain similar levels of CrhR protein with illumination (Fig. 5.4.D, lane 1) and after transfer into darkness 4 h (Fig. 5.4.D, lane 2). These effects of glucose and 3-OMG on CrhR levels correspond with the changes in relative abundance of the *crhR* mRNA described previously (section 4.2.1.2). The results demonstrate that, similar to the transcriptional regulation of *crhR*, the levels of the CrhR protein respond to alterations in illumination and glucose metabolism, albeit more slowly and with a lower magnitude of the induced changes.

#### **5.2.3.4 Alterations in CrhR Protein Levels Reflect the Plastoquinone-Mediated Redox Regulation of the *crhR* Transcript**

Since the pattern of CrhR expression appeared to mimic the regulation of *crhR* mRNA, Western analysis was performed following 3 h treatment with the electron transport inhibitors DCMU, DBMIB, KCN, and Mv. Relative to the levels present in untreated photoautotrophic cultures (Fig. 5.4.C, lane 1), CrhR decreases significantly following treatment with DCMU (Fig. 5.4.C, lane 2) but not with DBMIB (Fig. 5.4.C, lane 3). In contrast, neither DCMU nor DBMIB treatment of photomixotrophic cultures (Fig. 5.4.D, lanes 3 and 4, respectively) yield significant decreases relative to the untreated illuminated cultures (Fig. 5.4.D, lane 1). Recalling that *crhR* mRNA decreases only with DCMU-treatment of photoautotrophic cultures, these results for CrhR expression support a correlation between transcript and protein levels. Interestingly, the dramatic increases in *crhR* mRNA levels are not followed by corresponding increases in protein levels; this is similar to the lesser magnitude of CrhR induction compared to mRNA levels following illumination of dark-treated cultures.

Relative to the levels in untreated cells, CrhR declines somewhat when photoautotrophic cultures are treated with Mv (Fig. 5.4.C, lane 5). In contrast, CrhR is not detectable in photomixotrophic cultures treated with Mv (Fig. 5.4.D, lane 6). Once again this pattern mimics the general effects of Mv on transcript levels, where *crhR* mRNA is decreased only by prolonged treatment of photoautotrophic cultures while photomixotrophic cultures exhibit a general degradation of all RNA species that includes the absence of the *crhR* transcript. The addition of KCN appears to have similar effects on photoautotrophic (Fig. 5.4.C, lane 4) and photomixotrophic cultures (Fig. 5.4.D, lane 5): CrhR decreases significantly compared to the levels in untreated cultures. While in photomixotrophic cultures this corresponds with a decrease in the mRNA, *crhR* transcript levels apparently increase following KCN treatment of photoautotrophic cultures. This discrepancy is discussed below.

In general, but with the exception of KCN treatment noted above, the results of Western analysis indicate that the relative increase or decrease of the CrhR protein correlates with the presence or absence of *crhR* mRNA in response to net reduction of the plastoquinone pool.

#### **5.2.3.5 The Effect of Various Stress Treatments on CrhR Protein Levels**

In order to extend the comparison of transcriptional and translational expression patterns for the *crhR* gene, selected stress treatments were applied to photoautotrophic cultures prior to Western analysis, and are shown in duplicate. Cold-shock treatment and high salt conditions were investigated because of the dramatic effects on *crhR* transcript levels previously described (section 4.2.1.6; Suzuki *et al*, 2000; Vinnemeier and Hagemann, 1999). Relative to the untreated illuminated conditions (Fig. 5.4.E, lane 1) CrhR protein levels increase significantly following a temperature shift from 37°C to 22°C (Fig. 5.4.E, lanes 2 and 3). CrhR levels also increase following salt-shock (Fig. 5.4.E, lanes 4 and 5), although to a lesser extent than that seen with a temperature shift down.

The antibiotics tetracycline and chloramphenicol were also tested in order to differentiate between translational inhibition at the elongation versus initiation steps, respectively. Tetracycline treatment leads to a detectable decrease in CrhR levels after 2 h (Fig. 5.4.E, lanes 6 and 7) while the effects of chloramphenicol (Fig. 5.4.E, lanes 8 and 9) are not apparent until 4-6 h after addition. Significantly, these results are directly opposite to the effects of the two antibiotics on *crhR* mRNA levels, and are discussed



further in chapter seven.

## **5.2.4 Interaction of Other Proteins with CrhR**

### **5.2.4.1 FarWestern Analysis: Incubation of HIS:CrhR with Nitrocellulose-Immobilized Proteins**

Since many RNA helicases are found in association with other proteins, and since this is a logical requirement for the metabolism of the single-stranded RNA products, it was important to investigate this possibility with CrhR. This was initially pursued by FarWestern analysis, using a duplicate filter of the Western blot presented in Figure 5.4.A. The nitrocellulose-immobilized proteins were subjected to urea denaturation and progressive renaturation steps, and then incubated with a fresh preparation of affinity-purified HIS:CrhR. The interaction of HIS:CrhR with a particular protein(s) is expected to appear as a band at the position of the target peptide, following development as for Western blots. A reacting polypeptide of approximately 90 kDa (indicated by the arrow) is evident in four of the nine experimental lanes (Fig. 5.5.A). The presence or absence of this interaction does not correspond with the relative abundance of CrhR in the original extracts. Such a correlation might be expected if this protein interacts specifically with CrhR *in vivo*. Two further repetitions of the FarWestern procedure could not replicate this result therefore these results remain inconclusive and were not pursued further.

### **5.2.4.2 Addition of Anti-CrhR Antibodies Co-precipitates Two Proteins with CrhR**

As an alternative to FarWestern analysis, immunoprecipitations were performed by addition of the anti-CrhR antiserum to cell-free extracts of *Synechocystis*. Proteins were labeled *in vivo* by incorporation of <sup>35</sup>S-methionine and cells were lysed under non-denaturing conditions to preserve the integrity of multi-protein complexes. Since protein A-sepharose is added at the final step to facilitate precipitation and purification of antibody-protein complexes, the cell-free extracts were incubated with protein A-sepharose prior to the experimental addition of primary anti-CrhR antibodies. This treatment identifies and reduces the background signals that are due to non-specific interactions of soluble proteins with the protein A-sepharose. Following this treatment, a number of polypeptides are eluted from the protein A-sepharose (Fig. 5.5.B, lane 1), including proteins of 25.5 and 51 kDa. By comparison the elution following immunoprecipitation contains at least five proteins (Fig. 5.5.B, lanes 2 and 3): The protein of approximately 55 kDa is assumed to be CrhR, although attempts to confirm this by Western analysis were complicated by the presence of IgG. IgG is present in the polyclonal anti-CrhR antiserum, reacts with the secondary antibody used during Western

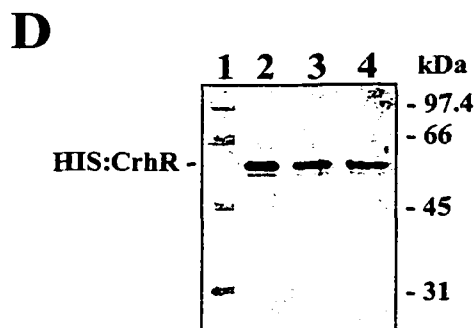
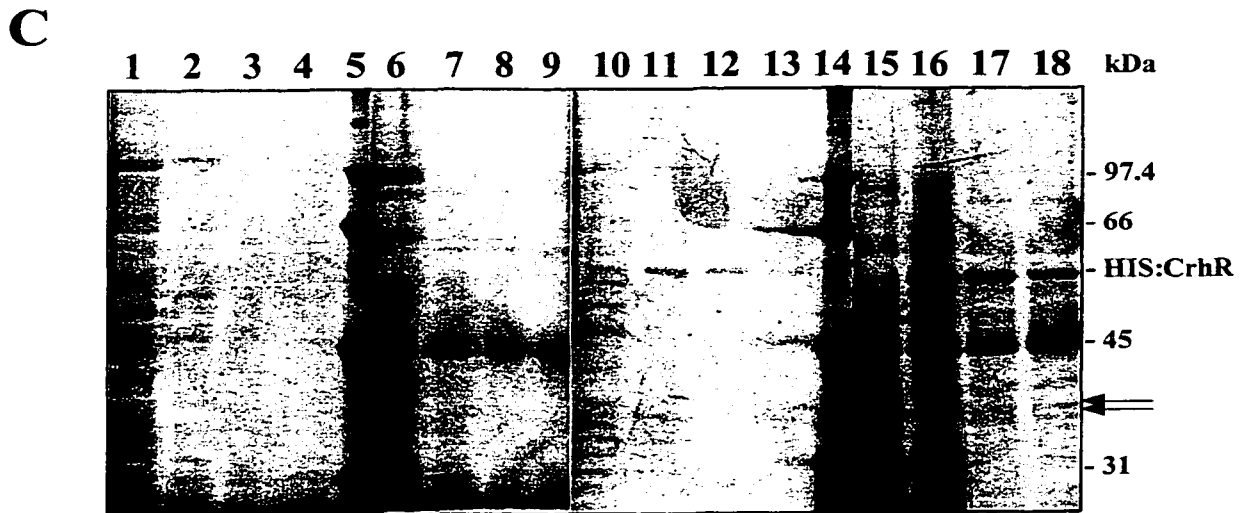
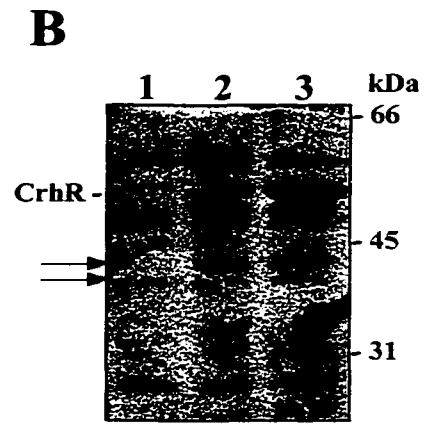
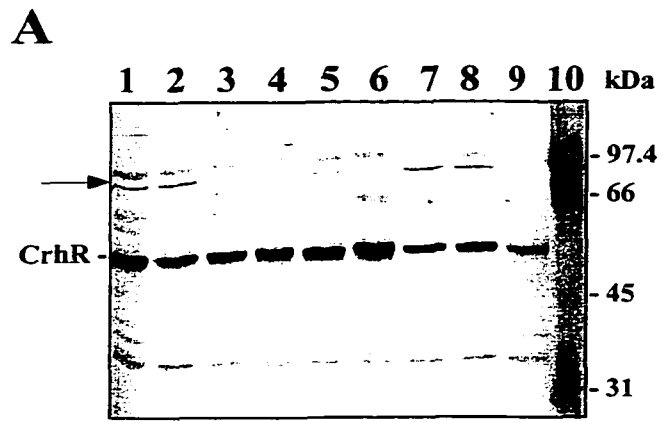
## **Figure 5.5 Potential Tertiary Associations of CrhR and HIS:CrhR with Soluble Proteins from *Synechocystis* Cell-Free Extracts**

**A. FarWestern analysis.** FarWestern analysis was performed on the membrane-immobilized samples from Fig. 5.4.A. Total soluble protein (30  $\mu$ g) was extracted from *Synechocystis* cultured photoautotrophically with illumination (lane 1), then treated with 4 h darkness (lane 2), 24 h darkness (lane 3), or 4 h dark followed by 30 min of re-illumination (lane 4). Photomixotrophic cultures were grown with illumination prior to treatment in darkness for 3 h (lane 5) or 24 h (lane 6). Alternatively, photoautotrophic cultures were pre-incubated for 4 h in darkness prior to addition of glucose and further incubation in darkness for 30 min (lane 7), or 2 h (lane 8), or addition of 3-OMG and further incubation in darkness for 3 h (lane 9). Rainbow marker (Amersham Pharmacia) is included as molecular weight size standards (lane 10).

**B. Co-precipitation of two proteins with CrhR.** Cell-free extracts were incubated with protein A-sepharose (lane 1) prior to performing immunoprecipitations by the addition of anti-CrhR antiserum using buffers and solutions that contain 50 mM NaCl (lane 2), or 140 mM NaCl (lane 3). Arrows indicate proteins that specifically co-precipitate with CrhR.

**C. Co-elution of two *Synechocystis* proteins with HIS:CrhR.** All samples were resolved by SDS-PAGE and visualized by silver-staining. Low molecular weight markers (BioRad) are included (lanes 5 and 14). Four separate Ni-NTA columns were incubated with cell-free extracts, washed successively with 50 mM (lanes 1, 6, 10, and 15), 100 mM (lanes 2, 7, 11, and 16), and 150 mM imidazole (lanes 3, 8, 12, and 17), and then eluted with 250 mM imidazole (lanes 4, 9, 13, and 18). As controls, cell-free extracts were obtained from *E. coli* JM109 cells (lanes 1-4), *Synechocystis* (lanes 6-9), and *E. coli* JM109(pRSET:*crhR*) (lanes 10-13). The experimental column was incubated with *E. coli* JM109(pRSET:*crhR*), washed with 20 mM imidazole and then incubated with *Synechocystis* cell-free extracts overnight (lanes 15-18). Arrows indicate proteins that specifically co-elute with HIS:CrhR.

**D. Western analysis of the experimental column fractions.** The samples from Fig. 5.5.C, lanes 16-18, were subjected to Western analysis in lanes 2-4, respectively. Low molecular weight markers (BioRad) are included for comparison (lane 1).



analysis, and migrates at the same position as CrhR. Some of the additional polypeptides, such as the 25.5 and 51 kDa proteins, result from non-specific interaction with protein A-sepharose since they also appear in the pre-treatment (Fig. 5.5.B, lane 1). The doublet of polypeptides of approximately 39 and 40.5 kDa are specific to the immunoprecipitation and are assumed to form a stable interaction or association with CrhR, under the lysis and precipitation conditions used. Since these proteins are present with either 50 mM (Fig. 5.5.B, lane 2) or 140 mM NaCl (Fig. 5.5.B, lane 3) in the buffers, this indicates that the interaction is stable at least within this range of ionic conditions.

During the course of immunoprecipitation experiments it was observed that the level of radioactively-labeled CrhR is significantly higher when the cells are labeled at 20°C versus 30°C. This is compatible with a hypothesis that the dramatic increase in CrhR levels following cold-shock is the result of *de novo* protein synthesis, with or without a concomitant increase in protein stability.

#### **5.2.4.3 Two Proteins from *Synechocystis* Co-elute with HIS:CrhR from an Ni-NTA Agarose Column**

In parallel with the immunoprecipitation experiments, a non-radioactive method was used to detect interactions of HIS:CrhR with peptides present in *Synechocystis* cell-free extracts. The experiment was performed by incubating cell-free extracts from various bacterial strains with Ni-NTA agarose, then collecting and concentrating the standard wash and elution fractions for further analysis by Western blot and silver staining. Two control columns were prepared with cell-free extracts from *E. coli* JM109 or *Synechocystis* to identify proteins that bind directly to the Ni-NTA agarose. A third control column was incubated with *E. coli* JM109(pRSET:*crhR*) to identify *E. coli* proteins that may co-purify with HIS:CrhR. The fourth, experimental column was also incubated with *E. coli* JM109(pRSET:*crhR*) to allow binding of HIS:CrhR, but was washed only at low stringency to remove *E. coli* protein contaminants. This fourth column containing immobilized HIS:CrhR was subsequently incubated with cell-free extracts from *Synechocystis* in order to concentrate and purify the proteins that interact with CrhR. The results indicate that there are no *E. coli* JM109 proteins that directly bind to the Ni-NTA agarose (Fig. 5.5.C, lanes 1-4), whereas *Synechocystis* cell-free extracts contain a 45 kDa nickel-binding polypeptide (Fig. 5.5.C, lanes 6-9). In addition to the 59 kDa HIS:CrhR protein, fractions from the experimental column (Fig. 5.5.C, lanes 15-18) contain a doublet of polypeptides migrating at approximately 38 and 39 kDa. These

proteins are specific to the experimental column, since they are not present in the samples from the control *E. coli* JM109(pRSET:*crhR*) column (Fig. 5.5.C, lanes 10-13). Furthermore, these are not breakdown products of CrhR since, unlike HIS:CrhR, they do not react with anti-CrhR antiserum in Western analysis of these fractions (Fig. 5.5.D). This provides evidence that two polypeptides interact with CrhR, results that are similar to those obtained by immunoprecipitation.

#### **5.2.4.4 Potential Candidate Proteins for Interaction with CrhR**

As a starting point in the identification of the two peptides that co-precipitate and co-elute with CrhR, the *Synechocystis* database of putative proteins was manually searched to identify proteins having a predicted molecular mass between 37 and 42 kDa (Table 5.1). Interestingly, this list includes the ribosomal protein S1, which has been previously suggested for interaction with the *Anabaena* DEAD-box RNA helicase CrhC (Yu, 1999).

### **5.3 Discussion**

CrhR is a DEAD-box protein with a molecular weight of approximately 55 kDa. The deduced amino acid sequence contains all conserved motifs that define this family of proteins. The consensus AxxGxGKT motif is found as SxxGxGKT in CrhR; a serine residue is similarly located in the yeast DEAD-box proteins PRP5 and Spb4 (de la Cruz *et al*, 1998). Further investigation of the relationship between the primary amino acid sequence and tertiary structure of the prokaryotic DEAD-box helicases will be necessary in order to determine if the proposed crystal structure of NS3 - the DExh-box RNA helicase from the Hepatitis C virus - may be extended to include CrhR.

#### **5.3.1 Over-Expression and Purification of Recombinant CrhR Proteins**

*E. coli* JM109(pGEX:*crhR*) was used successfully for the over-expression and purification of GST:CrhR. Thrombin digestion to separate CrhR from the GST moiety was achieved. However, the utility of the recombinant GST:CrhR protein is limited by a number of factors. The high molecular weight may contribute to insolubility and deposition in inclusion bodies. Solubilization is not a feasible method for obtaining CrhR because the use of detergents would denature the protein and the lengthy purification process may lead to loss of biochemical activity. Thrombin cleavage is necessary but impractical: the enzymatic activity of GST may interfere with the *in vitro* activity assays and the antigenicity of GST would contaminate the polyclonal anti-CrhR antiserum. Procedures for thrombin digestion are time-consuming and require removal of both the

**Table 5.1. Candidate Proteins for Interaction with CrhR**

Summary information obtained from Kaneko *et al* (1996a). Open reading frames (ORFs) encoding hypothetical proteins were not included in this list.

ORF Designation	Predicted MW (no. of a.a.)	Predicted product (Accession #)
slr1356	39 (328)	30S ribosomal protein S1 (D28752)
sll1110	43 (365)	peptide chain release factor (Z49782)
sll1689	43 (369)	RNA polymerase sigma factor (D10973)
sll0306	41 (345)	RNA polymerase sigma factor (D78583)
sll0569	42 (354)	RecA gene product (M29495)
slr1274	43 (367)	membrane protein (L28837)
sll0613	43 (361)	Holliday junction DNA helicase RuvB (U38892)
sll0998	41 (345)	LysR transcriptional regulator (U38804)
slr1245	36 (302)	transcriptional regulator (X89816)
slr1090	43 (368)	GTP-binding protein (U18997)
sll0782	43 (369)	putative protein kinase (A08709)
sll1590	41 (350)	sensory transduction histidine kinase (L09228)
sll1513	39 (334)	C-type cytochrome synthesis protein (U30821)
slr2094	41 (345)	GlpX protein (M97678)
slr0862	38 (326)	LmbP protein (X79146)
sll0222	38 (326)	alkaline phosphatase (X56656)
sll0644	39 (331)	esterase (L38252)

GST and thrombin proteins in order to obtain CrhR preparations of reasonable homogeneity.

*E. coli* JM109(pRSET:*crhR*) yields satisfactory quantity and purity of HIS:CrhR with a minimum of difficulty and a high level of reproducibility. The observation that CrhR breakdown products occur subsequent to collection of the wash and elution fractions may explain the time-dependent, temperature-sensitive loss of biochemical activity (section 6.2). This recombinant protein purification system is preferred over GST:CrhR. Soluble protein is more easily recovered; the HIS-tag moiety is smaller than GST and does not contribute significantly to insolubility. As a result, the expression and purification procedures involve fewer manipulations, can be performed in the absence of detergents, and give higher yields of soluble, non-denatured protein. The HIS-tag moiety has no intrinsic enzyme activity, thus eliminating the requirement for cleavage of the fusion protein. These factors contribute to the suitability of HIS:CrhR for use in biochemical assays and as an antigen to generate anti-CrhR antiserum.

### 5.3.2 Polyclonal Anti-CrhR Antibodies

The rabbit anti-HIS:CrhR antiserum demonstrates specificity for CrhR and recombinant CrhR proteins, and is able to detect these in wash and elution fractions from the two different affinity columns as well as in *Synechocystis* lysates. The antiserum reacts with denatured and native forms of CrhR, since it was used successfully for both Western analyses and immunoprecipitations.

The proteins that are detected in heterologous systems by Western analysis with polyclonal anti-CrhR antibodies will require further analysis to determine their identity and possible homology to CrhR. This is especially true for *Synechococcus*, in which DEAD-box proteins have not been significantly investigated. Failure to detect CrhC in *Anabaena* extracts may be attributed to the 30°C culture conditions, since this DEAD-box RNA helicase is expressed specifically following cold-shock. Some of the cross-reacting species in *E. coli* are expected to be DEAD-box proteins; for example, based solely on molecular weight comparisons the 46, 50, 54, and 57 kDa proteins may be DbpA, SrmB, RhlE, and RhlB, respectively. In particular CsdA might be expected to react with anti-CrhR antiserum, given the primary amino acid sequence homology and the similar pattern of expression in response to a down-shift in temperature. However, an *E. coli* polypeptide corresponding to 70 kDa (which is the molecular mass of CsdA) was

not detected with the antiserum, possibly because the cells were cultured under non-inducing conditions, i.e. 37°C.

### 5.3.3 Western Analyses to Elucidate the CrhR Expression Pattern

The CrhR expression pattern generally correlates with redox-regulated changes in accumulation of the mRNA as elucidated in chapter four. This indicates that transcription and translation are coordinated in the production of CrhR, and allows for the possibility that translational and post-translational controls or alterations may also be exerted under the particular growth conditions tested. The results of the Western analyses are most consistent with a hypothesis that the control of *crhR* gene expression occurs mainly at the level of transcription, superimposed with post-translational effects that are distinct from, but inter-dependent with, changes in transcript levels.

In this scenario, the possibility of translational or post-translational regulation is consistent with the following observations. It was noted that changes in the expression of CrhR occur slower than alterations in *crhR* mRNA levels. For example, with transfer into darkness, the decrease in CrhR becomes apparent only after 2 h, at which point the transcript is no longer detected. The effects of inhibiting translation are also not apparent until at least 2-4 h following addition of the appropriate antibiotic. Additionally, the magnitude of the increase or decrease in the amount of CrhR is less than the magnitude of the changes in mRNA levels. For example, illumination following a dark treatment causes a significant increase in the transcript but only restores CrhR to pre-dark levels. Similarly, the significant increase in *crhR* transcript in photomixotrophic cultures treated with DCMU or DBMIB is not observed at the level of protein. A possible explanation is that the 3 h treatment is too short or too long to reveal changes in protein expression. This is unlikely, however, since the time-course performed following transfer into darkness demonstrates that alterations in CrhR levels are detected within 3-4 h. Finally, the hypothesis that post-translational control is distinct from transcriptional changes is further supported by the observation that KCN, tetracycline, and chloramphenicol treatments yield changes in CrhR levels that are directly opposite to their effects on the accumulation of the transcript. According to this proposal these treatments create conditions where the post-translational effects are dominant to the transcriptional control. Furthermore the KCN treatment suggests that the presence of the CrhR protein reflects the integration of overlapping signal transduction pathways responding to additional metabolic cues, since the disparity is specific to the photoautotrophic cultures. This complexity in the regulation of an RNA helicase is not unexpected, since the modulation



of RNA secondary structure would presumably be integral to a diverse range of metabolic conditions.

The mechanism(s) of this postulated translational control remain to be determined. The timing of alterations in CrhR levels, as mentioned above, suggests that the protein has a low turnover rate. Since with few exceptions CrhR remains detectable by Western analysis, there appears to be a constitutive, basal level of CrhR protein maintained in the cells. This is consistent with the mutational analyses that suggested *crhR* is an essential gene (section 3.2.3). Since tetracycline and chloramphenicol treatments indicate that maintenance of CrhR levels requires continued translation of the transcript, it is possible that an undetectable level of *crhR* mRNA is constitutively transcribed and translated. The immediate and rapid transcriptional regulation of *crhR* may enable *Synechocystis* to simply modulate the relative levels of a highly stable RNA helicase protein. It is possible that CrhR protein stability is accomplished via associations within multimeric protein complexes, which would protect against proteolytic attack and degradation. Furthermore, the presence of CrhR as detected by Western analysis does not distinguish between catalytically active and inactive forms of the helicase. Therefore the CrhR levels detected by Western analyses may or may not directly correlate with the biological requirement for CrhR in RNA metabolism.

Notably, the most significant increase in CrhR levels was obtained by cold-shock treatment. The cold-induced expression of CrhR strongly suggests that in addition to the primary amino acid sequence homology with CsdA (*E. coli*) it may have a similar biological role, as discussed further in chapter seven.

#### **5.3.4 Potential *in vivo* Tertiary Interactions with CrhR**

The inability to detect tertiary interactions by FarWestern analysis is not altogether surprising, since a positive result depends on accurate *in vitro* reconstitution of the *in vivo* protein recognition and binding events. Thus, the results imply that tertiary conformation plays a critical role in enabling the protein-protein interactions involving CrhR. The native protein conformation may not be reconstituted during renaturation of the target proteins that are immobilized on the membrane. The interactions that directly involve CrhR may result from formation of a multi-subunit complex, such that the interactions between the other polypeptides strengthen or stabilize the interactions with CrhR. Finally, if the usual interaction between CrhR and other proteins is weak, this could explain both the absence of results from FarWestern analysis as well as the low level of protein observed for the co-eluting and co-precipitating species detected by alternate methods.

By comparison, methods that more closely approximate the *in vivo* conditions were able to detect potential tertiary interactions between CrhR and one or more (as yet unidentified) proteins. Two proteins are co-precipitated by the addition of anti-CrhR antiserum. Similarly, two proteins are co-eluted with HIS:CrhR from an Ni-NTA column following incubation of immobilized HIS:CrhR with *Synechocystis* cell-free extracts. In both experiments the proteins have estimated molecular weights of 37-42 kDa. Although it is theoretically possible that these two experiments identify four different proteins, it seems more plausible that the experiments identify the same two proteins. Hypothetical tertiary interaction of CrhR with these soluble *Synechocystis* proteins may occur as follows: CrhR may form two different complexes, in which it directly contacts only one of these proteins at a time. It is also possible that CrhR directly contacts both of these proteins simultaneously for the formation of a single multi-protein complex. Finally, CrhR may be in direct contact with only one of the two proteins, which in turn directly contacts the second protein. Further investigation will be necessary to differentiate between these scenarios and determine the influence of other proteins for the formation and/or maintenance of the interactions involving CrhR. It is likely that the successful isolation and purification of these proteins could be achieved by increasing the scale of co-purification experiments involving HIS:CrhR, but replacing the final elution buffer with a buffer lacking imidazole (and EDTA) while containing detergent to disrupt the protein-protein interactions, thus removing the associated peptides while leaving the HIS:CrhR bound to the affinity column.

The list of *Synechocystis* proteins in the size range of 37-42 kDa includes proteins with a variety of functions. Based on the predicted involvement of many DEAD-box RNA helicases with the ribosome (de la Cruz *et al*, 1999) and the continuing research into CrhC (El-Fahmawi and Owtrim, unpublished results; Yu, 1999; Yu and Owtrim, 2000), the ribosomal protein S1 is highly favoured as a candidate for interacting with CrhR. Interestingly, the S1 protein is known to have RNA unwinding activity, and to influence the affinity of the ribosome for translation initiation sequences in the mRNA. The possibility of ribosomal associations is compatible with a model for the biological role of CrhR as presented in chapter seven.

## **CHAPTER SIX**

### **Biochemical Analysis of the Recombinant CrhR Protein**

## 6.1 Introduction

DEAD-box proteins are presumed to possess RNA-dependent ATP hydrolysis and ATP-dependent RNA unwinding abilities, as demonstrated for key members of this family. Investigation of a newly identified DEAD-box protein requires confirmation of these biochemical properties.

The prototype DEAD-box RNA helicase is eIF4A, which exhibits *in vitro* ATP hydrolysis and RNA binding and unwinding activities that are dependent upon RNA and ATP, respectively (Grifo *et al*, 1984; Pause *et al*, 1993; Pause and Sonenberg, 1992; Rozen *et al*, 1990; Schmid and Linder, 1991). Initially, these activities were shown to be dependent upon a second initiation factor, eIF4B (Jaramillo *et al*, 1991; Rozen *et al*, 1990) that is homologous to the C-terminal extensions of other DEAD-box proteins and that harbours RNA binding motifs (Methot *et al*, 1994; Naranda *et al*, 1994). It was postulated that eIF4B provides an additional RNA-binding function which strengthens or stabilizes the interactions of eIF4A with mRNA (Jaramillo *et al*, 1991). More recently, Rogers and colleagues (1999) have demonstrated that the ATP-dependent RNA unwinding activity of eIF4A is in fact independent of, but significantly stimulated by, eIF4B. Furthermore, while eIF4A alone apparently exhibited non-processive RNA unwinding, the addition of eIF4B stimulated processive RNA helicase activity (Rogers *et al*, 1999). In wheat germ, the addition of eIF4B to eIF4A *in vitro* yielded a 10-fold increase in ATP binding activity, postulated to subsequently promote RNA unwinding (Bi *et al*, 2000).

This research into eIF4A and eIF4B illustrates the influence that protein-protein interactions may exert upon the biochemical activity of a particular RNA helicase. Similarly, the ATP hydrolysis and RNA unwinding activities of RhlB (*E. coli*) have been demonstrated only in association with the degradosome. Py and colleagues (1996) have detected an ATPase activity that could not be ascribed to the other components of the degradosome and that was inhibited specifically by anti-RhlB antibodies. More commonly, DEAD-box RNA helicases exhibit the typical biochemical activities as independent proteins; among the growing list of characterized RNA helicases the most recent cyanobacterial example is CrhC (Yu and Owtrim, 2000). Notably, *in vitro* assays may not yield the expected standard activities of RNA-dependent ATP hydrolysis and ATP-dependent RNA unwinding. Variations include ATP-independent RNA unwinding, referred to as helix-destabilizing activity, which is attributed to CsdA (*E. coli*) (Jones *et al*, 1996) and p68 (Hirling *et al*, 1989; Iggo and Lane, 1989). The RNA helicase activity of Vasa (*Drosophila*) is stimulated specifically by dsRNA rather than ssRNA, and RNA binding can occur in the absence of ATP (Liang *et al*, 1994). Interestingly, *in vitro*

assays with DbpA suggested that the RNA unwinding and ATPase activities are not coupled, rather there is competition between ATP binding and RNA binding (Fuller-Pace *et al.*, 1993). Variations in the *in vitro* requirements for ATP hydrolysis are illustrated by the yeast DEAD-box protein Rok1p, in which ATPase activity was demonstrated to be independent of ssRNA (Oh and Kim, 1999).

The first description of substrate specificity was elucidated for DbpA (*E. coli*) whose ATPase activity is highly stimulated by regions of 23S rRNA (Fuller-Pace *et al.*, 1993; Pugh *et al.*, 1999) and to a lesser extent by 16S rRNA (Boddeker *et al.*, 1997). In parallel helicase assays, RNA duplexes containing 16S or 23S rRNA were converted to ssRNA, whereas duplexes containing mRNA, synthetic RNA substrates, or DNA were left intact (Fuller-Pace *et al.*, 1993). Significantly, the newly characterized YxiN protein (*Bacillus subtilis*) exhibits ATP hydrolysis that is specifically stimulated by a 154 nt fragment of 23S rRNA (Kossen and Uhlenbeck, 1999). Since the C-terminal amino acid sequences are highly conserved between DbpA and YxiN, it is possible that the RNA substrate determinants localize to this region (Kossen and Uhlenbeck, 1999). Similar elucidation of an RNA substrate is expected for An3 (*Xenopus laevis*) following the observation that dATP hydrolysis is stimulated by total *Xenopus* oocyte RNA but not by the non-specific substrate, poly(U) RNA (Askjaer *et al.*, 2000). In the polar granules of *Drosophila* co-localization of Vasa with a number of transcripts, including *nanos*, provides circumstantial evidence for interaction between this DEAD-box RNA helicase and specific mRNAs (Gavis *et al.*, 1996). These results have fueled the hypothesis that specific RNA targets may exist for all DEAD-box proteins.

Furthermore, *in vitro* investigations may differentiate two separate interactions of RNA helicases with polynucleotide substrate(s). The 23S and 16S rRNA requirements of DbpA, as described above, illustrate the productive interaction that occurs when specific substrates stimulate the biochemical activity of an RNA helicase. In contrast, the demonstration that DbpA binds ssDNA, RNA, and poly(U) without concomitant enzymatic activation may be evidence for additional, non-productive interactions. This distinction between RNA binding and RNA unwinding is supported by the observation that Ded1 (*Saccharomyces cerevisiae*) exhibits increased affinity for dsRNA instead of ssRNA when ATP is present (Iost *et al.*, 1999). In agreement with current models for RNA helicase activity, and as observed for Vasa and CrhC in particular (Liang *et al.*, 1994; Yu and Owttrim, 2000), RNA binding may occur in the absence of ATP hydrolysis and possibly ATP binding, whereas RNA unwinding is energized by ATP hydrolysis (section 1.1.2 and 1.1.3).

The biochemical activities are typically dependent upon magnesium ions, since X-ray crystallography suggests that the first aspartate residue of the DEAD motif binds the gamma and beta phosphates of ATP via an intervening water molecule and  $Mg^{2+}$  (Hodgman, 1988). The initial interaction with the RNA substrate is thought to require single-stranded region(s), therefore various 5' and/or 3' overhangs are included in the artificial substrates for the RNA helicase assays. Subsequently, movement along one strand of the RNA yields processive unwinding of the dsRNA region, most likely by displacement of the second strand of RNA with which the helicase has relatively less contact (Hesson *et al.*, 2000). Recently, Jankowsky and colleagues (2000) have demonstrated a correlation between the amount of ATP hydrolyzed by NPH-II and the unwinding of RNA, in support of the processivity of RNA helicase activity on the dsRNA substrate.

In the absence of *in vivo* methods for demonstrating the biochemical activities of RNA unwinding coupled with ATP hydrolysis, *in vitro* assays are essential in the process of characterizing a DEAD-box protein. The *in vitro* results obtained for any particular RNA helicase are necessarily influenced by the attributes described above - namely, degree of specificity toward the RNA substrate, protein-protein interactions, and post-translational modifications. As a result, the *in vivo* significance of one or more of these factors may not be immediately apparent. Nonetheless, in concert with *in vivo* investigations such as Western analyses and immunoprecipitations the *in vitro* biochemical characterization may yield important information for elucidating the biological role of a particular DEAD-box protein.

The present study was performed to determine the biochemical activities of CrhR by applying recombinant HIS:CrhR protein to *in vitro* assays. ATP hydrolysis activity was assayed by a modified method of Rodriguez and Carrasco (1993), and 5'-3' RNA helicase activity was assayed following the method of Pause and Sonenberg (1995) as modified by Yu and Owtrim (2000). The requirements for RNA, ATP, and magnesium ions were examined by manipulation of the appropriate variables.

## 6.2 Results

For use in the *in vitro* assays HIS:CrhR was expressed in *E. coli* and affinity purified using Ni-NTA agarose. Column wash and elution buffers contain imidazole to disrupt the interaction between the HIS-tag and Ni-NTA agarose; unless otherwise indicated, the 250 mM elution fraction containing HIS:CrhR (or "column eluate") was

used in the assays. The concentration of HIS:CrhR was determined by the Bradford assay, with BSA as the standard, and confirmed by comparison with CBB-stained molecular weight standards on SDS-PAGE gels. Western analyses and CBB staining indicate that HIS:CrhR is the major protein species in the 150 mM wash and 250 mM elution fractions (see chapter five, section 5.2.1.2).

### 6.2.1 ATPase Activity

ATPase assays were performed *in vitro* to determine the ability of CrhR to hydrolyse ATP, measured as the release of the gamma phosphate (i.e.  $^{32}\text{P}_i$ ) from [ $\gamma$ - $^{32}\text{P}$ ]ATP. The two radioactive species were separated by cellulose TLC since the gamma phosphate product is mobile in the solvent phase, whereas the [ $\gamma$ - $^{32}\text{P}$ ]ATP substrate is not; following autoradiography these are identified as upper and lower spots, respectively. The spontaneous degradation of the gamma bond gives a background level of  $^{32}\text{P}_i$  formation, therefore control reactions lacking HIS:CrhR were included on each TLC plate (eg. Fig. 6.1.A, lane 1). An increase in the amount of radioactivity corresponding to  $^{32}\text{P}_i$  is evidence for the active hydrolysis of ATP. Quantitative analysis is limited to comparison of samples within a single TLC plate, from the same autoradiograph image.

#### 6.2.1.1 HIS:CrhR Exhibits ATPase Activity

The predicted ATP hydrolysis activity of CrhR is confirmed by the observation of dramatically higher levels of  $^{32}\text{P}_i$  released in the presence of HIS:CrhR (Fig. 6.1.A, lane 2) compared to the control reaction lacking HIS:CrhR (Fig. 6.1.A, lanes 1). ATP hydrolysis is stimulated specifically in the *in vitro* reactions that contain either the 250 mM elution (Fig. 6.1.A, lanes 2-6) or the 150 mM wash (Fig. 6.1.A, lane 7) fractions. This ATP hydrolysis activity can be ascribed to HIS:CrhR since the addition of increasing amounts of polyclonal anti-CrhR antiserum causes a corresponding decrease in the amount of  $^{32}\text{P}_i$  released (Fig. 6.1.B, compare lane 2 with lanes 3-5). Heat denaturation of the column eluate prior to addition to the reaction abolishes the release of  $^{32}\text{P}_i$  (Fig. 6.3.B, lane 8). During the course of these experiments, the ATPase activity of HIS:CrhR was generally observed to decline within 3-4 h when the column eluate was kept on ice or stored overnight at  $-20^\circ\text{C}$  (Fig. 6.1.C, lane 4); this precludes the use of extensive manipulations to increase the purity of the HIS:CrhR following elution from the column. Purified HIS:CrhR stored at  $-20^\circ\text{C}$  in 50% (v/v) glycerol for one week retained approximately 50% activity in the standard ATPase reactions (Fig. 6.3.A, lane 9), hence HIS:CrhR was prepared immediately prior to use.

### **Figure 6.1 HIS:CrhR Exhibits ATPase Activity**

All reactions were performed in standard buffer. Unless otherwise indicated, HIS:CrhR was added at 25 ng/ $\mu$ L to each reaction directly following affinity purification. RNA added to the reactions was prepared as total RNA from photoautotrophic cultures of *Synechocystis*. -, component omitted. +, component added exogenously.

**A. ATP hydrolysis by the recombinant HIS:CrhR.** Increasing amounts of total RNA were included in the reaction (lanes 2-6). \*, 25 ng/ $\mu$ L total protein from the 150 mM wash fraction. RNase, an aliquot of the eluate was treated with RNase A (1 ng) immediately prior to addition into the assay tube.

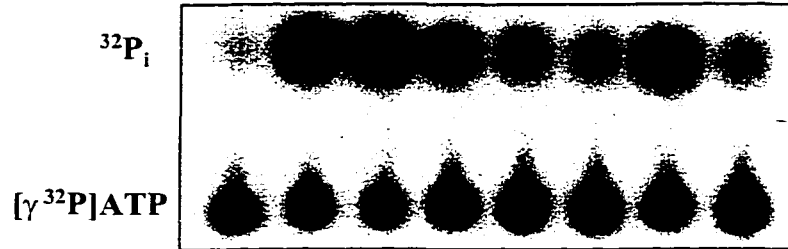
**B. ATP hydrolysis is inhibited by addition of anti-CrhR antibodies.** Polyclonal rabbit anti-CrhR antiserum was added to the final dilution (v/v) as indicated above each lane.

**C. Total RNA from *Synechocystis* stimulates ATP hydrolysis.** HIS:CrhR eluate was prepared following RNase treatment of *E. coli* JM109(pRSET:*crhR*) lysate during incubation with Ni-NTA agarose. #, HIS:CrhR elution fraction, after 24 h storage at -20°C. L, 5  $\mu$ g total RNA extracted from illuminated photoautotrophic cultures of *Synechocystis*. D, 5  $\mu$ g total RNA extracted from photoautotrophic cultures of *Synechocystis* following a 24 h dark incubation.

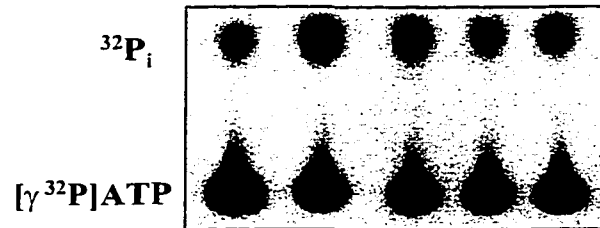


**A**

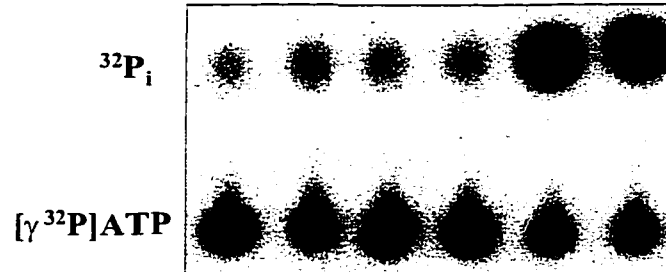
Lane	1	2	3	4	5	6	7	8
HIS:CrhR	-	+	+	+	+	+	*	+
RNA (μg)	-	-	5	10	15	20	-	-
RNase	-	-	-	-	-	-	-	+

**B**

Lane	1	2	3	4	5
HIS:CrhR	-	+	+	+	+
anti-CrhR antiserum	-	-	1/2000	1/200	1/20

**C**

Lane	1	2	3	4	5	6
HIS:CrhR	-	+	+	#	+	+
RNA	-	-	-	-	L	D
RNase	-	-	+	-	-	-



### 6.2.1.2 ATP Hydrolysis is RNA-dependent

Since ATP hydrolysis by DEAD-box RNA helicases is characterized as being dependent upon or stimulated by the presence of RNA, experiments were conducted to determine if this is true for CrhR. The initial results suggested that the ATPase activity of HIS:CrhR is independent of RNA, since the release of  $^{32}\text{P}_i$  occurred without addition of RNA to the reaction (Fig. 6.1.A, lane 2) and the addition of 250 ng/ $\mu\text{L}$  RNA did not cause an increase in the amount of ATP hydrolysis (Fig. 6.1.A, lane 3). In fact, it appeared that ATP hydrolysis may be inhibited by RNA since  $^{32}\text{P}_i$  decreases significantly with addition of increasing amounts of RNA (Fig. 6.1.A, lanes 3-6). These unexpected results were clarified by the inclusion of an important control reaction in which an aliquot of the HIS:CrhR eluate fraction was treated with RNase A (Fig. 6.1.A, lane 8). This RNase treatment results in ATP hydrolysis levels that are significantly lower in comparison to untreated eluate (Fig. 6.1.A, lane 2), approximating background levels of  $^{32}\text{P}_i$  release.

There are two possible explanations for the decrease in ATP hydrolysis following RNase treatment of HIS:CrhR. Since the RNase A is not removed from the eluate prior to addition into the ATPase reaction mixture, there may be a non-specific interference of this protein with HIS:CrhR. Alternatively, the RNase treatment may remove *E. coli* RNA that had become bound to or associated with HIS:CrhR during over-expression and purification. To differentiate between these two possibilities, the RNase treatment was performed during incubation of clarified *E. coli* JM109(pRSET:*crhR*) lysate with Ni-NTA agarose at 4°C, and removed during the HIS:CrhR purification process by increasing the volume of the low stringency wash. Similar to the RNase treatment of the column eluate, this pre-treatment of the lysate reduces the amount of  $^{32}\text{P}_i$  released (Fig. 6.1.C, lane 2). Repeating the RNase treatment of the 250 mM elution fraction from the RNase-treated column appears to further reduce ATP hydrolysis, suggesting that the initial digestion of RNA in the lysate was incomplete (Fig. 6.1.C, lane 3). Since the removal of RNA during preparation of HIS:CrhR was shown to have a significant effect on ATPase activity, cell-free extracts were routinely digested with RNase.

Following RNase treatment, CrhR clearly exhibits RNA-dependent ATPase activity. Addition of total RNA from illuminated photoautotrophic cultures of *Synechocystis* stimulates ATP hydrolysis by HIS:CrhR (Fig. 6.1.C, lane 5) above the levels observed in the absence of RNA (Fig. 6.1.C, lane 2). Similarly, addition of total RNA extracted from dark-treated photoautotrophic *Synechocystis* cultures stimulates the ATPase activity of HIS:CrhR (Fig. 6.1.C, lane 6). To determine the minimum and optimum concentrations of RNA for the *in vitro* assays, total RNA from *Synechocystis*

was added within the range of 5 ng/μL to 1 μg/μL. The results of a typical test are shown in Fig 6.2.A, and quantitated in Fig. 6.2.B. The results indicate that 5 ng/μL of RNA is sufficient to stimulate ATP hydrolysis by HIS:CrhR, however within the range of RNA concentrations tested there is no significant correlation between the magnitude of increase in RNA concentration and the level of ATPase activity (Fig. 6.2.A, lanes 1-8). It appears that the addition of *Synechocystis* chromosomal DNA also stimulates ATP hydrolysis by HIS:CrhR, although to a lesser extent than RNA (Fig. 6.3.A, lane 7). It is also possible that the DNA preparation was contaminated by RNA. These results confirm that the ATPase activity of CrhR is RNA-dependent; the potential stimulation by DNA requires further investigation.

It was desirable to determine the optimum concentration and the specific activity of HIS:CrhR in the standard *in vitro* ATPase assays. Three repetitions were performed with addition of increasing amounts of HIS:CrhR, from 5 ng/μL to 100 ng/μL and a representative autoradiogram is shown (Fig. 6.2.C, lanes 3-13). Since there was appreciable variance in the activity levels observed for independently prepared eluates, the three results are plotted separately (Fig. 6.2.D). The differences between HIS:CrhR preparations may be due to the time-dependent loss of activity during preparation of the eluates and the subsequent incubation on ice. All repetitions show the same general trend where the addition of HIS:CrhR, up to approximately 50 ng/μL, yields a corresponding increase in the release of  $^{32}\text{P}_i$  from the [ $\gamma$ - $^{32}\text{P}$ ]ATP substrate followed by a plateau in hydrolysis. For routine analysis 25 ng/μL HIS:CrhR was utilized since it yields an acceptable level of ATPase activity.

Interestingly, in the previous experiment a single reaction lacking MgOAc (Fig. 6.2.A, lane 9) seemed to yield identical ATPase activity as the corresponding reaction that includes MgOAc (Fig. 6.2.A, lane 6). This observation prompted a systematic investigation of the importance of each reaction component (Fig. 6.3.A, lanes 1-5). The results indicate that, in the absence of RNA, the presence of unlabelled ATP is not sufficient to stimulate ATP hydrolysis by HIS:CrhR (Fig. 6.3.A, lane 3). When RNA is included in the reaction ATP hydrolysis occurs both without (Fig. 6.3.A, lane 4) and with the addition of magnesium ions (Fig. 6.3.A, lane 5), as observed previously. However, in this experiment it appears that addition of MgOAc yields a higher level of ATPase activity compared to its absence, suggesting that magnesium ions do influence the rate of ATP hydrolysis and may be required to obtain maximum levels. These observations led to the hypothesis that divalent cations are necessary for ATP hydrolysis and are constitutively present in the *in vitro* reaction irrespective of the addition of MgOAc, perhaps bound to the HIS:CrhR or present in the eluate fraction. This was investigated in

**Figure 6.2 ATP Hydrolysis by HIS:CrhR is RNA-dependent *in vitro***

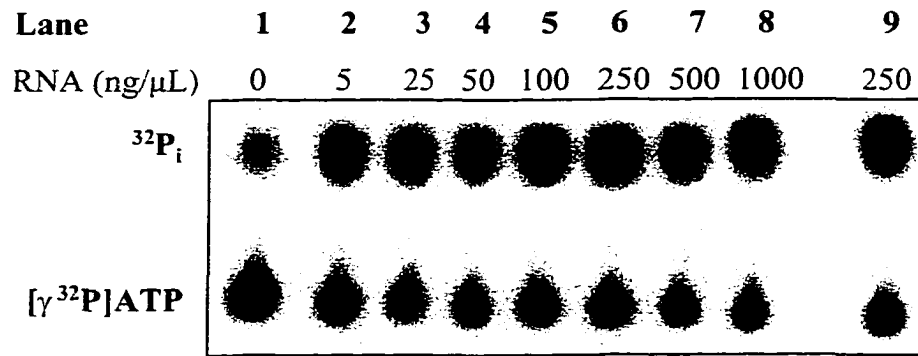
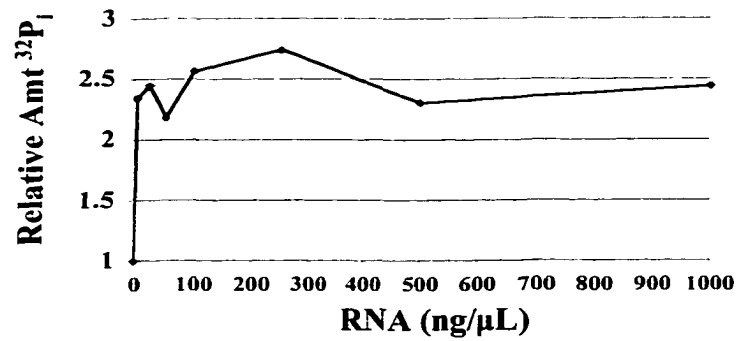
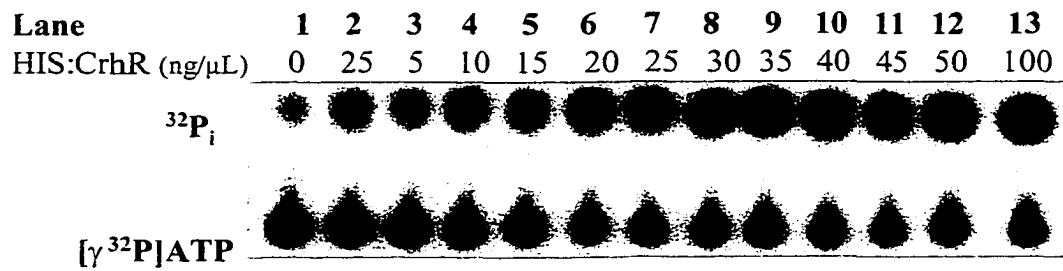
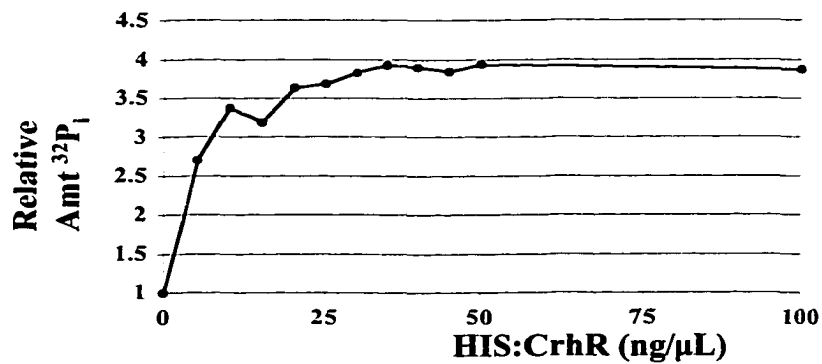
HIS:CrhR eluate was prepared following RNase treatment of *E. coli* JM109(pRSET:*crhR*) lysate, which was applied during incubation with Ni-NTA agarose.

**A. ATP hydrolysis in response to increasing RNA concentration.** All reactions contain 25 ng/ $\mu$ L HIS:CrhR, except for lane 1. 0.5 mM MgOAc, routinely added to all reactions, was omitted from lane 9.

**B. Quantitation of  $^{32}\text{P}_i$  released in response to increasing RNA concentration.** The amount of radioactive signal from the release of  $^{32}\text{P}_i$  in lanes 1-8 from the autoradiograph in 6.2.A was quantitated and normalized to the control reaction (lane 1), which is assigned a value of 1.

**C. ATPase Activity in response to increasing HIS:CrhR concentration.** Total RNA from *Synechocystis* sp. strain PCC 6803 (10 ng/ $\mu$ L) was omitted from lane 2.

**D. Quantitation of ATP hydrolysis activity in response to HIS:CrhR concentration.** Representation of the radioactive signal from the release of  $^{32}\text{P}_i$  was calculated as for Fig 6.2.B.

**A****B****C****D**

**Figure 6.3 Investigation of the Requirements for *in vitro* ATP Hydrolysis by HIS:CrhR**

HIS:CrhR eluate was prepared following RNase treatment of *E. coli* JM109(pRSET:*crhR*) lysate. -, component absent. +, component present.

**A. The effect of the *in vitro* assay components on ATP hydrolysis by HIS:CrhR.**

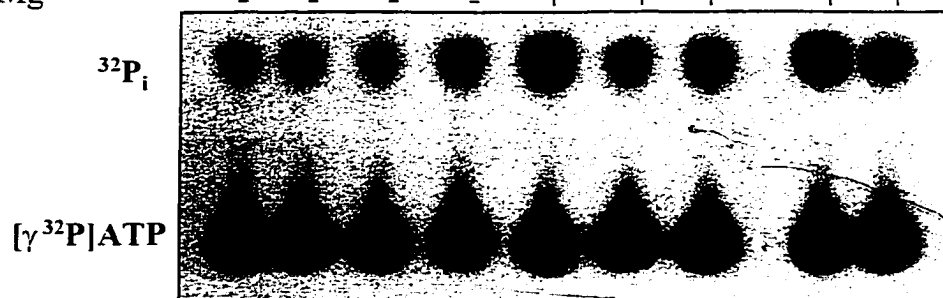
All components were added in the concentrations used for routine assays. RNA (10 ng/ $\mu$ L) was prepared from photoautotrophic cultures of *Synechocystis*. An aliquot of the HIS:CrhR eluate was treated with RNase A (lane 6). Chromosomal DNA from *Synechocystis* (lane 7), or 50 mM imidazole (lane 8) were added to the reaction. #, HIS:CrhR stored in 50% glycerol for 7 d (lane 9).

**B. ATP hydrolysis by HIS:CrhR is influenced by the presence of magnesium ions.** All reactions contain RNA (10 ng/ $\mu$ L) and HIS:CrhR (25 ng/ $\mu$ L). Other components were included as for routine assays. EDTA and MgOAc were added at a final concentration of 0.5 mM.

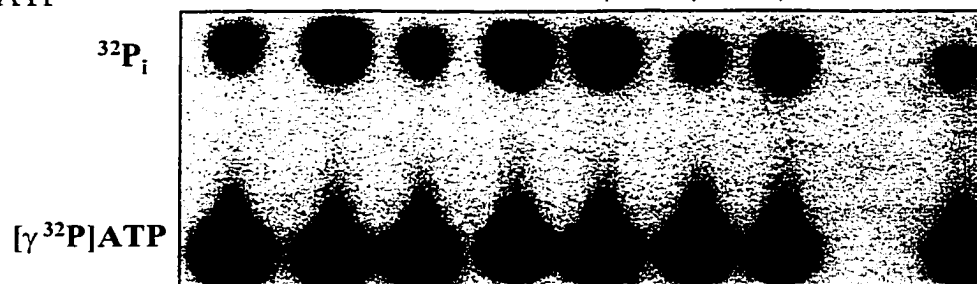
**C. Competition by unlabelled nucleotides in the ATPase assay to determine the nucleotide substrate specificity of HIS:CrhR.** The unlabeled competitor nucleotide species and its final concentration in the reaction are indicated above each lane.

**A**

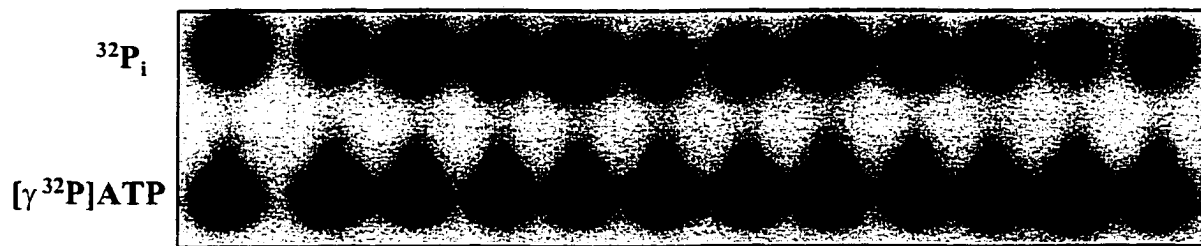
Lane	1	2	3	4	5	6	7	8	9
HEPES/DTT	+	+	+	+	+	+	+	+	+
HIS:CrhR	-	+	+	+	+	+	+	+	#
ATP	-	-	+	+	+	+	+	+	+
RNA	-	-	-	+	+	+	-	+	+
Mg	-	-	-	-	+	+	+	+	+

**B**

Lane	1	2	3	4	5	6	7	8
Mg	-	+	-	+	+	-	+	
EDTA	-	-	+	+	-	+	+	HIS:CrhR boiled
ATP	-	-	-	-	+	+	+	

**C**

Lane	1	2	3	4	5	6	7	8	9	10	11	12
	none	dATP	GTP	CTP	UTP	ATP	ATP	ATP	ATP	ATP	no CrhR	no RNA
		3 mM	3 mM	3 mM	3 mM	40 $\mu\text{M}$	0.4 mM	1 mM	3 mM	6 mM		



a set of experiments that include EDTA as a means of removing  $Mg^{2+}$  from the reaction. Notably, the addition of EDTA inhibits the release of  $^{32}P_i$  both in the absence (Fig. 6.3.B, lane 3) and presence of unlabeled ATP (Fig. 6.3.B, lane 6). In contrast, ATP hydrolysis occurs when MgOAc is added alone (Fig. 6.3.B, lane 2) or together with EDTA (Fig. 6.3.B, lane 4), irrespective of ATP addition (Fig. 6.3.B, lanes 5 and 7). These results support the previously stated hypothesis, since they indicate that magnesium ions do affect the ability of HIS:CrhR to hydrolyse ATP. Potential interference by imidazole, which is present in the HIS:CrhR eluate and which chelates divalent cations similar to EDTA, was tested by adding 50 mM imidazole to a standard reaction (Fig. 6.3.A, lane 8). Since the levels of  $^{32}P_i$  release are comparable to those of the corresponding untreated reaction (Fig. 6.3.A, lane 5), it is unlikely that the column elution buffer affects the *in vitro* ATP hydrolysis by HIS:CrhR by chelating magnesium ions.

### 6.2.1.3 Hydrolysis is Specific for Adenine Nucleotides

The nucleotide hydrolysis activity of DEAD-box RNA helicases is characteristically specific for ATP. Therefore, the substrate specificity of HIS:CrhR nucleotide hydrolysis was examined in competition experiments in which various unlabeled nucleotides were included in the *in vitro* reaction. A decrease in  $[\gamma\text{-}^{32}P]\text{ATP}$  hydrolysis is evidence that the unlabeled nucleotide is also a suitable substrate for the nucleotide binding activity of CrhR. In this assay, non-productive binding cannot be unequivocally distinguished from productive binding (i.e. binding that results in hydrolysis) of the unlabeled nucleotide since the release of unlabeled phosphate is not detectable. In comparison to ATP hydrolysis in the absence of unlabeled nucleotides (Fig. 6.3.C, lane 1) GTP, CTP, or UTP (Fig. 6.3.C, lanes 3-5) do not impair the release of  $^{32}P_i$ , suggesting that these nucleotides are not substrates for HIS:CrhR under the *in vitro* assay conditions. As expected, when unlabeled ATP is added within the range of 40  $\mu\text{M}$  to 6 mM (Fig. 6.3.C, lanes 6-10), all reactions exhibit at least slightly reduced  $^{32}P_i$  release compared to the control reaction lacking unlabeled ATP (Fig. 6.3.C, lane 1). Interestingly, the lowest concentration of unlabeled ATP (Fig. 6.3.C, lane 6) significantly reduces the released  $^{32}P_i$  levels, while the expected correlation between the magnitude of the increase in unlabeled ATP concentration and the magnitude of the decrease in  $^{32}P_i$  release is apparently absent under the *in vitro* assay conditions tested. Strikingly, the addition of 3 mM dATP (Fig. 6.3.C, lane 2) causes nearly complete inhibition of  $^{32}P_i$  release, and since the levels are comparable to background (Fig. 6.3.C, lane 11) dATP effectively competes with  $[\gamma\text{-}^{32}P]\text{ATP}$  as a substrate for binding and possibly hydrolysis. It appears that both dATP and ATP are substrates for CrhR.



## 6.2.2 RNA Helicase Activity

The *in vitro* helicase assay was performed using an artificial partially dsRNA substrate. The dsRNA region is formed by intermolecular base-pairing between a radioactively-labeled 41 nt ssRNA species and a non-radioactive 68 nt ssRNA species, leaving 5' single stranded overhangs. RNA helicase activity is seen as the conversion of the dsRNA to ssRNA, which has increased mobility in SDS-PAGE gels. This is detected by autoradiography or with a Phosphor Screen (Molecular Dynamics).

### 6.2.2.1 HIS:CrhR Exhibits RNA Unwinding Activity

Experimental reactions are compared to control reactions lacking enzyme (eg. Fig. 6.4.A, lane 1). It is obvious that a certain amount of ssRNA is initially present in the preparation containing the artificial RNA substrate. Heat denaturation of the substrate RNA is included to indicate the migration of the ssRNA (eg. Fig. 6.4.A, lane 2).

RNA unwinding occurs with addition of HIS:CrhR (Fig. 6.4.A, lane 5), whereas denaturing the HIS:CrhR protein by heat (Fig. 6.4.A, lane 3) or addition of SDS (Fig. 6.4.A, lane 4) abolishes the RNA helicase activity. With the addition of increasing amounts of the HIS:CrhR eluate (Fig. 6.4.B, lanes 3-7), the amount of dsRNA substrate decreases with a concomitant increase in the amount of ssRNA, compared to the control reaction in the absence of eluate. This suggests that HIS:CrhR mediates the conversion to the single-stranded form. Similarly, increasing the length of incubation yields a corresponding increase in the amount of dsRNA converted to ssRNA (Fig. 6.4.C, lanes 3-7). A 10-15 min incubation period is sufficient to achieve conversion of the duplex RNA substrate (Fig. 6.4.C, lane 4-5). These results demonstrate that HIS:CrhR possesses RNA helicase activity.

### 6.2.2.2 Non-specific RNA Stimulates Unwinding of the dsRNA Substrate

To further define the requirements for RNA unwinding by HIS:CrhR, the enzyme was prepared from a nickel column following addition of RNase A to the *E. coli* JM109(pRSET:crhR) lysate as described for the ATPase assays. Significantly, enzyme prepared in this manner lacks RNA helicase activity under standard assay conditions (Fig. 6.4.D, lane 3). In stark contrast, when unlabelled total RNA from *Synechocystis* is included in the reaction (Fig. 6.4.D, lane 2) or pre-incubated with HIS:CrhR (Fig. 6.4.D, lane 1) RNA unwinding is stimulated. By comparison, the addition of unlabelled RNA to reactions containing untreated HIS:CrhR neither decreased nor increased the efficiency of unwinding of the artificial substrate. This suggests that the helicase activity of CrhR may

## Figure 6.4 RNA Helicase Assays

Unless otherwise indicated, all reactions were incubated with 30 ng/μL HIS:CrhR at 37°C for 15 min.

**A. Artificial dsRNA substrate is converted to ssRNA in the presence of HIS:CrhR.** Reactions were performed without additions (lane 1), with heat denaturation for 2 min at 90°C (lane 2), or with addition of HIS:CrhR that was denatured by heating for 2 min at 90°C (lane 3), or by addition of 1% (w/v) SDS (lane 4), or left untreated (lane 5).

**B. RNA unwinding is dependent upon HIS:CrhR concentration.** Reactions were performed without additions (lane 1), with heat denaturation for 2 min at 90°C (lane 2), or with addition of 10 ng/μL (lane 3), 20 ng/μL (lane 4), 30 ng/μL (lane 5), 40 ng/μL (lane 6) or 50 ng/μL (lane 7) of HIS:CrhR.

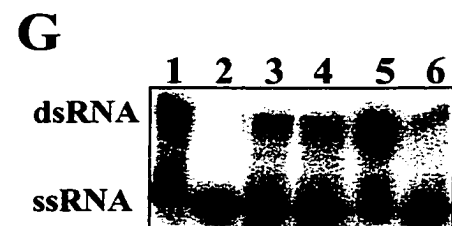
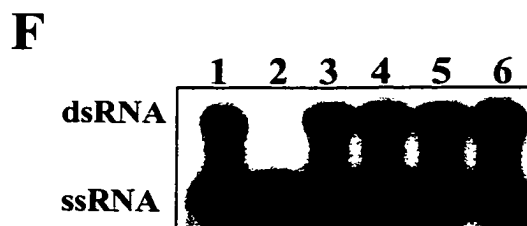
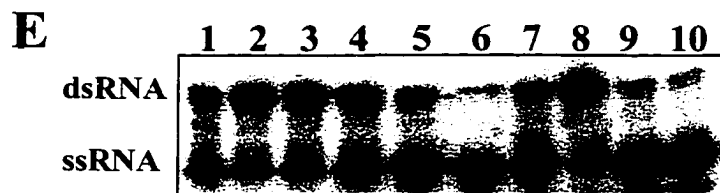
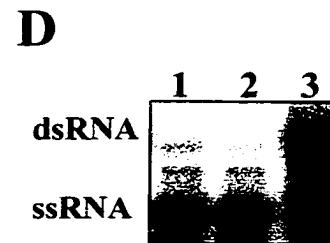
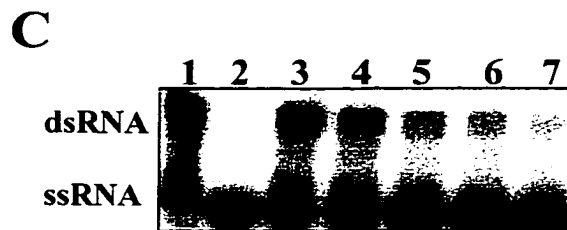
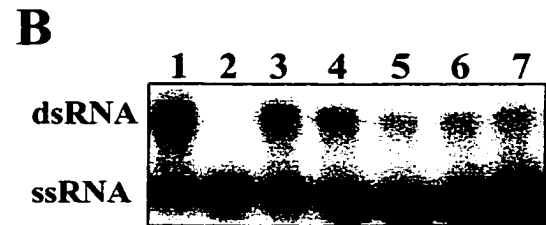
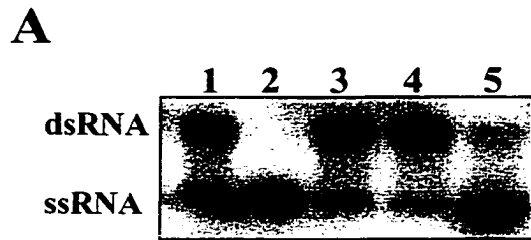
**C. RNA unwinding increases with incubation time.** Reactions were performed without additions (lane 1), with heat denaturation for 2 min at 90°C (lane 2), or with addition of HIS:CrhR for 5 min (lane 3), 10 min (lane 4), 15 min (lane 5), 20 min (lane 6), or 30 min (lane 7).

**D. Non-specific binding of RNA is a prerequisite for RNA unwinding activity.** Standard 10 min reactions were performed with HIS:CrhR that had been treated with RNase A prior to affinity-purification. Total RNA (2 μg) from *Synechocystis* was added to the HIS:CrhR prior to (lane 1) or simultaneous (lane 2) with incubation with the RNA substrate. Alternatively, total *Synechocystis* RNA was omitted from the reaction (lane 3).

**E. RNA unwinding is dependent upon ATP and Mg<sup>2+</sup>.** Standard 10 min reactions were performed without additions (lane 1), or with 0.6 μg HIS:CrhR and the following additions: 0.3 mM (lane 2), 1 mM (lane 3), 2 mM (lane 4), 3 mM (lane 5), or 6 mM ATP (lane 6); 3 mM ATP in the absence of MgCl<sub>2</sub> (lane 7), with 3 mM CaCl<sub>2</sub> (lane 8), 0.3 mM MgCl<sub>2</sub> (lane 9) or with 1 mM MgCl<sub>2</sub> (lane 10).

**F. ATP is the preferred nucleotide substrate.** Standard reactions were performed without additions (lane 1), with heat denaturation for 2 min at 90°C (lane 2), or with 3 mM ATP replaced by dATP (lane 3), UTP (lane 4), GTP (lane 5), or CTP (lane 6).

**G. The RNA helicase activity of HIS:CrhR is pH-dependent.** Standard reactions were performed without additions (lane 1), with heat denaturation (lane 2), with addition of HIS:CrhR at pH 8.5 (lane 3), pH 7.5 (lane 4), pH 9 (lane 5), or in the ATPase reaction buffer containing 5 mM MgOAc (lane 6). Except for the pH 9 buffer, which contains Tris-HCl, buffers contain HEPES-KOH.



be dependent upon an interaction with RNA in addition to the artificial dsRNA substrate. This effect is observed with total RNA from either *E. coli* (present during preparation of HIS:CrhR) or *Synechocystis* (added to the *in vitro* reaction).

### 6.2.2.3 RNA Unwinding is Dependent Upon ATP

In general, DEAD-box proteins possess RNA helicase activity that is dependent upon the hydrolysis of ATP, however there are reports of helix-destabilizing activity which is not ATP-dependent. Therefore the RNA unwinding activity of HIS:CrhR was examined in terms of the requirement for ATP. In the absence of ATP or at concentrations below 2 mM ATP no conversion of dsRNA is observed in the *in vitro* helicase assay (Fig. 6.4.E, lanes 2-4). An increase from 3 mM ATP (Fig. 6.4.E, lane 5) to 6 mM ATP (Fig. 6.4.E, lane 6) yields a corresponding increase in the amount of dsRNA converted to ssRNA during the same incubation period. The specificity of the requirement for ATP is demonstrated by the inability of dATP, UTP, GTP, or CTP (Fig. 6.4.F, lanes 3-6) to stimulate conversion of the artificial duplex RNA substrate into the single-stranded form. These results indicate that the RNA helicase activity of CrhR requires ATP.

Further investigations included testing the divalent cation requirement and the effects of pH on the efficiency of the RNA helicase activity of HIS:CrhR. While the reaction does proceed without exogenous addition of  $Mg^{2+}$  (Fig 6.4.E, lane 7), increasing the amount of  $MgCl_2$  (Fig. 6.4.E, lanes 9-10) or  $MgOAc$  (Fig. 6.4.G, lane 6) stimulates slightly higher levels of RNA unwinding. Interestingly, when  $MgCl_2$  is replaced with  $CaCl_2$ , the conversion to ssRNA is completely inhibited (Fig. 6.4.E, lane 8). These results suggest that the enzyme has a requirement for  $Mg^{2+}$  ions, and not simply for divalent cations, which may actually interfere with helicase activity. Finally, the *in vitro* conversion of dsRNA to ssRNA is favoured at a pH of 7.5 or 8.5 (Fig. 6.4.G, lanes 4 and 3, respectively) compared to pH 9 (Fig. 6.4.G, lane 5) under standard assay conditions.

## 6.3 Discussion

### 6.3.1 CrhR Exhibits Biochemical Activities Characteristic of an RNA Helicase

CrhR is a true DEAD-box RNA helicase, possessing RNA-dependent ATP hydrolysis, and ATP-dependent RNA-unwinding activities. The directionality of the RNA helicase activity was demonstrated to occur 5' to 3'; possible 3' to 5' activity remains to be investigated. RNA binding activity is inferred from the results obtained following RNase treatments. These biochemical activities were demonstrated by *in vitro*

assays using affinity-purified recombinant HIS:CrhR. Western analyses and SDS-PAGE have previously established that HIS:CrhR is the major polypeptide in the affinity column eluate that is applied to the assays (refer to chapter five). The activities are attributed to CrhR, as supported by the decrease in ATP hydrolysis with addition of anti-CrhR antiserum. The results presented here do not exclude the possibility that other proteins are present as minor species in the elution fraction and may interact with and/or modify HIS:CrhR activity. The successful demonstration of the enzymatic activities of HIS:CrhR implies that this recombinant protein undergoes proper folding and post-translational modifications that preserve the integrity of CrhR despite the presence of the N-terminal HIS-tag.

Both the RNA unwinding and nucleoside hydrolysis activities show specificity for ATP. The other nucleosides tested, namely GTP, CTP, and UTP, do not compete with ATP in the ATPase assay and do not support RNA unwinding in the helicase assay. This leads to the conclusion that these nucleosides are neither bound nor hydrolyzed by CrhR, and hence cannot serve as a source of energy for the biochemical activities. The results obtained with dATP are interesting: in competition assays dATP inhibits hydrolysis of [ $\gamma$ - $^{32}$ P]ATP to an even greater extent than the inhibition by unlabelled ATP, yet does not support RNA helicase activity. These observations are consistent with a hypothesis that dATP is bound by CrhR but cannot be hydrolyzed. In this scenario, non-productive binding to dATP inhibits the hydrolysis of the labeled ATP substrate by blocking the catalytic site and/or preventing turnover of the enzyme. By comparison, unlabeled ATP only slightly inhibits the reaction because it also serves as a substrate for hydrolysis, permitting enzyme turnover. If dATP is not hydrolyzed and also does not support RNA helicase activity, it follows that the unwinding of RNA by CrhR is normally driven by the energy derived from ATP hydrolysis.

The enzymatic requirement for divalent cations appears to be specific for magnesium. This is supported by the inhibition of ATPase activity when EDTA is added alone, and the observation that CaCl<sub>2</sub> completely blocks RNA helicase activity. These are interpreted as removal of and competition with magnesium ions, respectively. In light of this, and considering that most enzymes require magnesium, it seems plausible that CrhR also requires magnesium for its function. Hypothetically, the column eluate may contain sufficient Mg<sup>2+</sup> either free in solution or associated with HIS:CrhR, similar to the presence of RNA described above. This could occur if the HIS-tag, which is known to bind Ni<sup>2+</sup>, binds Mg<sup>2+</sup> with a lesser affinity but in sufficient quantities to function as a co-factor for the enzymatic activities of CrhR. Alternatively, perhaps nickel ions are co-eluted with HIS:CrhR and provide the same function as magnesium.

The RNase treatment of HIS:CrhR is significant because it provides a novel method for revealing the RNA-dependence of the ATP hydrolysis and RNA helicase activities. It also provides circumstantial evidence for the ability of CrhR to bind RNA. It is obvious that the presence (and presumably the binding) of this RNA is essential for the enzymatic activities, however the nature of the RNA species that effects the stimulation remains to be elucidated. The observation that both *E. coli* and *Synechocystis* RNA can activate CrhR implies that the particular RNA species is common to these two prokaryotes. Furthermore the artificial substrate alone is not able to stimulate the RNA unwinding activity of CrhR, despite the presence of both ssRNA and dsRNA in the preparation, which suggests that either it is not present in sufficient quantity or it is not an appropriate substrate for the binding. It is hoped that future research will determine whether binding requires dsRNA versus ssRNA, or whether it is specific for mRNA, rRNA, or tRNA.

### **6.3.2 CrhR and the Current Model for RNA Unwinding by DEAD-box Proteins**

The results from this study are consistent with the biochemical (Pause *et al.*, 1993) and structural (Cho *et al.*, 1999; de la Cruz *et al.*, 1999) models generally in use: CrhR interacts with both ATP and dsRNA substrates, and unwinds regions of base-paired RNA using the energy derived from the hydrolysis of ATP. The research presented here also supports the proposal that there are two separable sites for RNA binding: The first may be a non-productive interaction between CrhR and an RNA species that is common to *E. coli* and *Synechocystis*, such that the binding of this RNA does not result in its modification but rather it causes a conformational change in the protein. This type of interaction is often a proposed function of RNA binding motifs identified in the carboxy-termini of various DEAD-box proteins. If this initial interaction with RNA occurs simultaneously with ATP binding and/or hydrolysis this would suggest that it requires energy. Conversely, the binding of RNA may yield the active state of CrhR by potentiating the binding and hydrolysis of ATP as well as the active unwinding of dsRNA. According to this hypothesis the second RNA binding site is the cleft between domains 1 and 2 and domain 3, postulated as the "active" site for RNA helicase activity. Evidence in support of this proposal includes the observation that excess unlabeled RNA enables rather than competes with, the unwinding of the artificial dsRNA substrate in the helicase assay.

CrhR possesses biochemical activities consistent with an RNA helicase, activities that can be incorporated into a model predicting the biological function of CrhR as presented in chapter seven.

## **CHAPTER SEVEN**

### **A Model for the Regulation and Physiological Role of the RNA Helicase CrhR**

## **7.1 Introduction**

The research presented in this thesis establishes that the *Synechocystis* gene *crhR* encodes a DEAD-box RNA helicase. The characterization of this essential gene has a dual focus, being concerned not only with the physiological events that lead to expression of the cognate mRNA and protein, but also with the ensuing CrhR-mediated effects on RNA metabolism. In this chapter a model for the regulation and role of the RNA helicase is presented, summarized in Figure 7.1. The transcriptional and post-transcriptional regulation of *crhR* are described relative to changes in redox conditions, with the plastoquinone pool proposed to serve as the point of integration for the various stimuli that affect *crhR* gene expression. According to this model the interaction of plastoquinone with proximal membrane-bound complexes regulates the induction of overlapping signal transduction cascades. These are hypothesized to alter the activity of cytosolic DNA-binding factors that interact with *cis*-elements in the DNA sequence of *crhR*. Finally, the biological implications of a redox-regulated RNA helicase are discussed with regards to the biochemical activities and potential tertiary associations involving CrhR and other polypeptide(s).

## **7.2 Events Leading to the Expression of *crhR***

### **7.2.1 Redox-Regulated Gene Expression: The Role of Plastoquinone**

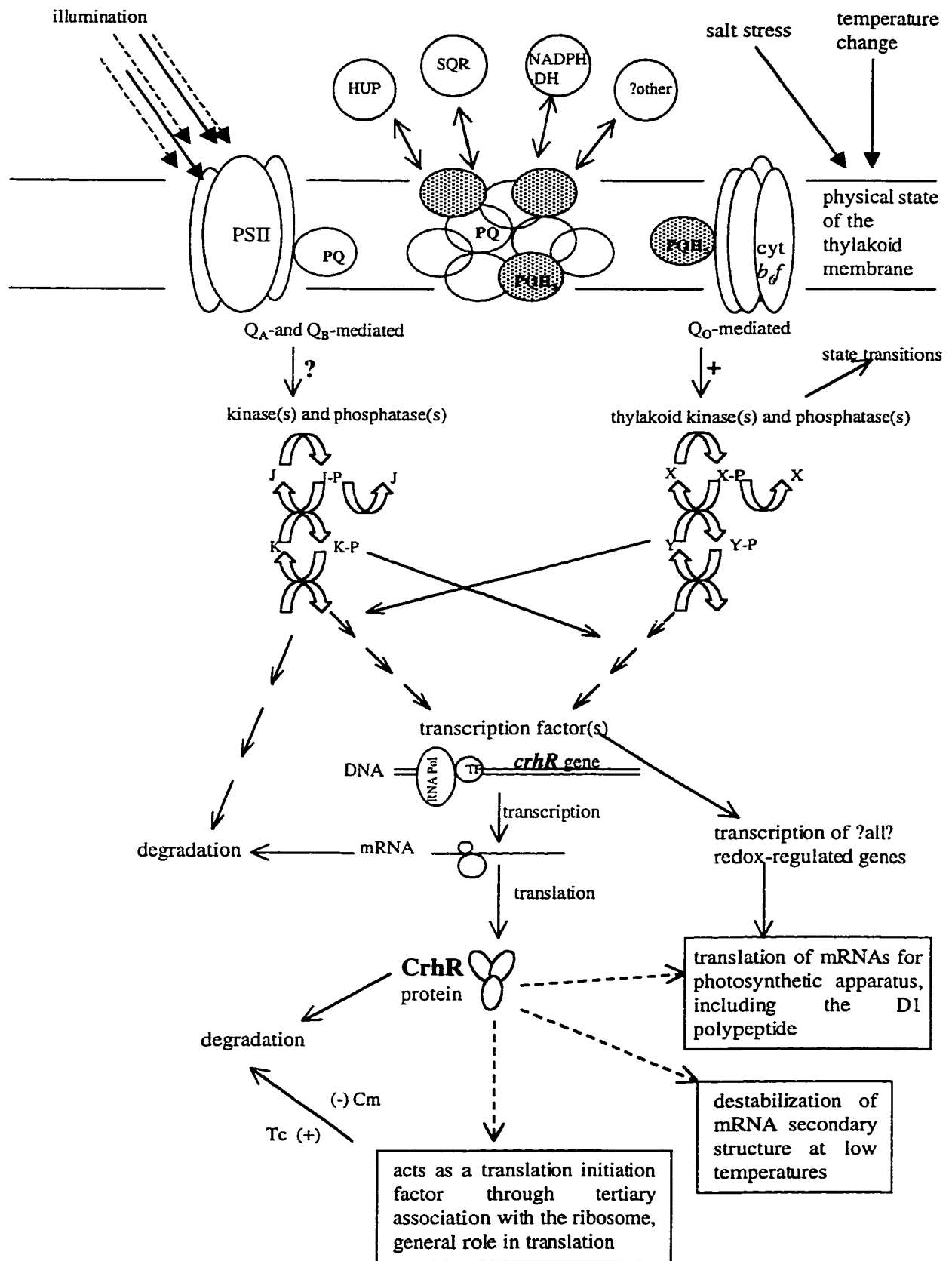
The expression of the *crhR* gene was elucidated following experimental manipulation of glucose metabolism, electron flow through the electron transport chain, wavelength and intensity of actinic illumination, and stress treatments. The results indicate that the regulation of *crhR* is consistent with physiological and molecular responses of photoautotrophic organisms to each of the experimental conditions, as previously described by various researchers. These investigations have revealed elements of redox control that may be traced to the involvement of plastoquinone. Thus, this section presents a proposal that plastoquinone lies at the intersection of the signaling pathways that regulate *crhR* expression.

According to this hypothesis, plastoquinone is a main integration point for various signal transduction networks in cyanobacteria, acting as a sensor for physiological and environmental alterations and then initiating changes that are detected in the present study as alterations in *crhR* expression. Plastoquinone is a suitable candidate for such a regulatory role for a number of reasons. Firstly, plastoquinone is located in the thylakoid membrane, which has a unique protein complement and photosynthetic function and which is therefore essential for the growth and survival of photoautotrophic cells. The



### **Figure 7.1 Model for Regulation and Role of the CrhR Helicase**

PQ, plastoquinone. PQH<sub>2</sub>, plastoquinol; also indicated by the shaded circles. PSII, photosystem II reaction centre. Cyt *b<sub>f</sub>*, cytochrome *b<sub>f</sub>* complex. HUP, uptake hydrogenase; SQP, sulfide quinone reductase: known or possible components which interact with plastoquinone in cyanobacteria (Kallas, 1994). J, K, X, and Y, hypothetical components in the proposed signal transduction pathways. The successive activation or de-activation of the signaling components and the possibility of cross-talk between the pathways are indicated by the arrows. TF, transcription factor regulating expression from the *crhR* promoter. Tc, tetracycline. Cm, chloramphenicol.



importance of this localization is seen in the fact that membranes have been previously suggested to be the sites for monitoring changes in temperature, osmotic pressure, or other stresses (Horvath *et al*, 1998). Secondly, the effects of a wide range of redox conditions converge at the point of plastoquinone. Therefore, a shift in the redox equilibrium of the plastoquinone pool has the potential to monitor redox changes from multiple external and internal signals. Thirdly, plastoquinone offers the advantages of a pool of individual molecules acting in concert. As such it is capable of a finer range of sensing and response modulations compared to a single molecule that exists in either active or inactive forms. Finally, the dynamic nature of electron flow yields rapid and constant adjustment in the redox state of the plastoquinone pool and its partners. Therefore, if plastoquinone functions as a homeostatic sensor it could rapidly "interpret" the magnitude and duration of redox contributions from many sources, combining these into a single common redox effect and then triggering changes in multiple signal transduction pathways via different affinities or redox potentials for interaction with the appropriate mediator(s).

Two of these hypothetical mediators may be *cyt b<sub>6</sub>f* and PSII, which co-localize with plastoquinone in the thylakoid membrane, and which could sense redox changes in the plastoquinone pool via interactions at the appropriate quinone or quinol binding sites. As detailed below, this prediction is supported by various independent research results implicating each of these integral membrane complexes in signal transduction pathways. Furthermore, this hypothesis is able to incorporate many of the effects of temperature and osmolarity on *crhR* expression by relating these to redox changes induced at the thylakoid membrane. The model is not intended to exclude other redox regulatory mechanisms, however the role of modulators such as thioredoxin remains to be investigated. Therefore, I believe this hypothesis could provide a tentative framework for understanding and predicting redox-regulated gene expression in cyanobacteria by linking it to a redox sensor (namely plastoquinone) that monitors and participates in maintaining the bioenergetic homeostasis.

### **7.2.2 Signal Transduction Pathways Initiated in Response to Interaction of the Plastoquinone Pool with *cyt b<sub>6</sub>f* and/or PSII**

The current model for plastoquinol-induced alterations in photosynthetic gene expression and protein phosphorylation patterns ascribes these to the thylakoid kinase and phosphatase(s) that are also responsible for effecting state transitions (Allen *et al*, 1995; Gal *et al*, 1997; Vener *et al*, 1998; section 4.1.1). It has been established that the plastoquinone pool interacts with the cytochrome *b<sub>6</sub>f* complex for electron transfer at the

quinol oxidase site,  $Q_O$ . Since the redox status of these two electron transport chain components is intimately linked, it is not surprising that redox regulation that is plastoquinol-responsive may also be *cyt b<sub>6</sub>f*-dependent, as indicated by the loss of redox-specific regulation in *cyt b<sub>6</sub>f* mutants (Gal *et al.*, 1987). Recently, Vener and co-workers (1995) have demonstrated that while a shift in the redox equilibrium of the plastoquinone pool towards plastoquinol induces the activity of the thylakoid kinase, it is the redox status of *cyt b<sub>6</sub>f* that prescribes the duration of the activated state. As the plastoquinone pool becomes more reduced, there is a corresponding increase in the frequency of electron transfer at  $Q_O$  as well as in thylakoid kinase activity, hence the key event for activation of the thylakoid kinase is postulated to be plastoquinol occupancy of  $Q_O$  (Alfonso *et al.*, 2000; Fujita *et al.*, 1994; Vener *et al.*, 1995). Thus, it is apparent that intracellular signaling events and downstream gene expression patterns are altered in response to the redox state of plastoquinone, in a *cyt b<sub>6</sub>f*-dependent manner (see Figure 7.1).

The interaction of plastoquinone with the PSII complex may similarly initiate signal transduction events that determine gene expression. Analogous to the thylakoid kinase activation mediated via  $Q_O$ , distinct but overlapping signaling pathways could be initiated in response to plastoquinone occupancy of the  $Q_A$  and/or  $Q_B$  sites in the D1 polypeptide or to electron transfer at these sites. For example, investigation of cyanobacterial adaptation to high intensity illumination conditions has suggested that efficient electron flow through PSII initiates a signal transduction pathway for altered pigment composition of the phycobilisomes (Minagawa *et al.*, 1999). PSII excitation pressure (which is a measure of electron flow through the complex) has also been proposed to regulate the biosynthesis of the D1 polypeptide itself through transcriptional control of *psbA*, and possibly at the point of translation or insertion of the D1 polypeptide into the membrane (Gombos *et al.*, 1992). As detailed previously (section 4.1.1), *psbA* is a redox-regulated gene whose expression correlates with changes in the redox status of the plastoquinone pool. These observations support the proposal that the redox interaction of plastoquinone with PSII could specify activation of a kinase analogous to the system described for *cyt b<sub>6</sub>f*. This PSII-dependent signaling pathway may become more significant under conditions of very high intensity illumination (photoinhibition - see section 1.2.3.3), when electron flow from PSII into the plastoquinone pool exceeds the rate of oxidation by *cyt b<sub>6</sub>f*. The resultant over-reduction of the plastoquinone pool subsequently favours the back-reaction that transfers electrons from  $Q_A$  or  $Q_B$  to P680 in the PSII reaction center (Krieger-Liszka and Rutherford, 1998, and references therein). Furthermore, the back-reaction generates a highly reactive chlorophyll species that leads

to oxidative damage and increased turnover of the D1 polypeptide (Krieger-Liszkay and Rutherford, 1998), which is presumably replaced in a redox-regulated manner.

Thus, in the model presented here the plastoquinone pool is a central redox control point, with differing thresholds for, but inter-dependent effects on, the two mediators PSII and *cyt b<sub>6</sub>f*. It is conceivable that the interaction of plastoquinone in the Q<sub>O</sub> site of *cyt b<sub>6</sub>f* is more significant under conditions where the plastoquinone pool is not completely reduced. The occupancy of the Q<sub>A</sub> and Q<sub>B</sub> sites in PSII is expected to increase as oxidation of plastoquinol by *cyt b<sub>6</sub>f* becomes rate-limiting. As light intensity increases, the interaction of plastoquinone with the PSII complex may become more important, until at photoinhibitory levels of illumination the back-reaction at Q<sub>A</sub> and Q<sub>B</sub> predominates. The respective redox-regulated kinases and downstream signal transduction cascades are expected to exert an effect on both photosynthetic and non-photosynthetic metabolism, at multiple levels including mRNA transcription and stability, as well as translational control and post-translational modifications.

The observed pattern of *crhR* expression is generally consistent with these predictions. Since *crhR* transcript levels decline following treatments that decrease the rate of redox exchange between the plastoquinone pool and *cyt b<sub>6</sub>f* or PSII, this suggests that in the absence of the respective kinase activities *crhR* is not actively expressed. In contrast, a shift in the equilibrium of the plastoquinone pool towards a more reduced status increases the frequency of Q<sub>O</sub> occupancy, resulting in increased activation of the *cyt b<sub>6</sub>f*-responsive kinase. Accordingly, *crhR* mRNA levels are constitutive with illumination, and are maintained when respiration of exogenous glucose sustains electron flow to plastoquinone in the dark. Altering the quality of the actinic light to preferentially excite PSI and increase the oxidation of plastoquinone versus increased excitation of PSII to increase the reduction of plastoquinone yields a relative decrease or increase, respectively, in the level of *crhR* mRNA. As the intensity of actinic light increases, *crhR* transcript accumulation is also enhanced, despite the increased instability of the mRNA. Significantly, the highest levels of *crhR* transcript were detected under conditions where the plastoquinone pool is predicted to be over-reduced, implying that the interaction of the plastoquinone pool with PSII at the Q<sub>A</sub> and Q<sub>B</sub> sites increases the *crhR* expression levels via a signaling pathway that is separate but additive with the *cyt b<sub>6</sub>f*-mediated pathway. Furthermore, if the signaling pathway initiated via Q<sub>A</sub> and Q<sub>B</sub> has an additive effect with the Q<sub>O</sub>-dependent pathway, the expected - and observed - outcome would be higher levels of *crhR* under photomixotrophic conditions with addition of DBMIB (which inhibits oxidation of plastoquinone at Q<sub>O</sub>) or DCMU (which acts as a competitive inhibitor in the Q<sub>B</sub> site). These results imply that *crhR* expression is

regulated by the separate but coordinated activities of multiple parallel and/or overlapping signal transduction pathways that originate due to redox exchanges within the thylakoid membrane.

### **7.2.3 Modulation of Plastoquinone-Mediated Signal Transduction Pathways by Alterations in the Thylakoid Membrane**

Since PSII and cyt *b<sub>6</sub>f* are integral membrane complexes and plastoquinone exists as a mobile pool of molecules within the thylakoid membrane, the electron transport components and reactions are significantly influenced by the physical state of the membrane. This affects the protein-protein interactions within and between the integral membrane complexes as well as with soluble thylakoid-associated peptides, thereby altering the efficiency of electron transfer. Therefore, it is plausible that manipulation of the membrane physical state could also affect the regulation of the proposed redox-responsive signaling pathways, and could be evidenced by changes in gene expression. A strength of the hypothetical model presented thus far is that it can accommodate various stress-induced alterations in *crhR* expression.

Changes in temperature yield the most obvious effects on the physical state of membranes. Stemming from the investigation of heat-shock protein expression in cyanobacteria, Horvath and colleagues (1998) have proposed a model describing the thylakoid membranes as the "cellular thermometer", linking temperature-induced changes in gene expression to the diffusion, and hence the redox status, of the plastoquinone pool. These researchers were able to mimic (induce) the heat-shock response through the use of membrane-fluidizing agents, whereas treatments that decrease membrane fluidity repressed the transcriptional activation and *de novo* synthesis of heat-shock proteins, including *dnaK* and *groESL*. These results were specific to *in vivo* treatment of the thylakoid membrane, but conspicuously absent following *in vivo* treatment of the cell membranes (Horvath *et al*, 1998). A decrease in temperature also alters the physical state of the thylakoid membrane and triggers long-term adaptations via shifts in the redox status (Gombos *et al*, 1992; Horvath *et al*, 1998; Kis *et al*, 1998). For example, as an adaptive response to the low-temperature decrease in fluidity of the thylakoid membranes, desaturation of the membrane fatty acids increases and is accomplished by the lipid desaturases (Kis *et al*, 1998). Treatment with inhibitors of transcription, translation, or electron transport has indicated that the light-induced expression of the lipid desaturase (*des*) genes requires *de novo* protein synthesis and is regulated at the level of transcription, mediated by a signaling pathway that includes factors generated in response to photosynthetic electron transport (Kis *et al*, 1998). These and similar

observations support the redox-mediated link between physical conditions that are sensed as alterations in the thylakoid membrane, and activation of signal transduction cascades for the regulation of gene expression.

Additionally, there is evidence that light and temperature exert a cooperative effect on membrane-localized redox events and downstream changes in gene expression. Studies of photosensitivity indicate that cells are more sensitive to photoinhibition at low light intensity when the temperature is also lower (Gombos *et al*, 1992; Kis *et al*, 1998; Miskiewicz *et al*, 2000), implying that light intensity is perceived to be higher when membrane fluidity - and hence the efficiency of electron transfer - decreases. This may be linked to the interaction of the D1 polypeptide with the plastoquinone pool at the  $Q_A$  and  $Q_B$  sites since the site of low-temperature photoinhibition was localized to the electron transport side of the PSII complex (Gombos *et al*, 1992). The modulation of total RNA synthesis, implying alterations in gene expression, has also been shown to be controlled by illumination conditions and modulated by temperature: The rate of RNA accumulation decreases following a temperature shift up and this effect is more pronounced when cells are simultaneously transferred into darkness (Suranyi *et al*, 1987). Since the pattern of RNA accumulation was dependent upon the light-dark regime performed immediately prior or subsequent to the heat-shock treatment, the effects of illumination appear to be dominant to temperature (Suranyi *et al*, 1987).

Osmolarity and pH may also be linked to signal transduction pathways mediated by redox changes at the thylakoid membrane. Vener and colleagues (1995) have used transient decreases in pH to activate the thylakoid kinase, presumably by shifting the membrane potential to yield the reduction of the plastoquinone pool. Adaptation to salt stress resembles state transitions by virtue of causing a decrease in energy transfer between the phycobilisomes and PSII (Hagemann *et al*, 1993), and hence altering the rate of electron flow through the thylakoid membrane-bound carriers. Furthermore, associated alterations in protein phosphorylation patterns in response to salt stress (Vinnemeier and Hagemann, 1999) imply that signal transduction pathways are affected.

According to the proposed model, therefore, the effects of modulating the physical state of the thylakoid membrane may be super-imposed upon the redox status conferred by photoautotrophic or photomixotrophic growth conditions. Insofar as they induce redox changes in plastoquinone, PSII, cyt *b<sub>6</sub>f*, or electron transfer, alterations in the thylakoid membrane physical state could also regulate the proposed signal pathways at  $Q_A/Q_B$  and  $Q_O$  and control gene expression. I believe that these predictions are generally borne out in the accumulation of *crhR* mRNA and protein as presented in this thesis. Following a temperature shift up, which would increase thylakoid membrane

fluidity and hence the rate of electron transfer, there is a decline in the abundance of the *crhR* mRNA. In contrast, cold-shock treatments decrease the efficiency of electron transport and lead to an increase in *crhR* expression in a pattern similar to that of the *desA* and *desB* transcripts (Kis *et al*, 1998), suggesting a common redox-regulated signal transduction pathway for these genes. Cold-shock is able to induce the accumulation of *crhR* mRNA and protein in the absence of light. Additionally, a cooperative effect of illumination and temperature is noted for *crhR* expression: The magnitude of the increase in *crhR* transcript levels following a downshift in temperature correlates with the increase in intensity of the actinic light. Furthermore, salt stress - which also causes a decrease in the electron transfer efficiency - similarly induces a significant increase in both transcript and protein levels, with or without illumination. Although the magnitude of the increase is lower with addition of salt than with cold-shock, it appears that both treatments generate redox changes that exert similar effects on the proposed signaling pathways from  $Q_O$  and/or  $Q_A/Q_B$ . These observations are consistent with a scenario whereby in the absence of light the expression of *crhR* is induced by cold or salt treatments via the  $Q_O$ -dependent signaling pathway. With illumination the additional electron flow through PSII could further regulate *crhR* expression via activation of the  $Q_A/Q_B$ -regulated signal transduction pathway, speculated above to be sensitive to the intensity of the light. While the effect of pH was not specifically investigated in the present work, experimental modulation of pH could be used in future research to confirm the involvement of the  $Q_O$ -dependent kinase in *crhR* expression, since the link between pH and thylakoid kinase activation has been established (Vener *et al*, 1998).

#### **7.2.4 Redox Regulation of Transcript Stability**

The present thesis research provides evidence that the *crhR* mRNA stability is redox-responsive but is regulated separately from transcription of the gene. Specifically, the mRNA stability increases when photosynthetic electron transport is altered by transfer into darkness or by addition of DCMU or DBMIB, irrespective of photoautotrophic versus photomixotrophic growth conditions. In the model presented in this chapter (Figure 7.1), regulation of the half-life of the *crhR* transcript is attributed to the PSII-dependent signaling pathway. This explanation is favoured because all other components, reactions, and/or products of photosynthetic electron transport would be affected by the metabolism of exogenous glucose and the subsequent increase in respiratory electron flow. Furthermore, while DCMU and DBMIB have opposite effects on the redox state of the plastoquinone pool, they both affect the redox reactions occurring at the  $Q_A$  and  $Q_B$  sites: PSII is inhibited by DCMU occupancy of the  $Q_B$  site;



the over-reduction of plastoquinone following addition of DBMIB could cause an increase in the excitation pressure of PSII and increase the plastoquinol occupancy at  $Q_A$  and  $Q_B$ . These inhibitors could be expected to affect PSII similarly, irrespective of glucose respiration.

Future investigation into the mechanisms of degradation and stability of the *crhR* mRNA will be revealing. It may be possible to elucidate the specific RNase that is responsible for degradation as well as the RNA sequence determinants for ribonucleolytic attack. This could be accomplished by determining the transcript half-life in various RNase<sup>-</sup> mutants of *E. coli* available in this laboratory, as has been previously performed for *crhC* (Chamot and Owtrim, personal communication). It should also be possible to elucidate the stability determinants, such as the formation of protective secondary structures in the *crhR* mRNA (suggested below) and/or interaction with proteins that act as RNA chaperones. Finally, it will be important to determine the effect of mRNA stability on translation for the synthesis of CrhR (see also section 7.2.6).

### **7.2.5 A Potential Transcription Factor in the Putative Signal Transduction Pathway to *crhR* Expression**

Thus far the model for redox-regulated gene expression, including *crhR*, predicts that the redox-regulated signal transduction pathways are not responding directly to the plastoquinone pool *per se*, but rather to the interaction of plastoquinone with cyt *b<sub>6</sub>f* or PSII. While the preceding discussion focuses on the activation of putative kinases, it is likely that additional control occurs through the coordinate regulation of various signal transduction phosphatases. Similar to the control of state transitions and according to the model of Allen and colleagues (1995), the strength and duration of the redox signal from the plastoquinone pool to *crhR* expression is determined by the balance between thylakoid kinase and phosphatase activities, both within and between the multiple parallel and/or opposing signal transduction pathways responsible for maintaining bioenergetic homeostasis. The hypothetical model for *crhR* expression invokes at least two potential signal transduction pathways, the complimentary or competing effects of which remain to be confirmed, including the proposed effects of alterations in the physical state of the thylakoid membrane.

Evidence for transcription factors controlling *crhR* expression was obtained by EMSA (section 4.2.4). A 228 bp region of the *crhR* gene and putative promoter sequences, extending from -39 to +188 (relative to the putative transcription initiation site), is the smallest region assayed that successfully forms complexes with a DNA-binding protein (or multi-protein complex) present in soluble cell-free extracts. Further

research is necessary to delimit and isolate the sequences that confer transcriptional regulation in promoter assays. Since the key *cis*-acting sequences appear to localize to the coding region of *crhR*, they may function as operator, enhancer, or down-regulatory sequences during transcription of *crhR* (as described for other redox-regulated genes in section 4.1.2). Alternatively, this region may function as an operator sequence for another, suitably located, gene in the surrounding DNA. In either case, it would be interesting to determine if this region of DNA is related to the differing severity of the two *crhR*<sup>-</sup> mutants since the point insertion mutant (*crhR::Sp*), in which disruption of the gene spacing is greater than in the deletion mutant (*crhRΔ::Sp*), also showed a more severe growth phenotype.

The DNA-binding effector that interacts with this region of DNA remains to be identified. Future research should focus on obtaining purified protein for N-terminal microsequencing as well as to confirm a productive interaction with the coding region of the *crhR* gene. Following identification of the coding region for this polypeptide, it would be interesting to determine the pattern of *crhR* expression in a site-directed mutant for this gene in *Synechocystis*. This would enable elucidation of the transcriptional effects of the DNA-effector complex *in vivo*.

A number of intriguing questions remain which are outside the scope of this thesis, the answers to which will impact the direction of future research into *crhR* expression. These concern the isolation and characterization of the Q<sub>O</sub>- and (postulated) Q<sub>A</sub>/Q<sub>B</sub>-regulated kinases, including confirmation of activity (Shi *et al*, 1999) and determination of the mechanism of transducing the redox signal into kinase activation (Vener *et al*, 1998). Equally significant will be the continued elucidation of the postulated phosphorylation cascades specifically in *Synechocystis*, for which the putative two-component signal transduction genes have been identified in the genome database (Mizuno *et al*, 1996). Initial investigations suggest that redox conditions may influence the activity of some of these sensor kinases and/or response regulators (Li and Sherman, 2000). This information will enable construction of *Synechocystis* mutants for specific kinases, phosphatases, transcription factors, and other signal transduction components. The role of these putative signal transduction components in *crhR* expression could then be determined by assessing transcript and protein levels in the mutants, using the Northern and Western procedures applied in this thesis. Alternatively, this goal could be accomplished by assaying for the expression of reporter genes fused to the *crhR* promoter region. In fact, the coding and/or promoter sequences of *crhR* may serve as an ideal reporter system for changes in redox-mediated signal transduction paths, since this non-photosynthetic gene is redox-regulated in concert with many photosynthetic transcripts.

### **7.2.6 Interdependence of Transcriptional and Translational Control of *crhR*: The Protein Expression Pattern**

The correlation between the redox status of the plastoquinone pool and *crhR* expression is strongest at the level of mRNA, whereas the link to CrhR protein accumulation is less direct. Under photoautotrophic growth conditions the CrhR protein, unlike the mRNA, is constitutively present with both illumination and darkness. This implies that the protein is very stable within the cells, since it persists in the absence of detectable *crhR* transcript. Despite the lack of *crhR* transcription in the dark, it is possible that CrhR protein levels are initially maintained as a result of the increased stability of *crhR* transcripts, which may permit a degree of continued translation. Nonetheless, alterations in the relative abundance of CrhR protein do correlate with increases or decreases in accumulation of the transcript, which suggests that the rate of synthesis of CrhR is coupled to the level of mRNA present.

Translational and/or post-translational controls may be inferred from a number of observations in which the presence of CrhR protein differs significantly from the accumulation of the mRNA. This includes the long half-life of the CrhR protein and the results obtained with KCN treatment of photoautotrophic and photomixotrophic cultures. These results imply that the protein is protected from general proteolysis and turnover, potentially via an association within a highly stable multimeric complex. Further evidence that translation of CrhR can be uncoupled from mRNA accumulation is observed following treatment with the translational inhibitors chloramphenicol and tetracycline: Addition of tetracycline has no effect on the level of *crhR* transcript but yields a significant decrease in CrhR protein levels. Similar treatment with chloramphenicol results in loss of the *crhR* transcript, however no decrease in protein levels is evident. Since the two inhibitors target different stages of the translational process - tetracycline prevents initiation of translation while chloramphenicol blocks the elongation on ribosomes that have already initiated - it is possible that the effects on CrhR accumulation are due to altered protein stability rather than altered synthesis. According to this proposal, CrhR may act as a translation initiation factor whose association with the ribosome actively protects it from degradation. It is possible that, by preventing the ribosomal subunits from binding to mRNAs, tetracycline also induces the dissociation of CrhR from the ribosome and thereby increases CrhR degradation. Since chloramphenicol has no immediate effect on CrhR protein levels, it is possible that once the ribosome is in the elongation stage of translation, the interaction with CrhR is more resistant to dissociation, or that CrhR may be protected within stalled initiation

complexes. As discussed below, the potential association of the ribosomal S1 protein with CrhR (section 7.3.4) would be in agreement with this hypothesis.

Interestingly, the differential effect of chloramphenicol and tetracycline on *crhR* transcript levels suggests that the stability of the *crhR* mRNA is coupled to its translation. The *crhR* transcript levels decrease significantly when translation is blocked at the elongation stage but translation initiation continues (addition of chloramphenicol); however, when translation initiation is prevented (addition of tetracycline) the transcript levels are apparently unaffected. These observations are consistent with a scenario whereby the act of ribosome docking onto the 5' end of the *crhR* mRNA removes protective secondary structures and subsequently permits active endo- and exonucleolytic degradation. Since *crhR* transcript stability was shown to be lower with illumination compared to darkness, it follows that initiation of translation may also be light-dependent. Additionally, if this is generally true for many of the photosynthetic transcripts that exhibit a similar pattern of mRNA stability and if elongation is light-independent, this would agree with the proposed mechanism of CrhR protein stability.

### **7.3 Biological Significance of CrhR**

#### **7.3.1 CrhR is a True RNA Helicase That is Essential for Viability and Growth of *Synechocystis***

CrhR is the sole DEAD-box protein in *Synechocystis* sp. strain PCC 6803. *In vitro* assays demonstrate that CrhR binds RNA constitutively and without apparent sequence specificity. This non-specific binding of RNA is essential for biochemical activation, in agreement with the RNA helicase models that differentiate between productive and non-productive interactions with RNA (section 6.1). Since CrhR exhibits RNA-dependent ATP hydrolysis and ATP-dependent (5'-3')-RNA-unwinding activities *in vitro*, it is presumed to play the biological role of an RNA helicase *in vivo*. Importantly, while detection of the transcript and/or protein under specific conditions indicates the manner in which *crhR* expression is regulated, this is not necessarily an indication of *in vivo* biochemical activity nor the magnitude of the biological effect since the CrhR protein has an enzymatic rather than structural function.

The genotype and phenotype of *Synechocystis* carrying gene disruption mutations in the *crhR* coding region, indicate that the RNA helicase function is essential to the growth and survival of this cyanobacterium. The pleiotropic effects point to a disruption or impairment of photosynthetic metabolism. The stability of the CrhR protein may have significant consequences for the generation of *crhR*<sup>-</sup> mutants, since it is likely that wild-

type CrhR would remain in the cells for a number of generations following the chromosomal segregation event that would generate the homozygous *crhR*<sup>-</sup> clone. Protein stability may also be related to the dominant phenotype of the mutant copy of *crhR* in the heterozygotes, since it may have augmented the deleterious effect of the C-terminally truncated CrhR peptide.

### **7.3.2 Biological Function of a Redox-Regulated RNA Helicase: Implications for RNA Metabolism**

Since *crhR* is essential for viability, the RNA helicase function is inferred to be critical for RNA metabolism. The conditions that elicit or alter the level of *crhR* expression are presumed to reflect a cellular requirement for modulation of RNA secondary structure, and to correlate with the presence of the appropriate RNA substrate. Therefore, coordinate regulation of *crhR* with the transcripts of other redox-responsive genes suggests possible biological functions for CrhR. The model proposed by Allen and colleagues (1995) emphasizes redox control of the genes whose products are directly involved in photosynthesis and postulates an unidentified translational control point. This control point likely involves an RNA helicase such as CrhR, which would remove secondary structures that inhibit proper or efficient translation of the mRNAs encoding the photosynthetic apparatus. For example, as illumination intensity increases the coordination between increased D1 turnover and accumulation of the *crhR* transcript could be interpreted as implicating CrhR in photoacclimation. Similarly, the significant accumulation of *crhR* mRNA and protein during salt stress treatment suggests that the helicase may be required for the process of osmotic adaptation, which includes *de novo* synthesis of glycosylglycerol and other osmoprotective compounds (Hagemann *et al*, 1997). Additionally, photosynthetic and photomixotrophic metabolism encompass an increased production of RNAs in general; all or some of these RNA species could require the CrhR helicase activity for their function. Whether CrhR has specific targets, such as redox-specific mRNAs, or plays a more general role, perhaps enabling or increasing the efficiency of translation or assembly of ribonucleoprotein complexes, remains to be determined.

### **7.3.3 CrhR Expression in Response to Cold-Shock and Cold-Acclimation: Similarities to CsdA from *E. coli***

Together with the amino acid sequence homology, the similar pattern of cold-shock-induced accumulation of both CsdA (*E. coli*) and CrhR suggests an analogous function during the adaptation to a decrease in temperature. As previously described

(section 1.1.5), in *E. coli* the RNA helicase CsdA is required for expression of  $\sigma^{32}$  during the process of cold acclimation. CsdA enables the translation of this sigma factor by destabilizing secondary structures in the 5' UTR of the transcript. It was also noted that at low temperature *csdA*<sup>-</sup> mutants exhibit impaired growth, aberrant cell division, and lack of de-repression of heat-shock proteins; these effects were attributed to the normal association of CsdA with the ribosome and postulated role in translation initiation at low temperatures (Jones *et al.*, 1996). Similar to CsdA, CrhR has a cold-induced expression pattern (section 4.2.1.6; Suzuki *et al.*, 2000; Vinnemeier and Hagemann, 1999). Therefore, CrhR may perform an analogous function during cold-acclimation in *Synechocystis*. If this is true, the phenotype of both *crhR* mutants could be interpreted as growth defects, and the lack of increase in the cell density of *crhR::Sp* and *crhRΔ::Sp* mutants may reflect failure of the cells to divide. If, like CsdA, CrhR facilitates the translation of a sigma factor, either an alternative one like  $\sigma^{32}$  or the housekeeping  $\sigma^{70}$  type, this would be compatible with the requirement for CrhR under all growth conditions and with the pleiotropic phenotypes of the mutants.

#### **7.3.4 Tertiary Association of CrhR with Other Proteins**

The involvement of RNA helicases in tertiary associations with other peptides is appropriate given the nature of the RNA unwinding reaction - since ssRNA is thermodynamically unfavorable it must be "utilized" immediately either to translate, degrade, splice, protect, or re-fold it. The results of immunoprecipitation and column purification experiments indicate an interaction of CrhR with at least two polypeptides. The preliminary purification and identification of these two proteins could provide circumstantial evidence for the physiological function of CrhR, assuming that their functions are linked or complementary to RNA unwinding. If the C-terminally truncated peptides synthesized in the *crhR::Sp* and *crhRΔ::Sp* mutants retain the sequence determinants for the tertiary interaction with the two peptides, it is conceivable that this could confer the observed dominant phenotype by interfering with productive protein-protein interactions involving the wild-type CrhR.

The possibility that one of these peptides is the ribosomal S1 protein would be compatible with predictions of a biological function for CrhR in ribosome biogenesis or translation, a function that has been suggested for many of the known DEAD-box RNA helicases (de la Cruz *et al.*, 1999). As described above, CrhR may have a biological role similar to that of eIF-4A, acting as a standard translation initiation factor that is required for general light-dependent translation efficiency. This function could become more essential under cold-shock conditions where the thermodynamic stability of secondary

structures in the mRNA increases. Additionally, the ribosomal association may afford protection of CrhR against degradation, and contribute to the long half-life of the protein. Additional support for this hypothesis is provided by continuing research into CrhC from *Anabaena* sp. strain PCC 7120. Preliminary results indicate that this cold-shock-induced cyanobacterial helicase may form tertiary associations with the ribosomal S1 protein and may also become more highly associated with the membrane following a decrease in temperature (El-Fahmawi and Owtrim, personal communication). If CrhR does interact with the S1 protein, the further possibility that CrhR is also membrane-associated (El-Fahmawi and Owtrim, personal communication) will require continued investigation. This could facilitate or correlate with an increased role of CrhR (and CrhC) in the translation occurring on the thylakoid-associated ribosomes.

Another possibility, related to the homology between CrhR and CsdA (*E. coli*), is that the two peptides which associate with CrhR may be ssRNA-binding proteins possessing RNA chaperone functions analogous to the accessory role of CspA. Namely, one or both of the peptides may bind to single-stranded regions of mRNAs in order to prevent re-annealing.

#### **7.4 Significance**

The significance of this research lies in the relatively novel demonstration of a *non-photosynthetic* gene that is regulated in response to alterations in redox conditions. The model for *crhR* expression, as presented in this chapter, seeks to provide a hypothesis that is compatible with the observed alterations in mRNA and protein accumulation and that can be tested in future research. The present work also supports the feasibility of isolating the DNA-binding effector that binds to the *crhR* promoter and proximal coding regions, with the exciting potential for characterizing a cyanobacterial transcription factor. It follows that a better understanding of the signal transduction pathways that control *crhR*, and other redox-regulated genes, would result. The preliminary observation of two polypeptides that interact with the CrhR protein provides a starting point for their identification, which should yield significant insight into the biological function and RNA substrates for CrhR. Together with the continuing investigation of other RNA helicases, this information will increase our understanding of the importance of RNA secondary structure and RNA metabolism for the physiology of photosynthesis in cyanobacteria as well as higher plants.

## **CHAPTER EIGHT**

### **References**



- Abath, F.G.C., and A.J.G. Simpson.** 1991. A simple method for the recovery of purified recombinant peptides cleaved from glutathione-S-transferase-fusion proteins. *BioTechniques* **10**: 178.
- Alfonso, M., I. Perewoska, and D. Kirilovsky.** 2000. Redox control of *psbA* gene expression in the cyanobacterium *Synechocystis* PCC 6803. Involvement of the cytochrome b(6)/f complex. *Plant Physiol.* **122**: 505-516.
- Allen, J.F.** 1992. Protein phosphorylation in regulation of photosynthesis. *Biochim Biophys Acta* **1098**: 275-335.
- Allen, J.F., K. Alexciev, and G. Hakansson.** 1995. Regulation by redox signaling. *Curr. Biol.* **5**: 869-872.
- Allen, J.F., M.A. Harrison, and N.G. Holmes.** 1989. Protein phosphorylation and control of excitation energy transfer in photosynthetic purple bacteria and cyanobacteria. *Biochimie* **71**: 1021-1028.
- Anandan, S., and S.S. Golden.** 1997. *cis*-Acting sequences required for light-responsive expression of the *psbDII* gene in *Synechococcus* sp strain PCC 7942. *J Bacteriol* **179**: 6865-6870.
- Anderson, S.L., and L. McIntosh.** 1991. Light-activated heterotrophic growth of the cyanobacterium *Synechocystis* sp. strain PCC 6803: A blue-light-requiring process. *J Bacteriol* **173**: 2761-2767.
- Aoki, S., T. Kondo, and M. Ishiura.** 1995. Circadian expression of the *dnaK* gene in the cyanobacterium *Synechocystis* sp. strain PCC 6803. *J Bacteriol* **177**: 5606-5611.
- Askjaer, P., R. Rosendahl, and J. Kjems.** 2000. Nuclear export of the DEAD box An3 protein by CRM1 is coupled to An3 helicase activity. *J Biol Chem.* **275**: 11561-11568.
- Aubourg, S., M. Kreis, and A. Lecharny.** 1999. The DEAD box RNA helicase family in *Arabidopsis thaliana*. *Nuc. Acids Res.* **27**: 628-636.
- Ausubel, F. M., R. Brent, R. E. Kingston, D. D. Moore, J. G. Seidman, J. A. Smith, and K. Struhl (eds.).** 1995. *Current Protocols in Molecular Biology*. John Wiley & Sons, Inc., U.S.A.
- Baginsky, S., K. Tiller, and G. Link.** 1997. Transcription factor phosphorylation by a protein kinase associated with chloroplast RNA polymerase from mustard (*Sinapis alba*). *Plant Mol. Biol.* **34**: 181-189.

- Barne, K.A., J.A. Bown, S.J. Busby, and S.D. Minchin.** 1997. Region 2.5 of the *Escherichia coli* RNA polymerase  $\sigma^{70}$  subunit is responsible for the recognition of the 'extended -10' motif at promoters. *EMBO J* **16**: 4034-4040.
- Bauer, C.E., and T.H. Bird.** 1996. Regulatory circuits controlling photosynthesis gene expression. *Cell* **85**: 5-8.
- Benz, J., H. Trachsel, and U. Baumann.** 1999. Crystal structure of the ATPase domain of translation initiation factor 4A from *Saccharomyces cerevisiae* – the prototype of the DEAD box protein family. *Structure Fold Des* **7**: 671-679.
- Bi, X., J. Ren, and D. Goss.** 2000. Wheat germ translation initiation factor eIF4B affects eIF4A and eIFiso4A helicase activity by increasing the ATP binding affinity of eIF4A. *Biochemistry* **39**: 5758-5765.
- Bloye, S.A., N.J. Silman, N.H. Mann, and N.G. Carr.** 1992. Bicarbonate concentration by *Synechocystis* PCC6803: Modulation of protein phosphorylation and inorganic carbon transport by glucose. *Plant Physiol.* **99**: 601-606.
- Boddeker, N., Stade, K., and F. Franceschi.** 1997. Characterization of DbpA, an *Escherichia coli* DEAD box protein with ATP-independent RNA unwinding activity. *Nuc. Acids Res.* **25**: 537-544.
- Bolivar, F., R.L. Rodriguez, R.J. Greene, M.C. Betlach, H.L. Heyneker, and H.W. Boyer.** 1977. Construction and characterization of new cloning vehicles. II. A multipurpose cloning system. *Gene* **2**: 95-113.
- Brandi, A., R. Spurio, C.O. Gualerzi, and C.L. Pon.** 1999. Massive presence of the *Escherichia coli* 'major cold-shock protein' CspA under non-stress conditions. *EMBO J.* **18**: 1653-1659.
- Browning, K.** 1996. The plant translational apparatus. *Plant Mol Biol.* **32**: 107-144.
- Buchanan, B.** 1991. Regulation of CO<sub>2</sub> assimilation in oxygenic photosynthesis: the ferredoxin/thioredoxin system. Perspective on its discovery, present status, and future development. *Arch. Biochem. Biophys.* **288**: 1-9.
- Buelt, M.K., B.J. Glidden, and D.R. Storm.** 1994. Regulation of p68 RNA helicase by calmodulin and protein kinase C. *J. Biol. Chem.* **269**: 29367-29370.
- Burger, F., M. Daugeron, and P. Linder.** 2000. Dbp10p, a putative RNA helicase from *Saccharomyces cerevisiae*, is required for ribosome biogenesis. *Nuc Acids Res.* **28**: 2315-2323.
- Bustos, S.A., and S.S. Golden.** 1991. Expression of the *psbDI* gene in *Synechococcus* sp. strain PCC 7942 requires sequences downstream of the transcriptional start site. *J Bacteriol* **173**: 7525-7533.

- Bustos, S.A., M.R. Schaefer, and S.S. Golden.** 1990. Different and rapid responses of four cyanobacterial *psbA* transcripts to changes in light intensity. *J Bacteriol* **172**: 1998-2004.
- Campbell, D., J. Houmard, and N. Tandeau de Marsac.** 1993. Electron transport regulates cellular differentiation in the filamentous cyanobacterium *Calothrix*. *Plant Cell* **5**: 451-463.
- Chamot, D., W. C. Magee, E. Yu, and G. W. Owttrim.** 1999. A cold shock-induced cyanobacterial RNA helicase. *J Bacteriol.* **181**: 1728-32
- Chamot, D., and G.W. Owttrim.** 2000. Regulation of cold shock-induced RNA helicase gene expression in the cyanobacterium *Anabaena* sp. strain PCC 7120. *J Bacteriol.* **182**: 1251-1256.
- Chien, Y., J.D. Helmann, and S.H. Zinder.** 1998. Interactions between the promoter regions of nitrogenase structural genes (*nifHDK2*) and DNA-binding proteins from N<sub>2</sub> and ammonium-grown cells of the Archaeon *Methanosarcina barkerii* 227. *J Bacteriol.* **180**: 2723-2728.
- Cho, H., N. Ha, L. Kang, K.M. Chung, S.H. Back, S.K. Jang, and B. Oh.** 1998. Crystal structure of RNA helicase from genotype 1b hepatitis C virus. A feasible mechanism of unwinding duplex RNA. *J Biol Chem.* **273**: 15045-15052.
- Chuang, R., P. Weaver, Z. Liu, and T. Chang.** 1997. Requirement of the DEAD-box protein Ded 1p for messenger RNA translation. *Science* **275**: 1468-1471.
- Clarke, A.K., and D. Campbell.** 1996. Inactivation of the *petE* gene for plastocyanin lowers photosynthetic capacity and exacerbates chilling-induced photoinhibition in the cyanobacterium *Synechococcus*. *Plant Physiol.* **112**: 1551-1561.
- Coburn, G., X. Miao, D. Briant, and G. Mackie.** 1999. Reconstitution of a minimal RNA degradosome demonstrates functional coordination between a 3' exonuclease and a DEAD-box RNA helicase. *Genes Dev.* **13**: 2594-2603.
- Cooley, J., C. Howitt, and W. Vermaas.** 2000. Succinate:quinol oxidoreductases in the cyanobacterium *Synechocystis* sp. strain PCC 6803: Presence and function in metabolism and electron transport. *J Bacteriol.* **182**: 714-722.
- Cozzone, A. J.** 1993. ATP-dependent protein kinases in bacteria. *J Cell Biochem.* **51**: 7-13.
- Curtis, S.E., and J.A. Martin.** 1994. The transcription apparatus and the regulation of transcription initiation. pp. 613-639. *In* D.A. Bryant (ed.), *The Molecular Biology of Cyanobacteria*. Kluwer Academic Publishers, Dordrecht, The Netherlands.

- Dalla Chiesa, M., G. Friso, Z. Deak, I. Vass, J. Barber, and P.J. Nixon.** 1997. Reduced turnover of the D1 polypeptide and photoactivation of electron transfer in novel herbicide resistant mutants of *Synechocystis* sp. PCC 6803. *Eur J Biochem.* **248**: 731-740.
- Danon, A., and S.P. Mayfield.** 1994. Light-regulated translation of chloroplast messenger RNAs through redox potential. *Science* **266**: 1717-1719.
- Daugeron, M., and P. Linder.** 1998. Dbp7p, a putative ATP-dependent RNA helicase from *Saccharomyces cerevisiae*, is required for 60S ribosomal subunit assembly. *RNA* **4**: 566-581.
- de la Cruz, J., D. Kressler, and P. Linder.** 1999. Unwinding RNA in *Saccharomyces cerevisiae*: DEAD-box proteins and related families. *TIBS* **24**: 192-198.
- de la Cruz, J. D. Kressler, M. Rojo, D. Tollervey, and P. Linder.** 1998a. Spb4p, an essential putative RNA helicase, is required for a late step in the assembly of 60S ribosomal subunits in *Saccharomyces cerevisiae*. *RNA* **4**: 1268-81.
- de la Cruz, J., D. Kressler, D. Tollervey, and P. Linder.** 1998b. Dob1p (Mtr4p) is a putative ATP-dependent RNA helicase required for the 3' end formation of 5.8S rRNA in *Saccharomyces cerevisiae*. *EMBO J.* **17**: 1128-1140.
- Dickey, L.F., M.E. Petracek, T.T. Nguyen, E.R. Hansen, and W.F. Thompson.** 1998. Light regulation of *Fed-1* mRNA requires an element in the 5' untranslated region and correlates with differential polyribosome association. *Plant Cell* **10**: 475-484.
- Dolganov, N.A.M., D. Bhaya, and A.T. Grossman.** 1995. Cyanobacterial protein with similarity to the chlorophyll *a/b* binding proteins of higher plants: Evolution and regulation. *PNAS USA* **92**: 636-640.
- Eberl, D., L. Lorenz, M. Melnick, V. Sood, P. Lasko, and N. Perrimon.** 1997. A new enhancer of position-effect variegation in *Drosophila melanogaster* encodes a putative RNA helicase that binds chromosomes and is regulated by the cell-cycle. *Genetics* **146**: 951-963.
- Escoubas, J., M. Lomas, J. LaRoche, and P.G. Falkowski.** 1995. Light intensity regulation of *cab* gene transcription is signaled by the redox state of the plastoquinone pool. *PNAS USA* **92**: 10237-10241.
- Fankhauser, C., and J. Chory.** 1997. Light control of plant development. *Annu. Rev. Cell Dev. Biol.* **13**: 203-229.
- Feinberg, A.P., and B. Vogelstein.** 1983. A technique for radiolabelling DNA restriction endonuclease fragments to high specific activity. *Anal. Biochem.* **132**:6-13.

- Ferino, F., and F. Chauvat.** 1989. A promoter-probe vector-host system for the cyanobacterium *Synechocystis* PCC6803. *Gene* 84: 257-266.
- Flores, E., and G. Schmetterer.** 1986. Interaction of fructose with the glucose permease of the cyanobacterium *Synechocystis* sp. strain PCC 6803. *J Bacteriol.* 166: 693-696.
- Frangioni, J.V., and B. G. Neel.** 1993. Solubilization and purification of enzymatically active glutathione *S*-transferase (pGEX) fusion proteins. *Anal Biochem.* 210: 179-187.
- Fujita, Y., A. Murakami, K. Aizawa, and K. Ohki.** 1994. Short-term and long-term adaptation of the photosynthetic apparatus: Homeostatic properties of thylakoids. pp. 677-692. *In* D.A. Bryant (ed.), *The Molecular Biology of Cyanobacteria*. Kluwer Academic Publishers, Dordrecht, The Netherlands.
- Fuller-Pace, F. V.** 1994. RNA helicases: modulators of RNA structure. *Trends in Cell Biology* 4: 271-274.
- Fuller-Pace, F., S. Nicol, A. Reid, and D. Lane.** 1993. DbpA: a DEAD box protein specifically activated by 23s rRNA. *EMBO J.* 12: 3619-3626.
- Gal, A., Y. Shahak, G. Schuster, and I. Ohad.** 1987. *FEBS Lett.* 221: 205-210.
- Gal, A., H. Zer, and I. Ohad.** 1997. Redox-controlled thylakoid protein phosphorylation. News and views. *Physiol Plant.* 100: 869-885.
- Gantt, E.** 1994. Supramolecular membrane organization. pp. 119-138. *In* D.A. Bryant (ed.), *The Molecular Biology of Cyanobacteria*. Kluwer Academic Publishers, Dordrecht, The Netherlands.
- Gavis, E.R., L. Lunsford, S.E. Bergsten, and R. Lehmann.** 1996. A conserved 90 nucleotide element mediates translational repression of *nanos* RNA. *Development* 122: 2791-2800.
- Giacometti, G.M., R. Barbato, S. Chiaramonte, G. Friso, and F. Rigoni.** 1996. Effects of ultraviolet-B radiation on photosystem II of the cyanobacterium *Synechocystis* sp. PCC 6803. *Eur J Biochem.* 242: 799-806.
- Gilmartin, P.M., L. Sarokin, J. Memelink, and N. Chua.** 1990. Molecular light switches for plant genes. *Plant Cell* 2: 369-378.
- Gingras, A., B. Raught, and N. Sonenberg.** 1999. eIF4 initiation factors: effectors of mRNA recruitment to ribosomes and regulators of translation. *Annu Rev Biochem.* 68: 913-963.
- Godbout, R., and J. Squire.** 1993. Amplification of a DEAD box protein gene in retinoblastoma cell lines. *PNAS USA* 90: 7578-7582.

- Golbeck, J.H.** 1994. Photosystem I in Cyanobacteria. pp 319-360. *In* D.A. Bryant (ed.), *The Molecular Biology of Cyanobacteria*. Kluwer Academic Publishers, Dordrecht, The Netherlands.
- Golden, S. S.** 1995. Light-responsive gene expression in cyanobacteria. *J Bacteriol.* **177**: 1651-1654.
- Golden, S.S., J. Brusslan, and R. Haselkorn.** 1987. Genetic engineering of the cyanobacterial chromosome. *Meth Enzymol.* **153**: 215-231.
- Gombos, Z., H. Wada, and N. Murata.** 1992. Unsaturation of fatty acids in membrane lipids enhances tolerance of the cyanobacterium *Synechocystis* PCC6803 to low-temperature photoinhibition. *PNAS USA* **89**: 9959-9963.
- Gorbalenya, A.E., and E.V. Koonin.** 1993. Helicases: amino acid sequence comparisons and structure-function relationships. *Curr Opin Struct Biol.* **3**: 419-429.
- Gorbalenya, A.E., E.V. Koonin, A.P. Donchenko, and V.M. Blinov.** 1988. A conserved NTP-motif in putative helicases. *Nature* **333**: 22.
- Gorbalenya, A.E., E.V. Koonin, A.P. Donchenko, and V.M. Blinov.** 1989. Two related superfamilies of putative helicases involved in replication, recombination, repair, and expression of DNA and RNA genomes. *Nuc Acid Res.* **17**: 4713-4730.
- Graumann, P., and M. Marahiel.** 1996. Some like it cold: response of microorganisms to cold shock. *Arch Microbiol.* **166**: 293-300.
- Gray, G.R., L. Chauvin, F. Sarhan, and N.P.A. Huner.** 1997. Cold acclimation and freezing tolerance; A complex interaction of light and temperature. *Plant Physiol.* **114**: 467-474.
- Gregor, J., and G. Klug.** 1999. Regulation of bacterial photosynthesis genes by oxygen and light. *FEMS Microbiol Lett.* **179**:1-9.
- Grifo, J.A., R.D. Abramson, C.A. Satler, and W.C. Merrick.** 1984. RNA-stimulated ATPase activity of eukaryotic initiation factors. *J Biol Chem.* **259**: 8648-8654.
- Grigorieva, G., and S. Shestakov.** 1982. Transformation in the cyanobacterium *Synechocystis* 6803. *FEMS Microbiol Lett.* **13**:367-370.
- Grossman, A., M. Schaefer, G. Chiang, and J. Collier.** 1993. The phycobilisome, a light-harvesting complex responsive to environmental conditions. *Microbiol Rev.* **57**: 725-749.
- Grossman, A., M. Schaefer, G. Chiang, and J. Collier.** 1994. The responses of cyanobacteria to environmental conditions: Light and nutrients. pp 641-675. *In*

- D.A. Bryant (ed.), *The Molecular Biology of Cyanobacteria*. Kluwer Academic Publishers, Dordrecht, The Netherlands.
- Hagemann, M., A. Schoor, R. Jeanjean, E. Zuther, and F. Joret.** 1997. The *stpA* gene from *Synechocystis* sp. strain PCC 6803 encodes the glucosylglycerol-phosphate phosphatase involved in cyanobacterial osmotic response to salt shock. *J Bacteriol.* **179**: 1727-33.
- Hagemann, M., D. Gollack, J. Biggins, and N. Erdmann.** 1993. Salt-dependent protein phosphorylation in the cyanobacterium *Synechocystis* PCC 6803. *FEMS Microbiol Lett.* **113**: 205-210.
- Hanahan, D.** 1983. Studies on the transformation of *Escherichia coli* with plasmids. *J Mol Biol.* **166**: 557-580.
- Harada, K., S. Martin, and A. Frankel.** 1996. Selection of RNA-binding peptides in vivo. *Nature* **380**: 175-179.
- Haselkorn, R.** 1991. Genetic systems in cyanobacteria. *Meth Enzymol.* **204**: 418-430
- Herschlag, D.** 1995. RNA chaperones and the RNA folding problem. *J Biol Chem.* **270**: 20871-20874.
- Hirano, M., K. Satoh, and S. Katoh.** 1980. Plastoquinone as a common link between photosynthesis and respiration in a blue-green alga. *Photosynth Res.* **1**: 149-162.
- Hodgman, T.C.** 1988. A new superfamily of replicative proteins. *Nature* **333**: 22-23.
- Horvath, I., A. Glatz, V. Varvasovszki, Z. Torok, T. Pali, G. Balogh, E. Kovacs, L. Nadasdi, S. Benko, F. Joo, and L. Vigh.** 1998. Membrane physical state controls the signaling mechanism of the heat shock response in *Synechocystis* PCC6803: Identification of *hsp17* as a "fluidity gene". *PNAS USA* **95**: 3513-3518.
- Howitt, C.A.** 1996. Amplification of DNA from whole cells of cyanobacteria using PCR. *BioTechniques* **21**: 32-34.
- Howitt, C.A., P.K. Udall, and W.F.J. Vermaas.** 1999. Type 2 NADH Dehydrogenases in the cyanobacterium *Synechocystis* sp. strain PCC 6803 are involved in regulation rather than respiration. *J Bacteriol.* **181**: 3994-4003.
- Iggo, R.D., and D.P. Lane.** 1989. Nuclear protein p68 is an RNA-dependent ATPase. *EMBO J.* **8**: 1827-1831.
- Iggo, R., S. Picksley, J. Southgate, J. McPheat, and D. Lane.** 1990. Identification of a putative RNA helicase in *E. coli*. *Nuc Acid Res.* **18**: 5413-5417.
- Iost I., and M. Dreyfus.** 1994. mRNAs can be stabilized by DEAD-box proteins. *Nature* **372**: 193-196.

- Iost, I., M. Dreyfus, and P. Linder.** 1999. Ded1p, a DEAD-box protein required for translation initiation in *Saccharomyces cerevisiae*, is an RNA helicase. *J Biol Chem.* **274**: 17677-17683.
- Jankowsky, E., C. Gross, S. Shuman, and A. Pyle.** 2000. The DExH protein NPH-II is a processive and directional motor for unwinding RNA. *Nature* **403**: 447-451.
- Jansson, C., R. Debus, H. Osiewacz, M. Gurevitz, and L. McIntosh.** 1987. *Plant Physiol.* **85**: 1021-1025.
- Jaramillo, M., T. Dever, W. Merrick, and N. Sonenberg.** 1991. RNA unwinding in translation: Assembly of helicase complex intermediates comprising eukaryotic initiation factors eIF-4F and eIF-4B. *Mol Cell Biol.* **11**: 5992-5997.
- Johnson, R., and D. McKay.** 1999. Crystallographic structure of the amino terminal domain of yeast initiation factor 4A, a representative DEAD-box RNA helicase. *RNA* **5**: 1526-1534.
- Jones, P. G., M. Mitta, Y. Kim, W. Jiang, and M. Inouye.** 1996. Cold shock induces a major ribosomal-associated protein that unwinds double-stranded RNA in *Escherichia coli*. *PNAS USA* **93**: 76-80.
- Kallas, T.** 1994. The cytochrome b6f complex. pp. 259-317 *In* D.A. Bryant (ed.), *The Molecular Biology of Cyanobacteria*. Kluwer Academic Publishers, Dordrecht, The Netherlands.
- Kalman, M., H. Murphy, and M. Cashel.** 1991. *rhlB*, a new *Escherichia coli* K-12 gene with an RNA helicase-like protein sequence motif, one of at least five such possible genes in a prokaryote. *New Biol.* **3**: 886-895.
- Kaneko, T., A. Tanaka, S. Sato, H. Kotani, T. Sazuka, N. Miyajima, M. Sugiura, and S. Tabata.** 1995a. Sequence analysis of the genome of the unicellular cyanobacterium *Synechocystis* sp. strain PCC6803. I. Sequence features in the 1 Mb region from map positions 64% to 92% of the genome. *DNA Research* **2**: 153-166.
- Kaneko, T., A. Tanaka, S. Sato, H. Kotani, T. Sazuka, N. Miyajima, M. Sugiura, and S. Tabata.** 1995b. Sequence analysis of the genome of the unicellular cyanobacterium *Synechocystis* sp. strain PCC6803. I. Sequence features in the 1 Mb region from map positions 64% to 92% of the genome (Supplement). *DNA Res.* **2**: 191-198.
- Kaneko, T., S. Sato, H. Kotani, A. Tanaka, E. Asamizu, Y. Nakamura, N. Miyajima, M. Hirose, M. Sugiura, S. Sasamoto, T. Kimura, T. Hosouchi, A. Matsuno, A. Muraki, N. Nakazaki, K. Naruo, S. Okumura, S. Shimpo, C. Takeuchi, T. Wada, A. Watanabe, M. Yamada, M. Yasuda, and S. Tabata.**



- 1996a. Sequence determination of the entire genome and assignment of potential protein-coding regions. *DNA Res.* **3**: 109-136.
- Kaneko, T., S. Sato, H. Kotani, A. Tanaka, E. Asamizu, Y. Nakamura, N. Miyajima, M. Hirose, M. Sugiura, S. Sasamoto, T. Kimura, T. Hosouchi, A. Matsuno, A. Muraki, N. Nakazaki, K. Naruo, S. Okumura, S. Shimpo, C. Takeuchi, T. Wada, A. Watanabe, M. Yamada, M. Yasuda, and S. Tabata.** 1996b. Sequence analysis of the genome of the unicellular cyanobacterium *Synechocystis* sp. strain PCC6803. II. Sequence determination of the entire genome and assignment of potential protein-coding regions (Supplement). *DNA Res.* **3**: 185-209.
- Kanervo, E., Y. Tasaka, N. Murata, and E. Aro.** 1997. Membrane lipid unsaturation modulates processing of the photosystem II reaction-center protein D1 at low temperatures. *Plant Physiol.* **114**: 841-849.
- Karpinski, S., C. Escobar, B. Karpinska, G. Creissen, and P.M. Mullineaux.** 1997. Photosynthetic electron transport regulates the expression of cytosolic ascorbate peroxidase genes in *Arabidopsis* during excess light stress. *Plant Cell* **9**: 627-640.
- Kennelly, P.J., and M. Potts.** 1996. Fancy meeting you here! a fresh look at "prokaryotic" protein phosphorylation. *J Bacteriol.* **178**: 4759-4764.
- Kim, J.L., K.A. Morgenstern, J.P. Griffith, M.D. Dwyer, J.A. Thomson, M.A. Murcko, C. Lin and P.R. Caron.** 1998. Hepatitis C virus NS3 RNA helicase domain with a bound oligonucleotide: the crystal structure provides insights into the mode of unwinding. *Structure* **6**: 89-100.
- Kis, M., O. Zsiros, T. Farkas, H. Wada, F. Nagy, and Z. Gombos.** 1998. Light-induced expression of fatty acid desaturase genes. *PNAS USA* **95**: 4209-4214.
- Knaut, H., F. Pelegri, K. Bohmann, H. Schwarz, and C. Nusslein-Bolhard.** 2000. Zebrafish *vasa* RNA but not its protein is a component of the germ plasm and segregates asymmetrically before germline specification. *J Cell Biol* **149**: 875-888.
- Kossen, K., and O. Uhlenbeck.** 1999. Cloning and biochemical characterization of *Bacillus subtilis* YxiN, a DEAD protein specifically activated by 23S rRNA: delineation of a novel sub-family of bacterial DEAD proteins. *Nuc Acids Res.* **27**: 3811-3820.
- Kotani, H., A. Tanaka, T. Kaneko, S. Sato, M. Sugiura, and S. Tabata.** 1995. Assignment of 82 known genes and gene clusters on the genome of the unicellular cyanobacterium *Synechocystis* sp. strain PCC6803. *DNA Res.* **2**: 133-142.

- Krieger-Liszkay, A., and A.W. Rutherford.** 1998. Influence of herbicide binding on the redox potential of the quinone acceptor in photosystem II: Relevance to photodamage and phytotoxicity. *Biochemistry* **37**: 17339-17344.
- Kujat, S.L., and G.W. Owttrim.** 2000. Redox-regulated RNA helicase expression. *Plant Physiol.* **124**: 703-713.
- Kulkarni, R.D., and S.S. Golden.** 1992. Transcriptional and post-transcriptional components of *psbA* response to high light intensity in *Synechococcus* sp. strain PCC 7942. *J Bacteriol.* **174**: 3775-3781.
- Kulkarni, R.D., and S.S. Golden.** 1997. mRNA stability is regulated by a coding-region element and the unique 5' untranslated leader sequences of the three *Synechococcus psbA* transcripts. *Mol Microbiol.* **24**: 1131-1142.
- Labarre, J., F. Chauvat, and P. Thuriaux.** 1989. Insertional mutagenesis by random cloning of antibiotic resistance genes into the genome of the cyanobacterium *Synechocystis* strain PCC 6803. *J Bacteriol.* **171**: 3449-3457.
- Lasko, P.F., and M. Ashburner.** 1988. The product of the *Drosophila* gene *vasa* is very similar to eukaryotic initiation factor-4A. *Nature* **335**: 611-617.
- Leroy, P., P. Alzari, D. Sassoon, D. Wolgemuth, and M. Fellous.** 1989. The protein encoded by a murine male germ cell-specific transcript is a putative ATP-dependent RNA helicase. *Cell* **57**: 549-559.
- Leskiw, B.K., R. Mah, E.J. Lawlor, and K.F. Chater.** 1993. Accumulation of *bldA*-specified tRNA is temporally regulated in *Streptomyces coelicolor* A3(2). *J Bacteriol* **175**: 1995-2005.
- Li, H., and L.A. Sherman.** 2000. A redox-responsive regulator of photosynthetic gene expression in the cyanobacterium *Synechocystis* sp. strain PCC 6803. *J. Bacteriol.* **182**: 4268-4277.
- Li, Q., and D. T. Canvin.** 1998. Energy sources for HCO<sub>3</sub><sup>-</sup> and CO<sub>2</sub> transport in air-grown cells of *Synechococcus* UTEX 625. *Plant Physiol.* **116**: 1125-1132
- Li, Q., H. Imataka, S. Morina, G. Rogers Jr, N. Richter-Cook, W. Merrick, and N. Sonenberg.** 1999. Eukaryotic translation initiation factor 4AIII (eIF4AIII) is functionally distinct from eIF4AI and eIF4AII. *Mol Cell Biol.* **19**: 7336-7346.
- Li, R., and S.S. Golden.** 1993. Enhancer activity of light-responsive regulatory elements in the untranslated leader regions of cyanobacterial *psbA* genes. *PNAS USA* **90**: 11678-11682.
- Li, R., N.S. Dickerson, U.W. Mueller, and S.S. Golden.** 1995. Specific binding of *Synechococcus* sp. strain PCC 7942 proteins to the enhancer element of *psbAII* required for high-light-induced expression. *J Bacteriol.* **177**: 508-516.

- Liang, L., W. Diehl-Jones, and P. Lasko.** 1994. Localization of vasa protein to the *Drosophila* pole plasm is independent of its RNA-binding and helicase activities. *Development* **120**: 1201-1211.
- Linder, P., P.F. Lasko, M. Ashburner, P. Leroy, P.J. Nielen, K. Nishi, J. Schnier, and P. Slonimski.** 1989. Birth of the D-E-A-D box. *Nature* **337**: 121-122.
- Madigan, M.T., J.M. Martinko, and J. Parker, eds.** 1997. *Brock Biology of Microorganisms*, 8<sup>th</sup> ed. Prentice-Hall, Inc., New Jersey, USA.
- Magee, W.C.** 1997. Characterization of a cyanobacterial RNA helicase gene. M.Sc. thesis. University of Alberta, Edmonton, Canada.
- Mann, N.** 1994. Protein phosphorylation in cyanobacteria. *Microbiology* **140**: 3207-3215.
- Mann, N., R. Rippka, and M. Herdman.** 1991. Regulation of protein phosphorylation in the cyanobacterium *Anabaena* strain PCC 7120. *J Gen Microbiol.* **137**: 331-339.
- Marmur, J.** 1961. A procedure for the isolation of deoxyribonucleic acid from microorganisms. *J. Mol. Biol.* **3**: 208-218.
- Marraccini, P., C. Cassier-Chauvat, S. Bulteau, S. Chavez, and F. Chauvat.** 1994. Light-regulated promoters from *Synechocystis* PCC6803 share a consensus motif involved in photoregulation. *Mol Microbiol.* **12**: 1005-1012.
- Mathews, C.K., and K.E. van Holde, eds.** 1990. *Biochemistry.* The Benjamin/Cummings Publishing Company, California, USA.
- Mattaj, I.** 1993. RNA recognition: a family matter? *Cell* **73**: 837-840.
- Maxwell, D.P., D.E. Laudenbach, and N.P.A. Huner.** 1995. Redox regulation of light-harvesting complex II and *cab* mRNA abundance in *Dunaliella salina*. *Plant Physiol.* **109**: 787-795.
- Mayfield, S. P., A. Cohen, A. Danon, and C. Yohn.** 1994. Translation of the *psbA* mRNA of *Chlamydomonas reinhardtii* requires a structured RNA element contained within the 5' untranslated region. *J Cell Biol.* **127**: 1537-1545.
- Mazouni, K., S. Bulteau, C. Cassier-Chauvat, and F. Chauvat.** 1998. Promoter element spacing controls basal expression and light inducibility of the cyanobacterial *secA* gene. *Mol Microbiol.* **30**: 1113-1122.
- Methot, N., A. Pause, J. Hershey, and N. Sonenberg.** 1994. The translation initiation factor eIF4B contains an RNA-binding region that is distinct and independent from its ribonucleoprotein consensus sequence. *Mol Cell Biol.* **14**: 2307-2316.
- Mian, I.S.** 1993. Sequence similarities between cell regulation factors, heat shock proteins and RNA helicases. *Trends Biochem Sci.* **18**: 125-127.

- Miczak, A., V. Kaberdin, C. Wei, and S. Lin-Chao.** 1996. Proteins associated with RNase E in a multicomponent ribonucleolytic complex. *PNAS USA* **93**: 3865-3869.
- Minagawa, J., Y. Narusaka, Y. Inoue, and K. Satoh.** 1999. Electron transfer between  $Q_A$  and  $Q_B$  in Photosystem II is thermodynamically perturbed in phototolerant mutants of *Synechocystis* sp. PCC 6803. *Biochemistry* **38**: 770-775.
- Misiewicz, E., A.G. Ivanov, J.P. Williams, M.U. Khan, S. Falk, and N.P. Huner.** 2000. Photosynthetic acclimation of the filamentous cyanobacterium, *Plectonema boryanum* UTEX 485, to temperature and light. *Plant Cell Physiol.* **41**: 767-775.
- Mizuno, T., T. Kaneko, and S. Tabata.** 1996. Compilation of all genes encoding bacterial two-component signal transducers in the genome of the cyanobacterium *Synechocystis* sp. strain PCC 6803. *DNA Res.* **3**: 407-414.
- Mohamed, A., and C. Jansson.** 1989. Influence of light on accumulation of photosynthesis-specific transcripts in the cyanobacterium *Synechocystis*. *Plant Mol Biol.* **13**: 693-700.
- Mohamed, A., and C. Jansson.** 1991. Photosynthetic electron transport controls degradation but not production of *psbA* transcripts in the cyanobacterium *Synechocystis* 6803. *Plant Mol Biol.* **16**: 891-897.
- Mohamed, A., J. Eriksson, H. Osiewacz, and C. Jansson.** 1993. Differential expression of the *psbA* genes in the cyanobacterium *Synechocystis*. *Mol. Gen. Genet.* **238**: 161-168.
- Mullet, J.E.** 1988. Chloroplast development and gene expression. *Annu Rev Plant Physiol Plant Mol Biol* **39**: 475-502.
- Mulligan, M., Jackman, D., and S. Murphy.** 1994. Heterocyst-forming filamentous cyanobacteria encode proteins that resemble eukaryotic RNA-binding proteins of the RNP family. *J Mol Biol.* **235**: 1162-1170.
- Mullineaux, C.W., and J.F. Allen.** 1986. The state 2 transition in the cyanobacterium *Synechococcus* 6301 can be driven by respiratory electron flow into the plastoquinone pool. *FEBS Lett.* **205**: 155-160.
- Mullineaux, C.W., and J.F. Allen.** 1990. State 1-state 2 transitions in the cyanobacterium *Synechococcus* 6301 are controlled by the redox state of electron carriers between photosystems I and II. *Photosynthesis Res.* **23**: 297-311.
- Mustilli, A.C., and C. Bowler.** 1997. Tuning in to the signals controlling photoregulated gene expression in plants. *EMBO J.* **16**: 5801-5806.
- Myers, J.** 1986. Photosynthetic and respiratory electron transport in a cyanobacterium. *Photosynth. Res.* **9**: 135-147.

- Nakajima, T., C. Uchida, S.G. Anderson, C. Lee, J. Hurwitz, J.D. Parvin, and M. Montminy.** 1997. RNA helicase A mediates association of CBP with RNA polymerase II. *Cell* 90: 1107-1112.
- Nanba, M., and S. Katoh.** 1984. Effects of dibromothymoquinone on oxidation-reduction reactions and the midpoint potential of the Rieske iron-sulfur center in photosynthetic electron transport of *Synechococcus* sp. *Biochim Biophys Acta* 767: 396-403.
- Nanba, M., and S. Katoh.** 1985. Electron transport from cytochrome b<sub>6</sub>-f complexes to photosystem I reaction center complexes in *Synechococcus* sp.: Is cytochrome c-553 a mobile electron carrier? *Biochim Biophys Acta* 808: 39-45.
- Naranda, T., W. Strong, J. Menaya, B. Fabbris, and J. Hershey.** 1994. Two structural domains of initiation factor eIF-4B are involved in binding to RNA. *J. Biol Chem.* 269: 14465-14472.
- Nicol, S., and F. Fuller-Pace.** 1995. The "DEAD box" protein DbpA interacts specifically with the peptidyltransferase center in 23S rRNA. *PNAS USA* 92: 11681-11685.
- Nishi, K., F. Morel-Deville, J. Hershey, T. Leighton, and J. Schnier.** 1988. An eIF-4A-like protein is a suppressor of an *Escherichia coli* mutant defective in 50S ribosomal subunit assembly. *Nature* 336: 496-498.
- Ogawa, T.** 1991. A gene homologous to the subunit-2 gene of NADH dehydrogenase is essential to inorganic carbon transport of *Synechocystis* PCC6803. *PNAS USA* 88: 4275-4279.
- Oh, J., and J. Kim.** 1999. ATP hydrolysis activity of the DEAD box protein Rok1p is required for *in vivo* ROK1 function. *Nuc Acids Res.* 27: 2753-2759.
- Ohmori, H.** 1994. Structural analysis of the *rhlE* gene of *Escherichia coli*. *Jpn J Genet.* 69: 1-12.
- Okanami, M., T. Meshi, and M. Iwabuchi.** 1998. Characterization of a DEAD box ATPase/RNA helicase protein of *Arabidopsis thaliana*. *Nuc Acids Res.* 26: 2638-2643.
- Omata, T., and N. Murata.** 1983. Isolation and characterization of the cytoplasmic membranes from the blue-green alga (cyanobacterium) *Anacystis nidulans*. *Plant Cell Physiol.* 24:1101-1112.
- Omata, T., and N. Murata.** 1984. Cytochromes and prenylquinones in preparations of cytoplasmic and thylakoid membranes from the cyanobacterium (blue-green alga) *Anacystis nidulans*. *Biochim Biophys Acta* 766: 395-402.

- Omata, T., and N. Murata.** 1985. Electron-transport reactions in cytoplasmic and thylakoid membranes prepared from the cyanobacteria (blue-green algae) *Anacystis nidulans* and *Synechocystis* PCC 6714. *Biochim Biophys Acta* **810**: 354-381.
- Owtrim, G.W., S. Hofmann, and C. Kuhlemeier.** 1991. Divergent genes for translation initiation factor eIF-4A are coordinately expressed in tobacco. *Nuc Acid Res.* **19**: 5491-5496.
- Owtrim, G.W., T. Mandel, H. Trachsel, A.A.M. Thomas, and C. Kuhlemeier.** 1994. Characterization of the tobacco *eIF-4A* gene family. *Plant Mol Biol.* **26**: 1747-1757.
- Pause, A., and N. Sonenberg.** 1992. Mutational analysis of a DEAD box RNA helicase: The mammalian translation initiation factor eIF-4A. *EMBO J.* **11**: 2643-2654.
- Pause, A., and N. Sonenberg.** 1993. Helicases and RNA unwinding in translation. *Curr Opin Struct Biol.* **3**: 953-959.
- Pause, A., N. Methot, and N. Sonenberg.** 1993. The HRIGRXXR region of the DEAD box RNA helicase eukaryotic translation initiation factor 4A is required for RNA binding and ATP hydrolysis. *Mol Cell Biol.* **13**: 6789-6798.
- Pemberton, J.M., I.M. Horne, and A.G. McEwan.** 1998. Regulation of photosynthetic gene expression in purple bacteria. *Microbiology* **144**: 267-278.
- Pfannschmidt, T., A. Nilsson, and J.F. Allen.** 1999. Photosynthetic control of chloroplast gene expression. *Nature* **397**: 625-628.
- Prentki, P., and H. M. Krisch.** 1984. *In vitro* insertional mutagenesis with a selectable DNA fragment. *Gene* **29**: 303-313.
- Pugh, G., S. Nicol, and F. Fuller-Pace.** 1999. Interaction of the *Escherichia coli* DEAD box protein DbpA with 23S ribosomal RNA. *J Mol Biol.* **292**: 771-778.
- Py, B., C. Higgins, H. Krisch, and A. Carpousis.** 1996. A DEAD-box RNA helicase in the *E. coli* RNA degradosome. *Nature* **381**: 169-172.
- Reyes, J.C., and F. J. Florencio.** 1995. Electron transport controls transcription of the glutamine synthetase gene (*glnA*) from the cyanobacterium *Synechocystis* sp. PCC 6803. *Plant Mol Biol.* **27**: 789-799.
- Reyes, J.C., M.I. Muro-Pastor, and F.J. Florencio.** 1997. Transcription of glutamine synthetase genes (*glnA* and *glnN*) from the cyanobacterium *Synechocystis* sp. strain PCC 6803 is differently regulated in response to nitrogen availability. *J Bacteriol.* **179**: 2678-2689.

- Richter, S., M. Hagemann, and W. Messer.** 1998. Transcription analysis and mutation of a *dnaA*-like gene in *Synechocystis* sp. strain PCC 6803. *J Bacteriol.* **180**: 4946-4949.
- Rippka, R.** 1988. Isolation and purification of cyanobacteria. *Methods Enzymol.* **167**: 3-27.
- Rippka, R., J. Deruelles, J.B. Waterbury, M. Herdman, and R.Y. Stanier.** 1979. Generic assignments, strain histories and properties of pure cultures of cyanobacteria. *J Gen Microbiol.* **111**: 1-61.
- Rodriguez, P.L., and L. Carrasco.** 1993. Poliovirus protein 2C has ATPase and GTPase activities. *J Biol Chem.* **268**: 8105-8110.
- Rogers, G. Jr., N. Richter, and W. Merrick.** 1999. Biochemical and kinetic characterization of the RNA helicase activity of eukaryotic initiation factor 4A. *J Biol Chem.* **274**: 12236-12244.
- Roos, S., S. Lindgren, and H. Jonsson.** 1999. Autoaggregation of *Lactobacillus reuteri* is mediated by a putative DEAD-box helicase. *Mol Microbiol.* **32**: 427-436.
- Rozen, F., I. Edery, K. Meerovitch, T. Dever, W. Merrick, and N. Sonenberg.** 1990. Bidirectional RNA helicase activity of eucaryotic translation initiation factors 4A and 4F. *Mol Cell Biol.* **10**: 1134-1144.
- Rozen, F., J. Pelletier, H. Trachsel, and N. Sonenberg.** 1989. A lysine substitution in the ATP-binding site of eucaryotic initiation factor 4A abrogates nucleotide-binding activity. *Mol Cell Biol.* **9**: 4061-4063.
- Sabaty, M., and S. Kaplan.** 1996. *mgpS*, a complex regulatory locus involved in the transcriptional control of the *puc* and *puf* operons in *Rhodobacter sphaeroides* 2.4.1. *J Bacteriol* **178**: 35-45.
- Saier Jr., M.H.** 1993. Introduction: Protein phosphorylation and signal transduction in bacteria. *J Cell Biochem.* **51**: 1-6.
- Salih, G.F., and C. Jansson.** 1997. Activation of the silent *psbA1* gene in the cyanobacterium *Synechocystis* sp. strain 6803 produces a novel and functional D1 protein. *Plant Cell* **9**: 869-878.
- Sambrook, J., E.F. Fritsch, and T. Maniatis.** 1989. Molecular cloning: a laboratory manual, 2nd ed. Cold Spring Harbor Laboratory Press, Cold Spring Harbor, N.Y.
- Sandmann, G., and R. Malkin.** 1983. NADH and NADPH as electron donors to respiratory and photosynthetic electron transport in the blue-green alga, *Aphanocapsa*. *Biochim Biophys Acta.* **725**: 221-224.
- Sato, N.** 1995. A family of cold-regulated RNA-binding proteins genes in the cyanobacterium *Anabaena variabilis* M3. *Nuc Acid Res.* **23**: 2161-2167.

- Scharnagl, M., S. Richter, and M. Hagemann.** 1998. The cyanobacterium *Synechocystis* sp. strain PCC 6803 expresses a DNA methyltransferase specific for the recognition sequence of the restriction endonuclease *PvuI*. *J Bacteriol.* **180**: 4116-4122.
- Scherer, S.** 1990. Do photosynthetic and respiratory electron transport chains share redox proteins? *TIBS* **15**: 458-462.
- Schmetterer, G.** 1994. Cyanobacterial respiration. pp. 409-435 *In* D.A. Bryant (ed.), *The Molecular Biology of Cyanobacteria*. Kluwer Academic Publishers, Dordrecht, The Netherlands.
- Schmid, S.R., and P. Linder.** 1991. Translation initiation factor 4A from *Saccharomyces cerevisiae*: analysis of residues conserved in the D-E-A-D family of RNA helicases. *Mol Cell Biol.* **11**: 3463-3471
- Schmid, S.R., and P. Linder.** 1992. D-E-A-D protein family of putative RNA helicases. *Mol. Microbiol.* **6**: 283-292.
- Shi, L., K.M. Bischoff, and P.J. Kennelly.** 1999. The *icfG* gene cluster of *Synechocystis* sp. strain PCC 6803 encodes an Rsb/Spo-like protein kinase, protein phosphatase, and two phosphoproteins. *J Bacteriol.* **181**: 4761-4767.
- Shi, L., M. Potts, and P.J. Kennelly.** 1998. The serine, threonine, and/or tyrosine-specific protein kinases and protein phosphatases of prokaryotic organisms: a family portrait. *FEMS Microbiol Rev.* **22**: 229-253.
- Smart, L.B., and L. McIntosh.** 1991. Expression of photosynthesis genes in the cyanobacterium *Synechocystis* sp. PCC6803: *psaA-psaB* and *psbA* transcripts accumulate in dark-grown cells. *Plant Mol. Biol.* **17**: 959-971.
- Smith, L.S., T. Lewis, and S. M. Matsui.** 1995. Increased yield of small DNA fragments purified by silica binding. *BioTechniques* **18**: 970-975.
- Snay-Hodge, C., H. Colot, A. Goldstein, and C. Cole.** 1998. Dbp5p/Rat8p is a yeast nuclear pore-associated DEAD-box protein essential for RNA export. *EMBO J.* **17**: 2663-2676.
- Sobczyk, A., G. Schyns, N. Tandeau de Marsac, and J. Houmard.** 1993. Transduction of the light signal during CCA in the cyanobacterium *Calothrix* sp. PCC 7601: DNA binding proteins and modulation by phosphorylation. *EMBO J.* **12**: 997-1004.
- Sonoda, M., H. Katoh, W. Vermaas, G. Schmetterer, and T. Ogawa.** 1998. Photosynthetic electron transport involved in PxcA-dependent proton extrusion in *Synechocystis* sp. strain PCC6803: Effect of *pxcA* inactivation on CO<sub>2</sub>, HCO<sub>3</sub><sup>-</sup> and NO<sub>3</sub><sup>-</sup> Uptake. *J Bacteriol.* **180**: 3799-3803.



- Stanier, R.Y., and G. Cohen-Bazire.** 1977. Phototrophic prokaryotes: The cyanobacteria. *Ann Rev Microbiol.* **31**: 225-274.
- Strauss, E.J., and C. Guthrie.** 1991. A cold-sensitive mRNA splicing mutant is a member of the RNA helicase gene family. *Genes Dev.* **5**: 629-641.
- Styhler, S., A. Nakamura, A. Swan, B. Suter, and P. Lasko.** 1998. *vasa* is required for GURKEN accumulation in the oocyte, and is involved in oocyte differentiation and germ-line cyst development. *Development* **125**: 1569-1578.
- Sugita, M., and M. Sugiura.** 1994. The existence of eukaryotic ribonucleoprotein consensus sequence-type RNA-binding proteins in a prokaryote, *Synechococcus* 6301. *Nuc Acid Res.* **22**: 25-31.
- Suranyi, G., A. Korcz, Z. Palfi, and G. Borbely.** 1987. Effects of light deprivation on RNA synthesis, accumulation of guanosine 3'(2')-diphosphate, and protein synthesis in heat-shocked *Synechococcus* sp. strain PCC 6301, a cyanobacterium. *J Bacteriol.* **169**: 632-639.
- Suzuki, I., D.A. Los, Y. Kanasaki, K. Mikami, and N. Murata.** 2000. The pathway for perception and transduction of low-temperature signals in *Synechocystis*. *EMBO J.* **19**: 1327-1334.
- Tandeau de Marsac, N., and J. Houmard.** 1988. Complementary chromatic adaptation: Physiological conditions and action spectra. *Methods Enzymol.* **159**: 318-328.
- Tandeau de Marsac, N.** 1994. Differentiation of hormogonia and relationships with other biological processes. pp. 825-842. *In* D.A. Bryant (ed.), *The Molecular Biology of Cyanobacteria*. Kluwer Academic Publishers, Dordrecht, The Netherlands.
- Thiel, T.** 1994. Genetic analysis of cyanobacteria. pp. 581-611. *In* D.A. Bryant (ed.), *The Molecular Biology of Cyanobacteria*. Kluwer Academic Publishers, Dordrecht, The Netherlands.
- Tiller, K., and G. Link.** 1993. Phosphorylation and dephosphorylation affect functional characteristics of chloroplast and etioplast transcription systems from mustard (*Sinapsis alba* L.). *EMBO J.* **12**: 1745-1753.
- Toone, W.M., K.E. Rudd, and J.D. Friesen.** 1991. *deaD*, a new *Escherichia coli* gene encoding a presumed ATP-dependent RNA helicase, can suppress a mutation in *rpsB*, the gene encoding ribosomal protein S2. *J Bacteriol.* **173**: 3291-3302.
- Trebst, A.** 1980. Inhibitors in electron flow: Tools for the functional and structural localization of carriers and energy conservation sites. *Meth Enzymol.* **69**: 675-715.

- Tseng, S., P. Weaver, Y. Liu, M. Hitomi, A. Tartakoff, and T. Chang.** 1998. Dbp5p, a cytosolic RNA helicase, is required for poly (A)+ RNA export. *EMBO J.* **17**: 2651-2662.
- Tsu, C. and O. Uhlenbeck.** 1998. Kinetic analysis of the RNA-dependent adenosinetriphosphatase activity of DbpA, and *Escherichia coli* DEAD protein specific for 23S ribosomal RNA. *Biochemistry* **37**: 16989-16996.
- Tuerk, C., and L. Gold.** 1990. Systematic evolution of ligands by exponential enrichment: RNA ligands to bacteriophage T4 DNA polymerase. *Science* **249**: 505-510.
- Tyystjarvi, T., E. Tyystjarvi, I. Ohad, E. Aro.** 1998. Exposure of *Synechocystis* 6803 cells to series of single turnover flashes increases the *psbA* transcript level by activating transcription and down-regulating *psbA* mRNA degradation. *FEBS Lett.* **436**:483-487.
- Van Bogelen, R., and F. Neidhardt.** 1990. Ribosomes as sensors of heat and cold shock in *Escherichia coli*. *PNAS USA* **87**: 5589-5593.
- Venema, J., C. Bousquet-Antonelli, J. Gelugne, M. Caizergues-Ferrer, and D. Tollervey.** 1997. Rok1p is a putative RNA helicase required for rRNA processing. *Mol Cell Biol.* **17**: 3398-3407.
- Vener, A.V., I. Ohad, and B. Andersson.** 1998. Protein phosphorylation and redox sensing in chloroplast thylakoids. *Curr Opin Plant Biol.* **1**: 217-223.
- Vener, A.V., P.J.M. van Kan, A. Gal, B. Andersson, and I. Ohad.** 1995. Activation/deactivation cycle of redox-controlled thylakoid protein phosphorylation: Role of plastoquinol bound to the reduced cytochrome *bf* complex. *J Biol Chem.* **270**: 25225-25232.
- Vermaas, W.F.J., G. Shen, and S. Styring.** 1994. Electrons generated by photosystem II are utilized by an oxidase in the absence of photosystem I in the cyanobacterium *Synechocystis* sp. PCC 6803. *FEBS Lett.* **337**: 103-108.
- Vinnemeier, J., and M. Hagemann.** 1999. Identification of salt-regulated genes in the genome of the cyanobacterium *Synechocystis* sp. strain PCC 6803 by subtractive RNA hybridization. *Arch Microbiol* **172**: 377-386.
- Vioque, A.** 1992. Analysis of the gene encoding the RNA subunit of ribonuclease P from cyanobacteria. *Nuc Acid Res.* **20**: 6331-6337.
- Vogelstein, B, and D. Gillespie.** 1979. Preparative and analytical purification of DNA from agarose. *PNAS USA* **76**: 615-619.

- Wang, Y., and C. Guthrie.** 1998. PRP16, a DEAH-box RNA helicase, is recruited to the spliceosome primarily via its nonconserved N-terminal domain. *RNA* **4**: 1216-1229.
- Wassarman, D. A., and J. A. Steitz.** 1991. Alive with DEAD proteins. *Nature* **349**: 463-464.
- Williams, J.G.K.** 1988. Construction of specific mutations in the photosystem II photosynthetic reaction center by genetic engineering methods in *Synechocystis* 6803. *Methods Enzymol.* **167**: 766-778.
- Wilmotte, A.** 1994. Molecular evolution and taxonomy of the cyanobacteria. pp. 1-25. *In* D.A. Bryant (ed.), *The Molecular Biology of Cyanobacteria*. Kluwer Academic Publishers, Dordrecht, The Netherlands.
- Wolk, C.P.** 1973. Physiology and cytological chemistry of blue-green algae. *Bacteriol Rev.* **37**: 32-101.
- Yao, N., T. Hesson, M. Cable, and H. Kwong, H. Le, and P. Weber.** 1997. Structure of the hepatitis C virus NS5A helicase domain. *Nat Struct Biol* **4**: 463-467.
- Yeh, K., S. Wu, J. Murphy, and J. Lagarias.** 1997. A cyanobacterial phytochrome two-component light sensory system. *Science* **277**: 1505-1508.
- Yu, E.** 1999. Characterizing a cold-induced RNA helicase. M.Sc. thesis. University of Alberta, Edmonton, Canada.
- Yu, E., and G.W. Owttrim.** 2000. Characterization of the cold stress induced cyanobacterial DEAD-box protein CrhC as an RNA helicase. *Nucl Acids Res.* **28**: 3926-3934.
- Yu, L., J. Zhao, U. Muhlenhoff, D.A. Bryant, and J.H. Golbeck.** 1993. PsaE is required for *in vivo* cyclic electron flow around photosystem I in the cyanobacterium *Synechococcus* sp. PCC 7002. *Plant Physiol.* **103**: 171-180.
- Zhao, J., and J.J. Brand.** 1989. Sequential events in the photoinhibition of *Synechocystis* under sodium stress. *Plant Physiol.* **91**: 91-100.
- Zhou, C., Y. Yang, and A.Y. Jong.** 1990. Mini-prep in ten minutes. *BioTechniques* **8**:172-173.
- Zoller, M.J., and M. Smith.** 1987. Oligonucleotide-directed mutagenesis: a simple method using two oligonucleotide primers and a single-stranded DNA template. *Meth Enzymol.* **154**: 329-350.

## Appendix A – Amino Acid Designations

The 20  $\alpha$ -amino acids and their one-letter and three-letter designations are grouped according to side chain characteristics.

### *Aliphatic amino acids*

G	Gly	Glycine
A	Ala	Alanine
V	Val	Valine
L	Leu	Leucine
I	Ile	Isoleucine

### *Aromatic amino acids*

P	Phe	Phenylalanine
Y	Tyr	Tyrosine
W	Trp	Tryptophan

### *Basic amino acids*

H	His	Histidine
K	Lys	Lysine
R	Arg	Arginine

### *Acidic amino acids*

D	Asp	Aspartic Acid
E	Glu	Glutamic Acid
N	Asn	Asparagine
Q	Gln	Glutamine

### *Amino acids with hydroxyl- or sulfur-containing side chains*

S	Ser	Serine
C	Cys	Cysteine
T	Thr	Threonine
M	Met	Methionine

### *Cyclic amino acid*

P	Pro	Proline
---	-----	---------